Organoid Models to Characterise Colonic Stem Cell Plasticity

Brittany-Amber Jacobs

University College

University of Oxford



A thesis submitted for the degree of

Doctor of Philosophy

Trinity 2022

DECLARATION

This thesis is submitted to the University of Oxford in support of my application for the degree of Doctor of Philosophy in Clinical Medicine. The work described herein was performed while I was a graduate student at the Ludwig Institute for Cancer Research, under the supervision of Professor Xin Lu and Professor Simon Leedham. All the work presented in this thesis is the result of my own work unless otherwise stated and has not been submitted in any previous application for any degree.

ACKNOWLEDGEMENTS

ABSTRACT

Cellular plasticity is the capability of cells to alter their phenotype in response to cues in the surrounding milieu, a vital property in several biological processes. The colon is a prime example of the importance of cellular plasticity in homeostasis as its epithelial lining is extremely dynamic, with cells constantly selecting between proliferation, differentiation, migration and apoptosis, depending on the needs of the tissue. While plasticity plays an important role in healthy tissues, genetic alterations and microenvironmental influences can also generate aberrant cellular plasticity which can mediate numerous diseases, including colorectal cancer. In colorectal cancer, the dysregulation of cellular plasticity causes phenotypic heterogeneity within the tumour, which is known to drive resistance to therapy. Consequently, despite progress in drug development in the past decades, curative treatment for this highly heterogeneous and metastatic disease remains difficult, with a significant proportion of cancer-related mortality worldwide attributable to colorectal cancer.

Understanding of the cellular plasticity mediating treatment resistance in colorectal cancer is a key step towards improving patient outcomes. In this study, in order to elucidate how genetic alterations and microenvironmental influences affected the cellular plasticity exhibited by colonic stem cells, a library of colon organoids (colonoids) harbouring driver gene mutations common in colorectal cancer were generated. Study of cellular plasticity was achieved by analysing this colonoid library with a novel, high-throughput, and unbiased organoid phenotyping platform, termed Shape, Appearance and Motion (SAM), which identified instantaneous mutant colonoid states and generated phenotype trajectories to compare mutant trait development over time. SAM analyses revealed that colorectal cancer-associated driver mutations significantly alter the cellular plasticity of colonoids and generate distinct genotype-phenotype profiles unique to each driver mutation. Notably, *Apc* mutant colonoids demonstrated a phenotypic dynamic that was particularly distinct from colonoids carrying all other driver mutations assessed, adopting a unique two-dimensional eccentric appearance.

To understand the molecular basis for the differences seen in cellular plasticity between the various mutant colonoids, phenotypic findings were integrated with single-cell RNA-sequencing. The distinct spatiotemporal dynamics exhibited by *Apc* mutant colonoids were found to be associated with a unique gene expression profile characterised by elevated Yap signalling and the acquisition of a regenerative stem cell and foetal gene signature. Furthermore, *Apc* mutant colonoids had decreased expression of tight junction proteins and increased expression of Yap-dependent extracellular matrix remodelling proteins. Together these findings suggest that *Apc* mutant colonoids are engaged in a Yap-mediated regenerative response, a process normally observed in the repairing intestinal epithelium. By combining these data with microscopic observation of developing *Apc* mutant colonoids, a mechanistic model for the unique *Apc* mutant colonoid phenotype is developed, whereby the two-dimensional eccentric appearance activates Yap-mediated mechanotransduction pathways and pushes the colonoids towards the regenerative stem cell molecular phenotype. Accordingly, the usual basal stem cell molecular phenotype imposed by the *Apc* mutation is overwritten by microenvironmentally influenced plasticity, which is able to induce a phenotypic shift towards a regenerative stem cell state regardless of the normal basal stem cell molecular phenotype associated with this mutation.

To extend this phenotypic study of mutant colonoids to model the subclonal dynamics and intratumoral heterogeneity driving tumour evolution and drug resistance in colorectal cancer, co-culture of mutant colonoids was employed. Findings suggested that mutant colonoids exhibit cooperative interactions in co-culture which significantly alter their individual phenotypes and increase their capacity for growth. scRNA-seq analysis on these co-cultured mutant colonoids showed that, while most mutant genotypes showed considerable transcriptomic changes during co-culture, *Apc* mutant colonoids were less susceptible to modifications of their transcriptomic profile in response to the presence of other mutant genotypes.

Finally, to advance the co-culture approach towards highly defined structures that more closely represent the clonal architecture of the tumour milieu, a novel organoid co-culture protocol

which provides spatial control and patterning of mutant colonoids and facilitates the incorporation of cells usually present in the tumour microenvironment was developed. The mixed colonoid model represents an exciting tool for future research to further understand the direct subclonal interactions, intratumoural heterogeneity, and cellular plasticity present in colorectal cancer tumours and clarify the influence that the tumour microenvironment has on tumour evolution. In summary, the findings and methods developed in this work using a driver mutation colonoid library provide further insight into how driver mutations co-opt cellular plasticity to drive colorectal cancer.

CONTENTS

Declaration……... i

Acknowledgements…….. ii

Abstract…….. iii

Contents…… vi

List of Figures…… xi

List of Tables……... xiv

List of Abbreviations…….. xv

1. **Introduction**

1.1. Colon Physiology…… 1

1.1.1. The Role of the Colon in the Digestive System…… 1

1.1.2. The Colon Epithelium: Structure and Function…… 2

1.1.2.1. Stem Cells……... 2

1.1.2.2. Colonocytes…… 4

1.1.2.3. Enteroendocrine Cells…… 5

1.1.2.4. Goblet Cells…….. 6

1.1.2.5. M Cells…….. 7

1.1.2.6. Tuft Cells…….. 8

1.1.3. Signalling Pathways in the Colonic Crypts…… 8

1.1.3.1. Wnt…… 9

1.1.3.2. Bmp…… 11

1.1.3.3. Hh…….. 12

1.1.3.4. Notch..... 13

1.1.4. Colon Epithelium Plasticity and Regeneration..…… 14

1.1.5. Colonic Diseases…… 15

1.2.Intestinal Organoids…….. 16
1.2.1. History of The Organoid…….…… 17
1.2.2. Organoids as Models for the Study of Intestinal Physiology……. 18
1.2.2.1. Morphogen Signals……... 18
1.2.2.2. The Microbiome…… 20
1.2.2.3. Immunity…… 21
1.2.3. Organoids as Models for the Study of Intestinal Pathologies…… 22
1.2.3.1. Hereditary Diseases…… 22
1.2.3.2. Infectious Diseases…….. 22
1.2.3.3. Inflammatory Bowel Disease and Colorectal Cancer…….…… 24
1.3. Colorectal Cancer in Detail…… 26
1.3.1. Genetics of Colorectal Cancer…….. 27
1.3.1.1. APC…… 28
1.3.1.2. KRAS…….. 28
1.3.1.3. SMAD4……... 28
1.3.1.4. TP53…… 29
1.3.2. Models of Colorectal Cancer…… 29
1.3.2.1. Adenoma-Carcinoma Sequence Model…… 29
1.3.2.2. Big Bang Model…… 31
1.3.3. Tumour Heterogeneity and Evolution in Colorectal Cancer…….. 32
1.4. Aims and Hypotheses...…….. 34
2. **Methods and Materials**
2.1. Colonoid Culture……... 36
2.1.1. Conditioned Medium and Genotype Specific Medium Constituents…… 36
2.1.2. Colonoid Derivation…… 37
2.1.3. Colonoid Maintenance, Cryopreservation and Thawing …….. 38
2.2. Fluorescent Labelling of Mutant Colonoids……... 38
2.2.1. Lentivirus Production…….. 38
2.2.2. Lentiviral Transduction of Colonoids…… 39

2.2.3. Cell Sorting…….. 39
2.3. Cre Recombinase Treatment of *p53*$^{LSL\text{-}R172H/R172H}$ and *Kras*$^{LSL\text{-}G12D/+}$ *CreERT2-EYFP* Colonoids…… 40
2.4. Polymerase Chain Reaction Confirming Colonoid Genotypes……... 40
2.5. Organoid Formation Assay…….. 40
2.5.1. Single Culture Conditions…….. 40
2.5.2. Co-Culture Medium Validation…….. 41
2.5.3. Co-Culture Conditions…… 41
2.6. Time-Lapse Microscopy for Shape, Appearance and Motion Analysis……. 42
2.6.1. Time-Lapse Confocal Microscopy…… 42
2.6.2. Time-Lapse Phase Contrast Microscopy……. 42
2.6.3. Shape, Appearance and Motion Analysis..…… 42
2.7. Reseeding 2D Eccentric *Apc*$^{min/+}$ mCherry Colonoids……..…… 44
2.8. Single-Cell RNA Sequencing……..…… 44
2.8.1. Sample Processing…… 44
2.8.2. Library Preparation…… 45
2.8.3. Data Analysis……... 45
2.9. Immunofluorescence Staining…… 46
2.10. Mixed Colonoids..…… 46
2.11. Ethics…….. 48
3. **Results**
3.1.Colonoids Harbouring Colorectal Cancer-Associated Driver Mutations Display Complex Spatiotemporal Dynamics…..……... 49
3.1.1. Introduction…….. 49
3.1.2. Chapter Aim…… 52
3.1.3. Generating Fluorescent Colonoids Harbouring Colorectal Cancer-Associated Driver Mutations……... 53
3.1.4. Mutant Colonoids Display Differences in Organoid Forming Ability……. 58

3.1.5. Shape, Appearance and Motion Analysis on Mutant Colonoids Reveals Intricate Spatiotemporal Dynamics……..... 59
3.1.6. Discussion…… 67
3.2.Colonoids Harbouring Colorectal Cancer-Associated Driver Mutations Exhibit Distinct Stem Cell Molecular Phenotypes……..... 72
3.2.1. Introduction…….. 72
3.2.2. Chapter Aim…… 75
3.2.3. scRNA-seq on Wild Type and Mutant Colonoids Reveals Unique Gene Expression Profiles…….. 76
3.2.4. Phenotypically distinct *Apc*$^{min/+}$ Colonoids Exhibit Activated Yap Signalling…….. 77
3.2.5. *Apc*$^{min/+}$ Colonoids Express a Regenerative and Foetal Stem Cell Gene Signature……. 80
3.2.6. *Apc*$^{min/+}$ Colonoids Exhibit Altered Expression of ECM Remodelling and Tight Junction Proteins…….…… 86
3.2.7. Discussion…… 90
3.3.Investigating the Influence of Colorectal Cancer-Associated Driver Mutations on Gene Expression and Subclonal Dynamics in Colonoid Co-Culture Models…..……..... 95
3.3.1. Introduction…….. 95
3.3.2. Chapter Aim…… 99
3.3.3. The Behaviour and Gene Expression of Mutant Colonoids is Altered Under Co-Culture Conditions……..…… 99
3.3.4. Mixed Colonoids: A Novel Organoid Co-Culture Model..…… 110
3.3.5. Discussion…… 112
4. **Conclusion…….. 118**
5. **Future Directions**
5.1.Investigating the Altered Stem Cell Molecular Phenotype and Morphological Change in *Apc*$^{min/+}$ Colonoids……... 123

5.1.1. Delineating the Role of Yap in Promoting the 2D Eccentric Phenotype and Regenerative Stem Cell Molecular Phenotype in *Apc*$^{min/+}$ Colonoids……. 123

5.1.2. Determining the Function of Ahr in *Apc*$^{min/+}$ Colonoids……..… 124

5.2. Examining the Unique Gene Expression Profile of *Kras*$^{G12D/+}$ Colonoids……...….. 127

5.3. Investigating the Potential Function of Wnt Antagonists in Mutant Colonoid Co-Culture Models…….. 129

5.4. Optimisation and Characterisation of Mixed Colonoids..…….. 131

6. **References…… 134**

7. **Appendix**

7.1. Cell Culture Media…….. 153

7.2. Conditioned Medium Activity Assay…...…….. 154

7.3.Lentiviral Transduction…… 156

7.4.Polymerase Chain Reaction…….. 156

7.5.Antibodies for Immunofluorescence Staining…….. 157

7.6.Reagents for Mixed Colonoid Culture…….…….. 157

LIST OF FIGURES

Introduction

Figure 1.1. Epithelial cells lining the colonic crypts of Lieberkühn…….. 3

Figure 1.2. Signalling pathways in the colonic crypts of Lieberkühn…….. 9

Figure 1.3. Wnt β-catenin signalling pathway……... 10

Figure 1.4. Bmp signalling pathway…… 11

Figure 1.5. Ihh signalling pathway……...12

Figure 1.6. Notch signalling pathway…… 13

Figure 1.7. Colon epithelium plasticity and regeneration……..…… 15

Figure 1.8. Intestinal organoid culture…… 18

Figure 1.9. The Adenoma-Carcinoma Sequence model of colorectal cancer……. 30

Figure 1.10. The Big Bang model of colorectal cancer…… 31

Methods and Materials

Figure 2.1. Shape, Appearance and Motion workflow…… 43

Figure 2.2. Mixed colonoid generation...…… 47

Results Chapter 3.1

Figure 3.1. Derivation of wild type and fluorescent mutant colonoids……... 54

Figure 3.2. PCR confirming the genotype of wild type and mutant colonoids……. 55

Figure 3.3. Confirmation of colonoid phenotype and fluorescent protein expression……. 57

Figure 3.4. Mutant colonoids display differences in organoid forming ability……... 58

Figure 3.5. Representative images from time-lapse confocal microscopy videos of mutant colonoids…… 60

Figure 3.6. SAM characterisation of mutant colonoids reveals 8 distinct phenotypic clusters……... 62

Figure 3.7. *Apc*$^{min/+}$ colonoids undergo drastic changes in phenotype over time.…… 63

Figure 3.8. *Apc*$^{min/+}$ colonoids exhibit increased eccentricity and mean speed over the course of 117 hours……..…….. 64

Figure 3.9. Mutant colonoids demonstrate unique trajectories through SAM space over time…… 65

Figure 3.10. Mutant colonoids demonstrate temporal variation in the frequency of each phenotype cluster…… 66

Results Chapter 3.2

Figure 3.11. Phenotypic fitness landscape model…… 73

Figure 3.12. Wild type and mutant colonoids exhibit unique gene expression profiles….. 76

Figure 3.13. Apcmin/+ colonoids overexpress Yap target genes and exhibit upregulated Yap signalling...…….…… 78

Figure 3.14. Yap is localised to the nucleus of 2D eccentric *Apc*$^{min/+}$ colonoids..…….. 79

Figure 3.15. *Apc*$^{min/+}$ colonoids express a regenerative stem cell signature…… 81

Figure 3.16. 2D eccentric *Apc*$^{min/+}$ colonoids stain positive for regenerative stem cell gene markers..……..…….. 82

Figure 3.17. *Apc*$^{min/+}$ colonoids express a foetal gene signature…….. 83

Figure 3.18. *Apc*$^{min/+}$ colonoids stain positive for foetal gene markers……..…… 85

Figure 3.19. 2D eccentric *Apc*$^{min/+}$ colonoids lose the capacity to efficiently form organoids…….. 87

Figure 3.20. *Apc*$^{min/+}$ colonoids exhibit increased expression of ECM remodelling proteins and decreased expression of tight junction proteins……..……. 89

Results Chapter 3.3

Figure 3.21. Co-culture medium does not significantly alter the organoid forming ability of mutant colonoids…… 101

Figure 3.22. Mutant colonoids have altered organoid forming ability in when grown in co-culture…….. 102

Figure 3.23. Gene expression profiles of mutant colonoids grown under standard and co-culture conditions……..……. 104

Figure 3.24. Gene expression profiles of mutant colonoids vary between standard and co-cultures conditions…… 105

Figure 3.25. Top upregulated genes expressed by mutant colonoids varies between standard and co-culture conditions…….. 107

Figure 3.26. Uniquely patterned mixed colonoids cultured with and without fibroblasts…… 111

Conclusion

Figure 4.1. Proposed mechanism behind the 2D eccentric phenotype adopted by *Apc*$^{min/+}$ colonoids……..…….. 120

Future Directions

Figure 5.1. *Apc*$^{min/+}$ colonoid-derived cells have elevated expression of *Ahr*……. 125

Figure 5.2. *Kras*$^{G12D/+}$ colonoids exhibit a unique gene expression profile…….. 128

Figure 5.3. Single and co-cultured *Apc*$^{min/+}$ colonoid-derived cells have elevated expression of Wnt antagonist *Notum*……... 130

Appendix

Figure 6.1. HEK293T luciferase reporter cell plate layout and medium requirements….. 154

Figure 6.2. An optimal luciferase assay result comparing the quality of an old and new batch of Wnt3A conditioned medium……... 155

Figure 6.3. Gating strategy applied to isolate successfully transduced organoid populations…….. 156

LIST OF TABLES

Methods and Materials

Table 2.1. Colonoid medium constituents…… 37

Results Chapter 3.3

Table 3.1. Significance of the top upregulated genes expressed by each genotype between culture conditions not focused on in this study…… 109

Appendix

Table 6.1. Polymerase Chain Reaction primers used to confirm the colonoid genotypes…… 156

Table 6.2. Polymerase Chain Reaction components and volumes used to confirm the colonoid genotypes…… 157

Table 6.3. ProFlex PCR System conditions used to confirm the mutant colonoid genotypes…… 157

Table 6.4. Primary and secondary antibodies used for immunofluorescent staining of colonoids…… 157

LIST OF ABBREVIATIONS

2D – Two-Dimensional

3D – Three-Dimensional

ACh – Acetylcholine

Ahr – Aryl hydrocarbon receptor

AKPm – *Apc*$^{min/+}$, *Kras*$^{G12D/+}$*:p53*^{Null} and *p53*$^{R12H/R172H}$ colonoids

AKPn – *Apc*$^{min/+}$, *Kras*$^{G12D/+}$*:p53*^{Null} and p*53*^{Null} colonoids

Ankrd1 – Ankyrin repeat domain 1

Anxa1 – Annexin a1

Apc – Adenomatous polyposis coli

Areg – Amphiregulin

Arg2 – Arginase 2

Ascl2 – Achaete scute-like 2

Atoh1 – Atonal homolog 1

Bmp – Bone morphogenetic protein

BSA – Bovine Serum Albumin

Bsg – Basigin

Car – Carbonic Anhydrase

CBC – Crypt Base Columnar

Ccn2 – Cellular communication network factor 2

CD – Chron's Disease

Cdh17 – Cadherin 17

Cdx2 – Caudal-type homeobox transcription factor 2

CF – Cystic Fibrosis

CFTR – Cystic Fibrosis Transmembrane Conductance Regulator

CIMP – CpG Island Methylator Phenotype

CIN – Chromosomal Instability

Ck1 – Casein kinase 1

Cldn15 – Claudin 15

Clu – Clusterin

CMS – Consensus Molecular Subtypes

Colonoid – Colon organoid

CRC – Colorectal Cancer

CSC – Cancer Stem Cell

DCP - Depth-Coloured Projection

Dkk1 – Dickkopf 1

Dmbt1 – Deleted in malignant brain tumours 1

DSS – Dextran Sulphate Sodium

EC – Enterochromaffin

ECM – Extracellular Matrix

EDTA – Ethylenediaminetetraacetic Acid

EEC – Enteroendocrine Cell

Egf – Epidermal growth factor

Egfr – Epidermal growth factor receptor

EMT – Epithelial-Mesenchymal Transition

Enpp2 – Ectonucleotide pyrophosphatase/phosphodiesterase 2

ENS – Enteric Nervous System

ENU – Ethylnitrosourea

FACS – Fluorescence-Activated Cell Sorting

FAK – Focal Adhesion Kinase

FAP – Familial Adenomatous Polyposis

FBS – Foetal Bovine Serum

GALT – Gut-Associated Lymphoid Tissue

GAP – Goblet cell-associated Antigen Passage

GC – Goblet Cell

Gdf15 – Growth differentiation factor 15

GI – Gastrointestinal

Gli1 – Glioma-associated oncogene 1

GPCR – G-protein-coupled receptor

GSEA – Gene Set Enrichment Analysis

Gsk3 – Glycogen synthase kinase 3

Guca2a – Guanylate cyclase activator 2a

HEPES – 4-(2-hydroxyethyl)-1-piperazineethanesulfonic Acid

Hes1 – Hairy and enhancer of split 1

Hh – Hedgehog

HIV – Human Immunodeficiency Virus

IBD – Irritable Bowel Disease

IBS – Irritable Bowel Syndrome

IF – Immunofluorescence

IFN – Interferon

Ihh – Indian hedgehog

IL – Interleukin

ISC – Intestinal Stem Cell

ITH – Intratumoural heterogeneity

Jnk – c-Jun N-terminal kinase

Kras – Kirsten Rat Sarcoma

Krt – Keratin

LDCV – Large Dense-Core Vesicle

Lef – Lymphoid enhancer-binding factor

Lgr5 – Leucine-rich G protein-coupled receptor 5

LPA – Lysophosphatidic acid

Lrig1 – Leucine rich repeats and immunoglobulin like domains 1

Lrp5/6 – Low-density lipoprotein receptor-related protein 5/6

LSL – Lox-Stop-Lox

Ly6a – Lymphocyte antigen 6 complex, locus a

Lypd8 – Ly6/Plaur domain containing 8

M – Microfold

MAPK – Mitogen-Activated Protein Kinase

Min – Multiple intestinal neoplasia

Mmp7 – Matrix metalloproteinase 7

MOI – Multiplicity of Infection

MSI – Microsatellite Instability

Msln – Mesothelin

Muc – Mucin

NHE3 – Sodium-hydrogen exchanger 3

NICD – Notch Intracellular Domain

Nod2 – Nucleotide binding oligomerization domain containing 2

OCT – Optimal Cutting Temperature

OFA – Organoid Formation Assay

Olfm4 – Olfactomedin 4

PBS – Phosphate Buffered Saline

PCA – Principal Component Analysis

PCR – Polymerase Chain Reaction

PDO – Patient-Derived Organoid

PFA – Paraformaldehyde

PFS – Progression-Free Survival

Pi3k – Phosphatidylinositol-3-kinase

Plaur – Plasminogen activator, urokinase receptor

Ras – Rat Sarcoma Virus

revSC – Revival Stem Cell

Rnt43 – Ring finger protein 43

Rock – Rho-Associated Protein Kinase

RSC – Regenerative Stem Cell

RT – Room Temperature

SAM – Shape, Appearance, Motion

SARS-CoV-2 – Severe Acute Respiratory Syndrome Coronavirus 2

SCFA – Short-Chain Fatty Acid

scRNA-seq – Single-cell RNA-sequencing

SEM – Standard Error of the Mean

SLMV – Smaller Synaptic-Like Microvesicle

Smad – Suppressor of Mothers Against Decapentaplegic

Spp1 – Osteopontin

Spink4 – Serine peptidase inhibitor kazal type 4

Sprr1a – Small proline rich protein 1a

Src – Steroid receptor coactivator

Tcf – T-cell factor

TA – Transit-amplifying

Tacstd2 – Tumour-associated calcium signal transducer 2

TC – Tuft Cell

Tff3 – Trefoil factor 3

Tgf – Transforming Growth Factor

TME – Tumour Microenvironment

TNF – Tumour Necrosis Factor

Tp53 – Tumour Protein p53

UC – Ulcerative Colitis

UMAP – Uniform Manifold Approximation and Projection

UMI – Unique Molecular Identifier

VST – Variance-Stabilizing Transformation

VSV-G – Vesicular Stomatitis Virus G Glycoprotein

Wnt – Wingless-related integration site

Yap – Yes-associated protein

Znrf3 – Zinc and ring finger 3

1. INTRODUCTION

1.1. Colon Physiology

1.1.1. The Role of the Colon in the Digestive System

The colon, also referred to as the large intestine, is the final portion of the gastrointestinal (GI) tract and can be divided into six main segments: the caecum, ascending colon, transverse colon, descending colon, sigmoid colon and the rectum[1]. The colon begins at the ileocecal valve, where the ileum (the last segment of the small intestine) meets the caecum and ends at the rectum. The primary function of the colon is to absorb water and electrolytes and propel any remaining indigestible material towards the rectum for elimination via the anus[2]. Through the establishment of a hypoxic environment conducive for bacterial growth, the colon is also responsible for production and absorption of B and K group vitamins[3].

The small intestine produces partially digested food (chyme), which is received at the initial/proximal portion of the colon by the pouch-shaped caecum. When the caecum is full, contractions are triggered in the muscular layer of the colon to move the chyme towards the ascending colon[2]. Haustral contractions, named after the haustra that give the colon its segmented appearance, are triggered by the presence of chyme and aim to move the chyme from one haustra to the next while simultaneously churning the chyme to aid absorption. Mass movements are strong contractions in the muscular layer of the colon responsible for rapid passage of the chyme towards the rectum[2].

Following the caecum, the chyme passes through the ascending and transverse colon. These segments of the colon are the major sites where residual water and electrolytes not taken up by the small intestine are absorbed. Water is absorbed via osmosis due to the gradient formed by absorption of electrolytes, namely sodium, potassium and chloride[2]. Sodium is absorbed as a result of active absorption through sodium channels. Depending on the concentration in the lumen created by the absorption of sodium, potassium is either passively absorbed or secreted. Chloride ions are absorbed across an electrochemical gradient via reciprocal anion exchange for bicarbonate ions[2,4].

The descending colon then receives and stores the solid material produced by the ascending and transverse colon. Contractions in the muscular layer of the sigmoid colon increase the pressure inside the colon and promote the movement of the indigestible material into the rectum prior to elimination via the anus[2].

1.1.2. The Colon Epithelium: Structure and Function

The colon is lined with an extremely dynamic single epithelial layer, which undergoes continuous proliferation, migration, differentiation and apoptosis. Structurally, the epithelium is organised into repetitive invaginations known as the crypts of Lieberkühn[5]. These powerful structural units are formed of stems cells that reside at the crypt base and terminally differentiated cell types which migrate upwards from the crypt base and line the lumen of the colon.

The cell types which constitute the epithelium can be broadly categorised into undifferentiated (intestinal stem cells) and post-mitotic differentiated cells. Differentiated cells can be further subdivided into absorptive (colonocytes), secretory (enteroendocrine, goblet and tuft cells) and M cells[6]. The characteristics of these epithelial cell types, whose arrangement in the colonic crypt is depicted in Figure 1.1, will briefly be discussed below.

1.1.2.1. Stem Cells

The cells of the colonic epithelium are under constant mechanical tension provided by the non-compressible endoluminal chyme and muscular contractions within the colon wall[7]. Furthermore, the epithelium is frequently exposed to pathogenic microorganisms and carcinogens present in the luminal contents. These persistent stressors lead to high rates of cell death and thus require daily self-renewal[8].

Small populations of intestinal stem cells (ISCs), which reside in the crypts of Lieberkühn, are responsible for this self-renewal[9]. The ISC is multipotent and self-renewing, meaning it has the ability to reconstitute the various cell types of the intestinal epithelium through differentiation while still maintaining the stem cell population[10].

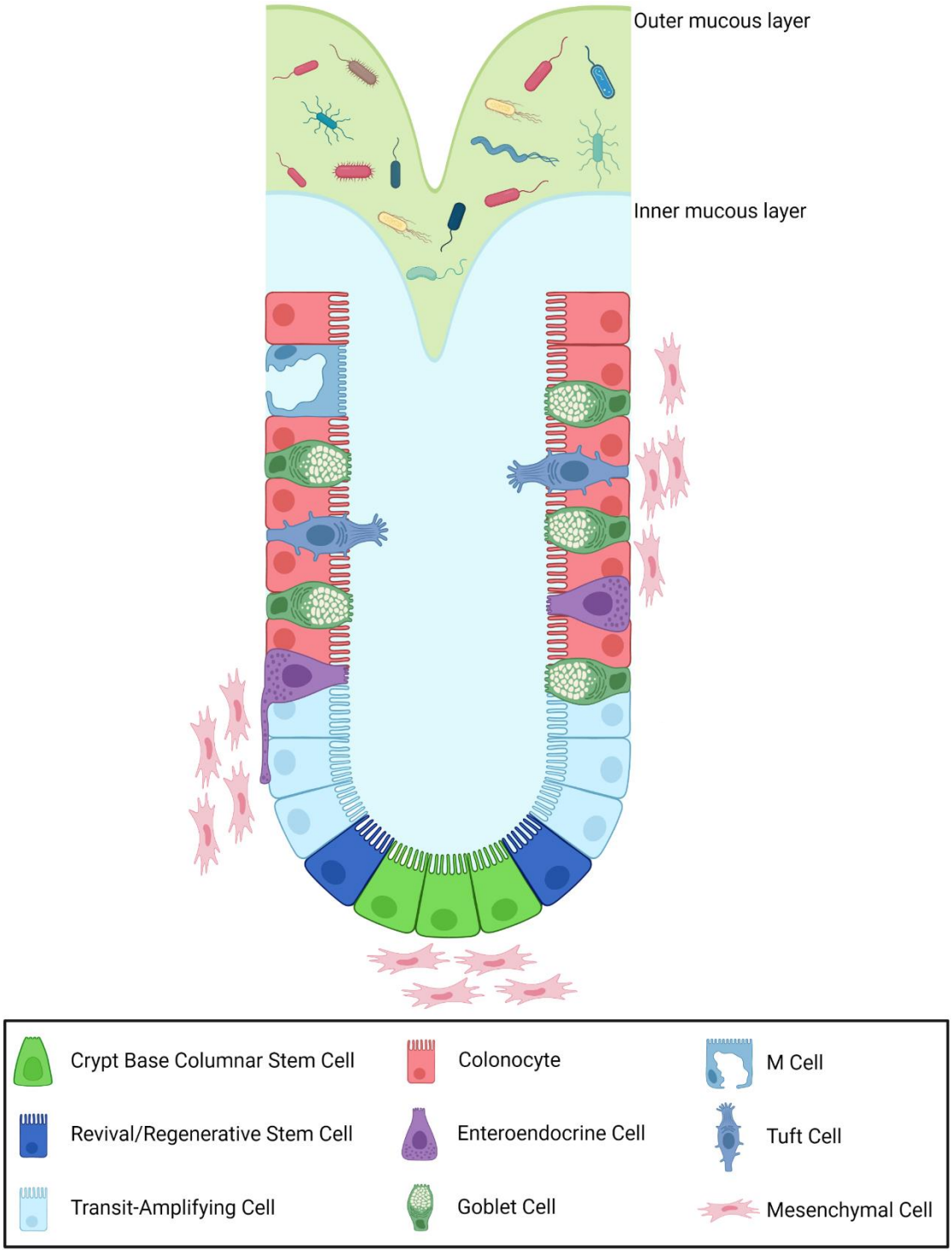


Figure 1.1. Epithelial cells lining the colonic crypts of Lieberkühn. The colon epithelium is made up of undifferentiated (intestinal stem cells) and post-mitotic differentiated cells. The differentiated cells are divided into absorptive (colonocytes) and secretory (enteroendocrine, goblet and tuft cells) lineages and M cells.

ISCs which reside at the crypt base are termed crypt base columnar (CBC) stem cells. These stem cells are regulated by the transcription factor Achaete scute-like 2 (Ascl2) and are marked

by the expression of *Leucine-rich G protein-coupled receptor 5* (*Lgr5*) and O*lfactomedin 4* (*Olfm4*)[10-13]. CBC stem cells are rapidly cycling/proliferating and can undergo both symmetric and asymmetric division[14-16]. Symmetric division generates two daughter ISCs and asymmetric division generates one active cycling daughter cell and another daughter cell to replace the parent stem cell. The rapidly cycling daughter cells are termed transit-amplifying (TA) cells. TA cells migrate towards the surface of the crypt and undergo a limited number of cell divisions before terminally differentiating into cells belonging to either the absorptive (colonocytes) or secretory (enteroendocrine, goblet and tuft cells) lineages or M cells[9].

In addition to CBC stem cells, a seminal study by Ayyaz *et al.* described a unique, damage-induced cell type which they termed revival stem cells (revSCs)[17]. These revSCs are marked by the expression of *Clusterin* (*Clu*) and are partly responsible for differentiating into the various intestinal epithelial cell types and for replacing the CBC stem cell pool during injury (see section 1.1.4 for further detail). *Clu* knockout mice exposed to a colitis (inflammation of the colon) inducing agent had shortened colons and reduced epithelial cell proliferation, crypt numbers and crypt lengths[17]. Interestingly, Yes-associated protein (Yap) a transcriptional regulator well known to play a role in intestinal epithelium regeneration, has now also been implicated in inducing revSCs and when knocked out leads to similar regenerative defects seen in *Clu* knockout mice[17,18]. Together, these findings confirm that revSCs are a distinct ISC population induced by intestinal damage in a Yap-dependent manner.

1.1.2.2. Colonocytes

Colonocytes are the most abundant cell type of the colonic epithelium and are mainly responsible for absorbing water, electrolytes and vitamins from the lumen through their apical surface and exporting them basally[6]. Microvilli, membrane protrusions supported by actin-based microfilaments, cover the luminal surface of colonocytes and aid in absorption by increasing the cell surface area[19]. These polarised columnar cells are also lined with tight junctions and therefore, together with the microvilli, contribute to the maintenance of barrier integrity[20].

In addition to their absorptive and mechanical functions, colonocytes maintain homeostasis by interacting with the microbiome. Colonocytes exhibit antimicrobial activity via the release of β-defensins, which exert microbicidal activity and regulate the adaptive immune response by attracting antigen presenting cells and memory T cells to the site of invasion[21]. The high oxygen consumption guaranteed by colonocyte metabolism further contributes to homeostasis by preserving anaerobic conditions[22]. This environment selects for obligate anaerobes, which benefit the human host by breaking down otherwise indigestible dietary fibre and producing short-chain fatty acids (SCFAs), such as butyrate[23]. SCFAs are absorbed by colonocytes and are essential for maintaining the regulatory T cell population in the mucosa and thus inhibiting intestinal inflammation[24]. Colonocytes also rely on signalling pathways activated by SCFAs to perform oxidative phosphorylation and consequently maintain a hypoxic environment[25]. A shift in homeostasis, which causes the epithelium to become oxygenated, can result in SCFA depletion and subsequent elevation of inflammatory signals, causing colonocytes to perform anaerobic glycolysis. These conditions are favourable for the growth of pathogenic facultative anaerobes and leads to dysbiosis[26]. Dysbiosis can occur as a result of antibiotic therapy, consumption of a high-fat diet and a range of human illnesses including cancer[27-32].

1.1.2.3. Enteroendocrine Cells

Enteroendocrine cells (EECs) are the primary chemosensory cell of the GI tract responsible for sensing carbohydrates, lipids and proteins in the luminal contents[33]. Despite being dispersed individually throughout the epithelium in relatively low numbers, EECs play an essential role in the endocrine/hormone producing system.

One of the features that distinguish EECs from other epithelial cell types is the existence of either large dense-core vesicles (LDCVs) or smaller synaptic-like microvesicles (SLMVs), which secrete regulatory peptide hormones in response to the luminal contents. EECs can be divided into two groups according to their location: open cells, which contain microvilli that extend into the lumen and directly sense its contents; and closed cells, which do not reach the epithelial surface and are instead regulated by the luminal contents indirectly via neural and humoral mechanisms. EECs of the colon all belong to the open group and are unique due to

the presence of both apical and basal processes[34-36]. There are multiple types of EECs, however those present in the colon are enterochromaffin (EC) cells, D cells and L cells. EC cells are the most abundant EEC type and are present along the entirety of the GI tract, D cells are relatively scarce in the colon but are also found throughout the GI tract and L cells are present at highest frequencies in the colon and increase in number from the caecum to the rectum[37].

EC cells release serotonin from vesicles found at both their apical and basal extensions, the latter of which is hypothesised to communicate with underlying neurons[38-40]. Serotonin release in the colon activates excitatory cholinergic neurones that innervate the underlying smooth muscle and cause increased gut motility and accelerated intestinal transit[41-43]. Furthermore, EC cell-derived serotonin production, induced in response to colorectal distension, leads to the secretion of electrogenic fluid and a decline in appetite[44,45].

D cells release somatostatin, which acts on somatostatin receptors to inhibit digestive endocrine and exocrine function and stimulate peristalsis and ion secretion[46,47]. Additionally, somatostatin acts on myenteric neurons to cause smooth muscle relaxation in the distal region of the colon[48].

Lastly, L cells release peptide hormones, namely peptide YY and proglucagon-derived peptides[49]. Peptide YY is involved in the anorexigenic response, where it functions to inhibit the release of orexigenic peptides in the hypothalamus and in doing so suppresses appetite[50]. Moreover, in response to unabsorbed nutrients, peptide YY is released and leads to reduced colonic transit time to allow for more effective absorption to take place. As a whole, proglucagon-derived peptides act on other EECs as well as enteric nerves to promote the proliferation of mucosal epithelial cells and stimulate insulin secretion in response to glucose in the luminal contents[51,52].

1.1.2.4. Goblet Cells

Goblet cells (GCs) are the second most abundant cell type in the colon and manage the synthesis and secretion of mucins forming the mucous layer[53]. The mucous layer maintains

barrier integrity by protecting the underlying epithelial cells from continuous mechanical stress and by physically separating these cells from luminal bacteria and potentially harmful microorganisms[54]. The mucous layer is also an important part of innate host defence due to its retention of antimicrobial peptides produced by colonocytes[55,56].

The mucous layer of the colon is made up of an inner and outer layer[57]. The inner layer is attached to the GCs and physically separates the epithelial cells from luminal bacteria. The outer layer expands into the lumen and is formed as a result of protease activity in the inner layer. Compared to the small pore sizes present in the inner layer, the expanded outer layer contains large pore sizes, which allow for bacterial penetration[57]. The mucous layer is made up of several proteins, the most abundant being the mucin Muc2[57]. Muc2 is stored in the secretory vesicles present in GCs and unfolds to form a net-like structure when secreted[58]. GCs present on the colonic surface continuously secrete their vesical contents in order to maintain the inner mucous layer whereas intracrypt GCs only do this upon stimulation by endocytosis or secretagogues (secretory inducing substances)[59,60].

Colonic GCs also play a role in the regulation of immunity by forming goblet cell-associated antigen passages (GAPs), which deliver luminal antigens to the antigen presenting cells in the underlying lamina propria[61]. GAP formation is regulated by GC responsiveness to acetylcholine (ACh) acting on muscarinic ACh receptor 4.

1.1.2.5. M Cells

Microfold (M) cells are primarily located in the follicle-associated epithelium, which covers multi-follicular lymphoid tissues termed gut-associated lymphoid tissue (GALT)[62]. Briefly, GALT is located throughout the intestine and is responsible for antigen sampling and inducing an adaptive immune response[63].

M cells play a critical role in mucosal immunity due to their ability to sample the luminal contents and relay macromolecules, antigens and pathogenic or commensal microorganisms to immune cells located at their basolateral surface[64]. M cells are able to transport whole microorganisms across the epithelium due to their limited lysosome machinery, lack of a

glycocalyx, a restructured apical membrane and deeply invaginated basolateral membrane[62]. The ability of M cells to traffic potentially pathogenic microorganisms across the epithelium is exploited by certain harmful microbes. Bacteria, including Salmonella, Yersinia and Shigella, viruses such as human immunodeficiency virus (HIV), and prions take advantage of this characteristic property of M cells to safely deliver them to the underlying tissue[65-67].

1.1.2.6. Tuft Cells

Tuft cells (TCs), also known as brush cells, are so named due to their distinctive characteristics: abundant apical vesicles which form a tubulovesicular system, a tuft of long, blunt microvilli that protrudes into the lumen, and actin, villin, and fimbrin microfilaments that extend from the tips of the microvilli[68,69].

While the exact function of TCs in the colon is less well understood, these cells are known to act as chemoreceptors and detect compounds with sweet, umami, bitter, sour and salty qualities. Upon activation, TCs express taste signal transduction proteins which allow the body to effectively respond to the luminal contents[70]. More recently, TCs have been shown to play a key role in immunity to parasites[71]. Chemosensory receptors, expressed by TCs, respond to parasitic helminth infections in the small intestine, and to a lesser extent the colon, and trigger an anti-inflammatory type 2 immune response through the release of interleukin (IL) 25[72-74]. IL25 causes the release of IL13 by innate lymphoid cells which induces TC expansion, GC hyperplasia and mucous production resulting in worm expulsion[75].

1.1.3. Signalling Pathways in the Colonic Crypts

In order to maintain the appropriate quantity and arrangement of the above described cell types within the crypt, stemness, proliferation, migration, and apoptosis along the crypt vertical axis is tightly controlled by polarised morphogen gradients generated by mesenchymal (underlying stromal cells) and epithelial cell-derived pathways present in the local microenvironment[76].

The manner in which crypt cells respond to these signals is determined by their position along the gradients. Key pathways involved in crypt organisation (Figure 1.2) which will be detailed

below include Wingless-related integration site (Wnt), Bone morphogenetic protein (Bmp), Hedgehog (Hh) and Notch signalling.

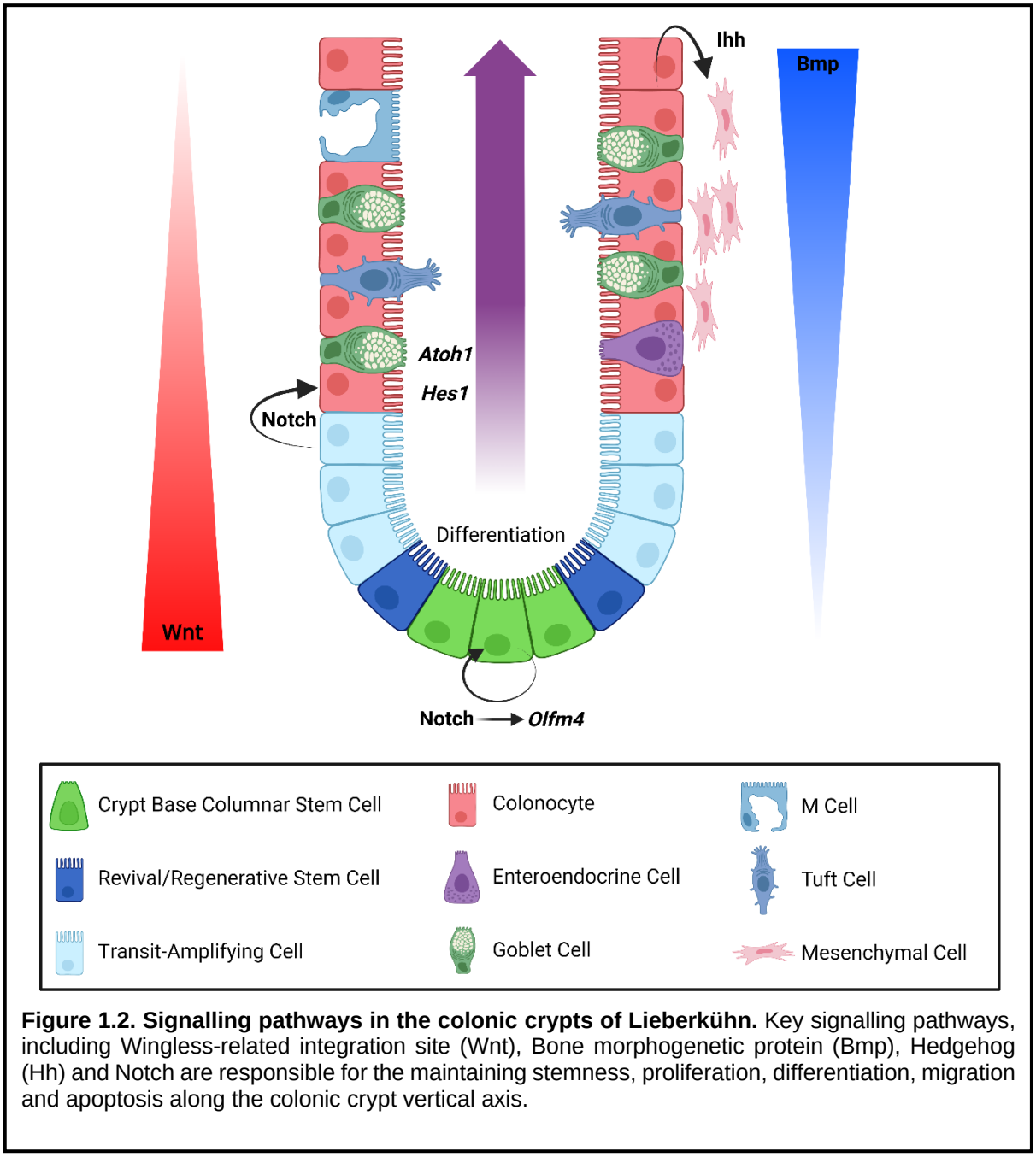


Figure 1.2. Signalling pathways in the colonic crypts of Lieberkühn. Key signalling pathways, including Wingless-related integration site (Wnt), Bone morphogenetic protein (Bmp), Hedgehog (Hh) and Notch are responsible for the maintaining stemness, proliferation, differentiation, migration and apoptosis along the colonic crypt vertical axis.

1.1.3.1. Wnt

The Wnt pathway is essential for controlling cell fate during embryonic development and continues to be a key regulator in self-renewing tissues, including the colon, during adulthood[77]. The canonical Wnt pathway is characterised by the formation of a β-catenin destruction complex made up of Glycogen synthase kinase 3 (Gsk3), Adenomatous polyposis coli (Apc), Casein kinase 1 (Ck1) and Axin. In the absence of Wnt, this destruction complex

phosphorylates cytoplasmic β-catenin and targets it for proteasomal degradation[78]. When present, Wnt binds the Frizzled receptor and Low-density lipoprotein receptor-related protein 5/6 (Lrp5/6) co-receptor and inhibits the formation of the destruction complex allowing for β-catenin stabilisation and translocation into the nucleus (Figure 1.3)[78,79]. β-catenin then associates with T-cell factor/Lymphoid enhancer-binding factor (Tcf/Lef) cofactors and induces the transcription of target genes such as *Lgr5*[78].

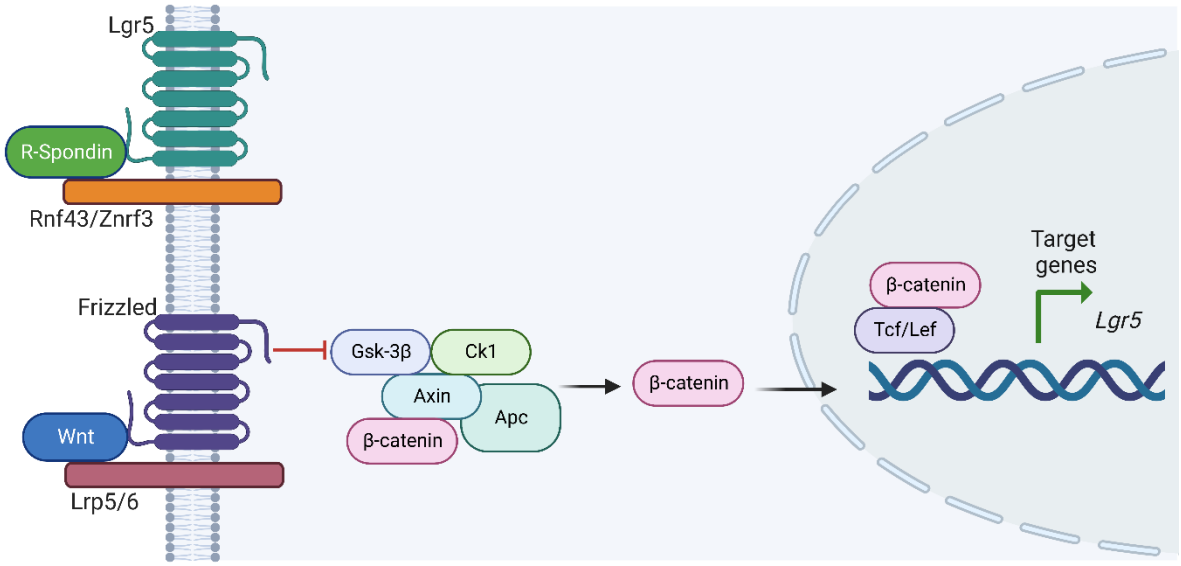


Figure 1.3. Wnt β-catenin signalling pathway. Wnt binds the Frizzled receptor and Lrp5/6 co-receptor and inhibits the formation of the β-catenin destruction complex. β-catenin is subsequently stabilised and translocates into the nucleus to associate with Tcf/Lef cofactors and induce the transcription of target genes such as *Lgr5*.

Wnt signalling can also be further enhanced by R-Spondin[80,81]. R-Spondin binds its receptor Lgr5 and inhibits the action of ubiquitin ligases Ring finger protein 43/Zinc and ring finger 3 (Rnt43/Znrf3), which usually degrade Frizzled receptors[82,83]. R-Spondin-driven Wnt signalling is highest at the colonic base, where it plays a critical role in promoting stemness by targeting CBC stem cells[10]. This key role has been confirmed by multiple studies, including those which knocked out *Lgr5* and its homolog *Lgr4* leading to the abolishment of crypt proliferation[81]. Moreover, Fevr *et al.* showed that β-catenin ablation led to the disruption of crypt structure, loss of TA cell populations and terminal differentiation of ISCs[84].

1.1.3.2. Bmp

Bmp is a part of the Transforming growth factor β (Tgfβ) superfamily of signalling proteins and results in the phosphorylation of Suppressor of mothers against decapentaplegic (Smad) proteins for signal transduction after ligand-receptor binding (Figure 1.4)[85]. Bmp receptors can also signal through non-Smad pathways such as p38, c-Jun N-terminal kinase (Jnk) and phosphatidylinositol-3-kinase (Pi3k) to regulate gene expression and several cellular functions[86].

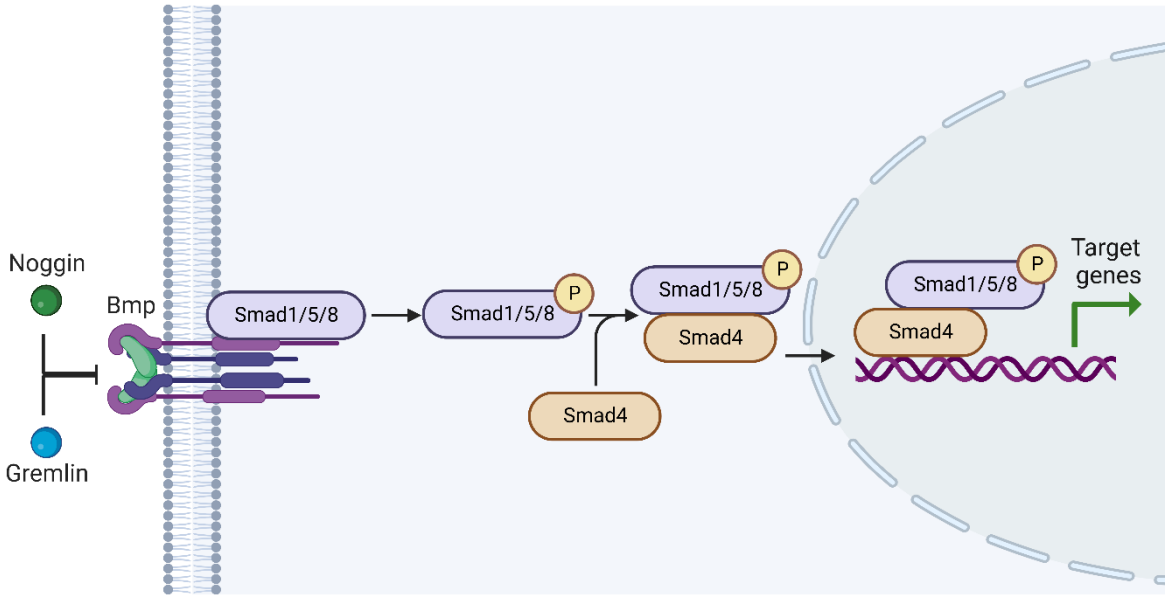


Figure 1.4. Bmp signalling pathway. Bmp signalling results in the phosphorylation of Smad proteins for signal transduction after ligand-receptor binding and induces the transcription of target genes important for promoting cell differentiation. Noggin and Gremlin act as antagonists to Bmp signalling.

While Bmp ligands are secreted by epithelial and mesenchymal intercrypt cells, Bmp antagonists, Gremlin and Noggin, are secreted by mesenchymal cells below the crypts[76,87]. As a result, a Bmp signalling gradient is formed with the highest concentration at the crypt surface. In contrast to Wnt, Bmp signalling promotes cell differentiation and has an important role in the control of stem cell self-renewal by repressing the transcription of stem cell signature genes including *Lgr5*[88,89].

1.1.3.3. Hh

During development, Hh signalling regulates the growth and specification of the gut tube mesenchyme and consequently plays an important role in maintaining homeostasis in the adult colon[90]. Briefly, Hh signalling involves the binding of Hh proteins to the patched receptors to initiate an intricate signalling cascade which results in the activation of the Glioma-associated oncogene 1 (Gli1) transcription factor and subsequent gene expression of Hh target genes (Figure 1.5)[91].

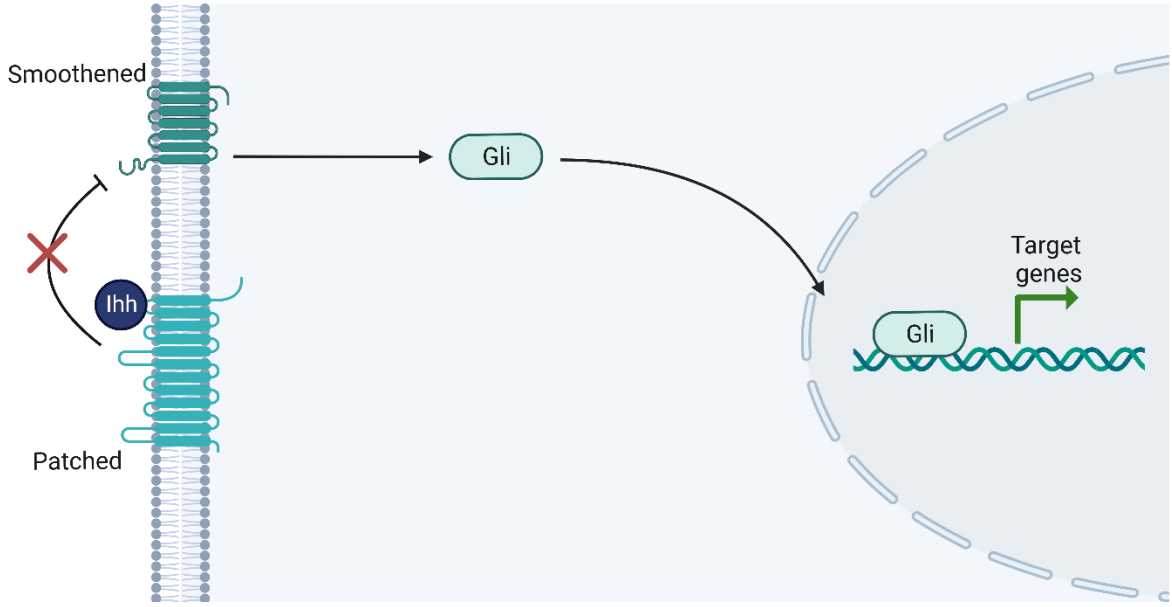


Figure 1.5. Ihh signalling pathway. Ihh signalling involves the binding of Ihh proteins to patched receptors resulting in the activation of the Gli1 transcription factor and subsequent gene expression of Hh target genes responsible for regulating the proliferation of the underlying mesenchyme and control the size and organisation of the crypt compartment.

Although there are several Hh proteins, *Indian hedgehog* (*Ihh*) is the most prevalent type expressed in the colon[92]. Ihh is secreted by mature colonocytes and acts upon mesenchymal cells in a paracrine manner to execute several tasks. Throughout development, Ihh signalling acts via a negative feedback loop to regulate the proliferation of the underlying mesenchyme and control the size and organisation of the crypt compartment[92-94]. Ihh further acts as an antagonist of Wnt signalling and restricts the expression of Wnt targets to the base of the colonic crypt, thereby regulating cell fate determination[92]. *Ihh* knock out mice exhibit reduced

ISC proliferation and differentiation as well as features typical of an aganglionic colon; a condition where certain nerves are absent from the underlying muscle layers[95].

1.1.3.4. Notch

Notch signalling is an evolutionary conserved master regulator of tissue patterning and is crucial in early cell fate determination in the colon[96]. When activated by ligands secreted by adjacent cells, Notch receptors are cleaved and release the Notch intracellular domain (NICD) from the membrane. NICD translocates into the nucleus to interact with DNA binding proteins and induce the transcription of target genes including *Hairy and enhancer of split 1* (*Hes1*, Figure 1.6)[97]. Via the regulation of Hes1, Notch signalling in CBC stem cells directly increases the expression of the key marker gene *Olfm4,* in an Atonal homolog 1 (Atoh1) independent manner, and thus is important for CBC stem cell proliferation and survival[98].

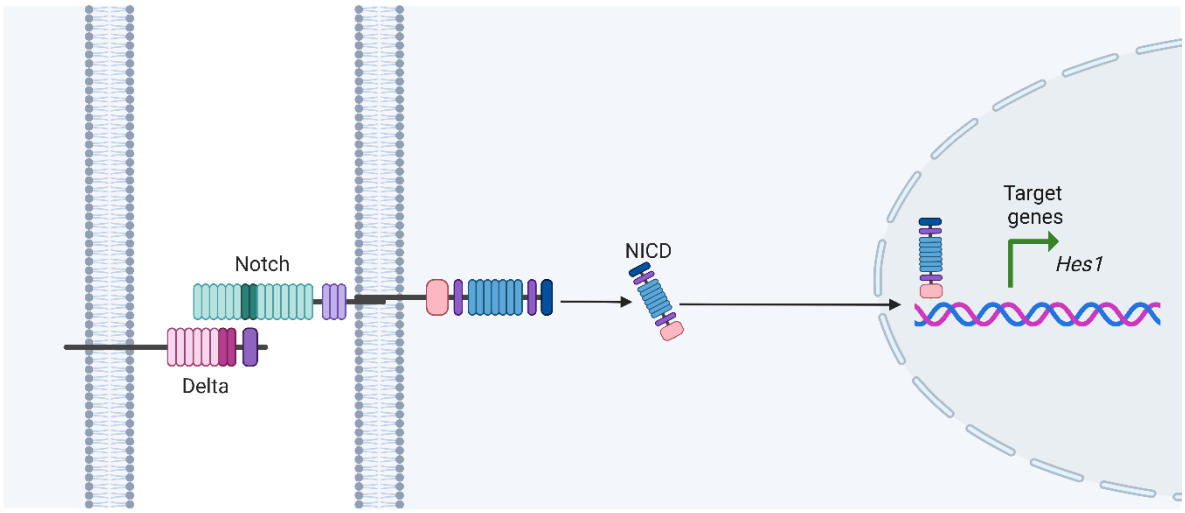


Figure 1.6. Notch signalling pathway. When activated by ligands secreted by adjacent cells, Notch receptors are cleaved and release the NICD from the membrane. NICD then translocates into the nucleus to induce the transcription of target genes including *Hes1* thereby promoting the absorptive cell fate.

Lastly, Notch signalling promotes absorptive cell fate by inhibiting secretory cell fate through Atoh1[98-100]. Notch signalling between neighbouring cells causes lateral inhibition and results in adjacent cells being driven towards different cell fates[101]. Ultimately, this leads to intermingled progenitor cells committed to either absorptive or secretory lineages.

1.1.4. Colon Epithelium Plasticity and Regeneration

In order to maintain homeostasis and ensure barrier integrity, the equilibrium between cell death and shedding of terminally differentiated cells at the crypt surface and the generation of new cells by ISCs is vital. This equilibrium is managed in a well organised spatial and temporal manner and allows for the complete renewal of the epithelium every five to seven days[102].

Under homeostatic conditions, CBC stem cells self-renew and give rise to the differentiated cells of the intestinal epithelium. These differentiated cells eventually undergo cell death and are shed into the lumen. However, in response to injury or infection the CBC stem cell population is diminished and the expression of stem cell markers and Wnt target genes, including *Lgr5*, declines[103,104]. Fortunately, the epithelium is highly plastic and is able to efficiently regenerate. This points to the existence of an additional "reserve" stem cell population. These specialised stem cells have proven difficult to identify as a unique gene signature has yet to be established, with several suggested markers also being expressed by CBC stem cells[105-107].

Recently it has been shown that in order to replenish the CBC stem cell pool, a process of dedifferentiation occurs during which the remaining partially differentiated cells acquire foetal-like stem cell characteristics and power regeneration of the CBC stem cell pool, and subsequently the full epithelium of the crypt. These foetal-like characteristics include the development of a gene signature (*Ly6a, Clu, Anxa1*) characteristic of the foetal endoderm, which is dependent on Hippo signalling and the Yap transcription factor[18,108]. The individual genes within this foetal transcriptional program, have been used to identify regenerative cells with stem cell properties – regenerative stem cells (RSCs, Figure 1.7)[17,18,108-110]. Taken together, in order for efficient regeneration to occur the adult epithelium must temporally revert to an embryonic state[108].

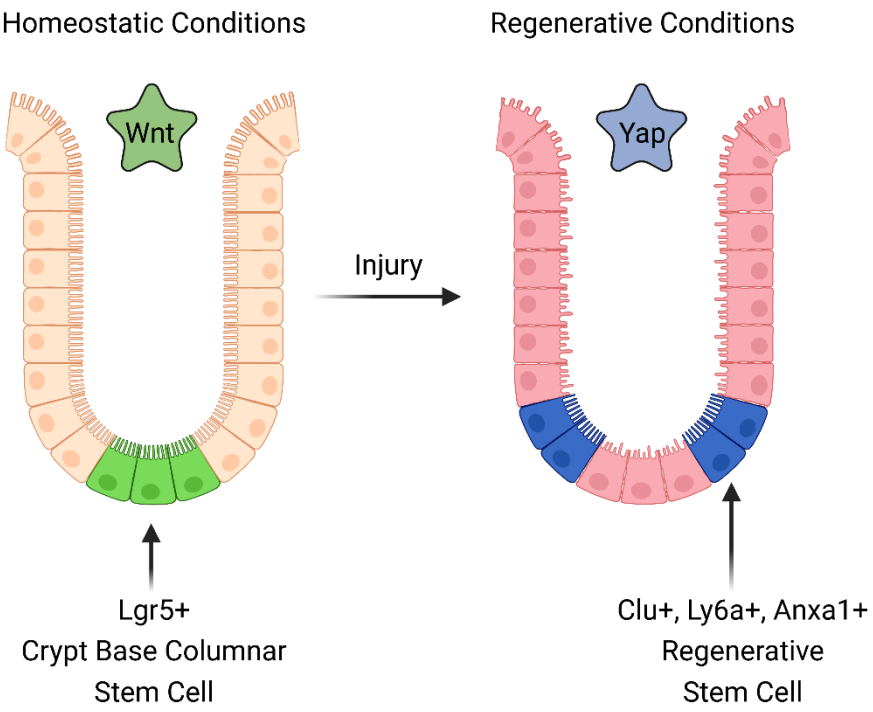


Figure 1.7. Colon epithelium plasticity and regeneration. Under homeostatic conditions, Lgr5-positive crypt base columnar stem cells self-renew and give rise to the differentiated cells of the intestinal epithelium. In response to injury, a process of dedifferentiation occurs where the remaining partially differentiated cells acquire foetal-like stem cell characteristics and power regeneration of the crypt base columnar stem cell pool. These regenerative cells are marked by the expression of *Ly6a*, *Clu*, *Anxa1* and are termed regenerative stem cells.

1.1.5. Colonic Diseases

There are several disorders of the colon, which hinder its proper functioning and can lead to significant illness. These include irritable bowel syndrome (IBS), inflammatory bowel disease (IBD), Hirschsprung disease, diverticulosis/diverticulitis and colorectal cancer (CRC, see section 1.3 for further detail)[2].

IBS is one of the most frequently diagnosed GI diseases with 10%-15% of the population suffering from it[111]. IBS is associated with severe abdominal pain and abnormal bowel habits (constipation or diarrhoea). While the exact aetiology of IBS is unknown motility, visceral sensation, brain-gut interaction and psychosocial distress can all play a role in its development.

IBD, a term mainly used to describe Chron's Disease (CD) and Ulcerative Colitis (UC), are chronic inflammatory disorders with increasing prevalence across both the developed and developing world[112]. While UC is confined to the colon, CD can occur anywhere in the GI tract,

from mouth to anus. IBD arises due a combination of genetic and environmental factors which lead to the dysfunctional activation of the mucosal immune system by the normal luminal microbiome[113]. This abnormal response occurs as a result of defects in both the barrier function of the epithelium and the mucosal immune system. This causes abdominal pain, abnormal bowel habits, rectal bleeding, fever, weight loss, fatigue and night sweats. The inherent heterogeneity characteristic of IBD makes it difficult to study and patients often suffer reduced quality of life, prolonged time to remission and relapse due to ineffective treatment options.

Hirschsprung disease is a genetic disorder diagnosed at or shortly after birth which occurs as a result of the absence of the enteric nervous system (ENS) in the distal colon[114]. This disease has significant effects on colon motility making it difficult to pass stool.

Lastly, diverticulosis is characterised by the development of pockets in the colonic mucosa[115]. These pockets form due to weaknesses in the muscular layer of the colon which occur over time as we age. Diverticulitis arises if these pockets become inflamed or infected, leading to abdominal pain and abnormal bowel habits.

The complexities associated with the above-described diseases make understanding them and identifying effective treatments particularly challenging. Consequently, physiologically accurate and relevant models are particularly needed.

1.2. Intestinal Organoids

Cell culture is a widely used technique in the study of development, disease, drug action and tissue engineering[116]. When it comes to cancer biology, most of the research is based on two-dimensional (2D) cell culture where cells are grown as a monolayer attached to a plastic surface. Unfortunately, 2D cell culture is accompanied by several limitations including forced apical-basal polarisation, abnormal cell morphology and division and the lack of cellular and extracellular environmental components[117].

2D cell culture fails particularly with regard to the study of the intestinal crypt as it lacks the cellular complexity and architecture present *in vivo*. This has led to the establishment and optimisation of three-dimensional (3D) cell culture models where cells are grown under

nonadherent conditions (either in suspension, in an extracellular matrix or on a scaffold) and are responsible for creating their own strict apical-basal polarisation[117].

1.2.1. History of The Organoid

Organoids are 3D *ex vivo* culture systems, which can be derived from either pluripotent (embryonic or induced) or organ-restricted adult stem cells[118,119]. These miniaturised organs capture the intrinsic propensity of stem cells to form a self-organised entity, which recapitulates the 3D architecture and signalling physiologically relevant to the originating tissue type[120,121].

The unique potential of the organoid was identified as early as the 1960s, where it referred to self-organised organotypic cultures[122]. Some 30 years later, 3D culture models were popularised by publications which demonstrated that a laminin-rich matrix was able to support *ex vivo* hepatocellular functions and could be used to study morphogenesis in healthy and malignant breast epithelial tissue[123-125].

Unfortunately, the inevitable genetic instability and loss of differentiation capacity made maintaining long-term *in vitro* stem cell-derived cultures demanding[121,122]. Fortunately, in 2009 Sato *et al.* reported an instrumental protocol to generate long-term 3D intestinal organoid cultures[11]. It was demonstrated that, in the presence of a defined cocktail of growth factors (Epidermal growth factor, Wnt, R-Spondin and Noggin), a single adult Lgr5-positive stem cell embedded in an extracellular matrix (ECM) is capable of giving rise to a fully differentiated cell aggregate with many of the cells discussed in section 1.1.2 arranged in a manner highly reminiscent of the *in vivo* crypt-villus architecture (Figure 1.8).

Of course, intestinal organoid culture is accompanied by certain constraints. These include the lack of consistent cellular organisation within and between experiments, limited accessibility to the apical (lumen facing) surface which is required for certain infections models, atypical physiology (crypt-villus projections outwards from the organoid) and reduced culture durations[126]. Despite these limitations, the power of the organoid has subsequently been harnessed across multiple fields, ranging from the study of human development to diseases,

including cancer, and its ability to recapitulate the 3D organisation of the crypt has made a keystone methodology for *ex vivo* study of the intestine[127-129].

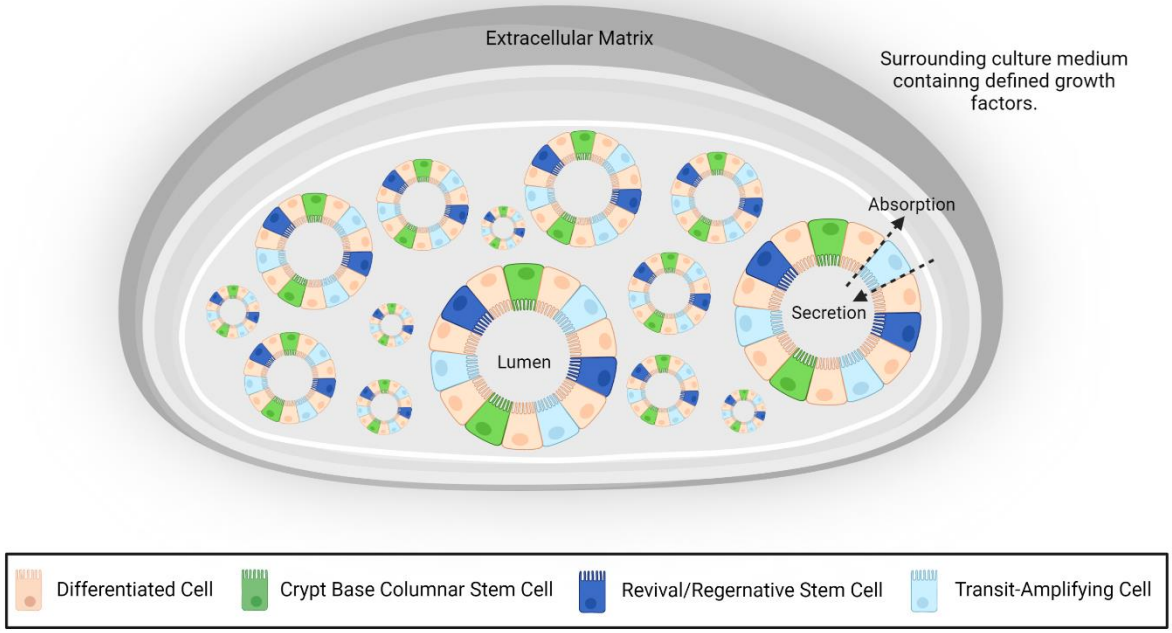


Figure 1.8. Intestinal organoid culture. In the presence of a defined growth factors, a single adult Lgr5-positive crypt base columnar stem cell embedded in an extracellular matrix is capable of giving rise to a fully differentiated cell aggregate reminiscent of the *in vivo* crypt-villus architecture.

1.2.2. Organoids as Models for the Study of Intestinal Physiology

The landmark study by Sato *et al.* has played a significant role in contributing to our current understanding of intestinal physiology. The key studies which utilised organoids to elucidate the biology of the intestine will be highlighted below.

1.2.2.1. Morphogen Signals

The tendency for cells within these "mini-intestines" to arrange in a manner resembling the *in vivo* organization within intestinal crypts has made organoids an important model for the study of processes which would otherwise be impossible to model using 2D cell cultures. These include mechanisms which control compartmentalisation, crypt folding, cell fate and cell migration[130,131].

It was demonstrated that as cells migrate from the basal surface of the crypt towards the lumen, they respond to morphogen signal gradients and readily differentiate into cells belonging to either the absorptive or secretory lineages once they reach a position in the crypt with a sufficient concentration of the appropriate morphogen[11,132]. As described above, one of the key signalling pathways controlling cell fate decisions between these linages is the Notch pathway. Organoids played a key role in the discovery of this phenomenon, as organoid cultures treated with inhibitors of the Notch pathway (γ-Secretase inhibitor dibenzazepine and Neurogenin-3) resulted in altered cell fate determination and the differentiation of stem cell progeny into those belonging to the secretory lineage[133].

Sustained *ex vivo* culture of intestinal organoids is impossible without the presence of essential morphogens in the culture medium and emphasises the critical role that they play in intestinal development and homeostasis *in vivo*. The key morphogens responsible for efficient intestinal organoid culture include Wnt, R-Spondin, Noggin and Epidermal growth factor (Egf).

Wnt signalling is responsible for regulating intestinal epithelial proliferation and stemness *in vivo*[10]. This was supported by the indefinite expansion exhibited by organoids grown in culture medium supplemented with Wnt3a, a canonical Wnt ligand, and their terminal differentiation when Wnt3a was withdrawn[134-136]. The removal of Wnt3a leads to loss of *Lgr5* expression, decreased cell proliferation and increased numbers of absorptive and secretory cell types[11]. Moreover, isolated primary intestinal epithelial cells failed to form organoids when treated with the Wnt antagonist Dickkopf 1 (Dkk1) [133].

R-Spondin binds its Lgr5 receptor and potentiates Wnt signalling by inhibiting the degradation of Wnt receptors[82,83]. When added to the medium of intestinal organoid cultures, R-Spondin increased CBC stem cell numbers and promoted organoid formation and growth suggesting an increased level of functional stem cell activity[133]. Additional evidence in support of the function of R-Spondin in sustained organoid growth was revealed when deletion of its receptors led to the inability of organoids to form[81].

Bmp signalling drives intestinal differentiation and maintains the ISC population by regulating the expression of stem cell signature genes[88,89]. Consequently, Noggin, a Bmp antagonist, is key in maintaining intestinal organoid cultures and when absent leads to the loss of *Lgr5* expression and decreased proliferation within two weeks[11].

Egf is important for epithelial cell proliferation and survival and promotes the long-term culture of intestinal organoids[137,138]. Indeed, human intestinal organoids ceased proliferation within one week of treatment with an EGF receptor (EGFR) inhibitor and those harbouring activating mutations in signalling pathways initiated by EGFR binding readily acquired EGF independence[139]. *Leucine rich repeats and immunoglobulin like domains 1* (*Lrig1*), a negative regulator of Egf, is highly expressed by ISCs and regulates the stem cell population by controlling Egf and other growth factor signalling pathways[140]. *Lrig1* knockout organoids, in which Egf signalling is disrupted, do not require the addition of Egf to the culture medium to grow efficiently thus suggesting that Egf signalling is also essential for the self-renewal of the intestinal epithelium[140,141].

As a result of the above, organoid models which aim to study cell differentiation in the intestine make use of culture medium lacking Wnt3a, R-Spondin, Noggin and Egf which all promote maintenance of a stem-like phenotype[136].

1.2.2.2. The Microbiome

Prior to the development of organoids it was not possible to accurately study the contribution of the microbiome to intestinal health and disease due to the challenges in controlling multiple external factors associated with conventional *in vitro* and *in vivo* models[142,143].

A seminal study by Kaiko *et al.* which utilised intestinal organoids, revealed that butyrate, a key microbiota-derived metabolite, inhibited the proliferation of ISCs and that differentiated colonocytes metabolised butyrate thereby protecting ISCs from this inhibitory effect[144]. Muramyl-dipeptide, another microbiota-derived metabolite, was further shown to promote intestinal organoid survival by binding to the cytosolic innate immune sensor Nucleotide

binding oligomerization domain containing 2 (Nod2) expressed by CBC stem cells and protecting against oxidative stress-mediated cell death[145]. Furthermore, the co-culture of intestinal organoids with commensal bacteria, such as *Bacteroides thetaiotaomicron* and non-pathogenic strains of *Escherichia coli*, induced mucus fucosylation and promoted a hypoxic environment respectively, emphasising the role that the microbiome has in supplying energy to other intestinal bacteria and providing a suitable environment for host-microbiome interactions[146,147].

1.2.2.3. Immunity

The ability to co-culture organoids with cells usually present in the surrounding microenvironment over extended periods has facilitated immunological research which aims to elucidate epithelial cell–immune cell interactions during intestinal homeostasis[148].

Recently, it was revealed that organoid derived ISCs can activate CD4+ T cells and induce the expression of T helper cell derived cytokines, which can in turn influence epithelial cell differentiation[149]. Intestinal organoids co-cultured with pre-activated T helper 2 cells or the associated cytokines IL4 and IL13 resulted in a decrease in ISC numbers and increased differentiation of goblet and tuft cells[73,149,150]. Similarly, co-culture with pre-activated T helper 1 or 17 cells or the associated proinflammatory cytokines Interferon (IFN) γ and IL17 respectively reduced ISC numbers and increased that of TA cells[149]. In contrast, treatment with the anti-inflammatory cytokines IL10 or IL22 or co-culture with regulatory T cells promoted the growth of intestinal organoids and increased ISC numbers[149,151]. Intestinal organoid models have also been used in studies of foetal development where it was shown that low doses of Tumour necrosis factor (TNF), produced by effector memory T cells, promoted fetal ISC proliferation whereas high doses had the opposite effect[152].

M cells, which are critical in inducing immune responses by sampling the luminal contents, have remained elusive for many years. However, the culture of intestinal organoids allowed for the identification of key ligands responsible for M cell differentiation and consequent establishment of a transcriptional signature associated with this cell type[153,154].

These organoid-generated findings reveal the key interplay between immune signalling and ISCs in maintaining the crypt architecture.

1.2.3. Organoids as Models for the Study of Intestinal Pathologies

Intestinal organoids allow for the sustainable *ex vivo* culture of both healthy and diseased tissue-derived cells. This has enabled the study of infection- and mutation-carcinogenesis, facilitated drug screening and guided the development of personalised therapy[155-160]. The role of organoid technology in understanding intestinal disease states will be detailed below.

1.2.3.1. Hereditary Diseases

Intestinal organoids have been implemented in the study of monogenic hereditary diseases, including cystic fibrosis (CF)[118]. Cystic fibrosis (CF) is the result of a range of mutations in the gene encoding the *Cystic fibrosis transmembrane conductance regulator* (*CFTR*) chloride channel, which is expressed by the epithelial cells of many organs[161]. While the impact that CF has on the epithelial cells of the lungs has been extensively studied, the impact that this disease has on the intestinal epithelial cells has remained elusive.

Dekkers *et al*. developed a forskolin-induced swelling assay to test CFTR functionality in organoids derived from rectal biopsies of CF patients carrying different *CFTR* mutations[162,163]. Forskolin activated CFTR by elevating intracellular cyclic AMP and led to fluid secretion into the lumen and swelling of healthy rectal organoids but not those from CF patients. The *ex vivo* drug responses exhibited by the rectal CF organoids positively correlated with clinical trial data and revealed that these organoids were valuable in determining which patients would benefit from certain drug treatment regimens. Consequently, the forskolin-induced swelling assay is currently being employed in patient drug screening protocols and has proven to exhibit superior predictive power than existing therapeutic strategies.

1.2.3.2. Infectious Diseases

Enteric pathogens cause significant annual morbidity and mortality. While the research surrounding these diseases has certainly progressed, many *in vitro* and *in vivo* systems which

aim to accurately model these infections are often unsuccesful[164]. Fortunately, the representative 3D model provided by intestinal organoid culture has facilitated a more realistic modelling of enteric infectious diseases, enabled the interrogation of host-pathogen relations and assisted in the exploration of therapeutic targets.

Intestinal organoids used to model rotavirus and norovirus infection were shown to be more tolerant of viral infection compared to immortalised cell cultures and supported the full life cycle of these viruses, thus allowing for the effective cultivation of previously uncultivatable pathogens[165,166]. These studies also allowed for the identification and validation of therapeutic methods to treat and prevent infection. Moreover, and in line with the recent COVID-19 pandemic, Lamers *et al.* demonstrated that human intestinal organoids were readily infected with Severe acute respiratory syndrome coronavirus 2 (SARS-CoV-2) and that the infected cells were able to efficiently produce infectious viral particles[167,168]. These findings contributed to the understanding of why infected individuals often present with GI symptoms.

In addition to viruses, intestinal organoids have also provided insight into host-bacterial pathologies, including *Clostridium difficile*, *Salmonella* and *E. coli*. The use of human colon organoids (colonoids) microinjected with cultured *C. difficile*, its related toxins or the faecal material of infected patients have confirmed and expanded on the current knowledge surrounding this bacterium and identified a druggable target, Sodium-hydrogen exchanger 3 (NHE3), which can be used to interfere with the manner in which *C. difficile* thrives in the host[169]. Furthermore, colonic crypts isolated from *C. difficile* infected mice were less efficient at forming organoids than uninfected controls, thus revealing that infection with this bacterium alters the functional capacity of colonic stem cells[170]. Live bacterial infection of organoids is also possible and co-cultures of live *Salmonella* with intestinal organoids revealed increased inflammatory cytokine expression and identified the direct effect that this bacterium has on epithelial tight junction proteins[171].

Intestinal parasitic infections can similarly be modelled using organoid systems. Infection with *Cryptosporidium parvum* resulted in the completion of the protozoans intricate life cycle as well as its' efficient propagation[172].

1.2.3.3. Inflammatory Bowel Disease and Colorectal Cancer

Unfortunately, many of the *in vitro* and *in vivo* animal models which aim to study IBD (described in section 1.1.5) and CRC do not accurately model disease progression and in the case of CRC, do not precisely recapitulate the patient's tumour. Consequently many of the therapeutics identified using these techniques have low efficacy when used in the clinic[173,174]. The establishment of physiologically relevant intestinal organoid models has vastly broadened our understanding of these inherently complicated diseases which often involve epithelial cell dysfunction[175].

Several groups, which have analysed the transcriptional signatures of organoids derived from IBD patients identified key genes as being differentially expressed between IBD and healthy control organoids[176-178]. These included genes associated with stemness (*LGR5*) which were upregulated and genes associated with differentiation (*Intestinal-type alkaline phosphatase, Villin 1, Chromogranin A* and *MUC2*) and junctional components (*Occludin*) which were downregulated. d'Aldebert *et al*. revealed that IBD-derived organoids exhibited an inflammatory phenotype, reduced size, budding capacity and tight junction protein expression, increased cell death and luminal debris and inverted polarisation[179]. This work has been supported by research using induced human UC-derived organoids. These organoids presented with the same histological and functional features of primary tissues from UC patients, including the lack of acidic mucous secretion and abnormal adherens junction patterning in the epithelium[180]. Furthermore, it was demonstrated that the inflammatory mediator *CXCL8/CXCR1* was overexpressed in the UC organoids but not healthy controls and inhibition of the CXCR1 lessened the progression of UC phenotypes.

IBD is a major risk factor for the development of CRC and over recent years research into the mechanisms behind CRC tumourigenesis which incorporate organoids has greatly increased[181]. In particular, biobanks containing CRC patient-derived organoid (PDO) cultures from both metastatic and matching normal colon have been successfully established by several groups[134,182-184]. The research on these PDOs demonstrated that they genetically and phenotypically resembled the originating healthy and tumour tissue and revealed important

correlations between drug responses and the presence of certain mutations[182]. The differences in mutational signatures exhibited between healthy and CRC PDOs is also reflected in the conditions that best support their establishment and sustained growth. Fuji *et al.* showed that certain CRC PDOs could only be derived when cultured under specific conditions, such as hypoxia or in medium lacking niche factors usually required by healthy PDOs[183]. CRC PDO biobanks have also been used for proteomic and transcriptomic analysis and have highlighted the differences in expression profiles between healthy and tumour organoids from the same patient and between patients[185].

The inherent genetic stability of healthy organoids has been combined with the powerful CRISPR–Cas9 genome editing technology to model CRC initiation and progression in PDOs. Targeted modification of the most commonly altered genes in CRC (see section 1.3.1 for further detail) in human ISCs resulted in the formation of mutant organoids which could be selected for by removing certain growth factors from the culture medium which would be essential for wild type cells in the stem cell niche[139,156]. When xenotransplanted into mice, organoids harbouring all of the common mutations were able to form tumours reminiscent of invasive carcinomas. Moreover, orthotopic transplantation of these engineered tumour organoids into mice resulted in lung and liver metastases[186-189].

Murine tumour-derived organoids have been incorporated into studies investigating the effects of cancer stem cells (CSCs) on CRC progression. Using an inducible *Lgr5* knockout model to specifically ablate stem cells, it was demonstrated that the loss of Lgr5-positive CSCs restricted primary tumour growth but did not result in tumour regression[190]. Interestingly, Lgr5-negative CSCs replenished the Lgr5-positive population which was important for the maintenance of liver metastasis. The overall findings of this study have been supported by more recent research which made use of a mouse model of CRC and identified that circulating disseminated CRC cells were Lgr5-negative and formed distant metastases where Lgr5-positive CSCs eventually reappeared[191].

One of the factors which hinder our understanding of tumour progression and the identification of additional therapeutic agents is the lack of a representative model for the tumour

microenvironment (TME)[192]. However, the co-culture of PDOs with immune and stromal cells have provided a way to realistically model the TME in CRC development and progression[193,194]. Specifically, PDOs co-cultured with immune cells and fibroblasts resulted in a T cell repertoire with clonal diversity similar to that present in the blood of patients; as such, these cultures have been used as a more accurate model to assess the effect of immune checkpoint therapies on CRC progression[193]. CRC PDOs have also been cultured with patient peripheral blood lymphocytes resulting in the generation of proliferative CD8+ T cell clones in response to the presence of PDO-derived neoantigens[194].

CRC PDOs have also proven valuable in evaluating individualised drug responses in a preclinical setting and have even shown strong correlation with treatment responses observed in patients enrolled in clinical trials[195-197]. Remarkably, in more recent studies, CRC PDOs have predicted responses to chemotherapy and chemoradiation[198,199]. Taken together, these studies emphasise the role that organoids play in accurately representing the 3D architecture of the tumour and developing personalised treatment strategies for patients with CRC.

While many disease states can be addressed using intestinal organoids, organoid interrogation of CRC provides perhaps one of the greatest opportunities to extend patients' lifespans. This is largely due to their ability to be successfully derived from both healthy and malignant tissue while retaining the intratumoural heterogeneity (ITH) unique to each patient. Furthermore, PDOs are significantly less perturbed than 2D cell lines. Taken together, PDOs more accurately represent clinical reality.

1.3. Colorectal Cancer in Detail

CRC, also referred to as colon or bowel cancer, is the third most commonly diagnosed cancer worldwide and the second leading cause of cancer mortality[200]. While CRC certainly has a genetic component, 90% of cases occur sporadically[200]. CRC incidence is highest in developed countries and thus it has been suggested that CRC risk may be associated with a lifestyle common in these countries where a lack of physical activity, a diet low in fibre, fruits and vegetables, obesity, excessive alcohol consumption and tobacco use are prevalent[200-204].

Unfortunately, CRC is a highly metastatic disease with as many as 50% of patients developing metastatic disease recurrence. While chemotherapeutic agents have shown some promise, surgical resection is still the only curative treatment[205,206]. There is a critical need in this setting to reduce time to detection, identify superior treatment strategies and ultimately increase survival time.

1.3.1. Genetics of Colorectal Cancer

CRC is a highly heterogenous disease which arises from one or more mechanisms of genetic or epigenetic dysregulation, particularly chromosomal instability (CIN), microsatellite instability (MSI) and CpG island methylator phenotype (CIMP)[207].

CIN is the most common pathway through which 65%-70% of CRC cases arise[208]. CIN occurs due to aberrant chromosomal segregation, loss of telomere viability and dysfunctional DNA-damage response machinery[209]. MSI is characterised by elevated genetic instability and is responsible for roughly 15% of CRC cases[210]. Hypermethylation caused by activating mutations in *BRAF* gives rise to CIMP. These mutations are correlated with serrated neoplasia and adenoma formation and are responsible for 15%-25% of CRC cases[211].

Based on which form of genetic/epigenetic dysregulation is present, in combination with tumour transcription profiles, CRC can be classified into four distinct consensus molecular subtypes (CMSs), which allows for efficient patient stratification and the identification of suitable therapies[212]. These subtypes are classified as: highly mutated with MSI and immune activation (CMS1), WNT and MYC activation (CMS2), metabolic dysregulations (CMS3) and stromal gene expression (CMS4)[213].

In addition to these broad dysregulation mechanisms, CRC patients often show alterations in four individual genes linked to CRC development and progression, namely *APC, Kirsten Rat Sarcoma (KRAS), SMAD4* and *Tumour Protein p53 (TP53)*. These genes and their role in CRC will be discussed next.

1.3.1.1. APC

Mutations in the *APC* gene are the most common in CRC and can either be inherited or arise sporadically[214]. Germline mutations in *APC* are associated with the development of Familial adenomatous polyposis (FAP), a colonic disorder which confers a significant risk of CRC development[215]. In contrast, mutations in *APC* are present in 50%-83% of sporadic CRC cases and are argued to be the earliest genetic alteration in the progression to sporadic CRC[214,216-218].

APC is a key regulator of the WNT signalling pathway and functions as a tumour suppressor by modulating intracellular β-Catenin levels (described in section 1.1.3.1). As a result of the truncated form of APC generated by 98% of the *APC* mutations in CRC, the β-Catenin destruction complex cannot form leading to its accumulation and subsequent translocation into the nucleus to promote the expression of WNT target genes[219,220]. Consequently, inactivating mutations in *APC* confer growth advantages to APC-deficient crypts and initiate their clonal expansion[214].

1.3.1.2. KRAS

KRAS is a proto-oncogene and essential mediator of the Mitogen-activated protein kinase (MAPK) pathway. A part of the Rat sarcoma virus (RAS) GTPase family, KRAS is activated upon ligand binding to the EGFR and regulates several processes, including cell cycle progression and cell growth, death and senescence[221,222]. Activating mutations in *KRAS* are present in 35%-45% of sporadic CRC cases and lead to the constitutive activation of downstream signalling pathways, promoting aberrant cell survival and proliferation even in the absence of EGFR ligands[220,223].

1.3.1.3. SMAD4

SMAD4 is a tumour suppressor and critical mediator of TGFβ signalling, which modulates cell proliferation, differentiation and regulation of the extracellular microenvironment[224]. The loss of *SMAD4* is considered to be a late event in CRC development and is present in 22% of late-stage cases compared to 5% in primary non-metastatic tumours[225]. SMAD4 has also been implicated as a negative prognostic marker of CRC as

mutations in *SMAD4* have been associated with clonal divergence and tumour evolution which correlate with metastasis and treatment resistance[226].

1.3.1.4. TP53

p53, which is encoded by *TP53*, is one of the most critical tumour suppressors identified and is a master regulator of the cell cycle. In response to oncogenic stress, p53 inhibits cell growth by inducing cell cycle arrest or apoptosis. In doing so, p53 functions to prevent tumour development[227]. Mutations in *TP53* have been suggested as the last genetic alteration in the progression from adenoma to invasive carcinoma and are present in 40%-50% of sporadic CRC cases[228]. The most common *TP53* mutations associated with sporadic CRC are missense mutations that lead to p53 dysfunction[228].

1.3.2. Models of Sporadic Colorectal Cancer

Sporadic CRC is thought to be initiated by a collection of benign or non-cancerous cells termed an adenomatous polyp. As a result of the accumulation of mutations, these pre-malignant polyps expand and protrude into the colon lumen and become ulcerated causing bleeding and bowel obstruction. Most adenomatous polyps will not progress into CRC, however if left undetected polyps can acquire further mutations and progress to a carcinoma. This process has been estimated to take roughly 10 years and highlights the importance of routine stool-based screening tests from the age of 50[229].

1.3.2.1. Adenoma-Carcinoma Sequence Model

As a hypothesis to describe the molecular origins of sporadic CRC, the Adenoma-Carcinoma Sequence model relies on the causative role of sequential alterations in the *APC*, *KRAS*, *SMAD4* and *TP53* genes (Figure 1.9)[230].

Specifically, the loss of *APC* induces the formation of an adenoma (premalignant precursor lesion) and successive mutations in *KRAS*, *SMAD4* and *TP53* genes promote the transformation of the adenoma into an invasive and metastatic carcinoma. This model, put forward by Vogelstein in 1988, states that mutations in these four genes are critical for the

development of CRC, and when present together, signify a worse prognosis and poorer response to therapy for CRC patients[228].

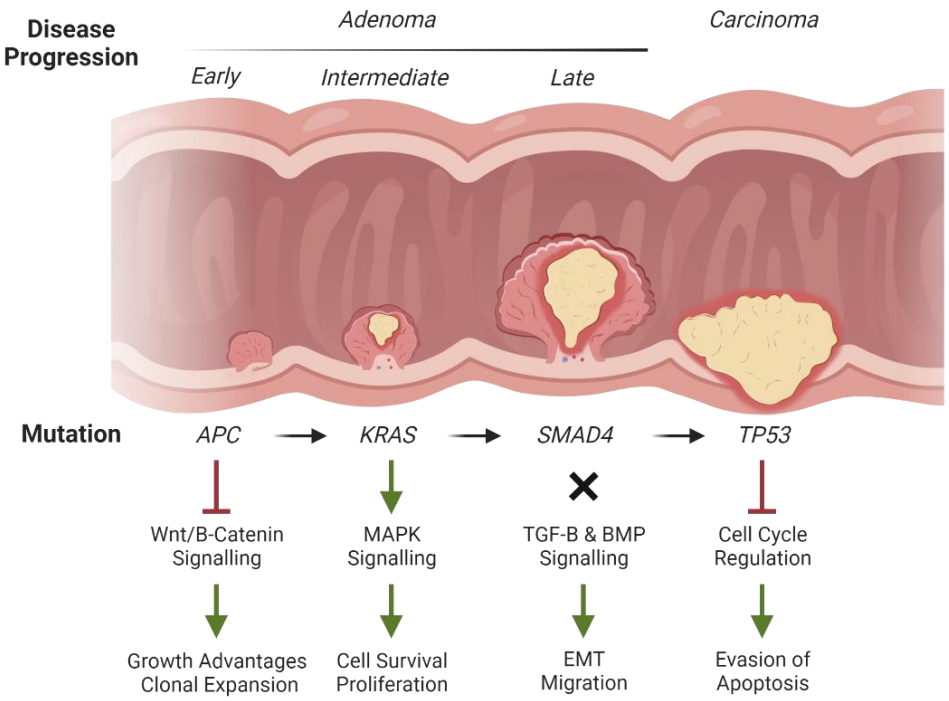


Figure 1.9. The Adenoma-Carcinoma Sequence model of colorectal cancer. Sequential alteration in the *APC*, *KRAS*, *SMAD4* and *TP53* genes promote the transformation of an adenoma into an invasive and metastatic carcinoma. This model states that mutations in these four genes are critical for the development of CRC and when present together, signify a worse prognosis and poorer response to therapy for colorectal cancer patients.

In view of this, organoid models have provided valuable insight into the correlation between mutations in *APC*, *KRAS*, *SMAD4* and *TP53* and CRC initiation and progression[231]. Using CRISPR-Cas9, oncogenic mutations in these four genes have been introduced in healthy PDOs, revealing the ability of these mutated organoids to form tumours in xenotransplant models[139,156]. This is thought to occur as a result of the mutations in these driver genes dysregulating pathways important for cell proliferation, differentiation and apoptosis, including WNT, RAS-MAPK, PI3K, TGFβ and p53, and conferring selective growth advantages on the mutated epithelium.

1.3.2.2. Big Bang Model

The development of robust sequencing technology has allowed for the more accurate characterisation of CRC tumours. Research from one of the groups which employed this technology revealed that only 6.6% of CRC tumours carried mutations in *APC*, *KRAS* and *TP53*[232]. This lack of detectable accumulation of all four mutations described in the Adenoma-Carcinoma Sequence model led to the accuracy of this model for sporadic CRC oncogenesis to be widely questioned. As an alternative hypothesis, Sottoriva *et al*. put forward the Big Bang model (Figure 1.10)[233].

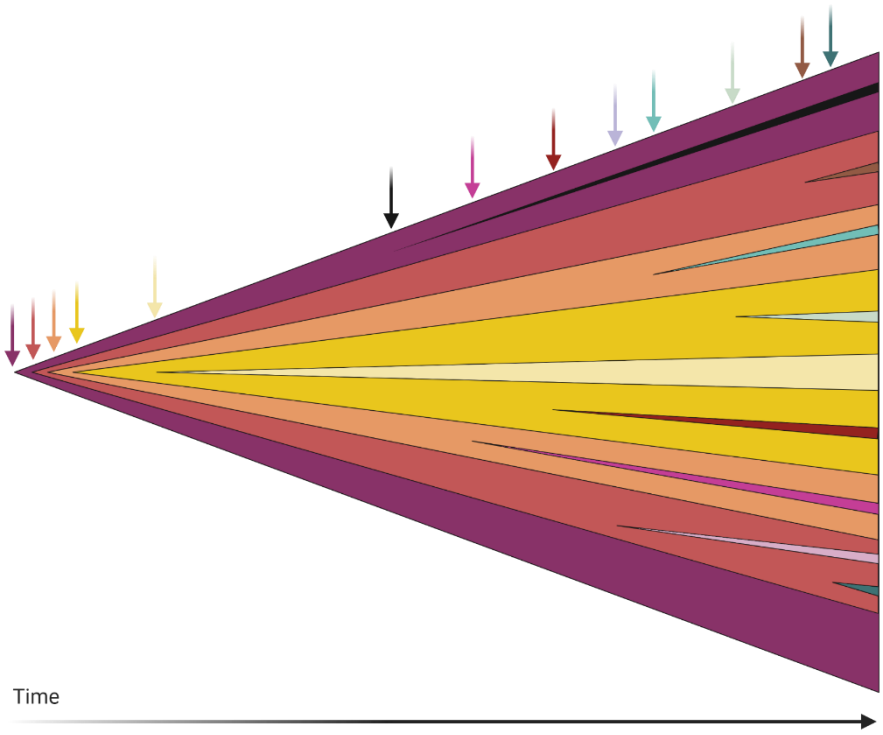


Figure 1.10. The Big Bang model of colorectal cancer. Following the initial transformation, tumours proliferate as a single expansion and produce several intermixed subclones. Public/clonal mutations are present in the first transformed cell and private/subclonal mutations occur early during tumourigenesis and persist throughout, while remaining non-dominant (coloured segments). Intratumoural heterogeneity results from the accumulation of private/subclonal mutations (arrows) that occur due to replication errors. Figure adapted form Sottoriva *et al.* 2015.

This model postulates that subsequent to an initial transforming mutation, CRC tumours proliferate as a single expansion and in doing so produce several intermixed subclones. Furthermore, during the precancerous stage, selective sweeps (clonal expansions that

significantly alter the clonal composition of the final tumour) do not occur and thus ITH and diverse subclone populations arise early during tumour development.

Evidence for the Big Bang model was provided by the genomic profiling of over 300 individual glands form several CRC tumours[233]. This revealed the lack of selective sweeps (which would be present if the accumulation of multiple specific driver genes were required), consistently high ITH and the intermixing of subclones in faraway regions indicating early malignant potential. Moreover, the origin of ITH was found to be the result of early private alterations.

1.3.3. Tumour Heterogeneity and Evolution in Colorectal Cancer

If correct, the Adenoma-Carcinoma Sequence model for sporadic CRC would result in the development of a homogenous tumour. However, sequencing analysis performed by several groups has proven that this is in fact not the case, and that CRC tumours are indeed highly heterogenous and carry mutations in a wide range of driver and non-driver genes[234-237]. Given this information, a tumour heterogeneity index, developed by Oh *et al.*, has now revealed an association between ITH and prognosis[238]. It was demonstrated that high index cases correlated with advanced CRC stages and low index cases correlated with earlier stages and longer periods of progression-free survival (PFS). This ability to stratify patients according to ITH could be crucial in disease management as ITH has been linked to resistance, recurrence and metastasis[239].

In further contrast to the Adenoma-Carcinoma Sequence model, extensive research on tumour evolution has shown that 48% of adenoma-carcinoma pairs did not acquire additional mutations during the shift from adenoma to carcinoma[240]. Additionally, a study on colorectal polyps revealed that 67% had mutations in *APC*, 15% had mutations in *KRAS* and 8% had mutations in *TP53* thus emphasising that premalignant lesions harbour the same driver mutations as CRC without exhibiting a malignant phenotype[241]. These results emphasise the existence of other mechanisms involved in the transition into a malignant phenotype.

The particularly high genetic diversity present in tumours has been suggested to occur as the result of non-Darwinian evolution, as Darwinian evolution tends to favour a decrease in genetic

diversity[242]. With regard to CRC, the Big Bang model supports this and postulates that the high ITH and varied subclone populations arise early during tumour development and that selective sweeps do not occur[233]. The tumour then undertakes neutral evolution with subsequent mutations being negatively selected against due to the spatial limitations of the rapidly growing tumour and the formation of microenvironmental niches.

It is entirely feasible that subclonal interactions within the tumour are in part responsible for the transition from a premalignant to malignant phenotype. In support of clonal competition, *Apc* mutant organoids upregulated the expression of Wnt antagonists and secreted them into the environment inducing paracrine downregulation of Wnt target genes by wild type organoids[243]. This finding was confirmed by a similar study which found that treatment with an inhibitor for Notum, a Wnt antagonist, reduced the ability of *Apc* mutant ISCs to colonise a crypt[244]. Clonal cooperation, via paracrine signalling or direct interactions, has also been demonstrated. One such study showed that cetuximab treated *KRAS* mutants cells secreted TGFα and Amphiregulin (AREG) in a paracrine manner and the resulting conditioned medium decreased the efficiency of cetuximab treatment when incubated with wild type *KRAS* cells[245]. Interestingly, although direct subclonal interactions have been studied in other cancers, it has not been observed in CRC[246].

In summary, the Adenoma-Carcinoma Sequence model has proven insufficient in fully describing the ITH observed in patient tumours, but the full mechanism behind subclone generation and the role that interactions between subclones play in CRC tumourigenesis remains to be understood.

1.4. Aims and Hypotheses

Study Aim

To determine the influence of defined colorectal cancer (CRC)-associated driver mutations on the cellular plasticity exhibited by colonic stem cells.

Study Hypothesis

Colon organoids (colonoids) harbouring CRC-associated driver mutations exhibit unique spatiotemporal and gene expression profiles resulting in intricate dynamics in cellular plasticity.

The above-stated aim will be fulfilled through the completion of the below.

Chapter 1: Aim and Hypothesis

Dysregulation in the ability of colon epithelial cells to exhibit cellular plasticity is directly linked to CRC and has been shown to promote treatment resistance and therapy evasion in models of this cancer type. The inherent plasticity demonstrated by colonic stem cells has led to the suggestion that cancer stem cells could represent the driving force behind CRC tumourigenesis. The genetic alterations harboured by these cancer stem cells associate with distinct alterations in cellular plasticity and result in the formation of a complex genotype-phenotype relationship. Research into the dynamics in cellular plasticity exhibited by stem cells harbouring CRC-associated mutations could provide significant insights into this intricate relationship and highlight the mechanisms behind CRC initiation and tumour evolution.

The first chapter of this study aims to efficiently model the genotype-phenotype relationship displayed by colon epithelial stem cells harbouring defined CRC-associated driver mutations. This will be achieved by employing an unbiased organoid phenotyping platform to perform an in-depth analysis of the unique spatiotemporal dynamics exhibited by mutant colonoids.

It is hypothesised that colonoids harbouring CRC-associated driver mutations either alone or in combination exhibit distinctive morphodynamic behaviours unique to each mutation.

Chapter 2: Aim and Hypothesis

Aberrant cellular plasticity and subsequent phenotypic heterogeneity are known to drive therapy evasion in CRC. Combining both phenotypic and transcriptomic analysis could further our understanding of CRC, highlight the molecular basis of disease and contribute to the prediction of suitable *in vivo* targets.

The second chapter of this study aims to execute single-cell RNA-sequencing (scRNA-seq) and immunofluorescence (IF) staining on mutant colonoids for integration with spatiotemporal analysis from chapter one.

It is hypothesised that the unique spatiotemporal dynamics exhibited by colonoids harbouring CRC-associated driver mutations is coupled with distinct gene expression profiles.

Chapter 3: Aim and Hypothesis

CRC is a dynamic disease characterised by significant genetic diversity, clonal expansion and clonal selection. The considerable intratumoural heterogeneity (ITH) exhibited by CRC tumours drives tumour evolution and fosters drug resistance leading to a poor prognosis for patients. To elucidate the role that CRC-associated driver mutations play in the progression from normal colonic epithelium to adenoma and carcinoma, including the mechanisms behind the development of the complex ITH seen in CRC, it is vital to understand how these diverse subclonal populations carrying different CRC driver mutations grow and interact during the early stages of tumour evolution.

The third chapter of this study aims to model ITH and changes in gene expression induced by subclonal interaction using co-cultured mutant colonoids assembled with novel cell patterning techniques.

It is hypothesised that subclonal interactions between colonoids harbouring CRC-associated driver mutations will result in changes in their behaviour and gene expression profiles compared to standard culture conditions.

2. METHODS AND MATERIALS

2.1. Colonoid Culture

2.1.1. Conditioned Medium and Genotype Specific Medium Constituents

HEK293T Rspo1-Fc cells (gifted by the laboratory of Professor Calvin Kuo, Stanford University), HEK293T Nog-Fc cells (gifted by the laboratory of Professor Gijs van den Brink[247]) and L Wnt3A (ATCC, CRL-2647™) cells were used to generate R-Spondin, Noggin and Wnt3a conditioned medium (Appendix 6.1). Wnt3a, R-Spondin and Noggin, are vital for stem cell maintenance, crypt hyperplasia and crypt expansion respectively and therefore are key components of organoid medium[134].

To produce sufficient quantities of conditioned medium, cells were initially grown to confluency in three T175 flasks containing the relevant selectable medium (Appendix 6.1) and then expanded into 15 T175 flasks containing the relevant non-selectable medium. HEK293T Rspo1-Fc cells and HEK293T Nog-Fc cells were grown in 50 ml of the relevant non-selectable medium for seven days before collection. L Wnt3A cells were grown in 25 ml of the relevant non-selectable medium for five days, followed by which the medium was collected, and 25 ml of fresh non-selectable medium added for a further two days. The two Wnt3a conditioned medium collections were then pooled together. The activity of the conditioned medium was assessed as described in Appendix 6.2.

In order to support the efficient growth of each colon organoid (colonoid) genotype, colonoids were cultured in media supplemented with or without specific growth factors (Table 2.1).

Table 2.1. Colonoid medium constituents. * Denotes those constituents excluded from *Apc*$^{min/+}$ colonoid medium, # denotes constituents included in *p53*$^{R172H/R172H}$ colonoid medium only and + denotes constituents included in the co-culture medium only.

Constituent	Company/Catalogue Number	Final Concentration
B27	ThermoFisher Scientific/17504001	1X
CHIR99021*	Sigma Aldrich/ SML1046	3 µM
EGF	ThermoFisher Scientific/PHG0311	50 ng/ml
N2	ThermoFisher Scientific/17502001	1X
Noggin	Conditioned Medium	20% of final volume
Nutlin-3#	Merck Lifesciences/ N6287	5 µM
R-Spondin*	Conditioned Medium	30% of final volume
Wnt3a*	Conditioned Medium	50% of final volume
Wnt3a+	Conditioned Medium	10% of final volume
Y-27632	StemCell Technologies/72308	10 µM

2.1.2. Colonoid Derivation

Murine colonoids were derived according to the protocols by Sato *et al.* and O' Rourke *et al.*[134,248]. The proximal colon was removed, and the tissue was cut into small (~ 5 mm) pieces and repeatedly washed with ice-cold Phosphate Buffered Saline (PBS) until the supernatant was clear. The tissue fragments were then washed once and incubated with cold 5 mM Ethylenediaminetetraacetic Acid (EDTA)-PBS (Fisher Scientific, BP2483) and placed on a roller at 4 °C for 15 minutes. To facilitate further dissociation, the tissue fragments were washed twice with ice-cold PBS and incubated in TrypLE (ThermoFisher Scientific, 12605010) at 37 °C for 30 minutes. Following a further two washes with ice-cold PBS, the sedimented tissue fragments were vigorously resuspended in ice-cold PBS and allowed to settle under gravity. The supernatant, now enriched with cells released from the tissue fragments, was then collected, passed through a 35 µm cell strainer (Corning, 352235) and centrifuged at 200 g for five minutes. The pellets were then embedded in Matrigel (Corning, 354230) and seeded in 24-well plates (~ 30 µl of Matrigel/well). The Matrigel was allowed to polymerise at 37 °C for five minutes and 500 µl of the appropriate medium (see Methods and Materials 2.1.1) was then overlaid and replaced every two days. To prevent anoikis (cell death induced upon detachment from the extracellular matrix), a Rho-associated protein kinase (Rock) inhibitor (Y-27632) and a Glycogen synthase kinase 3 (Gsk3) inhibitor (CHIR99021) were added to the medium for the first two days only. CHIR99021 has been shown to reduce the growth advantage of *Apc* mutant

cells while stimulating that of wild type cells[249]. Accordingly, to ensure that wild type cells did not dominate the culture, CHIR99021 was excluded from the *Apc*$^{min/+}$ colonoid medium.

Colonoids were maintained at 37 °C in an atmosphere of 5% CO_2 and 95% humidity. The method by which mutations were introduced into each colonoid genotype will be discussed in detail in the results section.

2.1.3. Colonoid Maintenance, Cryopreservation and Thawing

Colonoids were passaged every seven to 10 days at a ratio of 1:4. Using ice-cold PBS, the colonoids were retrieved from the Matrigel and briefly centrifuged. To aid dissociation, the pellet was vigorously resuspended in TrypLE and left at room temperature (RT) for five minutes. The colonoid fragments were then briefly centrifuged, embedded in Matrigel and seeded in a 24-well plate (~ 30 µl of Matrigel/well). The Matrigel was allowed to polymerise at 37 °C for five minutes and 500 µl of the appropriate medium was then overlaid and replaced every two days.

To cryopreserve, retrieved and pelleted colonoids were suspended in Freezing Medium Cryo-SFM (Merck, C-29912) and placed into a labelled cryovial. Cryovials were stored at -80 °C for 24 hours and then transferred to liquid Nitrogen for long-term storage.

When required, cryovials were retrieved from liquid Nitrogen and incubated in a 37 °C water bath. Once thawed, the colonoid suspension was transferred to a 1 ml eppendorf and briefly centrifuged. The pellet was then embedded in Matrigel and seeded in a 24-well plate (~ 30 µl of Matrigel/well). The Matrigel was allowed to polymerise at 37 °C for five minutes and 500 µl of the appropriate medium was then overlaid. Y-27632 and CHIR99021 were added to the medium of freshly thawed organoids for the first two days only. CHIR99021 was excluded from the *Apc*$^{min/+}$ colonoid medium.

2.2. Fluorescent Labelling of Mutant Colonoids

2.2.1. Lentivirus Production

To fluorescently label the *Apc*$^{min/+}$ and *p53*^{Null} mutant colonoids, lentiviruses expressing the mCherry and mBanana fluorescent proteins were individually produced. Phoenix cells

(ATCC, CRL-3213™, Appendix 6.1) were seeded in a 15 cm plate precoated with 0.01% poly-Lysine and allowed to reach confluency. The cells were then transfected with 15 µg of lentiviral vector (CSII pEF mCherry P2A 3F MCS and CSII pEF mBanana P2A 3F MCS), 12 µg of pCD/NL-BH*DDD (HIV-1 Gag/Pol, Tat, Rev) and 9 µg of VSV-G (Vesicular Stomatitis Virus G Glycoprotein) using Lipofectamine2000 and Opti-MEM as the transfection reagents. The following day, the medium was removed and replaced with 15 ml of fresh medium. After a further 24-hour incubation, the medium was collected, passed through a 0.45 µm filter and stored at 4 °C. 15 ml of fresh medium was then placed onto the cells for a further 24 hours, after which the medium was removed and filtered. The two collections were then pooled, aliquoted and stored at -80 °C.

2.2.2. Lentiviral Transduction of Colonoids

Apc$^{min/+}$ and *p53*^{Null} colonoids were transduced with a lentivirus expressing mCherry and mBanana fluorescent proteins respectively[250]. The medium was removed from at least six confluent wells of colonoids with the relevant genotype and the colonoids were retrieved from the Matrigel using ice-cold PBS followed by brief centrifugation. To aid dissociation, the pellet was vigorously resuspended in TrypLE and left at RT for five minutes. The colonoid fragments were then briefly centrifuged and the pellet resuspended in 5 ml of the relevant lentivirus containing-medium produced in 2.2.1. The colonoid/lentivirus suspension was added to a 6-well plate and centrifuged at 600 g at RT for one hour. The plate was then left to incubate at 37 °C for three hours. The labelled colonoids were collected, embedded in Matrigel, and seeded in a 24-well plate (~ 30 µl of Matrigel/well). The Matrigel was allowed to polymerise at 37 °C for five minutes and 500 µl of the appropriate medium was then overlaid and replaced every two days.

2.2.3. Cell Sorting

To generate a homogenous population of colonoids, which were all positive for the fluorescent protein of interest, a MA900 Multi-Application Cell Sorter (Sony Biotechnology) was used to sort colonoid-derived cells following the gating strategy depicted in Appendix 6.3. Transgenes were detected within 24 hours of lentiviral transduction.

2.3. Cre Recombinase Treatment of *p53*$^{LSL\text{-}R172H/R172H}$ and *Kras*$^{LSL\text{-}G12D/+\ CreERT2\text{-}EYFP}$ Colonoids

To derive *p53*$^{R172H/R172H}$ and *Kras*$^{G12D/+}$ colonoids, *p53*$^{LSL\text{-}R172H/R172H}$ (*p53*^{Null}) mBanana and *Kras*$^{LSL\text{-}G12D/+\ CreERT2\text{-}EYFP}$ colonoids were treated with a *Cre Recombinase* expressing Adenovirus (Vector Biolabs, 1045). To achieve this, colonoids were retrieved from the Matrigel using ice-cold PBS, centrifuged at 200 g for five minutes and incubated in TrypLE for 5 minutes at RT. The cell suspension was then passed through a 35 µm cell strainer, centrifuged at 200 g for five minutes and resuspended in serum free media. Cells were treated with a multiplicity of infection (MOI) of 50 for 3 hours in serum free medium. Following incubation, the cell/virus suspension was collected and centrifuged at 200 g for five minutes. The pellet was then embedded in Matrigel and seeded in 24-well plates (~ 30 µl of Matrigel/well). The Matrigel was allowed to polymerise at 37 °C for five minutes and 500 µl of the relevant medium was then overlaid and replaced every two days. The genotype of the colonoids was regularly checked (see Methods and Materials 2.4) and the above process repeated until the relevant mutation was fully expressed.

2.4. Polymerase Chain Reaction Confirming Colonoid Genotypes

To confirm that the colonoid genotypes were as expected, Polymerase Chain Reaction (PCR) was performed (Appendix 6.4). The DNA was extracted from the colonoids using the Zymo Research Quick-DNA Miniprep Plus Kit (D4068) and the quantity and quality of the extracted DNA was determined using a Nanodrop (ThermoFisher Scientific, ND-ONE-W). The components in Appendix 6.4 (Table 6.1 and 6.2) were combined and PCR was performed on a ProFlex PCR System (ThermoFisher Scientific) using the conditions specified in Appendix 6.4 (Table 6.3).

2.5. Organoid Formation Assay

2.5.1. Single Culture Conditions

An organoid formation assay (OFA) was performed in order to analyse the differences in the ability of each of the mutant colonoid genotypes to form an organoid from a single cell[251]. Mutant colonoids were retrieved from the Matrigel using ice-cold PBS, centrifuged at 200 g for

five minutes and incubated in TrypLE at RT for five minutes. The cell suspension was then passed through a 35 µm cell strainer and the filtered cell suspensions counted using an automated cell counter (Bio-Rad, TC20). 1000 single cells/genotype were embedded in Matrigel and seeded in a 24-well plate (4 wells/per genotype). The Matrigel was allowed to polymerise at 37 °C for five minutes and 500 µl of the appropriate medium was then overlaid and replaced every two days. Newly formed colonoids were manually counted on day three, five and seven.

2.5.2. Co-Culture Medium Validation

An OFA was similarly performed to analyse the differences in the ability of each of the colonoid genotypes to form an organoid from a single cell when grown alone in the co-culture medium. The colonoids were retrieved from the Matrigel using ice-cold PBS, centrifuged at 200 g for five minutes and incubated in TrypLE at RT for five minutes. The cell suspension was then passed through a 35 µm cell strainer and the filtered cell suspensions counted using an automated cell counter. 1000 single cells/genotype were embedded in Matrigel and seeded in a 24-well plate (4 wells/per genotype). The Matrigel was allowed to polymerise at 37 °C for five minutes and 500 µl of the co-culture medium was then overlaid and replaced every two days. Newly formed colonoids were manually counted on day three, five and seven.

2.5.3. Co-Culture Conditions

An OFA was performed to analyse the differences in the ability of each of the colonoid genotypes to form an organoid from a single cell when grown together in co-culture. The colonoids were retrieved from the Matrigel using ice-cold PBS, centrifuged at 200 g for five minutes and incubated in TrypLE at RT for five minutes. The cell suspension was then passed through a 35 µm cell strainer and the filtered cell suspensions counted using an automated cell counter. 1000 single cells/genotype were pooled together (either $Apc^{min/+}$ mCherry, $Kras^{G12D/+}$:$p53^{Null}$ EYFP and $p53^{Null}$ mBanana or $Apc^{min/+}$ mCherry, $Kras^{G12D/+}$:$p53^{Null}$ EYFP and $p53^{R172H/R172H}$ mBanana colonoids) and embedded in Matrigel and seeded in a 24-well plate (4 wells/per genotype). The Matrigel was allowed to polymerise at 37 °C for five minutes and 500 µl of the co-culture medium was then overlaid and replaced every two days. Newly formed

colonoids were imaged on a Zeiss 710MP confocal microscope, using the 5X objective, and manually counted on day three, five and seven.

2.6. Time-Lapse Microscopy for Shape, Appearance and Motion Analysis

2.6.1. Time-Lapse Confocal Microscopy

In order to analyse the spatiotemporal dynamics of the mutant colonoids, *Apc*$^{min/+}$ mCherry, *Kras*$^{G12D/+}$ EYFP, *Kras*$^{G12D/+}$*:p53*^{Null} EYFP, *p53*^{Null} mBanana and *p53*$^{R172H/R172H}$ mBanana colonoids were individually seeded in a 384-well plate and grown for 72 hours before being imaged on a Zeiss 710MP confocal microscope using the 10X objective. During the course of the time-lapse experiment, a z-stack was performed every two hours for 117 hours at each of the chosen positions.

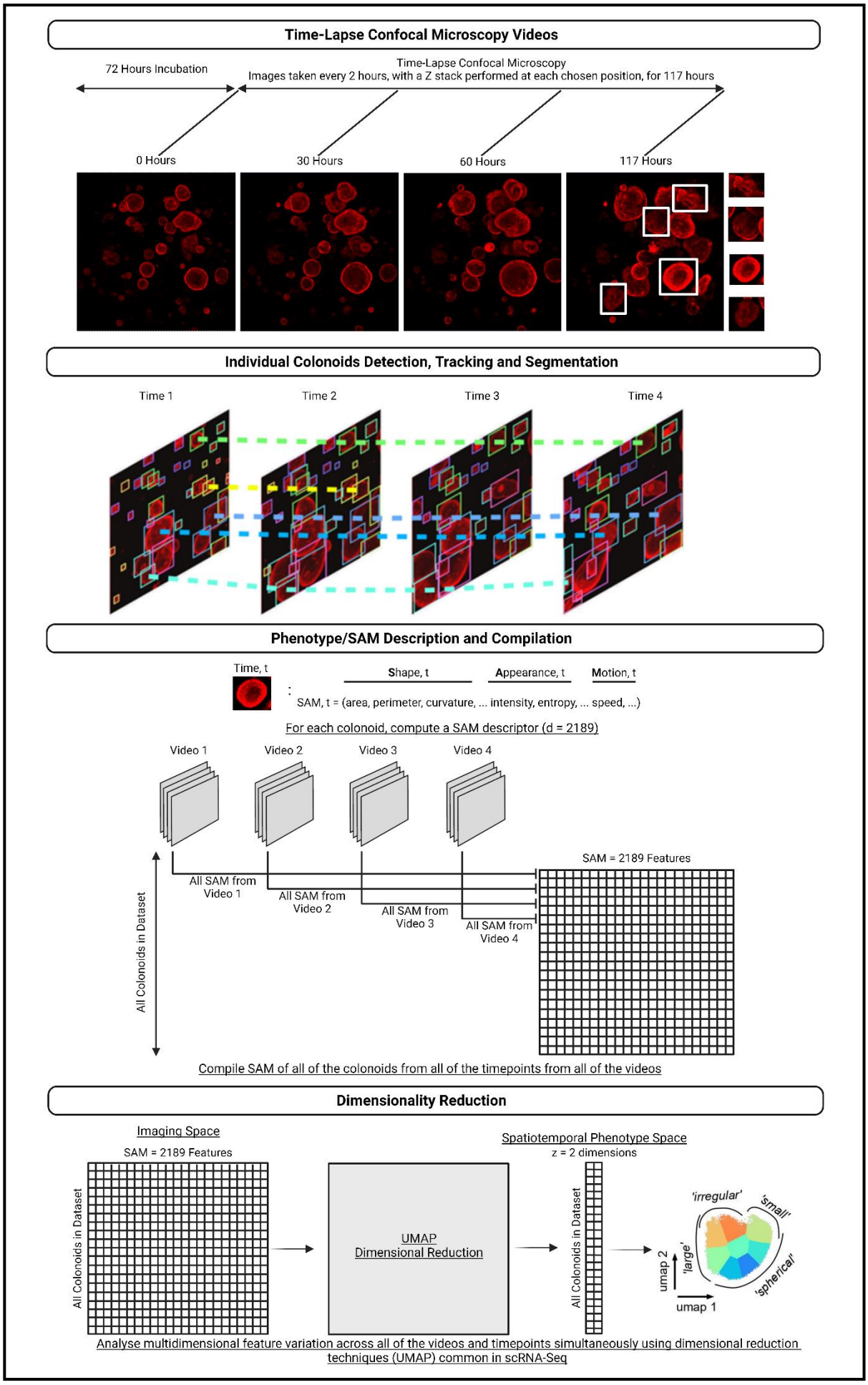
2.6.2. Time-Lapse Phase Contrast Microscopy

To analyse the spatiotemporal dynamics of the wild type colonoids and further validate that of the mutant fluorescent colonoids observed using time-lapse confocal microscopy, colonoids were individually seeded in a 96-well plate and grown for 72 hours before being imaged on a Nikon TE-2000e microscope using the 4X objective. During the course of the time-lapse experiment, a z-stack was performed every two hours for 117 hours at each of the chosen positions.

2.6.3 Shape, Appearance and Motion Analysis

Shape, Appearance and Motion (SAM) is a computational algorithm developed by Dr Felix Zhou. An overview of the workflow can be seen in Figure 2.1.

Briefly, once the time-lapse confocal and phase contrast microscopy videos were acquired, the individual colonoids were detected, tracked and segmented at each timepoint across the time course of each video. Each colonoid was then assigned a SAM descriptor by the algorithm, which is made up of 2189 features and encapsulates three fundamental conceptual properties: shape (S), object-level features such as area and perimeter; appearance (A), sub-object-level features such as image intensity; and motion (M), the movement of the object at time *t* in relation to the time before (*t-1*) and time after (*t+1*), such as speed statistics.


Time-Lapse Confocal Microscopy Videos
72 Hours Incubation
Time-Lapse Confocal Microscopy
Images taken every 2 hours, with a Z stack performed at each chosen position, for 117 hours
0 Hours
30 Hours
60 Hours
117 Hours
Individual Colonoids Detection, Tracking and Segmentation
Time 1
Time 2
Time 3
Time 4
Phenotype/SAM Description and Compilation
Time, t
Shape, t
Appearance, t
Motion, t
SAM, t = (area, perimeter, curvature, ... intensity, entropy, ... speed, ...)
For each colonoid, compute a SAM descriptor (d = 2189)
Video 1
Video 2
Video 3
Video 4
SAM = 2189 Features
All SAM from Video 1
All SAM from Video 2
All SAM from Video 3
All SAM from Video 4
All Colonoids in Dataset
Compile SAM of all of the colonoids from all of the timepoints from all of the videos
Dimensionality Reduction
Imaging Space
SAM = 2189 Features
All Colonoids in Dataset
UMAP
Dimensional Reduction
Spatiotemporal Phenotype Space
z = 2 dimensions
All Colonoids in Dataset
'irregular'
'small'
'large'
'spherical'
umap 2
umap 1
Analyse multidimensional feature variation across all of the videos and timepoints simultaneously using dimensional reduction techniques (UMAP) common in scRNA-Seq

Two allow for easier visualisation, these features were compiled across all timepoints from all videos and subjected to dimensionality reduction.

2.7. Reseeding 2D Eccentric *Apc*$^{min/+}$ mCherry Colonoids

To determine whether the morphologically distinct 2D eccentric *Apc*$^{min/+}$ mCherry colonoids retained their ability to form 3D organoids, the colonoids were cultured under normal conditions and monitored until the majority had flattened. To keep the few remaining 3D colonoids mostly intact, a 1 ml pipette tip with the end cut off and ice-cold PBS were used to retrieve the 3D cystic and 2D eccentric *Apc*$^{min/+}$ cells from the Matrigel. The suspension was centrifuged at 200 g for five minutes, the PBS removed and the remaining intact 3D colonoids were carefully removed from the top of the pellet. The pellet was then embedded in Matrigel and seeded in a 24-well plate (~ 30 µl of Matrigel/well). The Matrigel was allowed to polymerise at 37 °C for five minutes and 500 µl of the appropriate medium was then overlaid and replaced every two days. Cultures were monitored and imaged on a Zeiss 710MP confocal microscope using the 5X objective.

2.8. Single-Cell RNA Sequencing

2.8.1. Sample Processing

Single-cell RNA-sequencing (scRNA-seq) was performed on wild type and mutant fluorescent colonoids to determine the differences in their transcription profiles. Colonoids were individually seeded in a 384-well plate and cultured for seven days before processing. On day seven, the colonoids were retrieved from the Matrigel using ice-cold PBS, centrifuged at 300 g for five minutes and incubated in TrypLE at RT for 15 minutes. The dissociated organoids were then passed through a 35 µm cell strainer and the flow through centrifuged at 300 g for five minutes. The pellet was resuspended in 1 ml Cell Recovery Solution (Sigma Aldrich, DLW354253) and incubated for two hours at 4 °C under constant rotation. Samples were then centrifuged at 300 g for five minutes, the pellet resuspended in 1 ml 0.04% bovine serum albumin (BSA in PBS) and once again centrifuged at 300 g for five minutes. The pellet was then resuspended in 100 µl 0.04% BSA and dissociated organoids were passed through a 35 µm cell strainer. Filtered cell suspensions were then counted using an automated cell

counter, diluted to a concentration of 1 million total cells / ml in 0.04% BSA and kept on ice until encapsulation.

2.8.2. Library Preparation

scRNA-seq was conducted using a 5' scRNA-seq gene expression workflow (Chromium Single Cell Immune Profiling, Solution v1.1, 10x Genomics). Subsequent to the encapsulation of cells using the Chromium Controller, manufacturer's instructions were followed to perform GEM-RT, cDNA amplification and final library construction. The size profile and concentration of final libraries were determined using the Agilent 2100 Bioanalyzer (High Sensitivity DNA Kit, Agilent, 5067-4626) and Qubit (BR DNA Assay, ThermoFisher, Q32853) respectively. Sequencing of final libraries was achieved on the Illumina NextSeq 550 following 10x Genomics recommendations (26 cycles read 1, 8 cycles i7 index, 98 cycles read 2, targeting a minimum depth of 20,000 reads/cell).

2.8.3. Data Analysis

Pre-processing of scRNA-seq data was conducted using Cell Ranger (version 3.1.0). Briefly, FASTQ files were demultiplexed from raw BCL format using cellranger mkfastq. A custom Cell Ranger reference was then prepared (cellranger mkref) using a concatenation of the default Cell Ranger mouse genome sequence and annotation files (mm10-2020-A: GENCODE vM23/Ensembl 98) and custom sequence and annotation files for the fluorescent markers used in this study. Alignment to this custom reference, identification of true cells, and tabulation of Unique Molecular Identifier (UMI) counts for each sample was performed using cellranger count. The UMI counts for each sample were then combined into a single matrix using cellranger aggr without normalization.

Initial downstream processing was conducted using Seurat (v3.9.9.9038). As an initial filter for low-quality cells, cellular barcodes with less than 2000 genes detected or more than 10% mitochondrial reads were removed. Normalization, variance-stabilizing transformation (VST), and scaling were conducted on the remaining cells using Seurat's implementation of sctransform (v0.3.2.9002), and the scaled VST counts for the 3000 most variable features were extracted from the Seurat object (scale.data slot). Principal Component Analysis (PCA) was

performed on these scaled variance-stabilized counts, followed by Uniform Manifold Approximation and Projection (UMAP, umap-learn v0.5.0) for final dimensionality reduction. Clusters were identified using the FindClusters method within Seurat (Louvain algorithm). Marker genes were identified for each cluster/genotype using FindAllMarkers with a Wilcoxon signed-rank test performed for statistical analysis.

Gene Set Enrichment Analysis (GSEA) was performed using the fgsea package. The Yap signature used was previously published by Gregorieff *et al.* 2015[18].

2.9. Immunofluorescence Staining

To validate the scRNA-seq findings, immunofluorescence (IF) staining was performed on the wild type and mutant fluorescent colonoids. The colonoids were individually seeded in a 96-well plate and cultured for seven days before being processed for imaging. On day seven, the medium was removed and the colonoids were briefly washed with PBS. Colonoids were then fixed for 20 minutes in cold 4% paraformaldehyde (PFA, ThermoFisher Scientific, 28906) on a rocker. After fixation, colonoids were blocked in 10% donkey serum, 1% BSA and 0.5% Triton X-100 in PBS for one hour. Colonoids were incubated in primary antibody (Appendix 6.6) diluted in background reducing antibody diluent (Agilent Dako/S3022) at 4 °C overnight on a rocker. The colonoids were then washed in PBS (five x 10 minutes) and incubated in the appropriate secondary antibody (Appendix 6.6) diluted in antibody diluent (Agilent Dako/S0809) for two hours in the dark. Finally, samples were washed in PBS (five x 10 minutes) and mounted using 100 µl of Prolong GoldTM Antifade mountant (ThermoFisher Scientific, P36930) diluted 1:1 in PBS. Samples were imaged on a Zeiss 710MP confocal microscope using the 5X, 10X and 20X objectives.

2.10. Mixed Colonoids

To model the interaction between mutant colonoids when forced to grow in proximity under spatial control, a novel co-culture methodology, termed “mixed colonoids”, was developed (Figure 2.2).

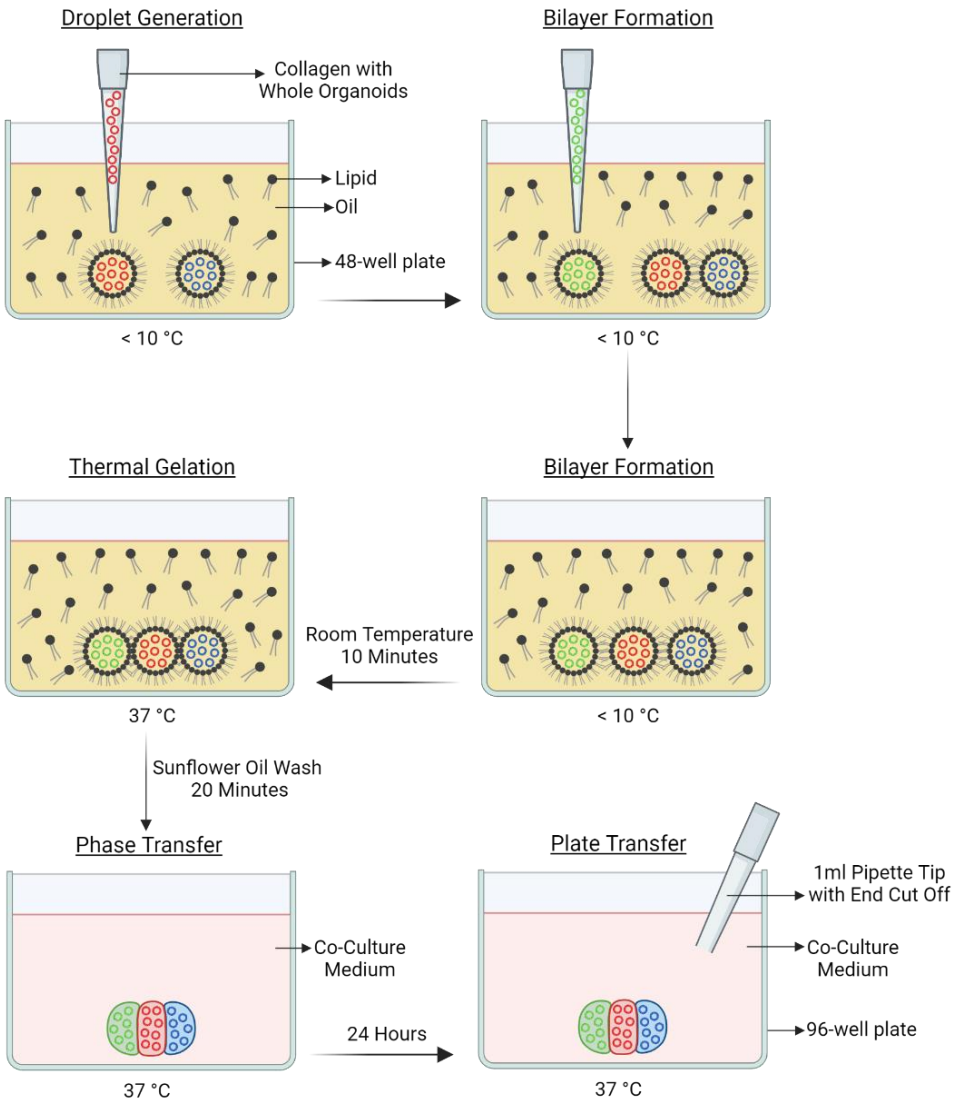


Figure 2.2. Mixed colonoid generation. Undigested mutant colonoids were resuspended in 50 µl of collagen only or collagen containing 1 x 10^6 colon-derived fibroblasts per ml and plated in 1 µl droplets into an oil/lipid bath kept on ice (< 10 °C) in a 48-well plate. Once each genotype (either *Apc*$^{min/+}$ mCherry, *Kras*$^{G12D/+}$*:p53*^{Null} EYFP and *p53*^{Null} mBanana or *Apc*$^{min/+}$ mCherry, *Kras*$^{G12D/+}$*:p53*^{Null} EYFP and *p53*$^{R172H/R172H}$ mBanana colonoids) had been plated per well, the culture was left at room temperature for 10 minutes to allow for thermal gelation and then incubated at 37 °C for a further 20 minutes. The oil/lipid bath was then carefully removed and replaced with sunflower oil. The sunflower oil was then removed and replaced with 400 µl of co-culture medium. Newly formed mixed colonoids were transferred to a 96-well plate 24 hours after plating and overlaid with 200 µl of co-culture medium, which was replaced every two days. Adapted from figure by Dr Linna Zhou.

Mixed colonoids were generated using a modified version of the previously reported lipid-bilayer-supported printing technique[252-254]. To keep the 3D colonoids mostly intact, a 1 ml pipette tip with the end cut off and ice-cold PBS were used to retrieve the colonoids from the Matrigel. Each mutant genotype (1 confluent well) was then briefly centrifuged and resuspended in collagen (Appendix 6.7) only or collagen containing 1 x 10^6 colon-derived

fibroblasts per ml. Resuspended colonoids were individually plated at close proximity into an ice-cold oil/lipid bath (Appendix 6.7) which enabled lipid bilayer formation between droplets and when removed resulted in droplet fusion to form a unified material. Once each genotype had been plated per well, the culture was left at RT to allow for thermal gelation and then incubated at 37 °C. The oil/lipid bath was then carefully removed and replaced with sunflower oil to remove excess oil/lipid. The sunflower oil was then replaced with co-culture medium. Newly formed mixed colonoids were transferred to a 96-well plate 24 hours after plating (using a 1 ml pipette tip with the end cut off) and overlaid with co-culture medium, which was replaced every two days. Mixed colonoids were regularly imaged on a Zeiss 710MP confocal microscope using the 5X objective.

2.11. Ethics

All animal work was approved by local ethical review and licensed by the UK Home Office (PPL 30/3451). Animals were bred and housed in individually ventilated cages at the Wellcome Trust Centre for Human Genetics, Oxford. Unless otherwise stated, 6-10-week-old C57BL/6 mice were used in all experiments.

3. RESULTS

3.1. Colonoids Harbouring Colorectal Cancer-Associated Driver Mutations Display Complex Spatiotemporal Dynamics

3.1.1. Introduction

Cellular plasticity is the capability of cells to alter their phenotype in response to cues in the surrounding milieu[255]. This characteristic is essential in numerous biological processes, such as development, homeostasis and repair, which require cells to readily adapt, acquire new properties and change fate. Indeed, the colon is a prime example of the important role of cellular plasticity in homeostasis; its epithelial lining is extremely dynamic and exhibits high degrees of cellular plasticity, with cells constantly undergoing proliferation, differentiation, migration and apoptosis[256].

Aberrant cellular plasticity is directly linked to diseases, including colorectal cancer (CRC), and has been shown to promote treatment resistance and therapy evasion in models of this cancer type[190,257-259]. Notably, the inherent plasticity demonstrated by stem cells has led to the suggestion that cancer stem cells (CSCs) could represent the driving force behind CRC tumourigenesis[260]. The genetic alterations harboured by these CSCs associate with distinct alterations in cellular plasticity and result in the formation of a complex genotype-phenotype relationship. Consequently, research into the dynamics in cellular plasticity exhibited by stem cells harbouring CRC-associated mutations could provide significant insights into this intricate relationship and highlight the mechanisms behind CRC initiation and tumour evolution.

The identification of Lgr5 as a functional marker of crypt base columnar (CBC) stem cells involved in normal crypt maintenance has driven research into whether an analogous Lgr5-positive CSC population may play a role in aberrant cellular plasticity during CRC development[10]. Previous work in mouse models of CRC employed xenotransplantation and lineage tracing techniques to identify a distinct population of Lgr5-positive cells capable of tumour initiation and differentiation into the malignant equivalent of each of the normal epithelial cell subtypes highlighted in the main introduction[261,262]. Despite this ability of Lgr5-

positive CSCs to generate the cell subtypes found in tumours, de Sousa e Melo *et al.* demonstrated that Lgr5-positive CSCs were not required for tumour maintenance, with genetic ablation of Lgr5-positive cells in orthotopically grafted CRC-derived organoids showing minimal effect on tumour growth[190]. Instead tumours were maintained by Lgr5-negative progenitor cells, which replenished the CSC pool and allowed for prompt tumour re-growth upon treatment cessation. This suggests that more differentiated tumour cells exhibit the plasticity evident in normal colon crypts and are able to offset the loss of CSCs. Further evidence for the plasticity demonstrated by CRC CSCs has been provided in a more recent study, which identified Lgr5-negative cells as the cell of origin of metastasis[191]. The plasticity of the stem cell pool allowed Lgr5-negative cells to regenerate the Lgr5-positive population at sites of new metastases and were able to successfully form CRC organoids *ex vivo*. This shows the phenotypic flexibility particularly of the Lgr5-negative CSC population in CRC, and the key roles that plasticity can play in CRC development and metastasis.

The underlying genetic changes enabling the high plasticity seen in CSCs and other populations in CRC is not yet well understood. However, the findings from the above-mentioned studies suggest that colon organoids (colonoids) could offer an ideal system to study the intricate genotype-phenotype relationship associated with defined genetic perturbations and dysregulated cellular plasticity as organoid research has been used as an accurate model to study the architecture and functionality of colonic stem cell populations. The precise modelling of this relationship could further our understanding of the molecular drivers of CRC and lead to the development of improved personalised therapeutics. Unfortunately, the high-throughput study of complex and evolving malignant organoid phenotypes and their dependence on genetic and environmental features is currently limited by the lack of effective analytical tools which can provide high-content phenotyping of organoids in a quantitative and spatiotemporal manner.

Current organoid phenotyping techniques mainly involve high-content imaging which applies automated microscopy and multiparameter algorithms to visualise and quantify numerous phenotypic alterations displayed by an organoid population[263]. This technology has been

employed by several groups and has certainly enabled successful multidimensional phenotyping, however the quantitative analysis associated with this technology is accompanied by various constraints. These include the dependence on fluorescent biomarker features and custom microscopy to specifically isolate and image single organoids or cells[264,265]. Furthermore, current computational pipelines associated with this method only focus on measuring pre-specified individual phenotypic or karyotypic traits but cannot measure previously unknown features which may be biologically relevant[266-271]. Taken together, these constraints hinder the accessibility of these analytical tools as they may not prove effective in research which aims to study overall phenotypic alterations in an unbiased manner. A recent publication by Freckmann *et al*. developed an analysis pipeline termed "Traject3d", which utilised label-free multi-day time-lapse imaging to identify heterogeneous states in 3D organoid culture and determine how these states culminate in unique phenotypes over time[272]. While insightful, the Traject3d incorporates existing software to extract very few features and does not consider regional features.

An unbiased organoid phenotyping platform, which extracts multiple local and regional features, has the potential to delineate the intricate cellular plasticity dynamics, which would otherwise be overlooked using common *in vitro* assays, associated with defined CRC mutations and contribute to our understanding of this complex disease.

Mutations in the well characterised CRC-associated genes *Apc*, *Kras* and *p53* are known inducers of cellular plasticity in 2D differentiated cell cultures[273-277]. Therefore, we hypothesise that colonoids carrying mutations in these genes either alone or in combination would exhibit distinctive morphodynamic behaviours. Through the use of more accurate and physiologically relevant models, the phenotypic features exhibited by these mutant colonoids have the potential to provide new insights into the complex genotype-phenotype relationship associated with dysregulated cellular plasticity in CRC.

3.1.2. Chapter Aim

Efficiently model the genotype-phenotype relationship displayed by colon epithelial stem cells harbouring defined CRC-associated driver mutations.

The aim of this chapter is to quantitatively examine the influence that three key genes associated with sporadic CRC (*Apc*, *Kras* and *p53)* have on the cellular plasticity displayed by colonic stem cells. This will be achieved by detecting subtle spatiotemporal changes in colonoid culture and will serve as the basis for the development of a new method for high-content organoid phenotyping.

The CRC-associated mutations focused on in this study were Apc^{min}, $Kras^{G12D}$ and $p53^{R172H}$ and will be briefly outlined below.

The *multiple intestinal neoplasia* (*min*) mutation is introduced into the murine *Apc* gene through treatment with a highly potent mutagen named ethylnitrosourea (ENU)[278,279]. The *min* mutation encodes a stop codon at codon 850 resulting in the premature truncation and inactivation of the Apc polypeptide. Consequently, the Wnt signalling pathway is constitutively activated leading to the stabilization of β-catenin and its translocation to the nucleus. Accordingly, processes which control cell adhesion and motility, cell cycle regulation, apoptosis and signal transduction become dysregulated[280]. Colonic crypts which carry the *min* mutation acquire proliferative abnormalities leading to the development of colon cancer in $Apc^{min/+}$ mice. As a result the $Apc^{min/+}$ model has been integrated into several studies which aim to investigate CRC tumourigenesis.

The $Kras^{G12D}$ mutation occurs due a point mutation at exon 2 of the *Kras* allele. This results in a single nucleotide change and an amino acid substitution of the glycine (G) at position 12 with an aspartic acid (D)[281]. $Kras^{G12D}$ mice carry a Lox-Stop-Lox (LSL) sequence followed by the *G12D* point mutation and when bred with a strain expressing *Cre recombinase*, Cre recombination deletes the LSL cassette and allows the expression of the mutant Kras protein. The constitutive activation of the Kras protein continually stimulates downstream signalling pathways, including cell proliferation and survival, thereby leading to tumorigenesis. The *G12D*

mutation is the most common *KRAS* mutation associated with CRC and often confers a significant resistance to several therapeutics and a poor prognosis for patients[281,282].

p53^{R172H} mice are generated using a conditional knock out model akin to that used to generate *Kras*^{G12D} mice[283]. The *p53*^{R172H} mutation arises due to a point mutation at exon 5 of the *Tp53* allele resulting in a single nucleotide change and an amino acid substitution of the arginine (R) at position 172 with a histidine (H)[284]. The murine *R172H* mutation corresponds to the highly prevalent human *R175H* mutation and similarly results in the dysregulation of cell proliferation, apoptosis and senescence processes[228]. CRC tumours developed by *p53*^{R172H} mice accurately recapitulate human CRC and thus provide an attractive model for the study of CRC tumourigenesis.

3.1.3. Generating Fluorescent Colonoids Harbouring Colorectal Cancer-Associated Driver Mutations

In order to execute the in-depth analysis of the spatiotemporal dynamics exhibited by colonoids harbouring the above-described CRC-associated driver mutations, wild type and mutant colonoids were made from the proximal colon of C57BL/6 mice (Figure 3.1). Tissue processing was conducted to isolate the stem cell containing intestinal crypts, and crypt cells were then cultured under the appropriate conditions relevant to each genotype (described in section 2.1.2) until colonoids had successfully formed.

Once the mutant colonoids had been derived it was important to establish a method by which each genotype could be easily and accurately distinguished from each other in downstream analyses. To this end, *Apc*$^{min/+}$ and *p53*$^{LSL\text{-}R172H/R172H}$ (*p53*^{Null}) colonoids were transduced with a lentivirus expressing mCherry and mBanana respectively and single cell sorted to obtain a homogenous fluorescent population. *p53*^{Null} mBanana and *Kras*$^{LSL\text{-}G12D/+\ CreERT2\text{-}EYFP}$ colonoids were treated with an adenovirus expressing *Cre recombinase* to obtain *p53*$^{R172H/R172H}$ mBanana and *Kras*$^{G12D/+}$ EYFP colonoids respectively. *Kras*$^{LSL\text{-}G12D/+\ CreERT2\text{-}EYFP}$*:p53*^{Null} mice were treated with tamoxifen *in vivo*, in order to express the *G12D* mutation, and consequently the mutant colonoids were EYFP-positive. Wild type colonoids were left without transduction of a fluorescent vector (Figure 3.1).

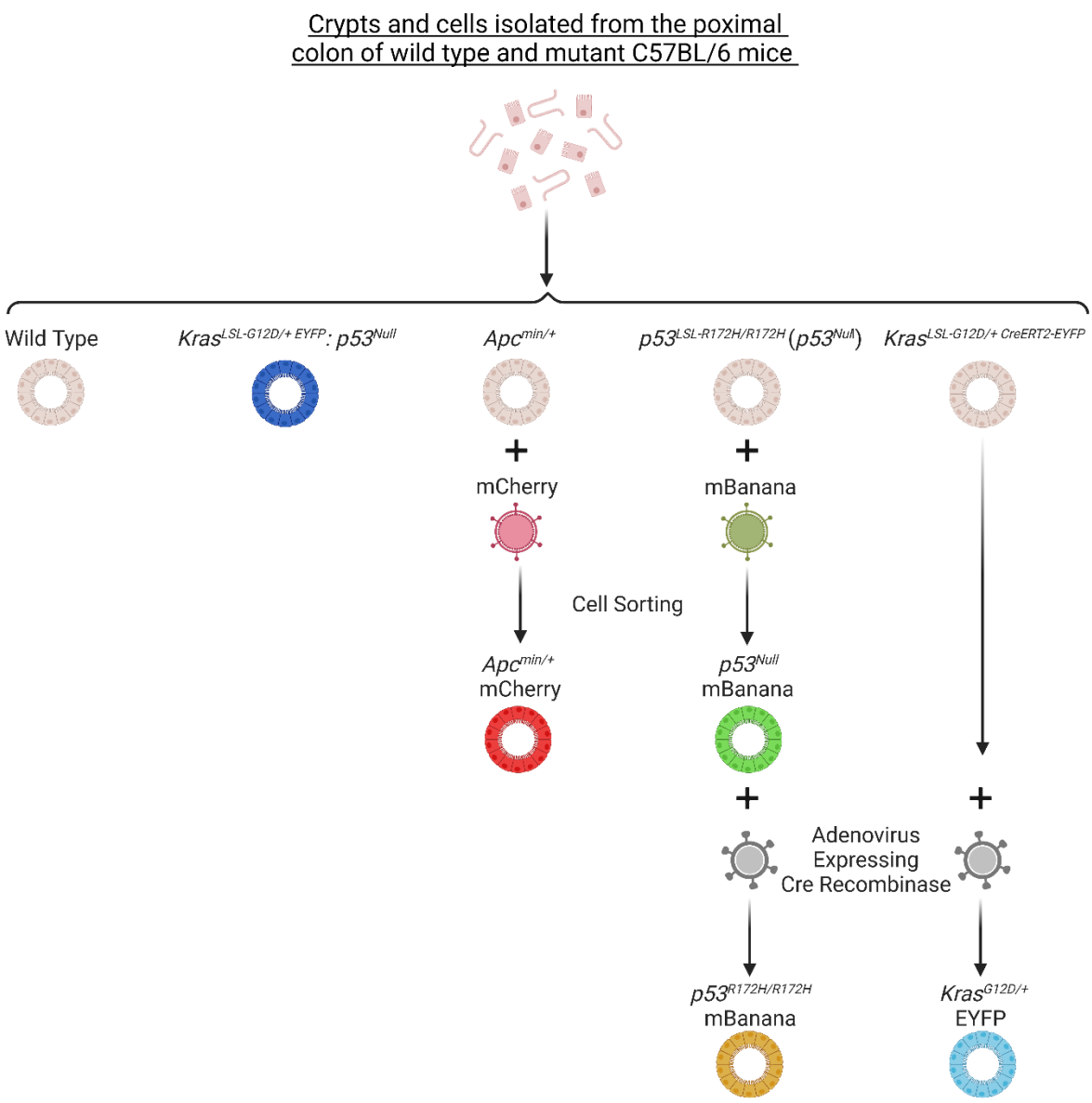


Figure 3.1. Derivation of wild type and fluorescent mutant colonoids. The proximal colon of wild type and mutant C57BL/6 mice was removed and processed. Isolated crypts and crypt cells were then cultured under the appropriate conditions until colonoids had formed. *Apc*$^{min/+}$ and *p53*$^{LSL-R172H/R172H}$ (*p53*^{Null}) colonoids were transduced with a lentivirus expressing mCherry and mBanana respectively and sorted to obtain a homogenous fluorescent population. *p53*^{Null} mBanana and *Kras*$^{LSL-G12D/+\ CreERT2-EYFP}$ colonoids were treated with an adenovirus expressing *Cre recombinase* to obtain *p53*$^{R172H/R172H}$ mBanana and *Kras*$^{G12D/+}$ EYFP colonoids respectively. *Kras*$^{G12D/+}$*:p53*^{Null} colonoids were made EYFP positive *in vivo* following tamoxifen treatment. Wild type colonoids were left untreated.

Next, PCR was performed to determine whether the resulting colonoids were indeed of the anticipated genotype (Figure 3.2).

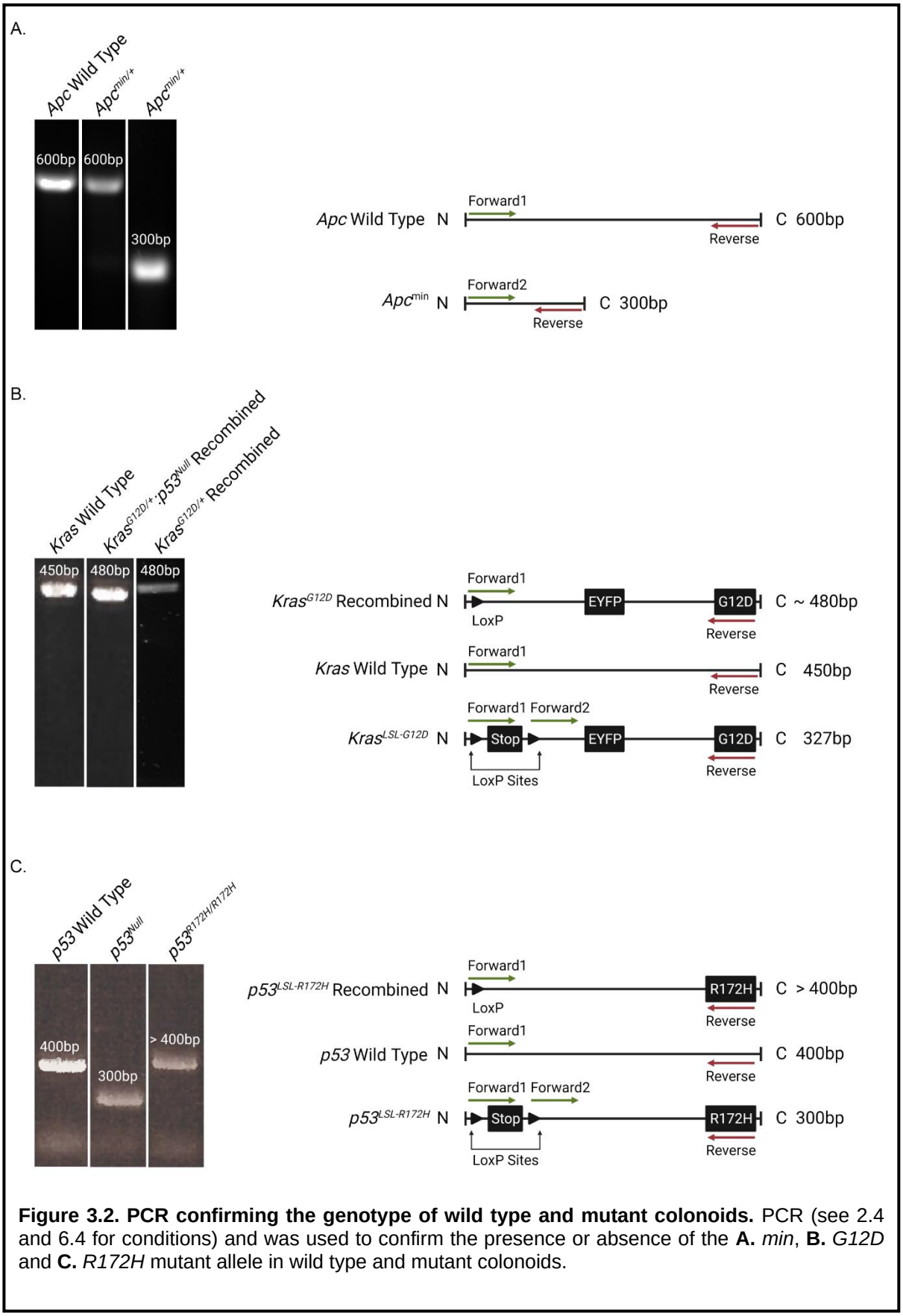


Figure 3.2. PCR confirming the genotype of wild type and mutant colonoids. PCR (see 2.4 and 6.4 for conditions) and was used to confirm the presence or absence of the **A.** *min*, **B.** *G12D* and **C.** *R172H* mutant allele in wild type and mutant colonoids.

Apc$^{min/+}$ colonoids had a band present at 600 bp (Figure 3.2. A, middle lane) and 300 bp (Figure 3.2. A, right lane), which corresponded to the wild type *Apc* and truncated mutant *min* alleles respectively and thus confirmed their heterozygosity. It is important to note that due to the fact that heterozygous *Apc*$^{min/+}$ colonoids were derived (owing to mouse availability), drift to bi-allelic population *Apc* loss is possible[249]. Moreover, the PCR genotyping strategy which was used in Figure 3.2 did not include the possibility of identifying contaminating populations. In the future, *Apc*$^{min/+}$ colonoids should be subject to further PCR analysis to determine the stability of the genotype over time and should include a restriction enzyme digest to test for contaminating populations.

Recombined *Kras*$^{G12D/+}$*:p53*^{Null} (Figure 3.2. B, middle lane) and recombined *Kras*$^{G12D/+}$ (Figure 3.2. B, right lane) colonoids had a band present at ~ 480 bp, corresponding to the recombined *G12D* allele. This band size is similar to the wild type *Kras* allele size of 450 bp and therefore confocal microscopy was later used to confirm that the stop codon had indeed been removed resulting in the expression of EYFP.

The untreated *p53*$^{LSL\text{-}R172H/R172H}$ colonoids had a band present at ~ 300 bp confirming that the stop codon had not been removed and that the colonoids were therefore *p53*^{Null} (Figure 3.2. C, middle lane). Recombined *p53*$^{LSL\text{-}R172H/R172H}$ colonoids had a band present at > 400 bp confirming that the stop codon had indeed been removed and that the *R172H* mutation was therefore being expressed (Figure 3.2. C, right lane).

Finally, wild type colonoids were confirmed to indeed be wild type for *Apc*, *Kras* and *p53* (Figure 3.2. A-C first lanes).

The wild type and fluorescent mutant colonoids were then viewed using brightfield and confocal microscopy respectively in order to ensure that the colonoids displayed the characteristic cystic shape associated with 3D intestinal organoid culture. Furthermore, confocal microscopy was used to ensure that the mutant colonoids were expressing the correct fluorescent protein which would be used to distinguish them from one another in downstream analyses (Figure 3.3).

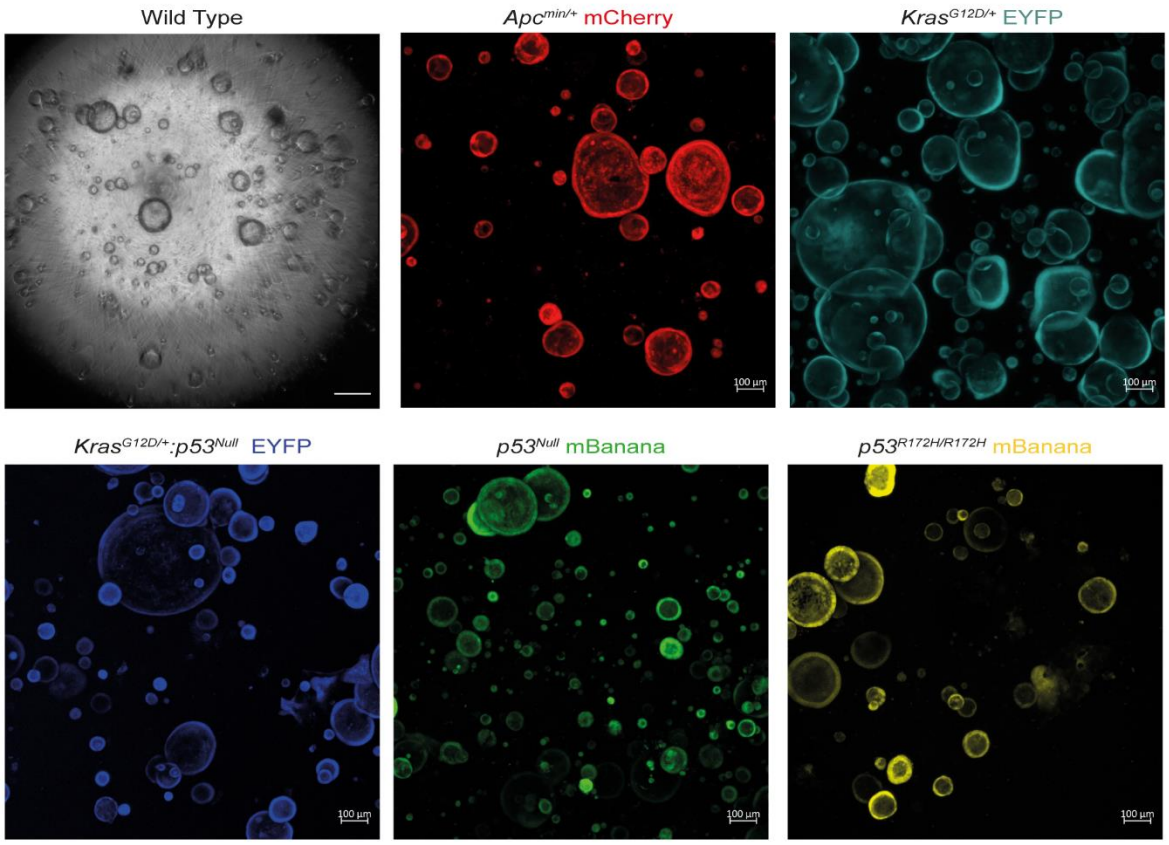


Figure 3.3. Confirmation of colonoid phenotype and fluorescent protein expression. Wild type and mutant colonoids were viewed 72 hours after passaging using brightfield and confocal microscopy to ensure they exhibited the appropriate 3D cystic shape. A Nikon TE-2000e microscope was used to view nonfluorescent wild type colonoids using the 4X objective. A Zeiss 710MP confocal microscope was used to view mutant colonoids and ensure the expression of the correct fluorescent protein using the 10X objective. Scale bars represent 100 µm. Fluorescent colonoids have been falsely coloured to allow for both EYFP and mBanana positive genotypes to be visually distinguished from one another.

Wild type and mutant colonoids were visualised 72 hours after plating and were all observed to adopt the 3D cystic appearance anticipated of intestinal organoid culture. *Apc*$^{min/+}$ colonoids were mCherry positive, *Kras*$^{G12D/+}$ and *Kras*$^{G12D/+}$*:p53*^{Null} colonoids were EYFP positive and *p53*^{Null} and *p53*$^{R172H/R172H}$ colonoids were mBanana positive. Wild type colonoids were left untreated and therefore did not express a fluorescent protein.

In this study, a range of techniques (endogenous tamoxifen treatment and lentiviral and adenoviral exposure) have been employed to fluorescently label the different mutant colonoid genotypes. Consequently, this may have generated confounding variables which would need controlling for. Future studies should either control for these variables or employ the same

technique to fluorescently label all of the mutant colonoid genotypes. This will further ensure that the results are accurate and reliable.

3.1.4. Mutant Colonoids Display Differences in Organoid Forming Ability

Prior to the in-depth spatiotemporal analysis, it was first determined whether the mutant colonoids presented with any efficiently quantifiable behavioural differences. Accordingly, an organoid formation assay (OFA) was performed (Figure 3.4).

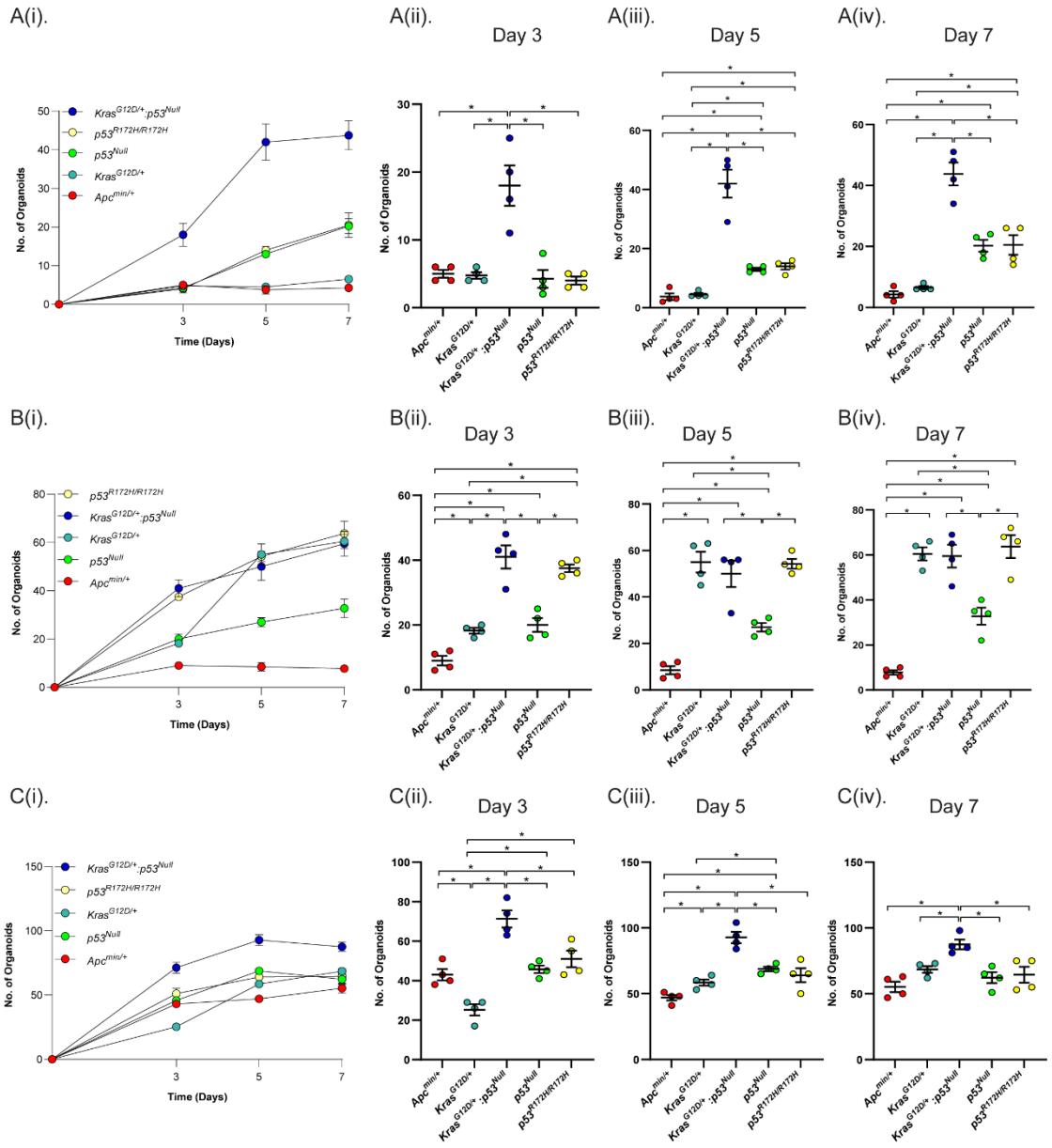


Figure 3.4. Mutant colonoids display differences in organoid forming ability. A(i)-Ci(). An organoid formation assay was performed to determine the ability of mutant colonoids to form an organoid from a single cell. 1000 single cells per genotype were plated in a 24-well plate in a flat matrigel bed and counted at **A(ii)-C(ii).** Day 3, **A(iii)-C(iii).** Day 5 and **A(iv)-C(iv).** Day 7. **A-C.** Shows the data from three independent experiments each performed in quadruplicate and analysed separately. The data were analysed using GraphPad Prism 9 and a nonparametric (Mann Whitney) unpaired t-test was performed *p<0.05 **p<0.01 ***p<0.001. Error bars represent Standard Error of the Mean (SEM).

The OFA was used to establish the capacity for the mutant colonoids to efficiently form organoids from a single cell and thus was used as a measure of stem cell functionality[251]. Due to the intra-experimental variation associated with the OFA, the results from three independent repeats have been plotted and analysed separately (Figure 3.4. A – C, this will be performed throughout this thesis). The intra-experimental variation arises due to the inability to reliably determine how many of the 1000 plated cells are indeed stem cells and will eventually form an organoid. Consequently, pooling the three independent repeats would result in the loss of statistical power. In the future, mutant colonoids could be live-cell stained with a range of stem cell markers (e.g. *Lgr5*), isolated using Fluorescence-activated cell sorting (FACS) and replated. This will ensure that most of the 1000 plated cells will form organoids and should reduce the intra-experimental variation.

The results from each experiment exhibited comparable results and revealed that *Kras*$^{G12D/+}$*:p53*^{Null} colonoids had the highest organoid forming ability, while *Apc*$^{min/+}$ colonoids had the lowest (Figure 3.4. A(i) – C(i)). In comparison, the remaining mutant colonoid genotypes had an intermediate organoid forming ability. Taken together, the results from the OFA suggest that *Kras*$^{G12D/+}$*:p53*^{Null} colonoids have an increased stem cell functionality compared to the remaining mutant genotypes and that *Apc*$^{min/+}$ colonoids have the lowest.

3.1.5. Shape, Appearance and Motion Analysis on Mutant Colonoids Reveals Intricate Spatiotemporal Dynamics

The OFA demonstrated significant behavioural differences between colonoids harbouring CRC-associated driver mutations, but the full effect of each mutation on the phenotype of the organoid was not known. These findings made the mutant colonoids an ideal test case to validate a new method for unbiased high-content organoid phenotyping, Shape, Appearance and Motion (SAM, developed by Dr Felix Zhou). SAM analysis (described in section 2.7.3) provides automated timeseries tracking of thousands of features per colonoid, and thus allowed for a more detailed analysis of the spatiotemporal dynamics displayed by these mutant colonoids.

SAM analysis was performed on time-lapse confocal microscopy videos of *Apc*$^{min/+}$ mCherry (red), *Kras*$^{G12D/+}$ EYFP (light blue), *Kras*$^{G12D/+}$*:p53*^{Null} EYFP (dark blue), *p53*^{Null} mBanana (green) and *p53*$^{R172H/R172H}$ mBanana (yellow) colonoids. The mutant colonoids were seeded in separate wells, cultured for 72 hours and then imaged on a confocal microscopy every 2 hours for 117 hours (Figure 3.5).

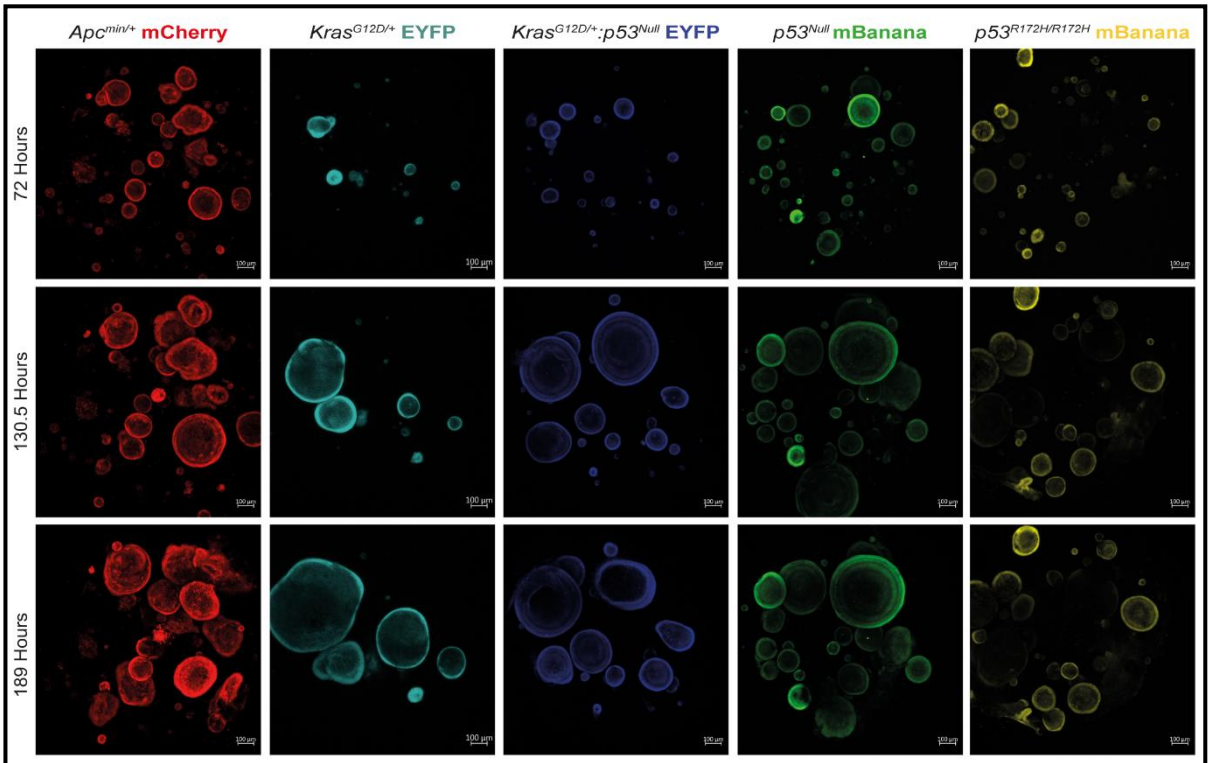


Figure 3.5. Representative images from time-lapse confocal microscopy videos of mutant colonoids. *Apc*$^{min/+}$ mCherry, *Kras*$^{G12D/+}$ EYFP, *Kras*$^{G12D/+}$*:p53*^{Null} EYFP, *p53*^{Null} mBanana and *p53*$^{R172H/R172H}$ colonoids were individually seeded in a 384-well plate and grown for 72 hours before being imaged on a Zeiss 710MP confocal microscope using the 10X objective. Scale bars represent 100 µm. During the course of the time-lapse experiment, a z-stack was performed every two hours for 117 hours at each of the chosen positions. Colonoids were in culture for a total of 189 hours.

Once the time-lapse confocal microscopy videos had been acquired, the individual colonoids were detected, tracked and segmented at each timepoint across the time course of each video. Each colonoid was then assigned a SAM descriptor, which is made up of 2189 features and encapsulates three fundamental conceptual properties: shape (S), object-level features such as area and perimeter; appearance (A), sub-object-level features such as image intensity; and motion (M), the movement of the object at time *t* in relation to the time before (*t-1*) and time after (*t+1*), such as speed statistics. To allow for easier visualisation of the overall structure of

the resulting dataset, these features were compiled across all timepoints from all videos and subjected to dimensionality reduction.

SAM segmented and measured a total of 59 593 colonoid instances pooled from three independent experiments from all timepoints and all mutant genotypes. To capture the full phenotypic variation the resulting SAM feature descriptors were analysed together by UMAP, revealing 8 phenotype clusters (Figure 3.6. A). Each of the 8 phenotype clusters was marked by a unique combination of SAM descriptor scores which related to a specific colonoid phenotype. The dynamics represented in Figure 3.6. B demonstrate the 'shape' (area and eccentricity/irregularity in shape), 'appearance' (intensity and entropy/ non-uniformity of image intensity in appearance) and 'motion' (mean speed) SAM features which are enriched in each cluster. Of the many features calculated by SAM in an unbiased manner, we selected these five as features with high interpretability showing high variability that appeared to associate with the overall structure of the UMAP.

Reflecting these phenotypic differences (Figure 3.6. B), each of the mutant colonoid genotypes mapped uniquely in UMAP space (Figure 3.6. C) and this was quantitatively reflected by different phenotypic cluster compositions (Figure 3.6. D). $Apc^{min/+}$ was enriched for/more likely to form 'irregular' (shape eccentricity) colonoids (clusters 7 and 8, combined 40%) relative to spherical ones (clusters 1 and 2) and had a modest hotspot enriched for 'small' colonoids (clusters 3 and 5). $Kras^{G12D/+}$ had a distinct hotspot representing the 'mean' colonoid (cluster 6) and was slightly enriched for 'large' (cluster 4) and 'spherical' (clusters 1 and 2) colonoids. $Kras^{G12D/+}$:$p53^{Null}$ was mostly enriched for 'large' (cluster 4) and 'spherical' (clusters 1 and 2) colonoids. $p53^{Null}$ and $p53^{R172H/R172H}$ were both enriched for 'small' (cluster 3) and 'spherical' (clusters 1 and 2) colonoids.

In summary, $Apc^{min/+}$ colonoids presented with an irregular or eccentric phenotype over time, while the remaining mutant colonoids presented with a spherical phenotype consistent with 3D intestinal organoid culture.

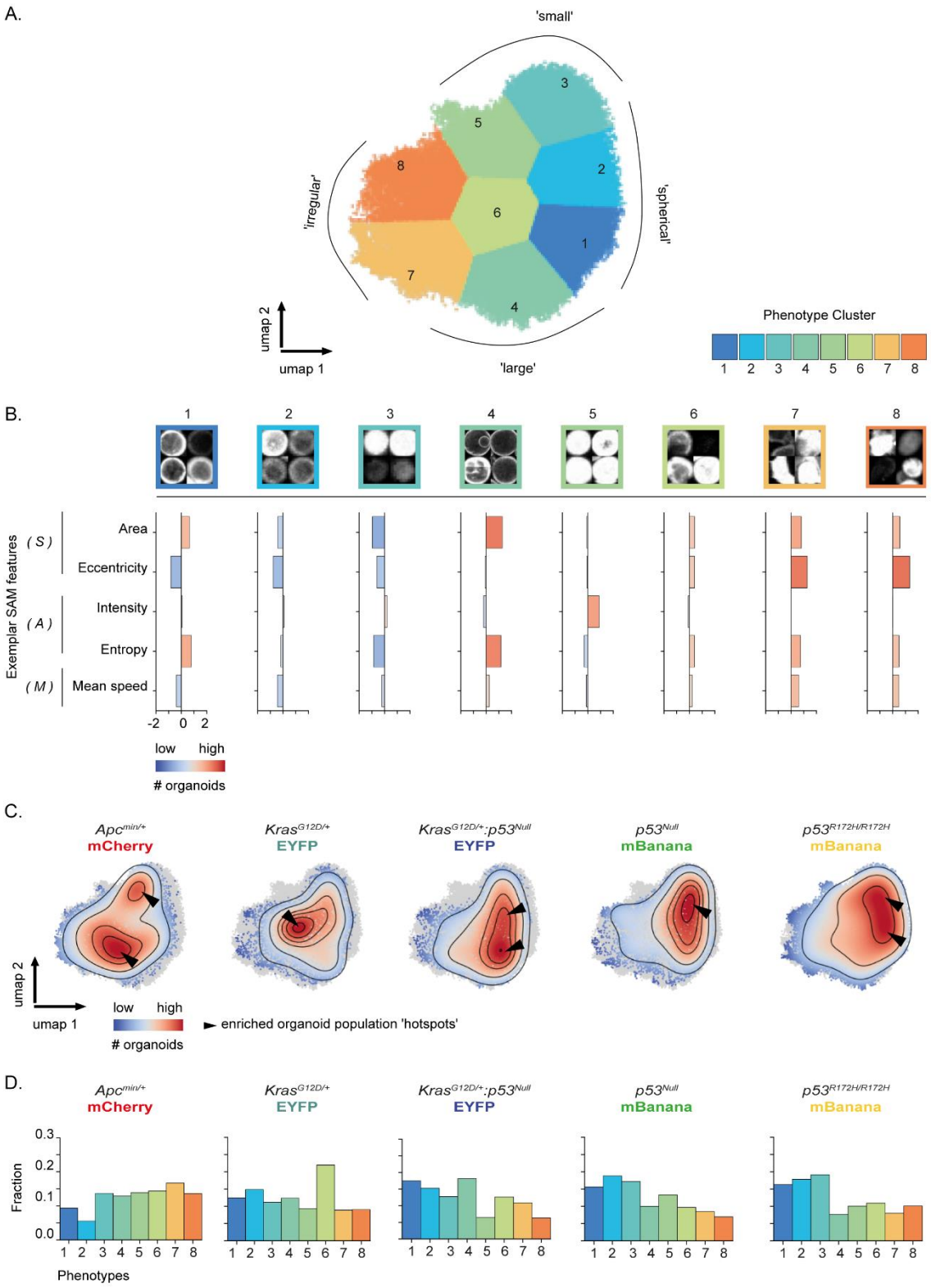


Figure 3.6. SAM characterisation of mutant colonoids reveals 8 distinct phenotypic clusters. **A.** UMAP projection of combined SAM features from a total of 64 time-lapse confocal microscopy videos. Each point represents a segmented colonoid instance (n = 59 593). **B.** Coloured heatmap bar plots of mean z-scores of select, interpretable SAM features for each phenotype cluster with four randomly sampled, cropped and resized to 64x64 pixel image patches above arranged as a 2x2 grid to illustrate the visual appearance of colonoids per cluster. **C.** Smoothed density heatmaps of all colonoids segmented from the respective indicated genotype. The region with darkest red colour reflects the organoids with defined SAM features at highest frequency. **D.** Frequency per phenotype cluster as a fraction of the total number of colonoids per indicated genotype. Analysis performed by Dr Felix Zhou. Figures adapted from those generated by Dr Felix Zhou.

The irregular phenotype dynamic exhibited by *Apc*$^{min/+}$ colonoids was particularly unique and warranted further investigation. This irregularity was reflected qualitatively in temporal snapshots taken from the time-lapse confocal microscopy videos and revealed that *Apc*$^{min/+}$ colonoids indeed underwent a drastic change in phenotype over time (Figure 3.7).

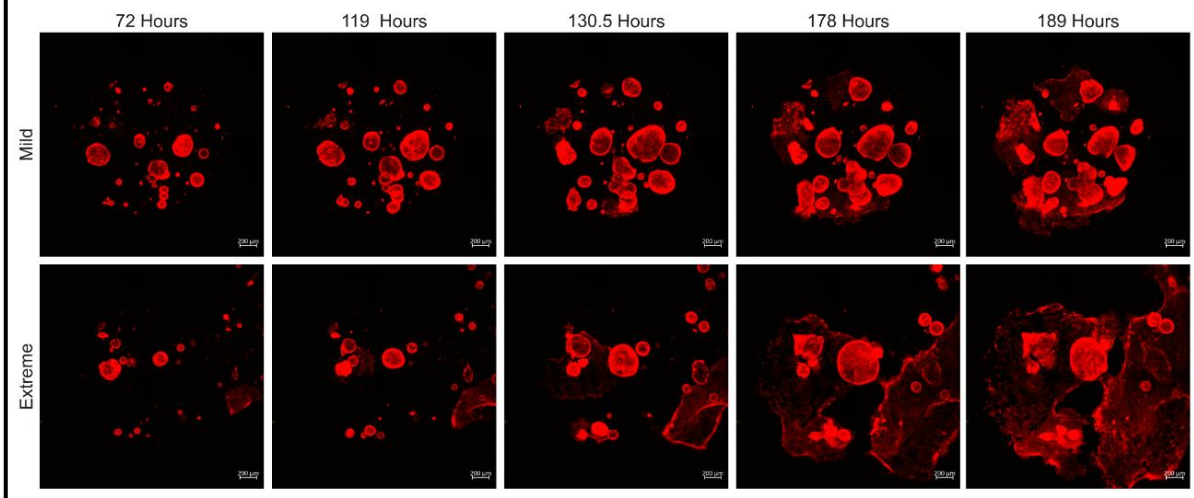


Figure 3.7. *Apc*$^{min/+}$ colonoids undergo drastic changes in phenotype over time. *Apc*$^{min/+}$ mCherry colonoids were individually seeded in a 384-well plate and grown for 72 hours before being imaged on a Zeiss 710MP confocal microscope using the 10X objective. Scale bars represent 200 µm. During the course of the time-lapse experiment, a z-stack was performed every two hours for 117 hours at each of the chosen positions. Colonoids were in culture for a total of 189 hours.

From 119 hours post-seeding, a visible subpopulation of colonoids appeared to lose the usual cystic phenotype associated with 3D intestinal organoid culture and adopt a 'flattened' morphology. This change in phenotype ranged from mild (Figure 3.7 top panel) to extreme (Figure 3.7 bottom panel). In the mild case, most of the *Apc*$^{min/+}$ colonoids remained as 3D cystic structures however, in the extreme case most of the colonoids lost sphericity and 'flattened' to attach to the plastic surface of the plate. These phenotypically distinct *Apc*$^{min/+}$ colonoids will be referred to as 2D eccentric from here on.

To further explore the change in phenotype observed in *Apc*$^{min/+}$ colonoids and allow for a more direct comparison between mutant genotypes, the SAM features that varied most between mutants, area, eccentricity (irregularity in shape), entropy (non-uniformity of image intensity in appearance) and mean speed, were individually selected and plotted over time (Figure 3.8).

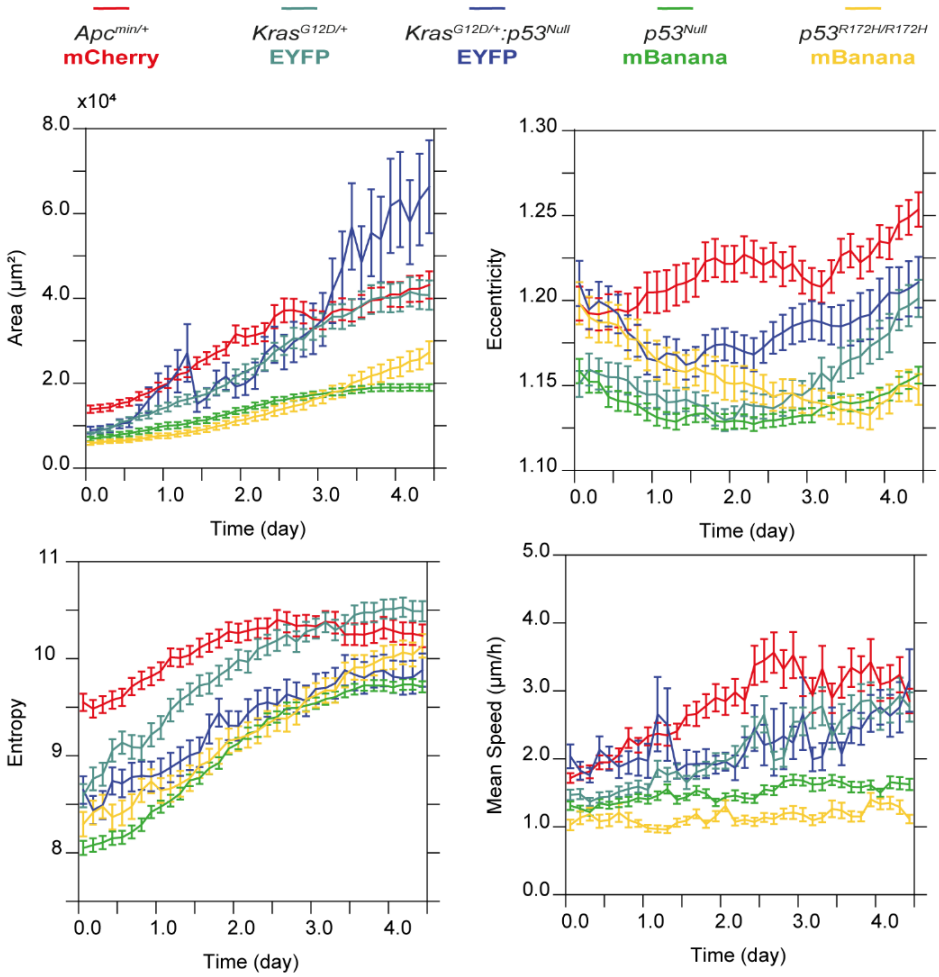


Figure 3.8. *Apc*$^{min/+}$ colonoids exhibit increased eccentricity and mean speed over the course of 117 hours. The individual SAM features real metric area, eccentricity, image entropy and mean speed were plotted as a function of time (0 to 4.5 days/117 hours). Error bars represent SEM of all segmented colonoids. Analysis performed by Dr Felix Zhou. Figures adapted from those generated by Dr Felix Zhou.

In accordance with their enrichment for the 'large' phenotypic characteristic, *Kras*$^{G12D/+}$ and particularly *Kras*$^{G12D/+}$*:p53*^{Null} colonoids exhibited an increased area covered over time. Comparatively, *p53*^{Null} and *p53*$^{R172H/R172H}$ colonoids covered a lesser area over time and this aligned with their 'small' phenotype dynamic. After just one day of time-lapse imaging, *Apc*$^{min/+}$ colonoids exhibited a much higher eccentricity and mean speed in motion. Taken together with the 2D eccentric phenotype displayed by *Apc*$^{min/+}$ colonoids (Figure 3.7), this supports a higher area covered which is comparable to that of *Kras*$^{G12D/+}$ colonoids and could imply a greater potential for migration and invasion. Furthermore, *Apc*$^{min/+}$ colonoids presented an increasing entropy score from the beginning of time-lapse video acquisition which then reached a plateau

by day two and stayed relatively constant until the end of imaging. This could reflect the dynamic changes observed in colonoid phenotypes (from 3D cystic to 2D eccentric) and may suggest a change from regularly organised colonic crypts to asymmetric structures with disrupted organisation. Over the course of the time-lapse videos, entropy scores for all of the mutant genotypes increased and ended within similar range of one another. This is likely to be as a result of the colonoids starting to die after 189 hours in culture and would be evident by the lumen filling with cell debris and causing a change in intensity.

To compare the phenotypic development of the mutant genotypes with each other, a temporal UMAP phenotype was calculated for each mutant colonoid depicting the mean trajectory through SAM space over time (Figure 3.9). This clearly highlighted an early deviation of the *Apc*$^{min/+}$ trajectory leftwards, towards increased average irregularity, compared to all other genotypes. This indicates a higher disposition of *Apc*$^{min/+}$ colonoids towards morphological change rather than pure growth, which is reflected in the trajectories of the other mutant genotypes through SAM space.

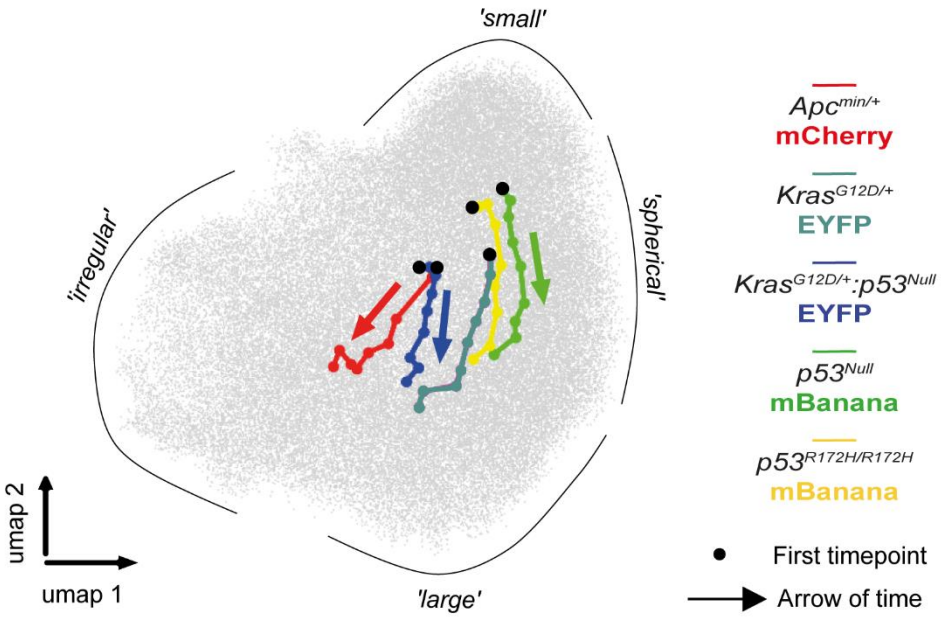


Figure 3.9. Mutant colonoids demonstrate unique trajectories through SAM space over time. Mean UMAP temporal trajectory as a function of time from 0 to 4.5 days (117 hours). Each coloured point denotes 0.5-day increments from the starting point (black point) on each trajectory. Analysis performed by Dr Felix Zhou. Figures adapted from those generated by Dr Felix Zhou.

Next, the temporal variation in the frequency of each phenotype cluster was visualised and compared between mutant genotypes (Figure 3.10). *Apc*$^{min/+}$ is clearly distinct, with expanding 'irregular' phenotype clusters (clusters 7 and 8) and decreasing 'spherical' phenotype clusters (clusters 1 and 2). *Kras*$^{G12D/+}$ and *Kras*$^{G12D/+}$*:p53*^{Null} exhibited expanding 'large' (cluster 4) and decreasing 'small' (cluster 3) phenotype clusters, while maintaining a constant 'spherical' phenotype cluster (clusters 1 and 2). Lastly, *p53*^{Null} and *p53*$^{R172H/R172H}$ exhibited expanding 'large' (cluster 4) and 'spherical' (cluster 1) phenotype clusters and decreasing 'small' (cluster 3) phenotype clusters. These temporal analyses show the manner in which SAM data can be parsed to reveal how important phenotypic features evolve over time.

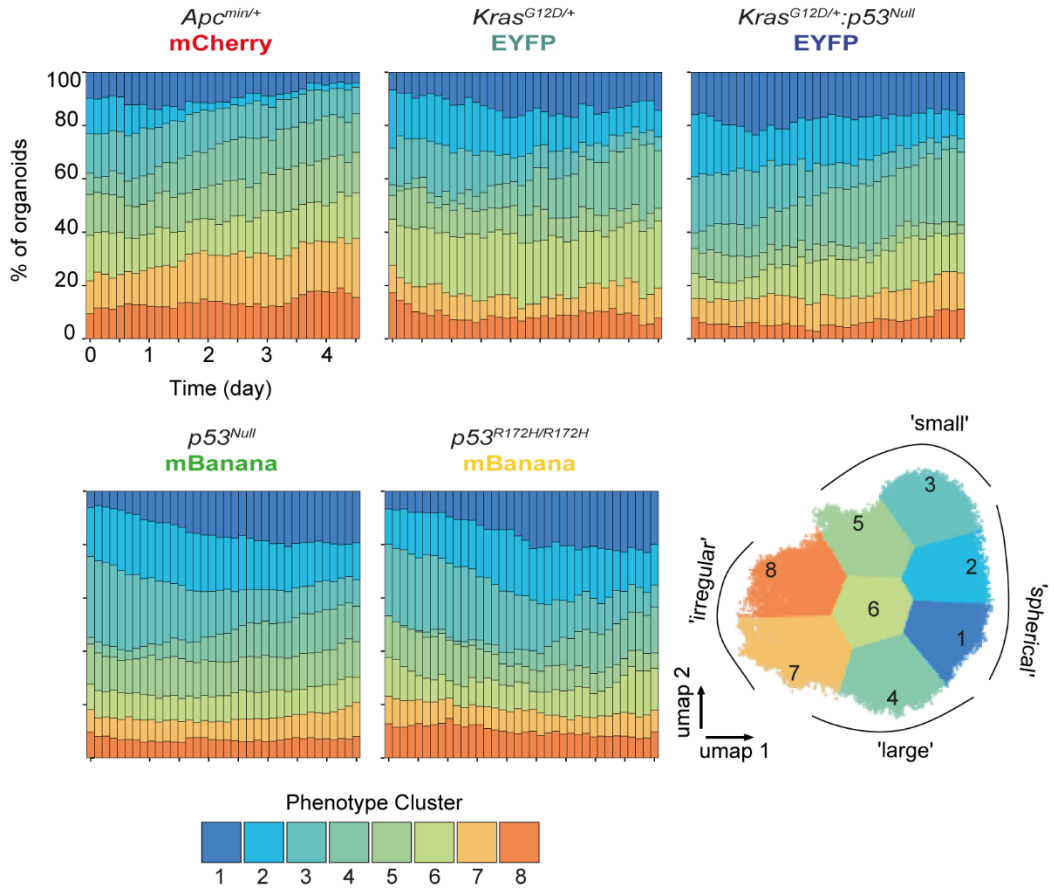


Figure 3.10. Mutant colonoids demonstrate temporal variation in the frequency of each phenotype cluster. Stacked bar plot showing temporal variation in the frequency of each phenotype cluster, as a percentage of all colonoids segmented from each genotype, aggregated and pooled together for analysis over the specified 1/8-day time interval over 0 to 4.5 days (117 hours) acquisition. Analysis performed by Dr Felix Zhou. Figures adapted from those generated by Dr Felix Zhou.

Here we have validated SAM and revealed that prominent CRC-associated mutations induce significant aberrations in cellular plasticity and spatiotemporal dynamics in colonoids. These results have the potential to provide useful information into the complexity behind CRC tumourigenesis and how certain mutations have the ability to alter disease outcome.

3.1.5. Discussion

The ability for cells to demonstrate cellular plasticity and readily respond to environmental signals is essential for the proper functioning of numerous biological processes. Undeniably, the colon epithelium presents a high degree of cellular plasticity, with cells constantly undergoing proliferation, differentiation, migration and apoptosis[257]. Dysregulation in the ability of colon epithelial cells to exhibit cellular plasticity results in various atypical phenotypic alterations and can lead to the development of several pathologies, including CRC[190]. Such dysregulation is associated with genetic alterations and results in the formation of a complex genotype-phenotype relationship. Efficient modelling of this relationship could enhance our knowledge of CRC tumourigenesis and aid in the identification of novel treatment regimes.

Here we have investigated the impact of CRC-associated driver mutations on the behaviour and cellular plasticity exhibited by colon organoids (colonoids). This was achieved via the unbiased and high-throughput, simultaneous measurement of Shape, Appearance and Motion (SAM) features, which identified instantaneous mutant colonoid states and generated phenotype trajectories for interpretative comparative analysis.

In this chapter, in order to enable SAM analysis, a library of mutant colonoids were successfully derived, characterised and fluorescently labelled. *Apc*$^{min/+}$ mCherry, *Kras*$^{G12D/+}$*:p53*^{Null} EYFP, *Kras*$^{G12D/+}$ EYFP, *p53*^{Null} mBanana and p53$^{R172H/R172H}$ mBanana colonoids were chosen due to the key role of these alterations in CRC initiation and progression[285].

An OFA revealed striking differences in the ability of the mutants to efficiently form colonoids from a single cell, suggesting key underlying phenotypic differences between these different driver mutations. Overall *Kras*$^{G12D/+}$*:p53*^{Null} had the highest organoid forming ability, while

Apc$^{min/+}$ colonoids had the lowest. Aberrant Wnt signalling, a key feature of *Apc* mutant tumours has been shown to decrease intestinal stem cell (ISC) functionality and lower organoid formation efficiency; thus it is possible that the decreased organoid formation seen in *Apc*$^{min/+}$ colonoids was a result of dysregulated Wnt signalling, leading to alterations in ISC fitness[286].

Next the spatiotemporal dynamics of the mutant colonoids was evaluated using SAM analysis of time-lapse confocal microscopy videos. SAM feature descriptors were together analysed by UMAP and revealed 8 phenotype clusters, which could be broadly categorised into 'small', 'large', 'spherical' and 'irregular' categories. Each of the mutant colonoid genotypes were composed of varying proportions of each of the 8 phenotype clusters and therefore, mapped uniquely in UMAP space. This result highlights the impact that CRC-associated driver mutations can have on cellular plasticity and that different alterations are responsible for generating different phenotype dynamics. This finding would not be as evident with if one were to rely solely on snapshot images of mutant colonoid cultures or if using computational pipelines tailored to only detect specific properties or traits.

Interestingly, *Apc*$^{min/+}$ was enriched in 'irregular' colonoids, while the remaining mutant genotypes were enriched in 'spherical' colonoids. The unique SAM phenotype clustering displayed by the *Apc*$^{min/+}$ colonoids, evident in the time-lapse confocal microscopy videos, were driven by a subset of colonoids which adopted a 2D eccentric appearance compared to the 3D cystic morphology usually displayed by intestinal organoids. This was further apparent by the elevated eccentricity and entropy SAM scores demonstrated by *Apc*$^{min/+}$ colonoids, which are measures of 'irregularity in shape' and 'non-uniformity of image intensity in appearance' respectively.

Although the exact mechanism behind this stark change in phenotype is not clear, it is possible that dysregulated Wnt signalling is inducing an altered response to microenvironmental signals and dysregulating the cellular plasticity of *Apc*$^{min/+}$ colonoids. In addition to regulating the ISC population, Wnt is known to drive CRC progression through epithelial-mesenchymal transition (EMT)[287-289]. EMT is associated with the progressive loss of epithelial features, such as cell-cell junctions and polarity, which results in increased cell motility[290]. Indeed this could provide

an explanation for both the increased mean speed scores observed in *Apc*$^{min/+}$ colonoids and the alteration in shape (eccentricity) observed in culture.

Lastly, temporal trajectory analysis on *Apc*$^{min/+}$ colonoid development presented a higher disposition towards morphological change rather than pure growth, which was highly unique when compared to the trajectories of the other mutant genotypes. Taken together with the above-mentioned changes, one could infer that the loss of *Apc* induces more drastic changes in cellular plasticity compared to other CRC-associated alterations.

It is important to note that the individual colonoid genotypes used throughout this study were each derived from a single C57BL/6 mouse. In order for concrete conclusions to be drawn from this data, further independent derivations of each colonoid genotype would need to be performed and downstream analysis repeated.

As is the case with any novel computational program, SAM analysis is accompanied by constraints and limitations which should be taken into account when interpreting the results. These will be briefly outlined below.

SAM analysis of the spatiotemporal dynamics exhibited by the different mutant colonoid genotypes is reliant on the intensity of the fluorescent proteins being expressed. If certain fluorescent proteins produce a more intense signal than others, the SAM features which relate to “appearance” could be interpreted incorrectly. Consequently, it is important that the fluorescent protein intensity is comparable between genotypes and experiments. This could be ensured by altering the power of the relevant lasers exciting the different fluorescent proteins and using the same microscope settings across experiments.

While the 2189 SAM features extracted and assigned to each colonoid instance undeniably provide an abundance of information relating to the spatiotemporal dynamics unique to each colonoid genotype, future SAM analysis should aim to eliminate feature redundancy. The current SAM analysis contains a degree of feature redundancy which has the potential to increase the likelihood of finding a significant result which may not exist. Eliminating feature

redundancy will ultimately decrease the overall number of SAM features; however the results will be more accurate and reliable.

SAM analysis is performed on 2D maximum intensity projections derived from the acquired z-stack images. This means that colonoids which completely overlap in 3D space are seen as one object and results in the loss of important information. Accordingly, it is vital that the colonoids are plated at a low density which will reduce the potential for significant overlapping to occur. Furthermore, only constant or reliable “tracks” are used to generate the final results figures following SAM analysis. Therefore, when two or more colonoids merge or overlap, the tracks for those colonoid instances at that timepoint are discarded. Only if the colonoids separate again will a new track be made for that colonoid instance at the later timepoint. Again, this will result in the loss of important information and further highlights the necessity for the colonoids to be plated at a low density. To further ensure that essential data is not lost, future analysis could monitor the colonoid/object number over time. A reduction in the object number could be used to identify the point at which segmentation error (when two distinct objects are newly classified as a single object) is too high indicating a suitable endpoint for the time-lapse experiment.

Lastly, following dimensionality reduction in the SAM analysis pipeline, k-means clustering is applied to the data to generate 8 phenotype clusters, with the number of clusters identified using the elbow selection method. Each colonoid instance is assigned to a cluster and bounded by lines drawn midway between the cluster centroids (the sum of the position of all colonoid instances in a single cluster divided by the number of colonoid instances) resulting in the formation of the depicted Voronoi partitions. K-means clustering may not be the most suitable clustering algorithm as it requires one to specify the number of clusters that will be created. This may not be appropriate in situations where the true number of clusters is unknown. Furthermore, the k-means algorithm is sensitive to outliers and assumes largely spherical clustering. Consequently, this algorithm does not perform well in situations with large outliers or irregularly shaped clusters. Future analysis could use the Louvain algorithm (as used in the scRNA-seq analysis) to determine the number of phenotype clusters more accurately.

While further investigation is warranted, this research has leveraged the power of novel advancements in high-content phenotyping methods (SAM) to reveal the impact that CRC-associated mutations have on cellular plasticity in colonic stem cells. These results form the basis for further exploration of the key phenotypic features distinguishing colonoids carrying various CRC driver mutations.

3.2. Colonoids Harbouring Colorectal Cancer-Associated Driver Mutations Exhibit Distinct Stem Cell Molecular Phenotypes

3.2.1. Introduction

The injured colon epithelium demonstrates a high degree of cellular plasticity and efficiently regenerates via the temporary disruption of morphogen signalling gradients and the easing of strict homeostatic controls over cell fate. While it is appreciated that many of the key signalling pathways essential during epithelial regeneration are commandeered during colorectal cancer (CRC), the exact role that distinct stem cell molecular phenotypes play in CRC tumourigenesis and progression is still largely unclear. Elucidating this role is vital as cellular plasticity and subsequent phenotypic heterogeneity are known to drive therapy evasion in cancer[110,291].

Key similarities in colon epithelium regeneration and CRC tumourigenesis and progression, namely altered stem cell plasticity and extracellular matrix (ECM) remodelling and Yap signalling will be the subject of this chapter.

Stem Cell Plasticity

In response to insult, the crypt base columnar (CBC) stem cell population, which usually drives cell turnover, is diminished and the expression of stem cell markers and Wnt target genes, including *Lgr5*, declines[103,104,292]. The CBC population is subsequently replenished via the dedifferentiation of remaining cell types and the acquisition of foetal-like stem cell characteristics through the activation of Yap signalling[108,109,257]. Consequently, efficient regeneration occurs through the temporary reversion of the adult epithelium to an embryonic state and is vital for re-establishing normal colon physiology. This Yap-mediated process has been associated with the expression of *Ly6a*, *Anxa1* and *Clu* and together have been used to identify stem cells with regenerative properties – regenerative stem cells (RSCs)[17,108,109,293].

While research into the role of RSCs in colon epithelial regeneration is developing, the molecular phenotype of stem cells involved in CRC is less apparent. Initially, CBC stem cells were thought to be the cell of origin for colon neoplasia as the loss of *Apc* in these stem cells led to prompt adenoma formation[294]. However, subsequent murine studies have demonstrated

that Lgr5-negative stem cells are also able to form neoplasia with inflammation and the disturbance of morphogen signals[295,296]. In support of this, genetic ablation of CBC stem cells in tumours derived from CRC organoids was shown to have little effect on tumour growth and that the cells responsible for metastatic tumour formation were largely disseminated Lgr5-negative stem cells[190,191]. These contradictory studies highlight the lack of complete understanding of the role that stem cells with different molecular phenotypes play in CRC tumourigenesis and progression.

In an attempt to understand the factors which control the molecular phenotype of stem cells involved in colon neoplasia, Gil Vasquez *et al.* put forward a phenotypic fitness landscape model (Figure 3.11).

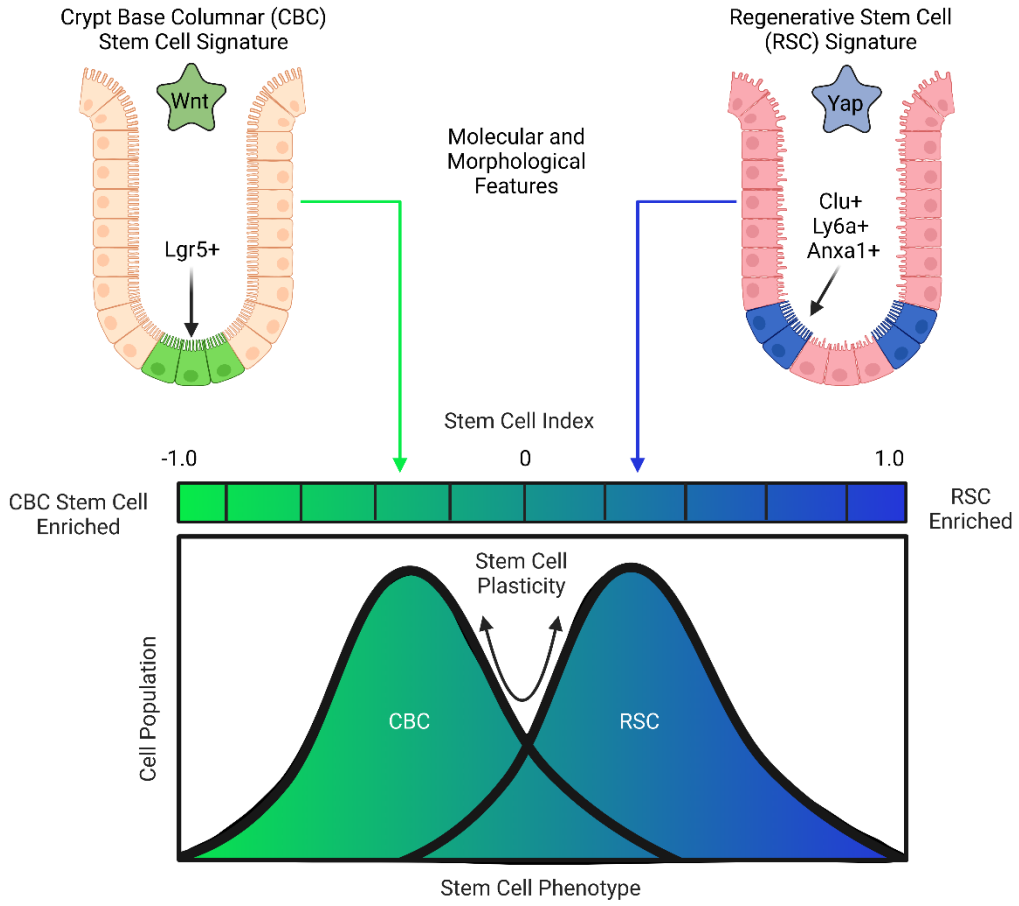


Figure 3.11. Phenotypic fitness landscape model. Molecular and morphological analysis on a range of intestinal lesions resulted in a proposed classification system for colorectal cancer stem cell molecular phenotype and neoplastic activity termed the stem cell index. The phenotypic fitness landscape model describes a phenotypic axis upon which crypt base columnar (CBC) stem cells and regenerative stem cells (RSCs) represent separate but interlinked fitness peaks. CBC stem cells and RSCs mark opposite ends of the phenotypic axis and shifts between fitness peaks represented stem cell phenotypic plasticity necessary for tumour adaption. Figure adapted form Gil Vazquez *et al.* 2022.

The authors performed molecular and morphological analysis on a range of intestinal lesions and proposed a classification system for CRC stem cell molecular phenotype and neoplastic activity termed the stem cell index[110]. This phenotypic fitness landscape model examined the relationship between neoplastic stem cell activity and phenotype and assessed the distribution of CBC stem cells and RSCs between lesions. The analysis revealed a phenotypic axis upon which CBC stem cells and RSCs represent separate but interlinked fitness peaks. CBC stem cells and RSCs mark opposite ends of the phenotypic axis and shifts between fitness peaks represented stem cell phenotypic plasticity necessary for tumour adaption. Moreover, the distribution of stem cell phenotypes along this axis is determined by the combination of epithelial cell mutations and microenvironmental extracellular signalling. For instance, mutations in *APC* associated with a CBC stem cell molecular phenotype, while activation of MAPK, YAP, TGFβ and inflammatory pathways associated with a RSC molecular phenotype.

Extracellular Matrix Remodelling and Yap Signalling

The temporary state assumed by the colonic epithelium during regeneration is partially instructed through the remodelling of the ECM and culminates in the activation of Yap signalling[108]. Briefly, remodelling of the ECM induces interactions between integrins (transmembrane receptors that link the ECM and the intracellular actin-cytoskeleton) and the ECM. This integrin-ECM interaction culminates in the activation of two nonreceptor intracellular tyrosine kinases, focal adhesion kinase (FAK) and steroid receptor coactivator (Src)[297]. Src then activates Yap allowing for its translocation into the nucleus and leading to the expression of genes necessary for efficient epithelial repair[108].

Both Wnt signalling and cell mechanics are essential for Yap activation and subsequent ISC reprogramming during colonic regeneration. The former promotes Yap activation via the inhibition of Apc and consequently the formation of the β-catenin destruction complex of which Yap is a part[108,298,299]. This was demonstrated by the impeded growth exhibited by *Apc* knockout organoids, cultured in a collagen ECM reminiscent of the repairing epithelium, and treated with a Yap inhibitor[108]. Similarly, cellular mechanics pathways are also required for cellular reprogramming in the regenerating epithelium, as the growth of *Apc* knockout

organoids was also reduced following the inhibition of Rho, an important mediator upstream of Yap in the mechanotransduction signalling pathway[108,300].

ECM remodelling and Yap signalling have also been implicated in promoting several cancers, including CRC[301]. During tumourigenesis the ECM is significantly modified in structure and composition and encourages cellular transformation, invasion and metastasis. These changes result in increased stiffness in the tissue, which culminates in aberrant Yap activation through similar mechanisms as seen during physiological colonic regeneration[300,302,303].

Due to their capacity to be successfully cultured in different ECMs types and stiffnesses, organoids have become and an attractive model for the study of the role of Yap in CRC tumourigenesis. Research using CRC PDOs has demonstrated that YAP plays a critical role in tumour organoid self-renewal and emphasised its role in the activation of CRC-specific enhancers[304]. Moreover, studies have shown a positive correlation between *YAP* expression levels and levels of EMT-inducing transcription factors and downstream EMT markers in human CRC tissue samples[305]. These findings suggest YAP activation in response to microenvironmental signals plays a key role in both tumourigenesis and progression in CRC.

Delineating the association between CRC-associated mutations and YAP-dependent alterations in stem cell molecular phenotype could reveal novel targets in CRC treatment.

3.2.2. Chapter Aim

Execute scRNA-seq and IF staining on mutant colonoids for integration with spatiotemporal analysis.

Shape, Appearance and Motion (SAM) analysis on colonoids harbouring CRC-associated driver alterations revealed differences in the spatiotemporal dynamics exhibited by colonoids with different mutant genotypes. In this chapter we aim to incorporate single-cell RNA sequencing (scRNA-seq) and immunofluorescence (IF) staining to determine whether these differences correlate with Yap-associated alterations in stem cell molecular phenotype and ECM remodelling which play key roles in CRC initiation and progression.

3.2.3. scRNA-seq on Wild Type and Mutant Colonoids Reveals Unique Gene Expression Profiles

The overall gene expression profile of wild type and mutant colonoids was determined using scRNA-seq. Generally, each genotype formed a discrete cluster of cells, demonstrating that colonoids carrying different driver mutations each express distinct transcriptional signatures (Figure 3.12).

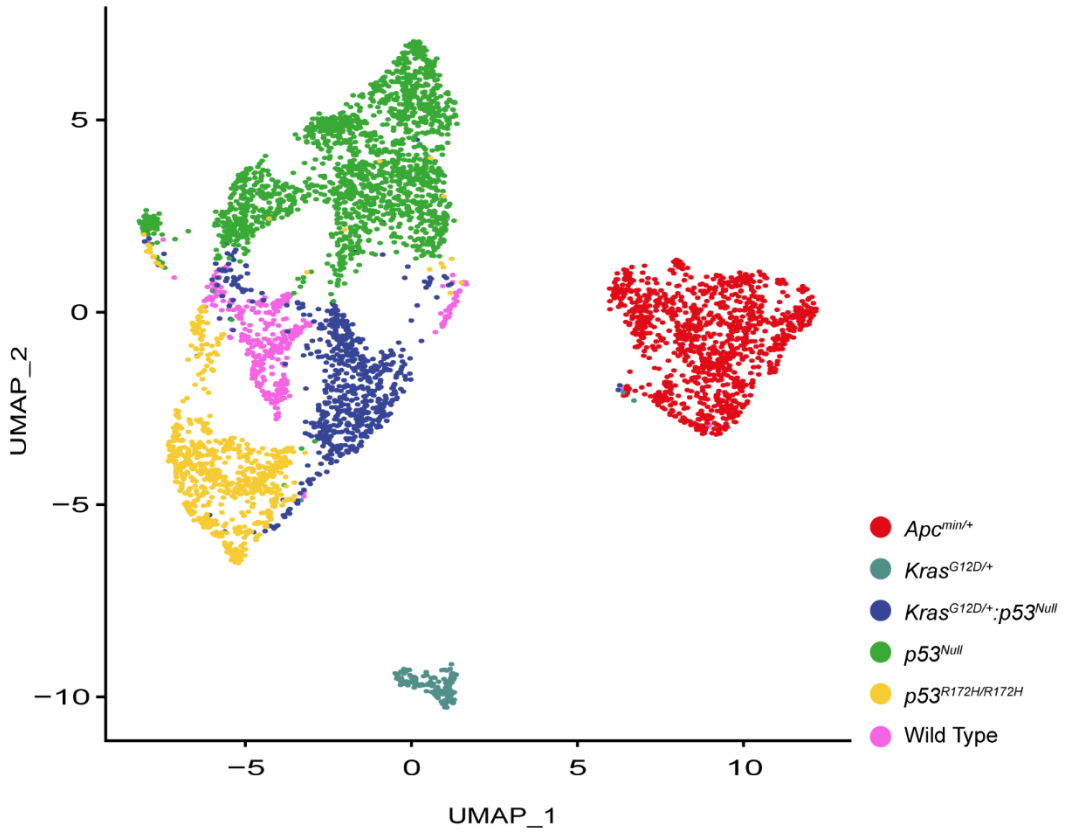


Figure 3.12. Wild type and mutant colonoids exhibit unique gene expression profiles. Wild type and mutant colonoids were individually seeded in a 384-well plate and cultured for seven days before processing. scRNA-seq was conducted using a 5' scRNA-seq gene expression workflow. Sequencing of final libraries was conducted on the Illumina NextSeq 550 and data analysis was conducted using Cell Ranger and Seurat. Analysis performed by Thomas Carroll and Brittany-Amber Jacobs.

Cells from wild type (pink) and *Kras*$^{G12D/+}$*:p53*^{Null} (dark blue) colonoid-derived cells showed some overlap with each other during dimensionality reduction (Figure 3.12); while the overlap was limited, this suggests the phenotype induced by these genotypes may be somewhat similar. *p53*^{Null} (green) and *p53*$^{R172H/R172H}$ (yellow) colonoid-derived cells showed a lesser

degree of overlap, showing that even a single driver mutation can generate unique transcriptional profiles. Strikingly, *Apc*$^{min/+}$ (red) and *Kras*$^{G12D/+}$ (light blue) colonoid-derived cells clustered completely separately to the aforementioned genotypes and each other, indicating their vastly different gene expression signatures compared to the other genotypes. These results show that a single driver mutation in colonoids is sufficient to drastically alter the transcriptome from its wild type state, and that some driver mutations induce more distinct transcriptional states than others.

To note, all of the cells in colonoid cultures were subject to scRNA-seq, in the case of *Apc*$^{min/+}$ colonoids this included the 3D cystic colonoids and the 2D eccentric colonoids.

3.2.4. Phenotypically Distinct *Apc*$^{min/+}$ Colonoids Exhibit Activated Yap Signalling

The highly distinct clustering of *Apc*$^{min/+}$ colonoid-derived cells by scRNA-seq appeared to validate the unique phenotype displayed by *Apc*$^{min/+}$ colonoids during SAM analysis. This justified further analysis of the scRNA-seq analysis to determine which transcriptional programs were responsible for the unique 2D eccentric phenotype exhibited by *Apc*$^{min/+}$ colonoids. Considering the current literature it was hypothesised that the unique spatiotemporal dynamics and gene expression profile exhibited by *Apc*$^{min/+}$ colonoids may be associated with an altered stem cell molecular phenotype.

In-depth analysis of the scRNA-seq data revealed that *Apc*$^{min/+}$ colonoid-derived cells highly expressed Yap target genes, namely *Ankyrin repeat domain 1 (Ankrd1)*, *Cellular communication network factor 2* (*Ccn2)* and *Plasminogen activator, urokinase receptor* (*Plaur,* Figure 3.13.A). *Ankdr1* was overexpressed by *Apc*$^{min/+}$ colonoid-derived cells compared to the other mutant and wild type colon-derived cells. *Ccn2* was similarly overexpressed, however *p53*$^{R172H/R172H}$ and *Kras*$^{G12D/+}$*:p53*^{Null} colonoid-derived cells expressed *Ccn2* at levels intermediate to that of *Apc*$^{min/+}$ and the remaining genotypes. *Apc*$^{min/+}$ and *p53*^{Null} colonoid-derived cells expressed comparable levels of *Plaur*, while the other genotypes exhibited low expression levels. Furthermore, Gene Set Enrichment Analysis (GSEA) showed that *Apc*$^{min/+}$ colonoid-derived cells exhibited an upregulation of the Yap signalling pathway (Figure 3.13.B).

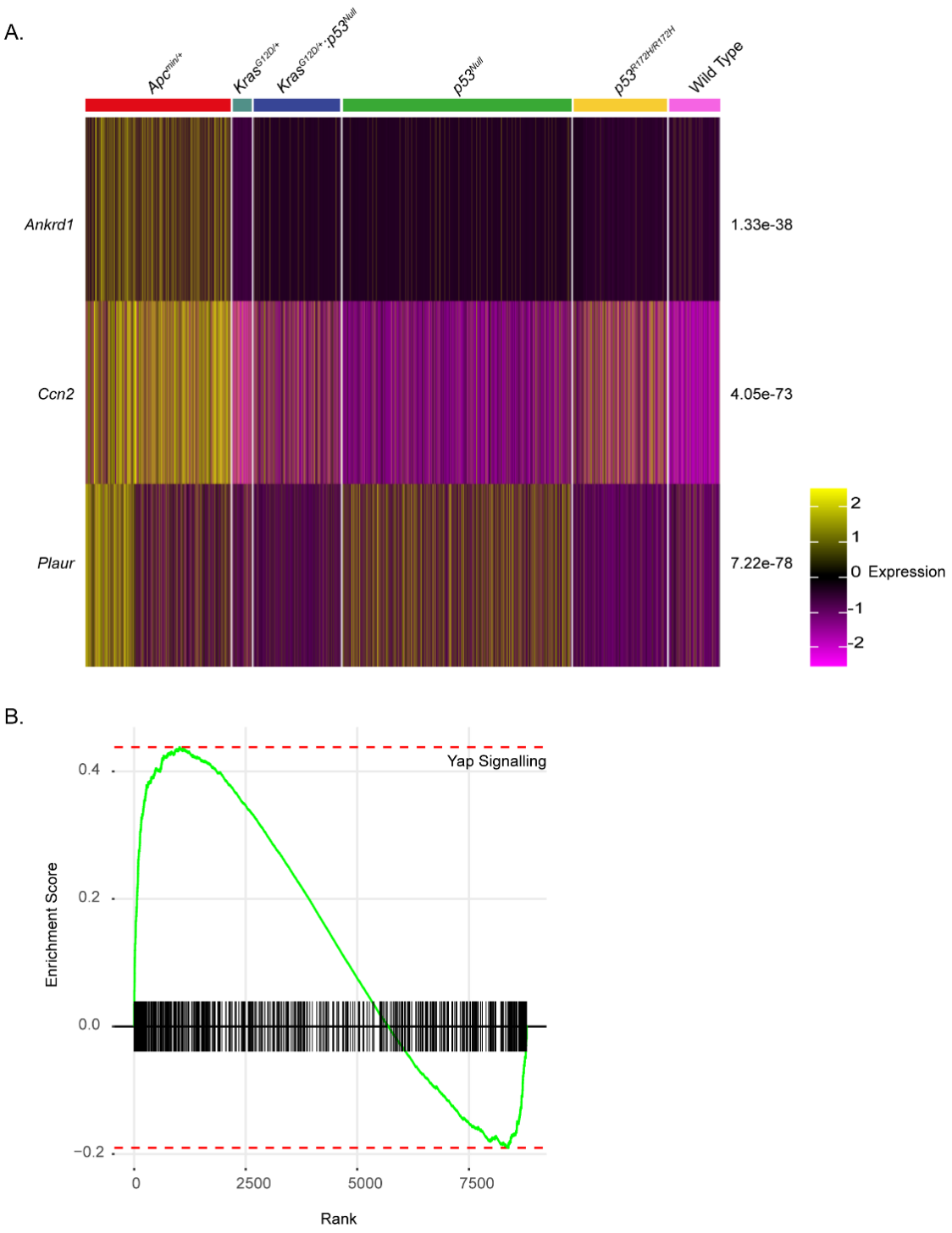


Figure 3.13. *Apc*$^{min/+}$ colonoids overexpress Yap target genes and exhibit upregulated Yap signalling. A. The expression of Yap target genes, *Ankyrin repeat domain 1* (*Ankrd1*), *Cellular communication network factor 2* (*Ccn2*) and *Plasminogen activator, urokinase receptor* (*Plaur*) was compared between wild type and mutant colonoids and visualised using a heatmap. The colour scheme represents the scaled normalized expression level of the given gene in each cell as calculated by Seurat. Adjusted p-values for the enrichment of each gene in *Apc*$^{min/+}$ colonoid-derived cells compared with all other genotypes are stated at the end of each row. **B.** Gene set enrichment analysis showing enrichment of Yap signalling between *Apc*$^{min/+}$ colonoid-derived cells and the remaining wild type and mutant genotypes.

The elevated Yap target gene expression exhibited by *Apc*$^{min/+}$ colonoid-derived cells suggested the possible activation of Yap signalling. To investigate this, IF staining was performed (Figure 3.14).

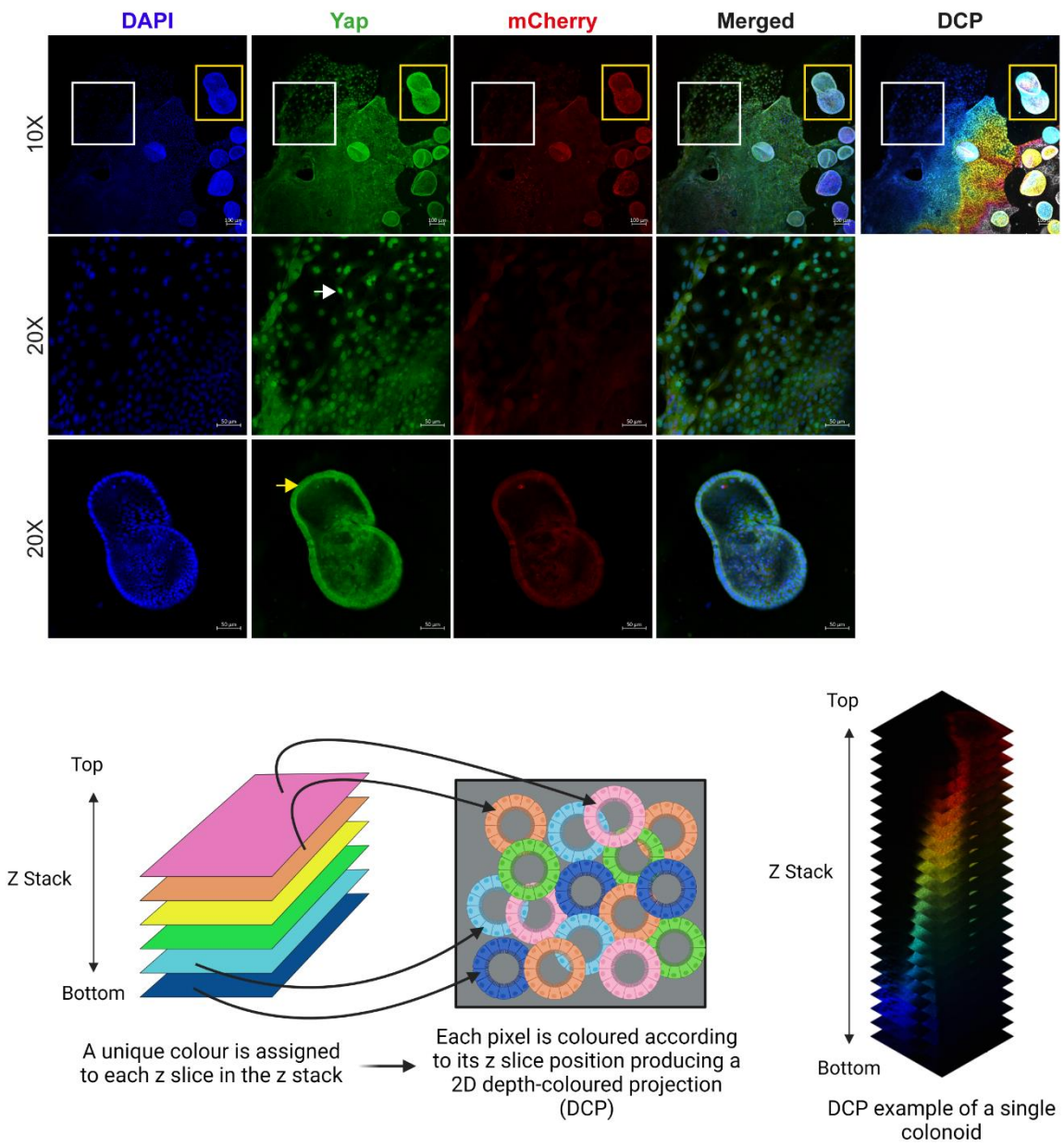


Figure 3.14. Yap is localised to the nucleus of 2D eccentric *Apc*$^{min/+}$ colonoids. *Apc*$^{min/+}$ colonoids were individually seeded in a 96-well plate and cultured for seven days before processing for immunofluorescence (IF) staining. Representative IF images of Yap (green) in fixed *Apc*$^{min/+}$ mCherry (red) colonoids, with nuclei counterstained with DAPI (blue). Depth-coloured projections (DCPs, explained in the bottom panel) were generated from images taken using the 405 nm (DAPI) laser only. Images were acquired on a Zeiss 710MP confocal microscope using the 10X (scale bar represents 100 µm) or 20X (scale bar represents 50 µm) objective as indicated. White and yellow boxes represent the areas focused on in higher magnification images. The images are representative of three independent experiments.

It was observed that the 2D eccentric *Apc*$^{min/+}$ colonoids (white box) which had lost the cystic shape characteristic of 3D intestinal organoid culture (see Figure 3.7) stained positive for nuclear Yap (white arrow). In contrast, 3D cystic *Apc*$^{min/+}$ colonoids (yellow box) stained positive for cytoplasmic Yap (yellow arrow). This suggested that 2D eccentric *Apc*$^{min/+}$ colonoids, but not 3D cystic ones, had activated Yap signalling.

Depth-coloured projections (DCPs, explained at the bottom of Figure 3.13) of the acquired confocal images revealed that 2D eccentric *Apc*$^{min/+}$ colonoids with nuclear Yap localisation were located at the bottom of the of the z-stack (blue) and therefore towards the bottom of the plate. 3D cystic *Apc*$^{min/+}$ colonoids with cytoplasmic Yap staining were higher up in the z-stack and therefore further way from the bottom of the plate and more centrally located in the Matrigel droplet. This finding could suggest that colonoids located at the bottom of the plate are experiencing an altered ECM stiffness leading to enhanced mechanotransduction and Yap activation.

Indeed, this is a significant finding, however it is important to note that the Yap signature was only detected in the sole colonoid genotype which adopts both a 3D and 2D phenotype and then compared genotypes which only adopt a 3D phenotype. In order to be certain that the elevated Yap signature exhibited by *Apc*$^{min/+}$ colonoids is unique to this genotype, one would need to plate all of the genotypes in 2D and repeat the scRNA-seq and IF staining to determine whether the non-*Apc*$^{min/+}$ colonoids exhibit elevated Yap signalling and nuclear Yap localisation.

3.2.5. *Apc*$^{min/+}$ Colonoids Express a Regenerative and Foetal Stem Cell Gene Signature

The activation of Yap signalling in intestinal stem cells (ISCs) has been coupled with the acquisition of a RSC gene signature. Consequently, the scRNA-seq dataset was assessed to determine whether the activated Yap signalling exhibited by *Apc*$^{min/+}$ colonoids was associated with alterations in stem cell molecular phenotype.

The analysis of the scRNA-seq data revealed that *Apc*$^{min/+}$ colonoid-derived cells highly expressed markers associated with a RSC gene signature, namely *Clusterin* (*Clu*), *Annexin*

a1 (*Anxa1*) and *Lymphocyte antigen 6 complex, locus a* (*Ly6a*, Figure 3.15). In comparison with the wild type and other mutant genotypes, *Apc*$^{min/+}$ colonoid-derived cells overexpressed *Clu* and *Anxa1* and to a lesser extent *Ly6a*.

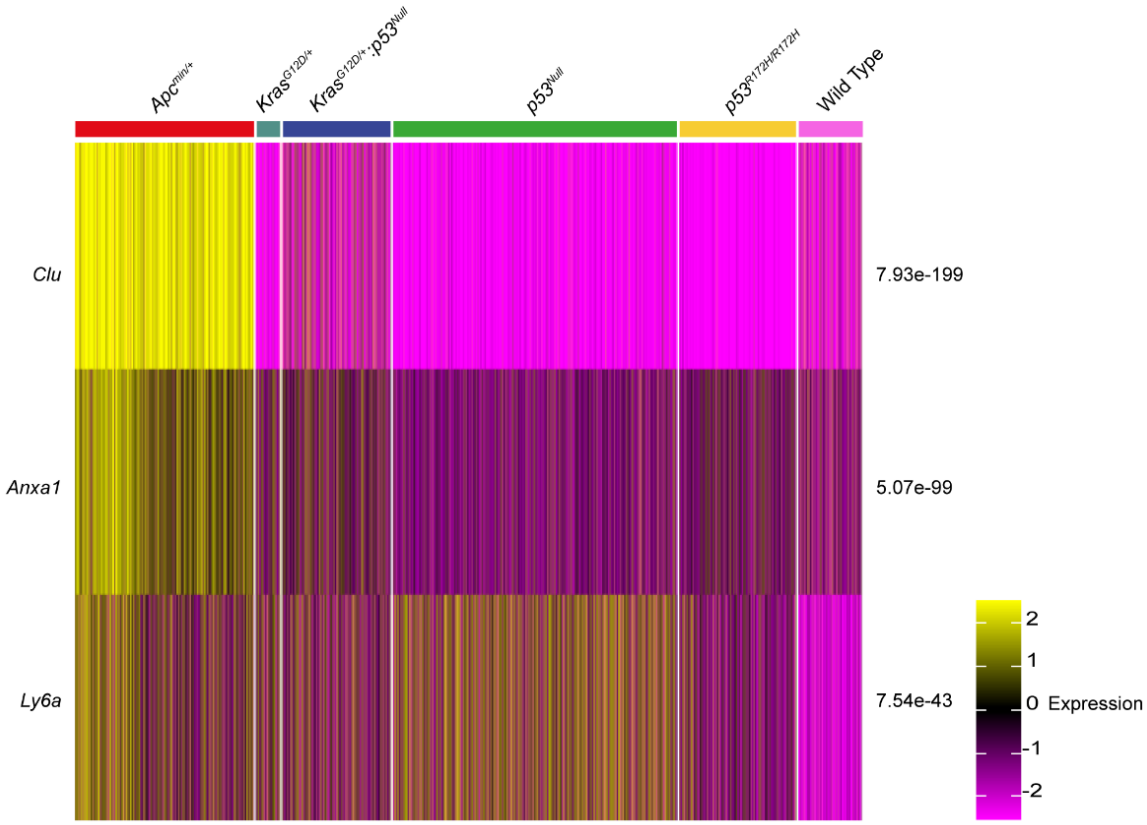


Figure 3.15. *Apc*$^{min/+}$ colonoids express a regenerative stem cell signature. The expression of regenerative stem cell markers, *Clusterin* (*Clu*), *Annexin A1* (*Anxa1*) and *lymphocyte antigen 6 complex, locus a* (*Ly6a*) was compared between wild type and mutant colonoids and visualised using a heatmap. The colour scheme represents the scaled normalized expression level of the given gene in each cell as calculated by Seurat. Adjusted p-values for the enrichment of each gene in *Apc*$^{min/+}$ colonoid-derived cells compared with all other genotypes are stated at the end of each row.

To validate the RSC gene signature expressed by *Apc*$^{min/+}$ colonoid-derived cells, IF staining was performed (Figure 3.16).

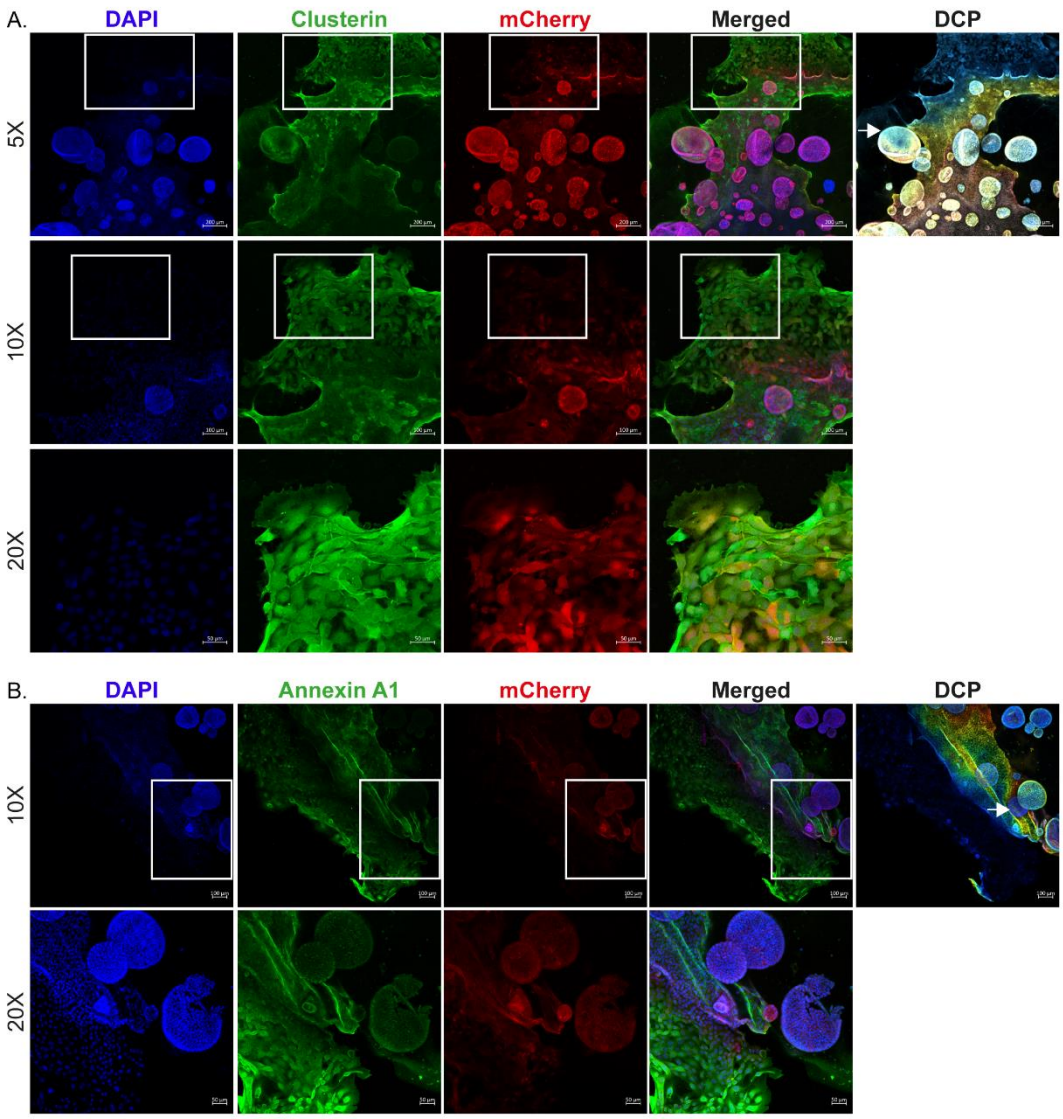


Figure 3.16. 2D eccentric *Apc*$^{min/+}$ colonoids stain positive for regenerative stem cell gene markers. *Apc*$^{min/+}$ colonoids were individually seeded in a 96-well plate and cultured for seven days before processing for IF staining. Representative IF images of **A.** Clusterin (green) and **B.** Annexin A1 (green) in fixed *Apc*$^{min/+}$ mCherry (red) colonoids, with nuclei counterstained with DAPI (blue). DCPs were generated from images taken using the 405 nm (DAPI) laser only. Images were acquired on a Zeiss 710MP confocal microscope using the 5X (scale bar represents 200 µm), 10X (scale bar represents 100 µm) or 20X (scale bar represents 50 µm) objective as indicated. White boxes represent the areas focused on in higher magnification images. The images are representative of three independent experiments.

IF staining showed that the 2D eccentric *Apc*$^{min/+}$ colonoids stained positive for both Clu (Figure 3.16. A) and Anxa1 (Figure 3.16. B) RSC markers. DCPs of the acquired confocal images revealed that Clu and Anxa1 positive 2D eccentric *Apc*$^{min/+}$ colonoids were located at the

bottom of the plate. While a few 3D cystic *Apc*$^{min/+}$ colonoids exhibited a degree of positive staining for Clu and Anxa1, this was only observed in colonoids which were near the bottom of the plate (white arrows) in a z-plane similar to that of the 2D eccentric *Apc*$^{min/+}$+ colonoids. Again, this could suggest that colonoids located at the bottom of the plate are experiencing an altered ECM stiffness leading to Yap activation and the expression of RSC marker genes.

As the Yap-induced RSC gene signature have been associated with the acquisition of a foetal gene signature, the dataset was next interrogated for markers of this primitive state, particularly for foetal genes known to be associated with the regenerating intestinal epithelium. For this reason, the expression of foetal genes associated with the regenerating colonic epithelium was examined between wild type and mutant colonoid-derived cells (Figure 3.17).

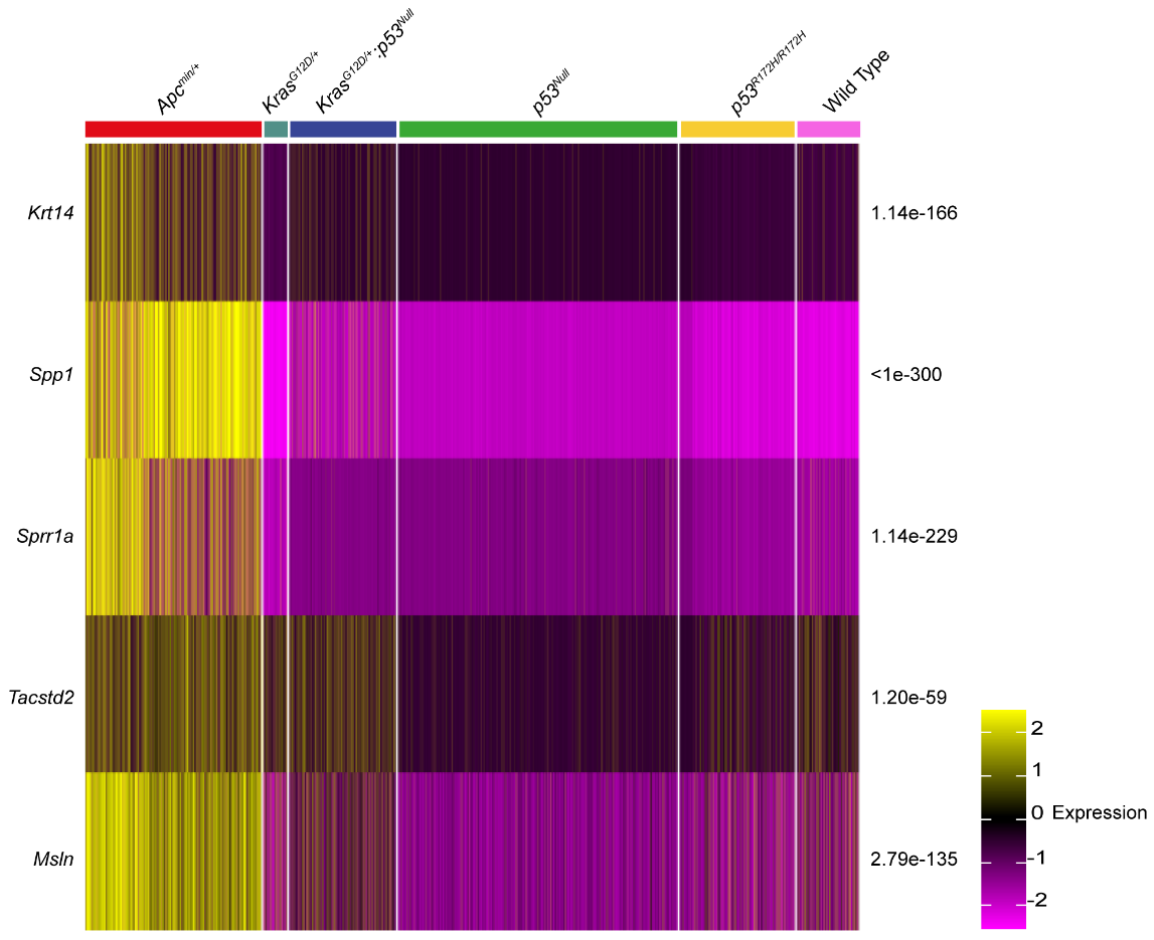


Figure 3.17. *Apc*$^{min/+}$ colonoids express a foetal gene signature. The expression of foetal gene markers, *keratin14* (*Krt14*), *osteopontin* (*Spp1*), *small proline rich protein 1A* (*Sprr1a*), *tumour-associated calcium signal transducer 2* (*Tacstd2*) and *mesothelin* (*Msln*) was compared between wild type and mutant colonoids and visualised using a heatmap. The colour scheme represents the scaled normalized expression level of the given gene in each cell as calculated by Seurat. Adjusted p-values for the enrichment of each gene in *Apc*$^{min/+}$ colonoid-derived cells compared with all other genotypes are stated at the end of each row.

This revealed that *Apc*$^{min/+}$ colonoid-derived cells showed much higher expression of foetal genes than other mutant genotypes, namely *Keratin 14* (*Krt14)*, *Osteopontin* (*Spp1*), *Small proline rich protein 1a* (*Sprr1a*), *Tumour-associated calcium signal transducer 2* (*Tacstd2*) and *Mesothelin* (*Msln*). *Spp1*, *Sprr1a* and *Msln* were overexpressed by *Apc*$^{min/+}$ colonoid-derived cells and to a lesser extent so were *Krt14* and *Tacstd2*.

To validate the foetal gene signature expressed by *Apc*$^{min/+}$ colonoid-derived cells, IF staining was once again performed (Figure 3.18). 2D eccentric *Apc*$^{min/+}$ colonoids stained positive for Spp1 (Figure 3.18. A), Sprr1a (Figure 3.18. B) and Krt14 (Figure 3.18. C) foetal markers. Similar to what was observed with the IF staining for Yap and RSC markers, DCPs of the acquired confocal images revealed that Spp1, Sprr1a and Krt14 positive 2D eccentric *Apc*$^{min/+}$ colonoids were located at the bottom of the z-stack and therefore the bottom of the plate. 3D cystic *Apc*$^{min/+}$ colonoids with positive staining for these foetal markers were near the bottom of the plate (white arrows) in a z-plane similar to that of the 2D eccentric *Apc*$^{min/+}$ colonoids.

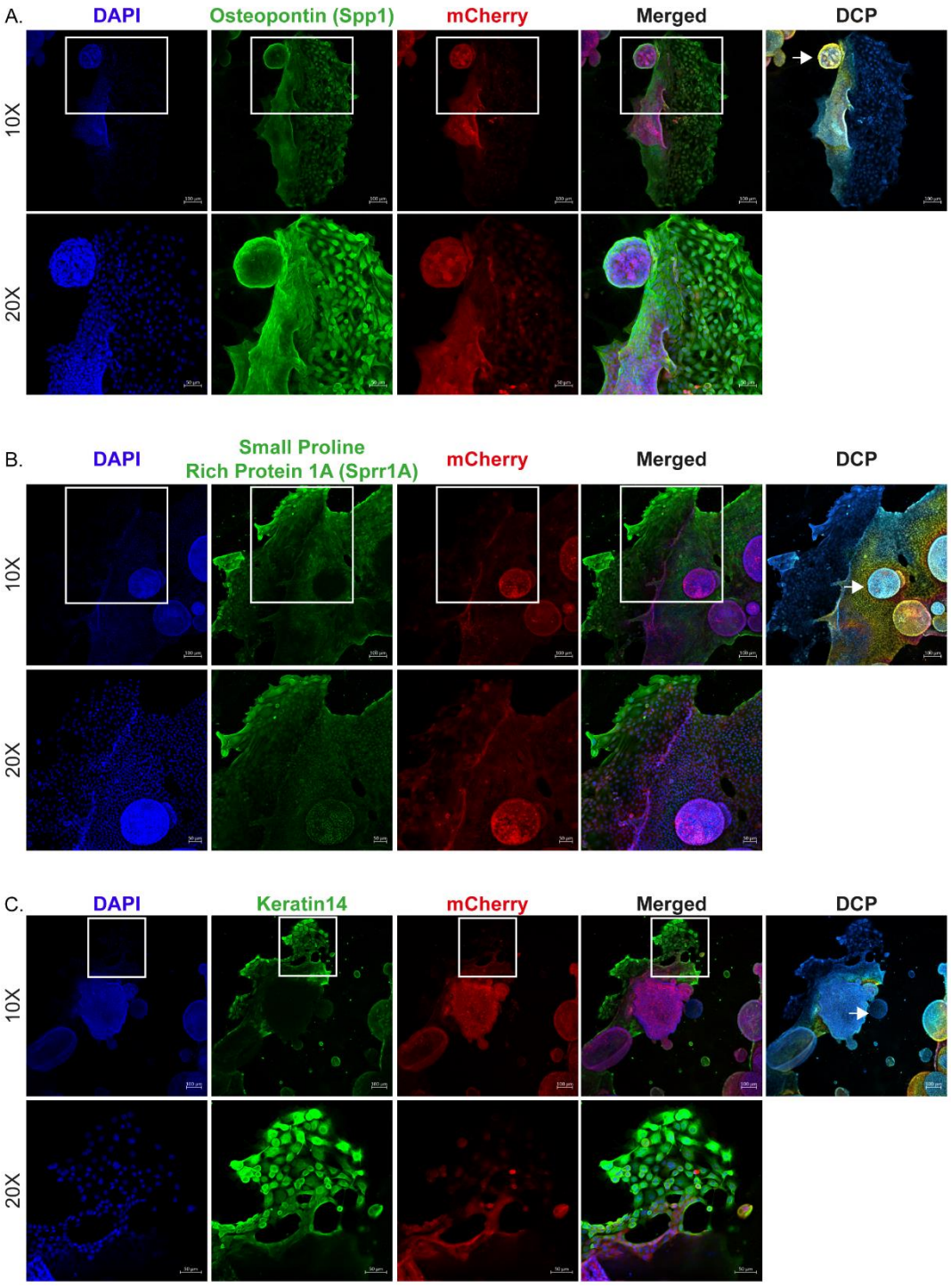


Figure 3.18. *Apc*$^{min/+}$ colonoids stain positive for foetal gene markers. *Apc*$^{min/+}$ colonoids were individually seeded in a 96-well plate and cultured for seven days before processing IF staining. Representative IF images of **A.** Osteopontin (Spp1, green), **B.** Small proline rich protein 1A (Sprr1A, green) and **C.** Keratin 14 (green) in fixed *Apc*$^{min/+}$ mCherry (red) colonoids, with nuclei counterstained with DAPI (blue). DCPs were generated from images taken using the 405 nm (DAPI) laser only. Images were acquired on a Zeiss 710MP confocal microscope using the 10X (scale bar represents 100 µm) or 20X (scale bar represents 50 µm) objective as indicated. White boxes represent the areas focused on in higher magnification images. The images are representative of three independent experiments.

In summary, Yap activation and induction of RSC and foetal gene signatures all appeared to be found in *Apc*$^{min/+}$ colonoids at the bottom of culture wells, particularly in colonoids showing a 2D eccentric phenotype unique to this driver mutation.

3.2.6. *Apc*$^{min/+}$ Colonoids Exhibit Altered Expression of ECM Remodelling and Tight Junction Proteins

In order to determine whether the 2D eccentric *Apc*$^{min/+}$ colonoids retained stem cell functionality and therefore the ability to form organoids, the colonoids were cultured past the usual passaging point to encourage the development of a 2D eccentric phenotype in a larger proportion of colonoids and were then reseeded before significant cell death was observed (Figure 3.19).

On day 12 (Figure 3.19. A), cell suspensions enriched for 2D eccentric *Apc*$^{min/+}$ colonoid-derived cells (represented by the blue cells in the DCP image) were reseeded and monitored. After the first reseed, 3D cystic *Apc*$^{min/+}$ colonoids had efficiently formed (Figure 3.19. B left) and were further observed until assuming a 2D eccentric phenotype again (Figure 3.19. B right). 3D cystic *Apc*$^{min/+}$ colonoids had efficiently formed by day six after the second reseed (Figure 3.19. C left), however by day 13 (Figure 3.19. C right) the colonoids detached from the Matrigel into the surrounding medium. It is unclear what this may represent, however it could suggest that extended periods of culture which promote the 2D eccentric phenotype acquired by *Apc*$^{min/+}$ colonoids ultimately reduces the stem cell functionality in *Apc* mutant cells.

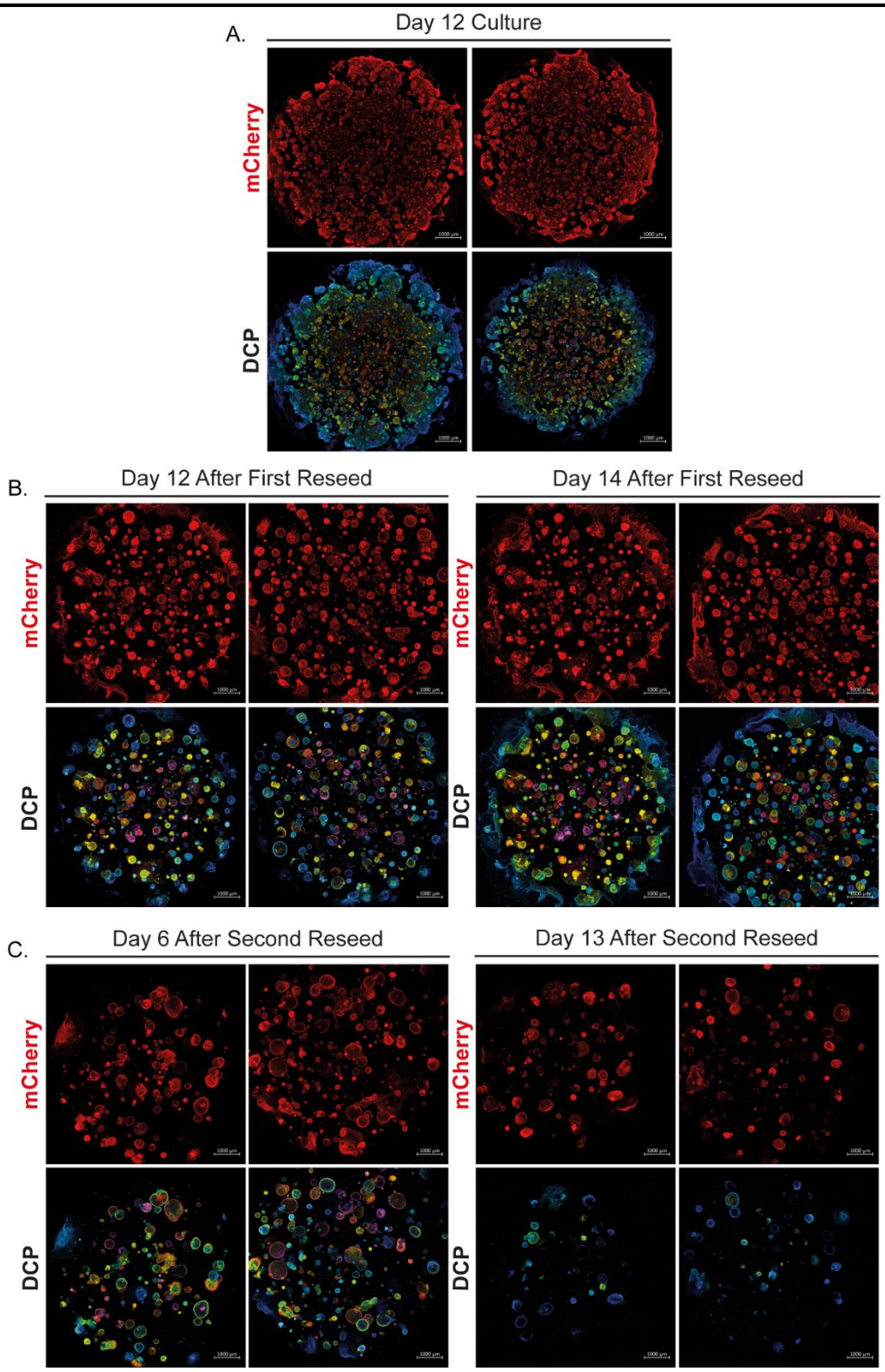


Figure 3.19. 2D eccentric *Apc*$^{min/+}$ colonoids lose the capacity to efficiently form organoids. *Apc*$^{min/+}$ colonoids were individually seeded in a 24-well plate and monitored until the majority had "flattened"/become eccentric. 2D eccentric colonoid-derived cells were separated from intact colonoids by centrifugation and reseeded. Representative images of **A.** Day 12 *Apc*$^{min/+}$ colonoid cultures before reseeding, **B.** Day 12 (left) and day 14 (right) *Apc*$^{min/+}$ colonoid cultures after the first reseed and **C.** Day 6 (left) and day 13 (right) *Apc*$^{min/+}$ colonoid cultures after the second reseed. DCPs were generated from images taken using the 594 nm laser used to acquire mCherry fluorescence. Images were acquired on a Zeiss 710MP confocal microscope using the 10X (scale bar represents 100 µm) objective. The images are representative of seven biological replicates.

The ability for *Apc*$^{min/+}$ colonoids to undergo significant phenotypic alterations and escape from the Matrigel suggested that these mutants may exhibit differences in the expression of ECM remodelling and tight junction associated proteins. Indeed, it is highly likely that the attachment to a 2D growth surface (the plate bottom) activates mechanotransduction and promotes the RSC molecular phenotype and foetal gene signature despite the presence of the *Apc* mutation.

Indeed scRNA-seq data revealed that a subset of *Apc*$^{min/+}$ colonoid-derived cells (far right cluster, see Figure 3.12) showed strong overexpression of *Matrix metalloproteinase 7* (*Mmp7*), a Mmp associated with ECM degradation and elevated Yap signalling (Figure 3.20. A)[306]. Furthermore, *Apc*$^{min/+}$ colonoid-derived cells had similarly lost the expression of tight junction proteins *Claudin 15* (*Cldn15*, Figure 3.20. B) and *Cadherin 17* (*Cdh17*, Figure 3.20. C). Among other targets, *Cdh17* expression is known to be regulated by the master intestinal differentiation marker Caudal-type homeobox transcription factor 2 (Cdx2), whose loss is correlated with metastasis and a poor prognosis in CRC patients[307-310]. Interestingly, *Apc*$^{min/+}$ colonoid-derived cells appeared to have lost the expression of *Cdx2*, which was highly expressed by cells from all other genotypes (Figure 3.20. D). This suggests *Apc*$^{min/+}$ colonoids show unique dysregulation of ECM interactions, which appears to be mediated through a variety of transcriptional mechanisms including a loss of *Cdx2* expression.

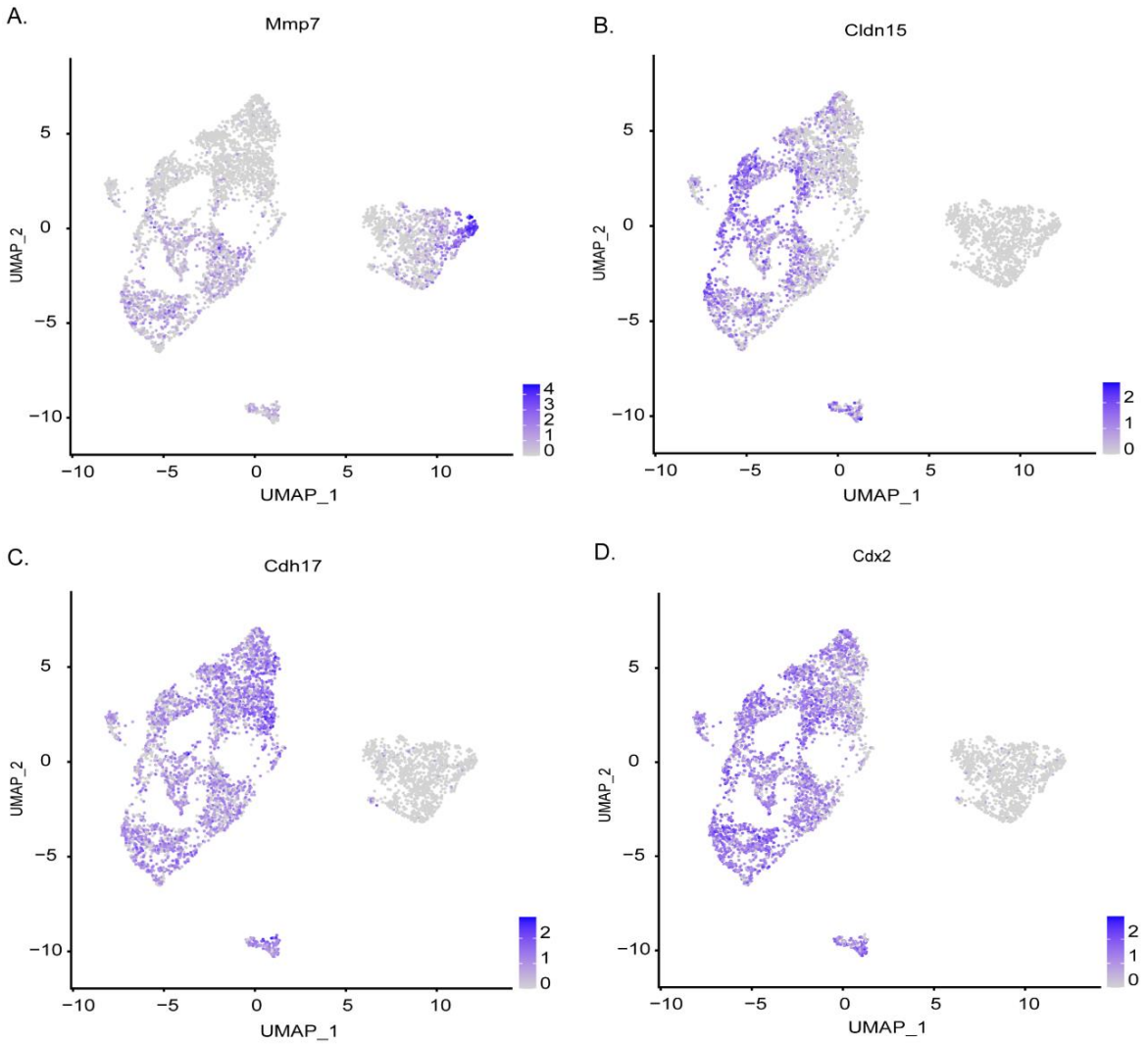


Figure 3.20. *Apc*$^{min/+}$ colonoids exhibit increased expression of ECM remodelling proteins and decreased expression of tight junction proteins. The expression of **A.** *Matrix metalloproteinase 7* (*Mmp7*), **B.** *Claudin 15* (*Cldn15*), **C.** *Cadherin 17* (*Cdh17*) and **D.** *Caudal-Type Homeobox Transcription Factor 2* (*Cdx2*) was visualised using FeaturePlot. Colour scale represents normalized expression values for each cell as calculated by Seurat.

Taken together these results highlight the impact that different CRC-associated driver mutations have on the gene expression of colonic stem cells. Furthermore, the distinct spatiotemporal dynamics and phenotypic alterations exhibited by the colonoids harbouring these mutations can be linked to the development of gene signatures associated with the activation of Yap signalling, alterations in stem cell molecular phenotype and ECM remodelling. This suggests that driver mutations set the phenotypic tone but the microenvironment can superimpose this.

These insights provide further information regarding the role that certain CRC-associated mutations play in CRC tumourigenesis and highlight potential targets for the development of novel therapeutics.

3.2.6. Discussion

The SAM analysis on colonoids harbouring CRC-associated driver mutations revealed that genetic alterations can indeed dysregulate cellular plasticity and induce morphological modifications. Here, we aimed to integrate phenotypic and transcriptomic analysis by determining whether the spatiotemporal dynamics identified and validated using the SAM algorithm were associated with changes to the gene expression profile of mutant colonoids. Ultimately, combining both phenotypic and transcriptomic analysis could further our understanding of CRC, highlight the molecular basis of disease and contribute to the prediction of suitable *in vivo* targets.

scRNA-seq on wild type and mutant colonoid-derived cells revealed the distinct effect that CRC-associated driver mutations can have on the transcriptional profiles of cells. Similar to the observations made following SAM analysis (Figure 3.6. C), $Apc^{min/+}$ and $Kras^{G12D/+}$ colonoid-derived cells clustered distinctly compared to the remaining genotypes. Furthermore, $Kras^{G12D/+}$:$p53^{Null}$, $p53^{Null}$ and $p53^{R172H/R172H}$ colonoid-derived cells showed a degree of overlap although to a lesser extent than was observed from the SAM analysis. These results highlight the importance of integrating phenotypic and transcriptomic analysis rather than relying solely on one readout.

Together with the apparent spatiotemporal dynamics displayed by $Apc^{min/+}$ colonoids, specifically the 2D eccentric phenotype adopted over time, a more in-depth analysis of the gene expression profile of the $Apc^{min/+}$ colonoid-derived cells was performed. This revealed that $Apc^{min/+}$ colonoid-derived cells had elevated expression of Yap target genes (*Ankrd1*, *Ccn2* and *Plaur*), exhibited an upregulation of the Yap signalling pathway and were characterised by a RSC and foetal gene signature associated with the expression of *Clu*, *Anxa1* and *Ly6a* and *Krt14*, *Spp1*, *Sprr1a*, *Tacstd2* and *Msln* respectively. These features appeared to be key

contributors to the transcriptional programmes differentiating *Apc*$^{min/+}$ colonoid-derived cells from cells derived from all other colonoid genotypes.

Following intestinal injury, a reversible Yap-driven process ensues whereby the CBC stem cell pool is replenished through the dedifferentiation of remaining cell types and acquisition of RSC and foetal gene markers[17,108,109,257]. In light of this, the findings presented in this chapter would suggest that *Apc*$^{min/+}$ colonoids are engaged in a Yap-mediated regenerative response[17,108]. Interestingly, the deletion of *Yap* in *Apc*$^{min/+}$ mice has been demonstrated to prevent adenoma formation, suggesting that the Yap-mediated regenerative response is commandeered during neoplasia to promote the progression of Apc-deficient foci to adenomas[18,311].

In a recent study, Gil Vasquez *et al.* utilised their phenotypic fitness landscape model (Figure 3.11) and mapped the distribution of the proposed stem cell index on TCGA lesions stratified by key CRC driver mutations[110]. This indicated that ligand independent Wnt mutations, including *APC*, were present in 84% of CBC and 35% of RSC predominant tumours. Similar results were observed in mouse tumours, where loss of or mutations in *Apc* was associated with a CBC signature. It is possible that the CBC molecular phenotype predominates in early *APC* mutant adenomas but as the lesion grows and the adenoma matrix alters then this induces a YAP-mediated shift in the polyp phenotype towards the RSC molecular phenotype. This has been supported by a study which found that CRC patient-derived organoids (PDOs) treated with a sublethal dose of chemotherapy were shown to acquire a persistent quiescent-like phenotype characterised by a YAP-dependent foetal gene signature which persisted even after DNA damage resolution[276]. These organoids displayed an enhanced *in vivo* metastatic capacity and predicted a poor prognosis for patients with stages II and III CRC. Through the incorporation of IF staining, further analysis of the mutant colonoid library revealed that Yap signalling was active in the morphologically distinct 2D eccentric *Apc*$^{min/+}$ colonoids which likewise stained for RSC and foetal gene markers. Depth-coloured projections (DCPs) on *Apc*$^{min/+}$ colonoid cultures revealed that the 2D eccentric colonoids were located at the bottom of the plate and had a unique capacity to escape 3D culture in the Matrigel, suggesting strong changes in how these colonoids interact with the ECM. Moreover, reseeded 2D eccentric

Apc$^{min/+}$ colonoids, similarly localised to the bottom of the plate, failed to efficiently form new colonoids and ultimately detached from the Matrigel. A similar result was observed by Cheung *et al.* which demonstrated that *Apc* knockout organoids with constitutive Yap activation lost their 3D cystic appearance after just three days of culture and failed to efficiently form organoids after passaging[312]. These *Apc* knockout organoids had decreased expression of Wnt target genes and presented with a regenerative gene signature marked by the expression of RSC makers *Anxa1* and *Ly6a*. Taken together, this would suggest that the RSC phenotypic shift induced in 2D eccentric *Apc*$^{min/+}$ colonoids is somehow imprinted and prevents subsequent 3D growth. In the phenotypic fitness landscape model proposed by Gil Vasquez *et al.* this finding would be represented by the skewing of the phenotype onto one molecular stem cell fitness peak preventing efficient reconstitution of the stem cell equilibrium that is necessary for outgrowth[110].

The ability for *Apc*$^{min/+}$ colonoids to undergo significant phenotypic alterations and escape from the Matrigel suggested that *Apc*$^{min/+}$ colonoids are involved in an ECM remodelling processes. Indeed, the expression of *Mmp7*, which has been associated with ECM degradation and elevated Yap signalling, was elevated in *Apc*$^{min/+}$ colonoid-derived cells[306]. It is well understood that Yap is a crucial mechanoreceptor which relays signals to the cell nucleus according to ECM rigidity and cell shape[313]. With this in mind, it is plausible that altered Wnt signalling and the absence of the β-catenin destruction complex characteristic of *Apc*$^{min/+}$ colonoids predisposes cells to a Yap-driven regenerative response and when coupled with a change in ECM rigidity (the bottom of the plate compared to Matrigel) Yap is free to translocate into the nucleus activating the expression of RSC and foetal gene markers as well as ECM remodelling proteins. It is highly likely that 2D growth activates mechanotransduction and pushes *Apc*$^{min/+}$ colonoids towards a RSC molecular phenotype despite the presence of the *Apc* mutation which has previously been reported as the strongest drive for the CBC phenotype[110]. This highlights the possibility that epithelial mutations set the underlying basal stem cell molecular phenotype but that microenvironmental influence (in this case mechanotransduction) can superimpose a phenotypic shift regardless of the mutation status.

Apc$^{min/+}$ colonoid-derived cells had also lost the expression of *Cdx2*, a marker of intestinal differentiation which when lost correlates with metastasis and a poor prognosis in CRC patients[308-310]. In accordance with the loss of *Cdx2* expression, *Apc*$^{min/+}$ colonoid-derived cells did not express *Cdh17*. Cdh17 is a cell adhesion molecule of the intestinal epithelium, regulated by Cdx2 and used as a prognostic marker for colonic adenocarcinomas where decreased *CDH17* expression correlates with high tumour grade, lympho-vascular permeation, lymph node metastasis and a poor prognosis[307,314,315]. Furthermore, *Apc*$^{min/+}$ colonoid-derived cells had lost the expression of another tight junction protein, namely *Cldn15*, which has similarly been observed to be downregulated in CRC patients[316]. Alterations in the expression of ECM remodelling and tight junction proteins, including *Cdh17* and *Cldn15*, are known to promote EMT of CRC and consequently increase cell motility[317-320]. This could indeed explain the increased mean speed displayed and validated by SAM analysis on *Apc*$^{min/+}$ time-lapse videos, and perhaps also the unique capability of *Apc*$^{min/+}$ organoids to escape the Matrigel. Furthermore, the increased cell motility could be promoting the Yap-mediated regenerative response by facilitating the *Apc*$^{min/+}$ colonoids in reaching an ECM of differing stiffness to the Matrigel (i.e. the bottom of the plate).

To note, a few 3D cystic *Apc*$^{min/+}$ colonoids stained positive for RSC and foetal gene markers. While the exact reason for this is unclear, the fact that these colonoids were located in similar z-planes as the 2D eccentric ones suggests that they may be in the process of transitioning towards a 2D eccentric phenotype.

In this chapter, a link between the spatiotemporal dynamics and gene expression profiles exhibited by colonoids harbouring CRC-associated driver alterations has been established. We show that the distinct spatiotemporal phenotype exhibited by *Apc*$^{min/+}$ colonoids is associated with a distinct transcriptional state unique to this mutation, which appears to be driven by a shift in stem cell molecular phenotype and alterations in expression of genes involved in ECM remodelling. These results suggest that microenvironmental influences and Yap activation are able to alter stem cell molecular phenotype regardless of the mutation status

and highlight the importance of combining both phenotypic and transcriptomic analyses in order to accurately model and understand CRC tumourigenesis and progression.

3.3. Investigating the Influence of CRC-Associated Driver Mutations on Gene Expression and Subclonal Dynamics in Colonoid Co-Culture Models

3.3.1. Introduction

CRC is a dynamic disease characterised by significant genetic diversity, clonal expansion and clonal selection[321,322]. The considerable intratumoural heterogeneity (ITH) exhibited by CRC tumours drives tumour evolution and fosters drug resistance leading to a poor prognosis for patients[234-238]. The unique ITH and clonal dynamics associated with CRC are elegantly described by the Big Bang model[233]. This model postulates that selective sweeps (clonal expansions that significantly alter the clonal composition of the final tumour) do not occur at the precancerous stage and thus ITH and diverse subclone populations arise early during tumour development. Following tumour formation, neutral evolution dominates and subsequent mutations are negatively selected against due to the spatial constraints conferred by the rapidly expanding clonal populations. To elucidate the role that CRC-associated driver mutations play in the progression from normal colonic epithelium to adenoma and carcinoma, including the mechanisms behind the development of the complex ITH seen in CRC, it is vital to understand how these diverse subclonal populations carrying different CRC driver mutations grow and interact during the early stages of tumour evolution.

Following the seminal study by Sato *et al.* in 2009 there have been rapid advances in the use of organoids models to study CRC tumourigenesis. One such development included the demonstration that patient-derived colonoids carrying targeted modifications in *APC*, *KRAS*, *TP53* and *SMAD4* grew efficiently in medium deprived of essential intestinal stem cell (ISC) niche growth factors, which are otherwise required for colonoid growth[139,156]. Furthermore, when xenotransplanted into mice, only those organoids which harboured mutations in all of the driver genes were able to form tumours reminiscent of invasive carcinomas. Through the use of more relevant orthotopic transplantation techniques it was later shown that these engineered mutant organoids were able to form lung and liver metastases in mice[186-189]. While these studies provided valuable insight into the importance of these driver genes in CRC, they did

not assess interactions between subclonal populations carrying individual driver mutations, and therefore may not accurately model the early stages of tumour formation.

Competitive cell interactions are essential in development and homeostasis; however they have also been implicated in promoting tumour growth. Evidence for this has been provided through time-lapse imaging of organoids formed by combining wild type organoid-derived cells and cancer organoid-derived cells each labelled with a different fluorescent protein[323]. Through careful observation it was found that the number of cancer cells, which harboured mutations in *Apc*, *Kras* and *Tp53,* increased over time and the number of wild type cells decreased. It was concluded that the cancer cells outcompeted the wild type cells via the induction of apoptosis, thus showing how competitive cell interactions can drive the expansion of tumours at the expense of normal tissues.

Interestingly, *Apc* mutant ISCs have recently been identified as “supercompetitors” in CRC tumour initiation and development[243]. It is proposed that *Apc* mutant ISCs establish clonal fixation (colonisation of an entire crypt) and initiate CRC through the secretion of Wnt antagonists which promote the differentiation and elimination of wild type ISCs by diminishing the Wnt-high stem cell niche required for wild type ISC maintenance. Notum has been identified as one likely mediator of this competitive effect through Wnt antagonism, as conditioned medium from *Apc* mutant organoid cultures suppressed the growth of wild type organoids, but this inhibitory effect was abrogated when Notum was inhibited[244]. Moreover, the knockout of *Notum* in *Apc* mutant mice resulted in a decrease in intestinal tumour burden and an increase in the experimental endpoint time from 60 to 85 days.

Another example of mutant-specific competitive interactions as a mechanism of tumour progression was identified by Yum *et al*., whereby *Kras* mutant crypts modified the cellular organisation of neighbouring wild type crypts and reduced ISC activity through the secretion of BMP ligands[324]. This resulted in an increased proportion of differentiation in wild type crypt cells and therefore an increased proportion of mutant cells relative to stem and transit-amplifying (TA) cells.

In addition to competitive cell interactions, cooperation between mutant cells seems to also play a role in CRC. Conditioned medium transferred from cetuximab treated *KRAS* mutant human CRC cells to *KRAS* wild type human CRC cells decreased the effectiveness of drug treatment[245]. This was proven to be due to the paracrine secretion of Transforming growth factor α (TGFα) and amphiregulin (AREG) by *KRAS* mutant cells. TGFα and AREG are Epidermal growth factor receptor (EGFR) ligands which by binding to the EGFR provide protection against EGFR targeting therapeutics. Furthermore, CRC cells cultured in the conditioned medium from oxaliplatin treated chemo-resistant cells displayed increased survival than those cultured in standard culture medium. This finding was associated with the secretion of Progranulin by the chemo-resistant human CRC cells which activates the EGF pathway to promote cell proliferation[325].

The above outlined literature has undoubtedly contributed to our knowledge on the subclonal interactions which may contribute to CRC tumourigenesis, however there is still a distinct lack of organoid co-culture protocols which more closely reconstruct the spatial architecture of subclonal interactions within defined colonic crypt structures that occur during early tumourigenesis. Furthermore, there is a lack of research which investigates the behaviour of single-driver mutants when combined with a different single-driver mutant, despite that likely being an important occurrence during early CRC tumourigenesis. Models which address these issues would support the thorough investigation of direct subclonal interactions and in doing so more accurately mimic ITH, giving researchers a better opportunity to understand and counteract its role in mediating treatment resistance.

One attempt to model these interactions has been developed using 3D cell aggregates or spheroids. Andersen *et al.* developed a co-culture model between cerebral cortex spheroids and cervical spinal cord spheroids in an attempt to study cortical circuits[326]. These “cortico-spinal assembloids” sustained long-term culture and supported the establishment of synaptic connections between cortical and spinal neurons. Cortico-spinal assembloids were further cultured with skeletal muscle spheroids to form three-part patterned “cortico-motor assembloids” which efficiently formed connections between spinal-derived motor neurons and

the muscle spheroids. This work highlights the capacity for 3D cultures to self-assemble and form functional systems for the study of development and disease, properties which could be particularly useful in the study of CRC subclonal interactions.

Assessing the impact of subclonal spatial interactions is limited by the difficulty in placing subclonal populations into defined arrangements using traditional laboratory techniques. To overcome these limitations, the Bayley laboratory have developed a sophisticated lipid-bilayer-supported printing technique whereby droplets containing cells and biocompatible ECM (collagen or Matrigel) are printed in a predefined pattern into a lipid bath[252,253]. This method allows cellular material to be layered into complex 3D structures with high resolution resembling the architecture of native tissues[327]. After printing, removal of the lipid bath surrounding the cellular material results in the formation of a unified material which supports intercompartmental interaction. This technique has been further modified for the bioengineering of gastrointestinal (GI) tissues using organoids[254]. Human duodenal organoids were embedded in collagen and printed into lipid immersed tubular moulds reminiscent of the tubular intestinal structure. The organoids were observed to migrate to the luminal surface of the collagen tubes and fuse to form a continuous epithelial layer similar to that of the intestinal epithelium. Furthermore, these collagen tubes were adapted to contain fibroblasts plated at a range of densities, whose contraction over time formed intricate structures that recapitulated the change in lumen diameter present throughout the GI tract. These fabricated tubes supported the growth of gastric and colon epithelial cancer cells which, similar to the duodenal organoids, formed a continuous layer lining the lumen of the tube.

The development of a CRC organoid model which utilises this technology and allows for spatial control and patterning could contribute to the understanding of direct subclonal interactions and how these interactions influence ITH during tumour development.

3.3.2. Chapter Aim

Model intratumoural heterogeneity and changes in gene expression induced by subclonal interaction using co-cultured mutant colonoids assembled with novel cell patterning techniques.

scRNA-seq on mutant colonoids revealed the unique gene expression profiles associated with each genotype when grown alone under standard conditions. In this chapter we aim to incorporate scRNA-seq and lipid-bilayer-supported printing techniques to investigate the influence of co-culture conditions on the gene expression profiles and subclonal dynamics exhibited by the mutant colonoids. These methods will allow us to assess the development of ITH during early tumour progression under more physiological conditions than previous methods have allowed.

It is important to note that the results contained within this chapter do not contain *Kras*$^{G12D/+}$ EYFP colonoids. These colonoids were generated after the completion of the below described experiments.

3.3.3. The Behaviour and Gene Expression of Mutant Colonoids is Altered Under Co-Culture Conditions

While the growth of *Apc* mutant organoids is independent of Wnt supplementation, *Kras* and *Tp53* single mutants organoids cannot survive in medium lacking Wnt[328-330]. Accordingly, in this study, the standard culture medium for *Apc* mutant colonoids lacked Wnt and the standard culture medium for *Kras* and *Tp53* mutant colonoids contained 50% Wnt (final volume, described in section 2.1.1).

To allow for assessment of the effect mutant colonoids may have on one another when grown in co-culture, a suitable medium was first developed which could support the growth of colonoids containing each common CRC driver mutation. The literature is clear that Wnt supplementation is a key aspect to balance when preparing a co-culture medium suitable for colonoids with common CRC driver mutations. Importantly, organoids which harbour mutations in *Apc*, *Kras* and *Tp53* in the same cell do not require Wnt supplementation to drive expansion

due to the constitutive activation of the Wnt pathway associated with the *Apc* mutation[139,156]. Taking this knowledge into account, the single mutant colonoids were co-cultured in medium supplemented with 10% Wnt (final volume, described in section 2.1.1). This concentration was chosen as it would not inhibit the growth of *Apc*$^{min/+}$ colonoids and would be sufficient in sustaining the growth of *Kras* and *Tp53* mutant colonoids which would also be exposed to paracrine signalling from *Apc*$^{min/+}$ colonoids.

An organoid formation assay (OFA) was first performed to determine whether the identified co-culture medium significantly altered the organoid forming ability of the mutant colonoids (Figure 3.21. A). Due to the intra-experimental variation associated with the OFA (described in Figure 3.4), the results from two independent repeats have been plotted and analysed separately (Figure 3.21. B and C). The results from each experiment exhibited the same trends and revealed that compared to the standard culture medium for each mutant genotype (described in section 2.1.1), the co-culture medium did not significantly change the organoid forming ability of the mutant colonoids on day 3 (Figure 3.21. B(i) – C(i)), day 5 (Figure 3.21. B(ii) – C(ii)) or day 7 (Figure 3.21. B(iii) – C(iii)).

Notably, there tended to be a trend towards reduced organoid forming ability of the mutant colonoids when grown in the co-culture medium in comparison to their organoid forming ability in standard culture medium. While this is important to be aware of, a slight reduction is to be expected, as the co-culture medium was established in order to take into account the paracrine signalling between mutants grown under co-culture conditions which would not be present when grown under standard culture conditions. Colonoids harbouring multiple CRC-associated mutations as well as those derived from CRC tumours have been shown to grow independently of niche factors usually essential for wild type or single mutant colonoids[139,156]. Thus it is not surprising that the co-culture medium slightly reduced the organoid forming ability of mutant colonoids as essential paracrine signalling from the other mutants and niche factors usually present in the standard culture medium would be absent. Notably, the co-culture medium did not result in the death of the mutant colonoids. Taken together, the co-culture medium was deemed adequate for use in future experiments.

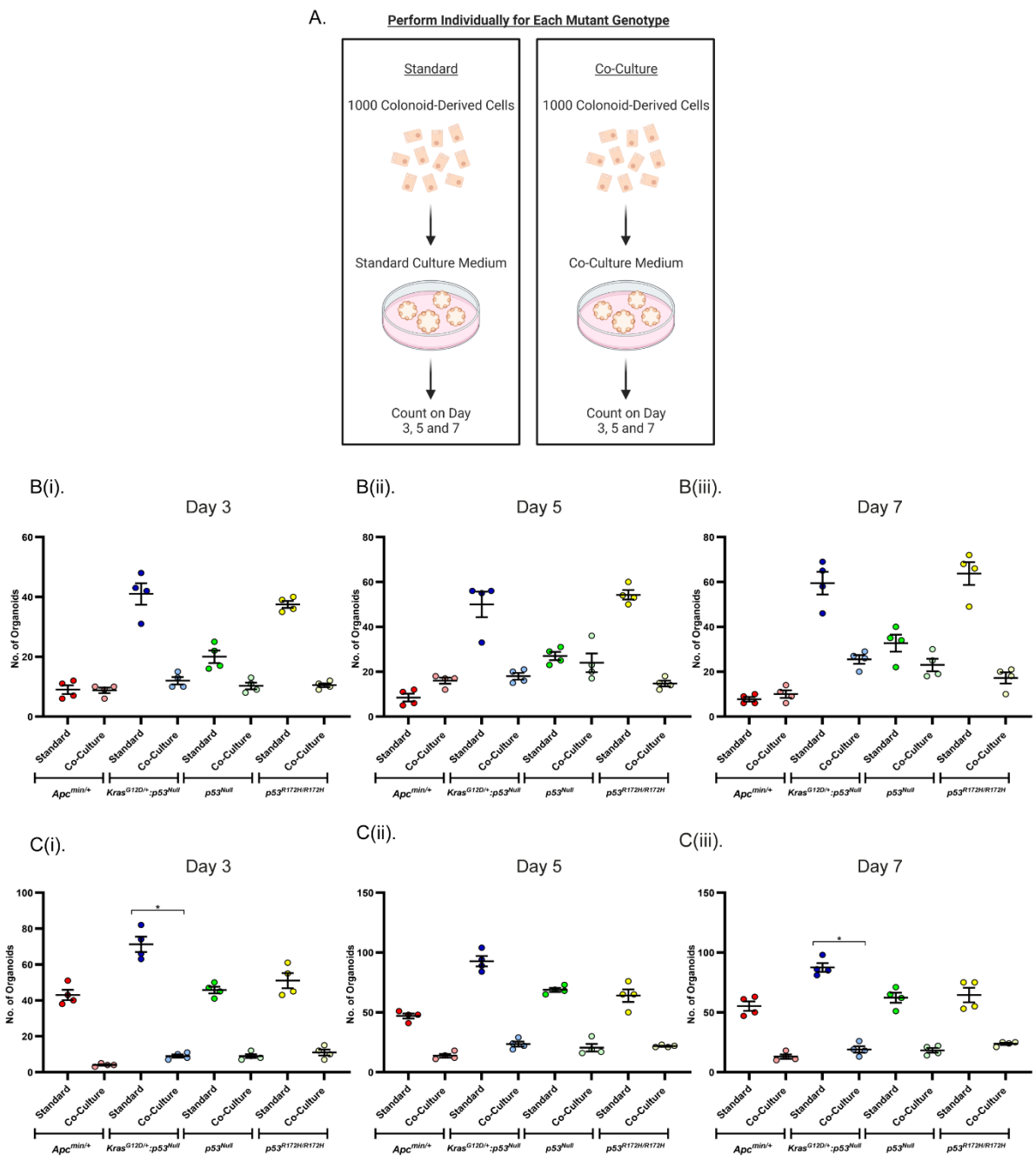


Figure 3.21. Co-culture medium does not significantly alter the organoid forming ability of mutant colonoids. An organoid formation assay (OFA) was performed to investigate the influence of the identified co-culture medium on the ability of the individual mutant colonoids to form an organoid from a single cell. **A.** 1000 single cells were plated in a 24-well plate in a flat matrigel bed, overlayed with standard or co-culture medium and counted at **B(i)-C(i).** Day 3, **B(ii)-C(ii).** Day 5 and **B(iii)-C(iii).** Day 7. **B-C.** Shows the data from two independent experiments each performed in quadruplicate and analysed separately. The data were analysed using GraphPad Prism 9 and a Kruskal-Wallis test was performed with p-value correction for multiple testing *p<0.05 **p<0.01 ***p<0.001. Error bars represent Standard Error of the Mean (SEM).

Once this suitable co-culture medium had been identified and characterised, additional OFAs were conducted to determine whether mutant colonoid behaviour was altered when grown in co-culture with other mutant colonoid genotypes (Figure 3.21).

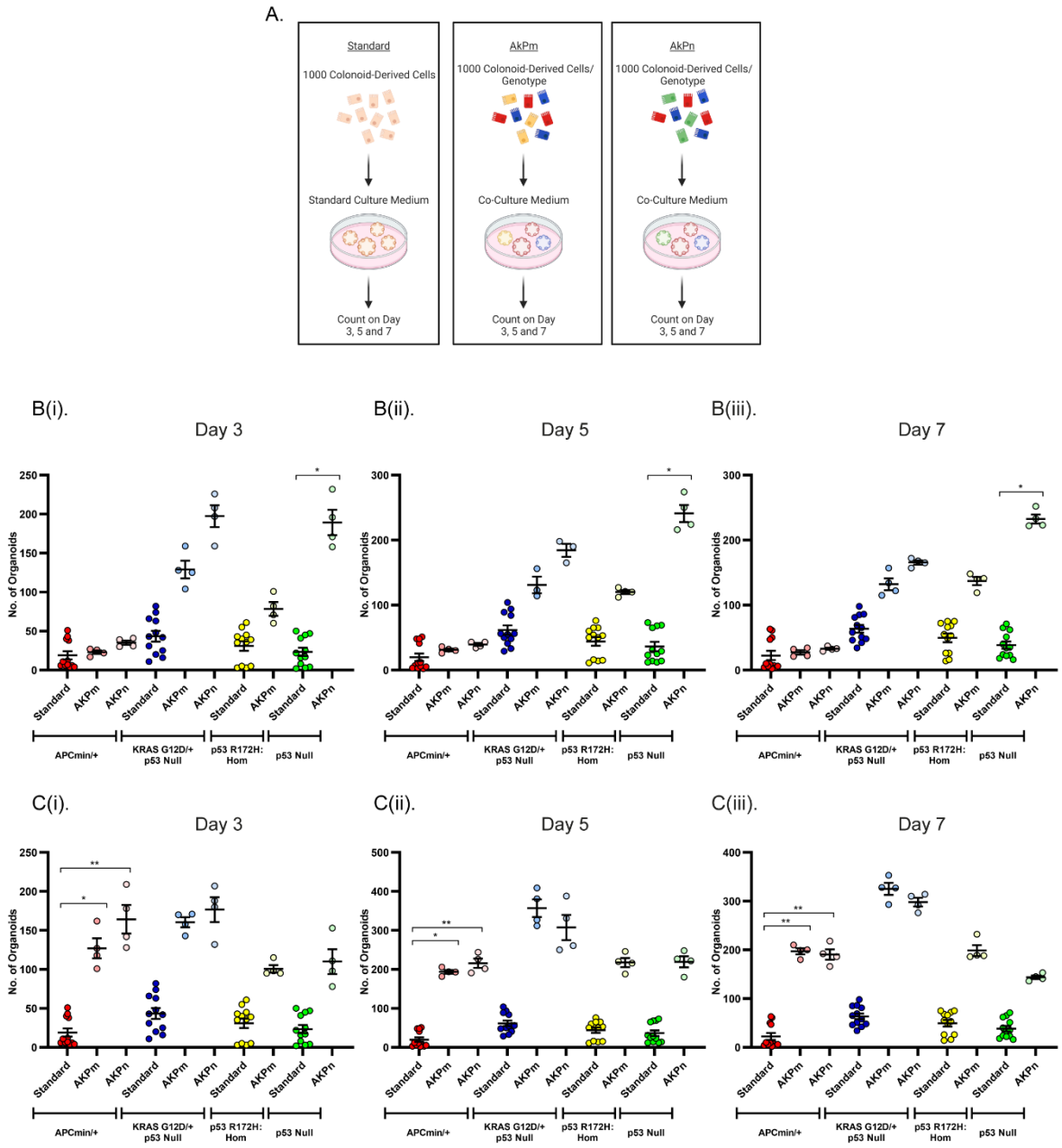


Figure 3.22. Mutant colonoids have altered organoid forming ability when grown in co-culture. An OFA was performed to investigate differences in the ability of mutant colonoids to form an organoid from a single cell when grown in co-culture with other mutants. **A**. 1000 single cells per genotype were either cultured alone under standard conditions (left panel) or mixed together to form AKPm (middle panel) and AKPn (right panel) co-cultures. Colonoid-derived cells were plated in a 24-well plate in a flat matrigel bed, overlayed with standard or co-culture medium and counted at **B(i)-C(i).** Day 3, **B(ii)-C(ii).** Day 5 and **B(iii)-C(iii).** Day 7. **B-C.** Shows the data from two independent experiments each performed in quadruplicate and analysed separately. The data were analysed using GraphPad Prism 9 and a Kruskal-Wallis test was performed with p-value correction for multiple testing *p<0.05 **p<0.01 ***p<0.001. Error bars represent SEM. Refer to Figure 3.4 for statistical comparisons between the organoid forming ability of mutant colonoids grown under standard conditions.

To achieve this, equal numbers of *Apc*$^{min/+}$, *Kras*$^{G12D/+}$*:p53*^{Null} and *p53*$^{R172H/R172H}$ (referred to as AKPm) and *Apc*$^{min/+}$, *Kras*$^{G12D/+}$*:p53*^{Null} and *p53*^{Null} (referred to as AKPn) colonoid-derived single cells were mixed together and newly formed colonoids of each genotype were counted over the course of a week using a confocal microscope (Figure 3.22. A). Due to the intra-experimental variation associated with the OFA (described in Figure 3.4), the results from two independent repeats have been plotted and analysed separately (Figure 3.22. B and C). The results from each experiment exhibited the same trends and showed that each mutant genotype formed more colonoids when grown in the presence of other mutants compared to when grown under standard conditions. Similar to the results from the OFA of mutant colonoids grown under standard culture conditions (Figure 3.4), *Kras*$^{G12D/+}$*:p53*^{Null} colonoids had the highest organoid forming ability compared to the other mutants, while *Apc*$^{min/+}$ colonoids had the lowest. In comparison, *p53*$^{R172H/R172H}$ and *p53*^{Null} mutant colonoid genotypes had an intermediate organoid forming ability. These results do not provide evidence of predominant subclonal competition between mutant populations, but instead suggest that subclonal cooperation is a key dynamic present between subclonal populations carrying different driver mutations, and likely contributes to a more aggressive tumour phenotype.

Given the striking evidence for subclonal cooperation seen above, gene expression profiles were next assessed to determine the mechanisms responsible for these effects. Accordingly, the influence of co-culture conditions on the gene expression profile of the different mutant colonoids was investigated. Mutant colonoid co-cultures were grown for seven days and subjected to scRNA-seq (Figure 3.23).

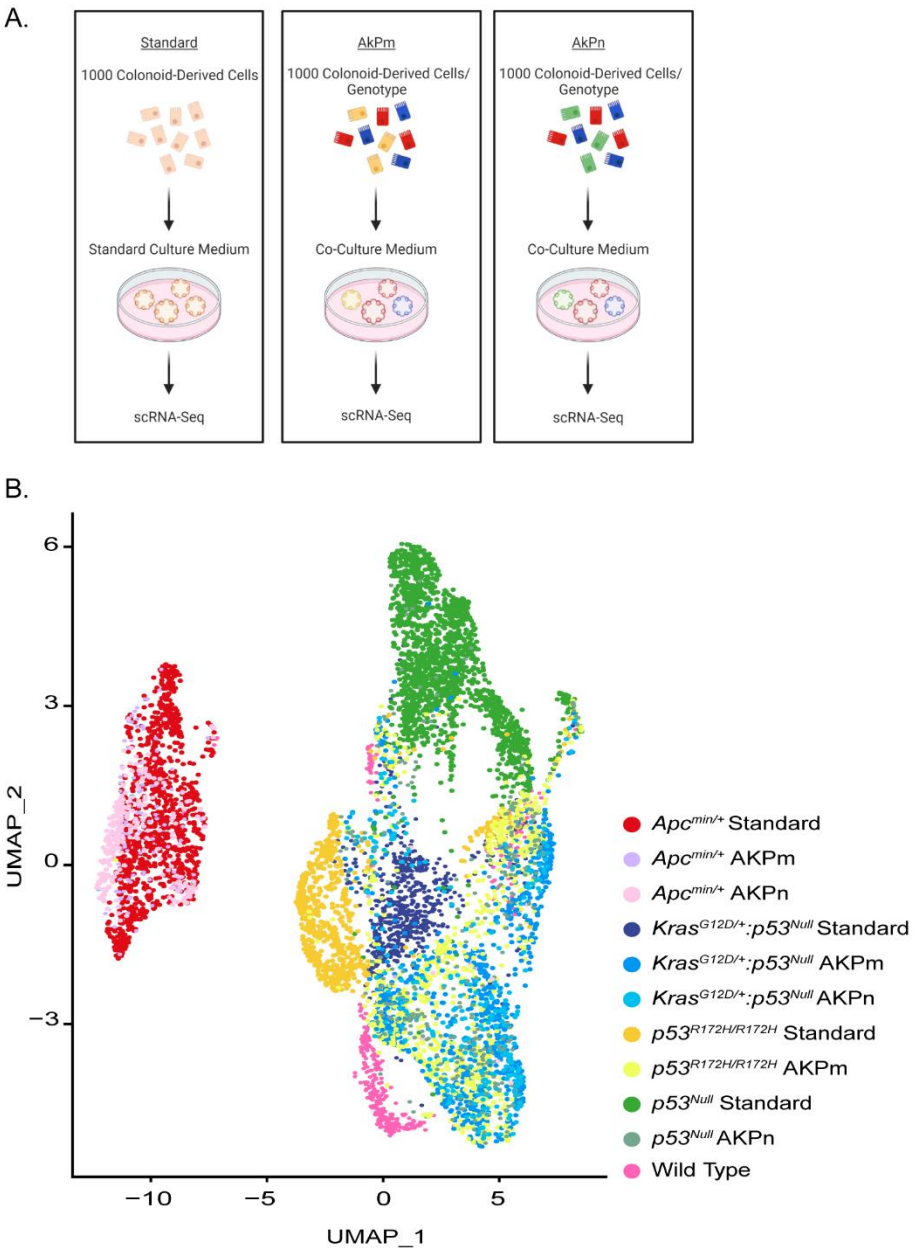


Figure 3.23. Gene expression profiles of mutant colonoids grown under standard and co-culture conditions. A. 1000 single cells per genotype were either cultured alone under standard conditions (left panel) or mixed together to form AKPm (middle panel) and AKPn (right panel) co-cultures. Colonoid-derived cells were plated in a 384-well plate, overlayed with standard or co-culture medium and cultured for seven days before processing. **B.** UMAP clustering of colonoid-derived cells grown in single or co-culture conditions. scRNA-seq was conducted using a 5' scRNA-seq gene expression workflow. Sequencing of final libraries was conducted on the Illumina NextSeq 550 and data analysis was conducted using Cell Ranger and Seurat. Analysis performed by Thomas Carroll and Brittany-Amber Jacobs.

For ease of comparison between standard and co-culture conditions, the UMAP clustering of the different genotypes was individually visualised (Figure 3.24).

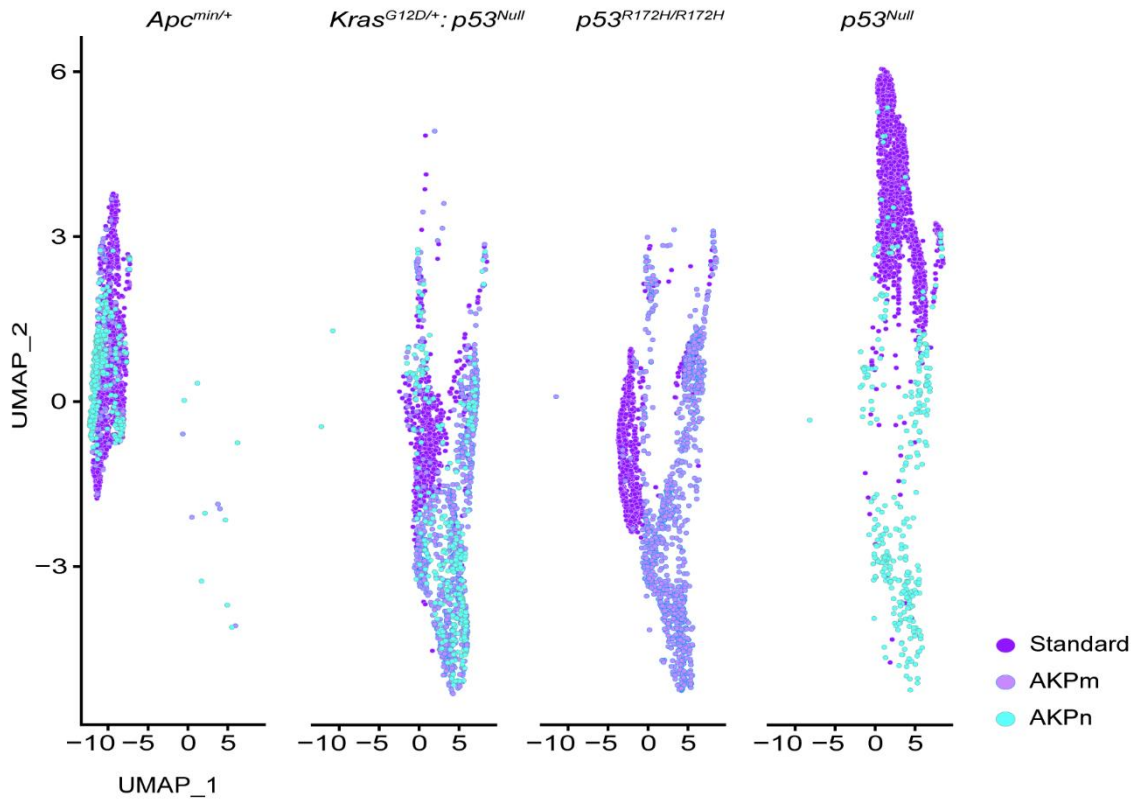


Figure 3.24. Gene expression profiles of mutant colonoids vary between standard and co-culture conditions. Variations in the clustering of mutant colonoid-derived cells when grown under standard versus co-culture conditions per genotype.

Apc$^{min/+}$ colonoid-derived cells from both AKPm and AKPn co-cultures were observed to cluster similarly to those grown under single culture conditions suggesting that the co-culture conditions had little effect on the gene expression profile of *Apc*$^{min/+}$ colonoids. In contrast, the gene expression profiles of *Kras*$^{G12D/+}$*:p53*^{Null}, *p53*$^{R172H/R172H}$ and *p53*^{Null} colonoid-derived cells were strikingly different between standard and co-culture conditions. Interestingly, while the gene expression profile of *p53*$^{R172H/R172H}$ and *p53*^{Null} colonoid-derived cells grown in standard culture were vastly different from one another, the gene expression profiles of these cells were comparable under co-culture conditions suggesting their phenotypes converge only in the presence of subclones carrying other driver mutations. Furthermore, *Kras*$^{G12D/+}$*:p53*^{Null} colonoid-derived cells from AKPm co-cultures clustered similarly to those from AKPn co-culture as well as those from *p53*$^{R172H/R172H}$ (AKPm) and *p53*^{Null} (AKPn).

It is important to note that this experiment did not include scRNA-seq data from single mutant colonoids cultured in the co-culture medium. Without this control it is not possible to conclude with absolute certainty that the changes in gene expression observed between culture conditions are a result of the presence of other mutants or a result of the co-culture medium. However, when coupled with the increasing organoid formation potential of each genotype seen in co-culture, it is likely that the major changes seen in transcriptomes of most mutants under co-culture conditions are driven at least in part by the same phenotypic changes that increase organoid formation potential in response to signalling from other subclonal populations.

To assess the transcriptomic changes behind the increasing OFA potential of each mutant seen under co-culture conditions, the top ten upregulated genes expressed by each mutant genotype were compared between culture conditions (Figure 3.25). While *Apc*$^{min/+}$ colonoid-derived cells appeared in similar regions of the UMAP plot following dimensionality reduction in both standard and co-culture conditions, there was still strong differential expression in a number of genes between these groups. This included decreased expression of the RSC marker *Clu* and foetal gene markers *Krt14* and *Sprr1a* in AKPm and AKPn co-cultured colonoid-derived cells (Figure 3.25. A). Intriguingly, these cells also had decreased average expression of columnar epithelial markers *Kerartin19 (Krt19)*, *Keratin8 (Krt8)* and *Keratin18* (*Krt18)*. Co-cultured *Apc*$^{min/+}$ colonoid-derived cells had an increased average expression of several interesting genes compared to those from standard cultures. The colonoid-derived cells from AKPm co-cultures had increased average expression of cell cycle regulator *Cdkn1a* (p21) and *growth differentiation factor 15 (Gdf15)* which have been shown to promote EMT and metastasis in CRC[331,332]. The colonoid-derived cells from AKPn co-cultures had increased average expression of colonic epithelial markers *carbonic anhydrase 1* (*Car1)* and *carbonic anhydrase 2 (Car2)* and *Basigin (Bsg)* which has been shown to promote CRC cell migration, proliferation and invasion[333,334]. These findings suggest the loss of the standard RSC and foetal molecular phenotype in favour of a more aggressive phenotype which could promote tumour progression.

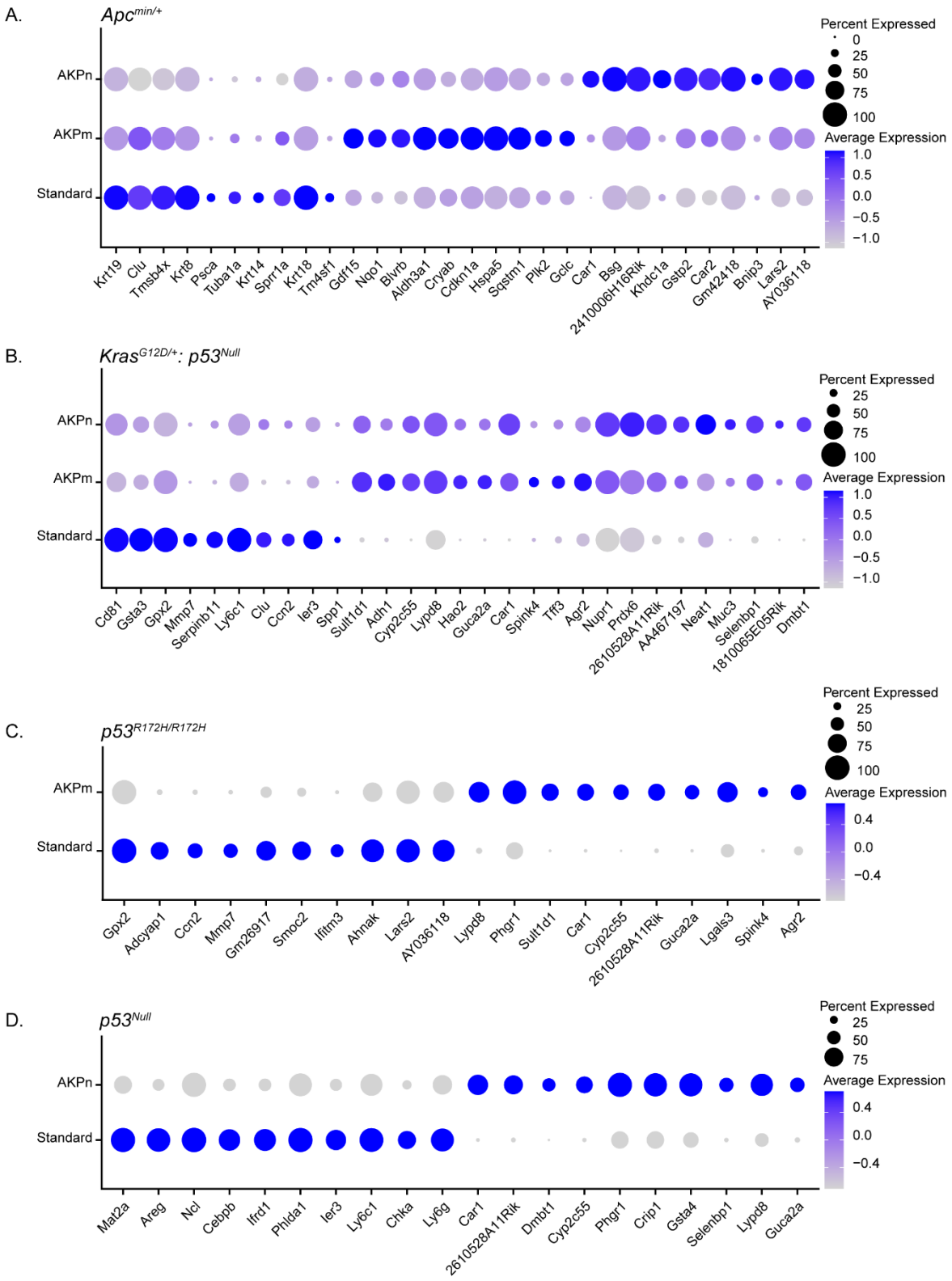


Figure 3.25. Top upregulated genes expressed by mutant colonoids varies between standard and co-culture conditions. Wild type and mutant colonoids were seeded as single or co-cultures in a 384-well plate and cultured for seven days before processing. scRNA-seq was conducted using a 5' scRNA-seq gene expression workflow. Sequencing of final libraries was conducted on the Illumina NextSeq 550 and data analysis was conducted using Cell Ranger and Seurat. The top ten upregulated genes expressed by **A.** *Apc*$^{min/+}$, **B.** *Kras*$^{G12D/+}$*:p53*^{Null}, **C.** *p53*$^{R172H/R172H}$ and **D.** *p53*^{Null} colonoid-derived cells was compared between single and co-culture conditions and visualised by DotPlot. All genes shown displayed highly significant differences between co-culture and standard conditions (all adjusted p-values < 8.77e-01).

Kras$^{G12D/+}$*:p53*^{Null}, *p53*$^{R172H/R172H}$ and *p53*^{Null} colonoid-derived cells displayed even more distinct differences in expression between standard and co-culture conditions for the top differentially expressed genes. Co-cultured *Kras*$^{G12D/+}$*:p53*^{Null} colonoid-derived had decreased average expression levels of *Clu*, foetal gene marker *Spp1*, ECM remodelling protein *Mmp7* and Yap target gene *Ccn2* (Figure 3.25. B). Furthermore, these cells had increased average expression levels of *Car1*, goblet cell (GC) markers *trefoil factor 3 (Tff3), Arginase 2 (Arg2), serine peptidase inhibitor kazal type 4 (Spink4)* and *mucin 3 (Muc3)* and *deleted in malignant brain tumours 1 (Dmbt1)* which serves as a negative prognostic marker in CRC[53,335]. These results suggest the loss of RSC and foetal gene markers in favour of specific lineage markers and markers of a more aggressive CRC phenotype.

Co-cultured *p53*$^{R172H/R172H}$ colonoid-derived cells had decreased average expression levels of *Mmp7* and *Ccn2* and increased average expression levels of *Car1*, *Arg2* and *Spink4* (Figure 3.25. C). Interestingly, these cells also had increased average expression levels of *Ly6/Plaur domain containing 8 (Lypd8)* which has proven to play a tumour suppressive role in CRC[336]. These findings highlight that very similar phenotypic changes are induced in co-cultured *p53*$^{R172H/R172H}$ colonoids as seen in *Kras*$^{G12D/+}$ colonoids, although the phenotype may be slightly less aggressive due to the upregulation of tumour suppressive genes. This matches the results of the OFA assays, where *Kras*$^{G12D/+}$ colonoids tended to exhibit higher OFA in co-culture than *p53*$^{R172H/R172H}$ colonoids.

Co-cultured *p53*^{Null} colonoid-derived cells had decreased average expression of epidermal growth factor receptor (Egfr) ligand *Areg*, with increased average expression levels of *Car1*, *Dmbt1* and *Lypd8* (Figure 3.25. D)[337]. Notably *Car1* and *Lypd8* were also upregulated by co-culture for *p53*$^{R172H/R172H}$ mutants, suggesting these genes could help drive the converging phenotypes of these cells in co-culture as assessed by UMAP.

Additional top differentially expressed genes from these analyses which were not discussed in this section but do have a known role in CRC have been summarized in Table 3.1.

Table 3.1. Significance of the top upregulated genes expressed by each genotype between culture conditions not focused on in this study.

Colonoid Genotype	Culture Condition	Gene Name	Significance in CRC
Apc$^{min/+}$	Standard	Tmsb4x	Marker of poor prognosis[338]
		Tm4sf1	Promotes EMT and stemness[339]
	AKPm	Nqo1	Marker of poor prognosis[340]
		Cryab	Tumour suppressor functions[341]
		Hspa4	Promotes development by inhibiting ferroptosis[342]
		Sqstm1	Inhibits apoptosis and promotes cell proliferation[343]
		Plk2	Marker of poor prognosis[344]
Kras$^{G12D/+}$; *p53*^{Null}	Standard	Cd81	Promotes EMT[345]
	AKPm and AKPn	Nupr1	Promotes tumour growth[346]
		Prdx6	Promotes EMT[347]
		Neat1	Marker of poor prognosis[348]
		Selenbp1	Tumour suppressor functions[349]
p53$^{R172H/R172H}$	Standard	Adcyap1	Associated with shorter disease-free survival time[350]
		Smoc2	Tumour suppressor[351]
		Ifitm3	Promotes progression and metastasis[352]
		Ahnak	Tumour suppressor[353]
	AKPm	Phgr1	Marker of lymph node metastasis[354]
		Lgals3	Promotes metastasis[355]
p53^{Null}	Standard	Mat2a	Promotes metastasis and invasion[356]
		Ncl	Promotes proliferaton[357]
		Cebpb	Decreases tumour growth, migration and invasion[358]
		Ifrd1	Marker of poor prognosis[359]
		Phlda1	Promotes tumour growth[360]
		Chka	Marker of poor prognosis[361]
	AKPn	Phgr1	Marker of lymph node metastasis[354]
		Crip1	Promotes migration and invasion[362]
		Gsta4	Marker of invasive carcinomas[363]
		Selenbp1	Tumour suppressor functions[349]

3.3.4. Mixed Colonoids: A Novel Organoid Co-Culture Model

The scRNA-seq of mutant colonoid-derived cells which had been co-cultured with other mutant colonoids revealed that the different mutants are likely altering the expression profiles and thus the phenotype of one another. These findings warranted further investigation into the subclonal dynamics present between mutant colonoids, and how they are affected by variation in spatial architecture and their physiological microenvironment. Such a model does not currently exist; therefore, as a first step towards this goal, a novel organoid co-culture model based on the droplet-based printing approaches from the Bayley laboratory was developed to facilitate spatial control and patterning of fluorescently labelled mutant colonoids. This represents a significant advance over the simple co-culture of mutant colonoids, as mutant colonoid cells can be placed in defined arrangements and proportions to combine into a single mixed colonoid of known composition, more closely resembling the mixed subclonal composition of the developing tumour. These "mixed colonoids" can thus be used to contribute to the understanding of subclonal interactions and ITH in CRC.

Mixed colonoids were generated using a modified version of the previously reported lipid-bilayer-supported printing technique (described in Figure 2.2)[252-254]. Briefly, undigested (i.e. not dissociated using TrypLE) mutant colonoids were resuspended in collagen and individually plated at close proximity into an oil/lipid bath. The oil/lipid bath enabled lipid bilayer formation between droplets and when removed resulted in droplet fusion to form a unified material (Figure 3.26. A). The generated mixed colonoids were small (~ 3 mm in length), robust and supported efficient growth for up to three weeks. Mixed colonoids were generated in various predefined patterns and imaged by confocal microscopy to visualise movement between regions within the mixed colonoid (Figure 3.26. B). The defined patterns were maintained for roughly one week before the colonoids started to migrate between compartments.

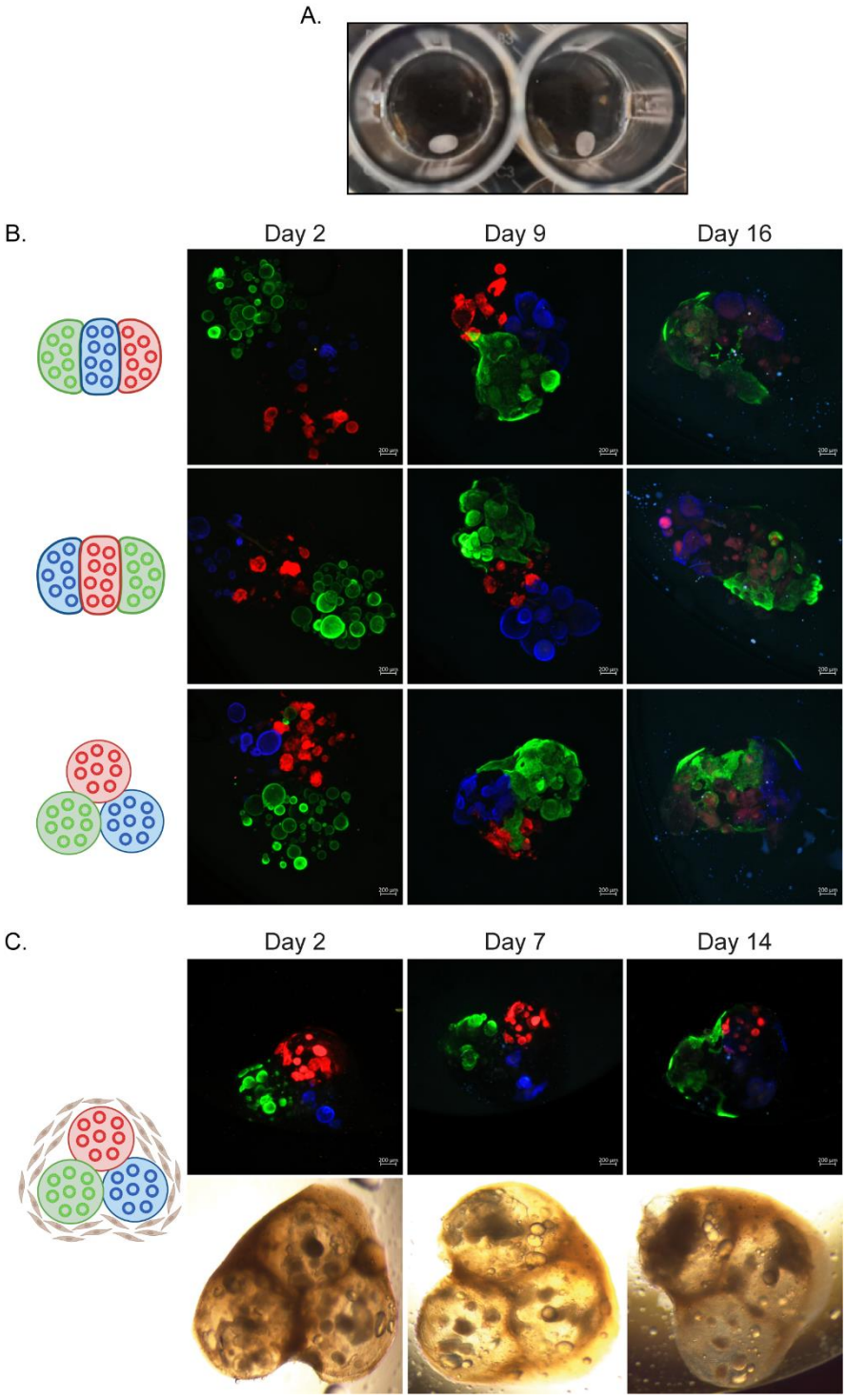


Figure 3.26. Uniquely patterned mixed colonoids cultured with and without fibroblasts. Intact *Apc*$^{min/+}$ mCherry, *Kras*$^{G12D/+}$ EYFP, and *p53*^{Null} mBanana colonoids were resuspended in collagen alone or collagen containing fibroblasts and individually plated in 1 µl droplets into an oil/lipid bath in a 48-well plate. Colonoids were plated in different patterns as indicated. After thermal gelation at RT, cultures were incubated and the oil/lipid bath carefully removed and replaced with sunflower oil. The sunflower oil was replaced with co-culture medium and the **A**. newly formed mixed colonoids were transferred to a 96-well plate. **B.** After seeding, mixed colonoids were visualised on day 2, 9 and 16. **C.** Mixed colonoids generated using collagen containing 1 million/ml colon fibroblasts (*p53*^{Null} in this case) were imaged on day 2, 7 and 14. Images were acquired on a Zeiss 710MP confocal microscope using the 5X objective. Scale bars represent 200 µm. Mixed colonoids made with the help of Dr Linna Zhou.

To further increase the physiological relevance of this model by representing the tumour microenvironment (TME), a process was also developed to form mixed colonoids containing both colonoids and colon fibroblasts (Figure 3.26. C). In this case, undigested mutant colonoids were resuspended in collagen which contained 1 million fibroblasts/ml and then individually plated into the oil/lipid bath. As previously observed the fibroblasts contracted over time which forced the compartment size to decrease and bring mutant colonoids closer together[254]. While this modification to the mixed colonoids protocol requires further optimisation, it certainly suggests that mixed colonoids could be used to study the role of the TME in CRC tumourigenesis and progression, in addition to ITH.

In summary, the mixed colonoid model developed in this section represents an advance in the ability of the field to model the spatial interaction of subclonal populations with or without their physiological microenvironment. This model therefore provides a promising tool for future studies to delve further into the mechanisms by which subclonal cooperation, as identified in this work through OFA and gene expression profiling, may contribute to CRC tumourigenesis and progression.

3.3.5. Discussion

SAM and scRNA-seq analysis on colonoids harbouring CRC-associated mutations revealed that each exhibited unique spatiotemporal dynamics and gene expression profiles respectively. It was however unclear whether these mutants would exhibit altered behaviour and gene expression when cultured in the presence of other mutants, as occurs between the subclonal populations with varying driver mutations known to exist in CRC tumours. This has yet to be investigated and could provide valuable insight into how mutations in driver genes influence each other and drive subclonal evolution in CRC tumourigenesis.

Prior to any co-culture experiments being performed a suitable co-culture medium was developed. While *Apc*$^{min/+}$ colonoids do not require Wnt supplementation in order to grow efficiently, colonoids which harbour mutations in *Kras* or *Tp53* do[328-330]. Moreover, due to the aberrant Wnt signalling characteristic of colon adenomas, organoids derived from these tissues and harbour mutations in *Apc*, *Kras* and *Tp53* do not require Wnt supplementation to

drive expansion[134]. Consequently, the co-culture medium established here was supplemented with 10% Wnt. This percentage of Wnt was sufficient in supporting the growth of *Kras*$^{G12D/+}$*:p53*^{Null}, *p53*^{Null} and *p53*$^{R172H/R172H}$ colonoids and did not inhibit the growth of *Apc*$^{min/+}$ colonoids. This was demonstrated by the fact that although the co-culture medium slightly reduced the organoid forming ability of the individual mutant colonoids it was not significant and the co-culture medium did not result in the death of the mutant colonoids. The identified co-culture medium was thus deemed suitable for use.

An OFA was then performed in order to determine whether the mutants exhibited altered behaviour when grown under co-culture conditions. This revealed that the co-culture of different mutant colonoids increased the organoid forming ability of each mutant compared to standard culture conditions. This finding implies cooperativity between mutant colonoids which results in increased stem cell functionality and potentially increased oncogenic potential[156].

Subsequent scRNA-seq of the co-cultured colonoid-derived cells showed that the altered organoid forming ability was accompanied by alterations in gene expression profiles. The gene expression profile of co-cultured *Apc*$^{min/+}$ colonoid-derived cells was altered to a lesser extent than that of the other co-cultured genotypes; however, a number of key differentially expressed genes were still identified in all genotypes upon co-culture, including *Apc*$^{min/+}$. Interestingly, co-culture conditions induced similar changes to the gene expression profiles of *p53*$^{R172H/R172H}$ and *p53*^{Null} colonoid-derived cells which were drastically different under standard culture conditions. Furthermore, the gene expression profiles of co-cultured *p53*$^{R172H/R172H}$ and *p53*^{Null} colonoid-derived cells were comparable to that of co-cultured *Kras*$^{G12D/+}$*:p53*^{Null} colonoid-derived cells. Together, these results suggest that co-culture conditions could be inducing similar phenotypic changes in *Kras*$^{G12D/+}$*:p53*^{Null}, *p53*$^{R172H/R172H}$ and *p53*^{Null} colonoids and that the transcriptome of *Apc*$^{min/+}$ colonoids is less susceptible to modifications induced by the presence of other mutant genotypes. *Apc*$^{min/+}$ colonoids have been described as “supercompetitors” in CRC tumour initiation[243]. With this in mind it is plausible that *Apc*$^{min/+}$ colonoids secrete signalling molecules to alter the oncogenic potential of surrounding mutants but are less dependent on signalling from other subclones for phenotype determination. However, before any finite conclusions can

be established, scRNA-seq needs to be performed on mutant colonoids cultured alone in the co-culture medium.

Comparisons between the top upregulated genes expressed by each mutant between culture conditions revealed that co-cultured *Apc*$^{min/+}$ colonoid-derived cells have decreased expression of RSC and foetal genes makers. This suggests that co-cultured *Apc*$^{min/+}$ colonoids may be losing the regenerative molecular phenotype observed in standard culture. Unexpectedly, these cells also had decreased expression of columnar epithelial markers which have been associated with CRC progression and the activation of Wnt signalling[364,365]. *Apc*$^{min/+}$ colonoid-derived cells also upregulated the expression of different gene sets between AKPm and AKPn co-cultures. The genes upregulated by co-cultured *Apc*$^{min/+}$-colonoid-derived cells have been associated with both CRC tumour promoting and tumour supressing functions, thus it is challenging to interpret whether these cells in fact exhibit increased oncogenic potential under co-culture conditions. For example, *Apc*$^{min/+}$ colonoid-derived cells from AKPm co-cultures had elevated expression of *Gdf15* which promotes EMT and metastasis, and elevated expression of *Cdkn1a* which is associated with a better prognosis in CRC patients[331,332]. Moreover, *Apc*$^{min/+}$ colonoid-derived cells from AKPn co-cultures had elevated expression of colonic epithelial markers *Car1* and *Car2* and *Bsg* which promotes migration, proliferation and invasion in CRC[333,334]. The mixed potential impact of these differentially expressed genes could suggest intermediate phenotypes among a wide range able to be induced in response to signalling from neighbouring subclones.

The differences in expression of the top upregulated genes by *Apc*$^{min/+}$ colonoid-derived cells between culture conditions was mainly observed at the average gene expression level, however *Kras*$^{G12D/+}$*:p53*^{Null}, *p53*$^{R172H/R172H}$ and *p53*^{Null} colonoid-derived cells displayed both greater differences in the average gene expression and the percentage of cells expressing the top upregulated genes between culture conditions. This highlights the possibility that *Apc*$^{min/+}$ colonoids are less impacted by the presence of other mutants compared to *Kras* and *Tp53* mutant colonoids. Interestingly, *Kras* and both *Tp53* conditions showed a degree of overlap in some of the top differentially expressed genes, suggesting a converging of phenotypes to

some extent under the co-culture conditions assayed. Co-cultured *Kras$^{G12D/+}$:p53^{Null}* colonoid-derived cells had decreased average expression levels of RSC and foetal gene markers as well as ECM remodelling proteins and Yap target genes. Notably, these cells had increased average expression levels of GC markers. The expression of differentiated cell type markers, including those of colonocytes, enteroendocrine cells and GCs, is usually reduced in CRC compared to normal colon tissue, however the elevated expression of GC markers has recently been associated with the consensus molecular subtype 3 (CMS3) of CRC[213]. Co-cultured *Kras$^{G12D/+}$:p53^{Null}* colonoid-derived cells also had elevated expression of *Dmbt1* which serves as a negative prognostic marker in CRC[335]. Significantly, all of the characterised top upregulated genes expressed by co-cultured *Kras$^{G12D/+}$:p53^{Null}* colonoid-derived cells are associated with CRC progression and a worse outcome for patients.

Similar to that of *Kras$^{G12D/+}$:p53^{Null}*, co-cultured *p53$^{R172H/R172H}$* colonoid-derived cells had decreased expression levels of ECM remodelling proteins, Yap target genes and increased expression levels of GC markers. Interestingly, co-cultured *p53^{Null}* colonoid-derived cells had decreased average expression of Egfr ligand *Areg* which has been identified as a marker of clonal cooperation[245]. Given the cooperativity seen in the OFAs, this result could represent a negative feedback loop following successful cooperation to prevent an overly cooperative environment. Lastly, co-cultured *Kras$^{G12D/+}$:p53^{Null}*, *p53$^{R172H/R172H}$* and *p53^{Null}* colonoid-derived cells had increased expression of *guanylate cyclase activator 2a (Guca2a)* which is associated with a better prognosis for CRC patients[366]. Co-cultured *p53$^{R172H/R172H}$* and *p53^{Null}* colonoid-derived cells also had elevated expression of *Lypd8* which has proven to play a tumour inhibitory role in CRC[336].

While the difference between AKPm and AKPn co-cultures is merely a missense versus a null mutation, it is important to note that significant differences were still observed between co-cultures. The murine *R172H* mutation corresponds to the human *R175H* mutation which is the most prevalent *TP53* mutation found in CRC patients (TCGA). Cells which harbour the *R172/5H* mutation are known to lose tumour suppressing abilities and gain oncogenic functions by dysregulating cell proliferation, apoptosis and senescence processes[228]. Mice

harbouring the *R172H* mutation have been observed to develop CRC tumours with enhanced proliferative and metastatic properties compared to those from p53 null mice[367]. Consequently, it is anticipated that AKPm co-cultures would have increased oncogenic potential compared to AKPn co-cultures.

While difficult to interpret in terms of CRC progression, these results highlight the fact that the co-culture conditions significantly altered the behaviour and gene expression profiles exhibited by colonoids harbouring CRC-associated mutations suggesting that CRC models that more closely recapitulate the subclonal heterogeneity of the tumour are required to fully understand this disease. As a tool to allow for further research of spatial interactions between mutant subclones, a novel co-culture protocol involving droplet-based printing techniques was developed in this work, which was termed “mixed colonoids”. Mixed colonoids facilitate both patterning and spatial control and allow for the investigation of direct subclonal interactions. Furthermore, by bringing different clones together mixed colonoids have the potential to accurately mimic ITH. The mixed colonoids can be generated in any pattern desired, are highly robust and support efficient colonoid growth for up to three weeks. After one week, colonoids migrate between compartments highlighting the ability for them to self-assemble and form functional systems. Lastly, through the incorporation of fibroblasts into the mixed colonoid culture system the interaction between the microenvironment and driver mutations can be studied. In future research, these mixed colonoids may thus provide an important tool to achieve the recapitulation of subclonal interactions needed to fully understand and combat ITH in CRC.

It is interesting to note that chimeric colonoids were very rarely observed during these experiments. Chimeric organoids have previously been noted to form between wild type organoid-derived cells and cancer organoid-derived cells however, despite multiple attempts using a similar protocol, the colonoids used in this study did not form chimeric colonoids with one another[323]. Although the exact reason behind this is unclear, it is possible that the mutant colonoids will only form a chimeric colonoid with wild type cells which impose little competitive threat. It is also conceivable that chimeric colonoids may form but disappear before

visualisation using confocal microscopy (usually performed 72 hours after plating). In order to address this, colonoid co-cultures could be viewed soon after plating to observe whether chimeric colonoids may be forming. This would provide a useful model for studying whether different mutant genotypes are able to outcompete one another depending on their abundance in an individual chimeric colonoid.

In summary, this chapter uses OFAs and scRNA-seq to identify cooperative interactions between subclonal populations in co-culture which significantly alter their individual phenotypes and develops mixed colonoids as a tool to explore the implications of these interactions more fully.

4. CONCLUSION

CRC is a highly metastatic disease responsible for a significant proportion of cancer-related mortality worldwide[200,205,206]. While chemotherapeutic agents have shown some promise, surgical resection is still the only curative treatment for this cancer type which only leads to a further decline in the patient's quality of life. Despite progress in treatment strategies, the median overall survival for metastatic CRC with standard of care is still only 30 months[368]. Consequently, there is a critical need to reduce time to detection, identify superior treatment strategies and ultimately increase survival time for patients with CRC.

Sporadic CRC, which accounts for 90% of CRC cases, is characterised by considerable interpatient heterogeneity making the exact mechanism behind how this complex cancer type arises and progresses difficult to elucidate[200]. Alterations in individual driver genes, namely *APC*, *KRAS*, and *TP53*, are well known to play an important role in CRC tumourigenesis, yet the exact impact that these mutations have on the plasticity of cells within the growing tumour is still unclear. Aberrant cellular plasticity results in various atypical phenotypic alterations and has the potential to promote CRC development[190,257]. Such phenotypic aberrations are associated with genetic alterations and result in the formation of a complex genotype-phenotype relationship. Until now, this relationship has yet to be accurately modelled.

In this study the impact of *Apc*, *Kras*, and *Tp53* driver mutations on the cellular plasticity exhibited by colonic stem cells was investigated. This was achieved using a novel, high-throughput and unbiased organoid phenotyping platform, termed Shape, Appearance and Motion (SAM). SAM simultaneously measured more than 2000 features per mutant colon organoid (colonoid) to identify instantaneous colonoid states and generate unique phenotype trajectories over time. The analysis enabled by this unique platform revealed that CRC-associated driver mutations indeed alter the spatiotemporal dynamics and cellular plasticity of colonoids and generate distinct genotype-phenotype profiles unique to each alteration. Notably, $Apc^{min/+}$ colonoids demonstrated a phenotypic dynamic that was particularly distinct from colonoids carrying all other driver mutations assessed, adopting a 2D eccentric

appearance and increased mean speed over time. Furthermore, *Apc*$^{min/+}$ colonoids had a higher disposition towards morphological change rather than pure growth. From these findings it can be inferred that the loss of functional *Apc* induces more drastic changes in cellular plasticity compared to other CRC-associated alterations.

To understand the molecular basis for the differences seen in cellular plasticity between the various mutant colonoids, these phenotypic findings were integrated with transcriptomic analysis by performing scRNA-seq on the same mutant colonoids. The distinct spatiotemporal dynamics exhibited by *Apc*$^{min/+}$ colonoids were found to associate with a unique gene expression profile characterised by elevated Yap signalling and the acquisition of a regenerative stem cell (RSC) and foetal gene signature. Intriguingly, *Apc*$^{min/+}$ colonoid-derived cells were also found to have decreased expression of tight junction proteins and increased expression of Yap-dependent ECM remodelling proteins[306]. These findings suggest that *Apc*$^{min/+}$ colonoids are engaged in a Yap-mediated regenerative response usually observed in the repairing intestinal epithelium[17,108-110,257].

Due to the key role of mechanotransduction in Yap signalling, it is highly likely that the 2D eccentric growth exhibited by *Apc*$^{min/+}$ colonoids activates Yap-mediated mechanotransduction pathways and pushes *Apc*$^{min/+}$ colonoids towards the RSC molecular phenotype observed with scRNA-seq[313]. This occurs despite the presence of the *Apc* mutation which has previously been associated with a crypt base columnar (CBC) stem cell molecular phenotype[110]. Taken together it is hypothesised that the dysregulated Wnt signalling characteristic of *Apc* mutant cells induces a loss of tight junction proteins, increases cell motility and predisposes colonoids to a Yap-driven regenerative response. When coupled with a change in ECM rigidity, Yap translocates into the nucleus activating the expression of RSC and foetal gene markers as well as ECM remodelling proteins. This culminates in the 2D eccentric phenotype adopted by *Apc*$^{min/+}$ colonoids in areas of increased ECM stiffness (Figure 4.1). This highlights the possibility that epithelial mutations set the underlying basal stem cell molecular phenotype but that microenvironmental influences (in this case mechanotransduction) can superimpose a phenotypic shift along a wide range of possible states for each driver mutation.

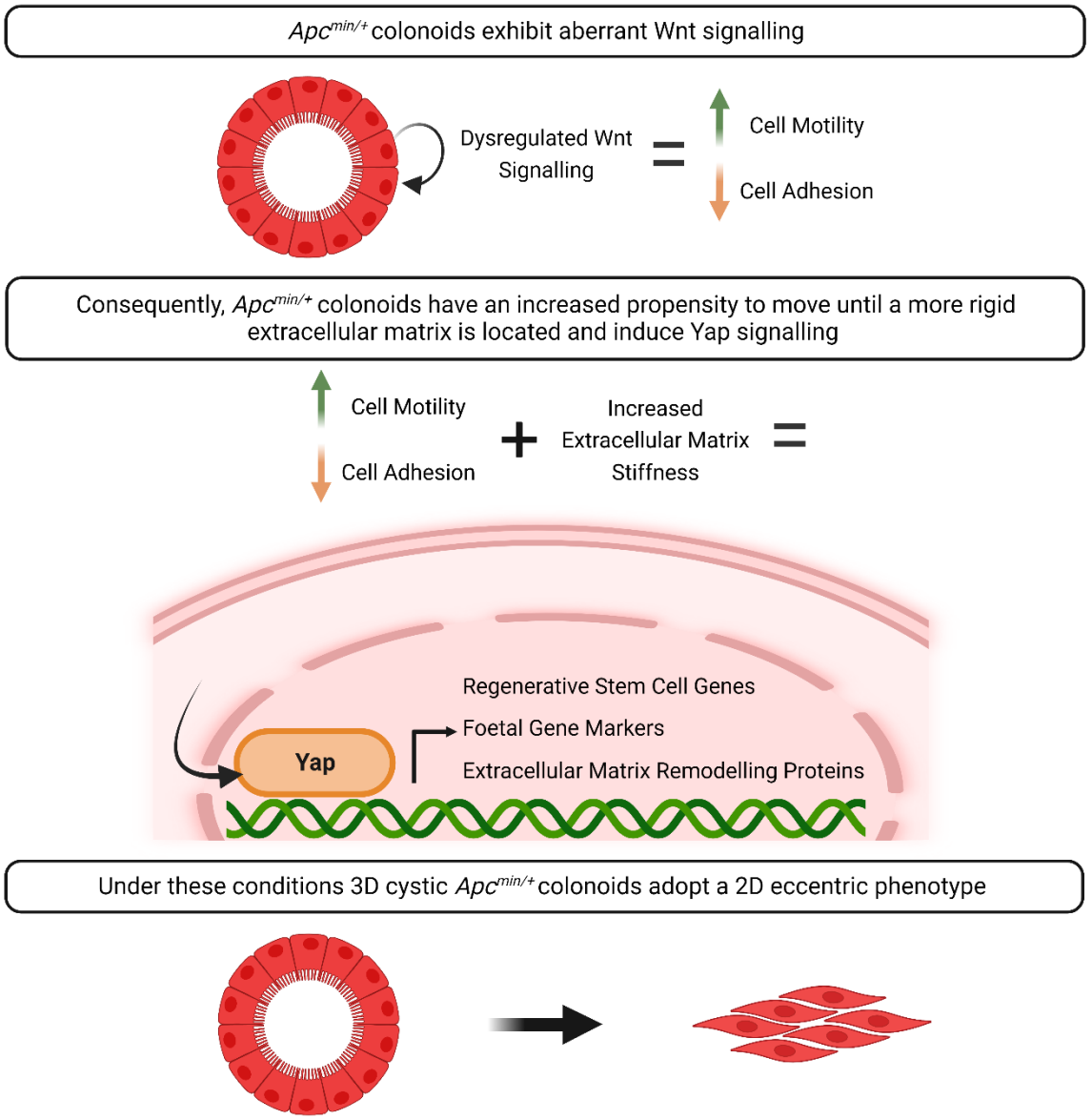


Figure 4.1. Proposed mechanism behind the 2D eccentric phenotype adopted by *Apc*$^{min/+}$ colonoids. The dysregulated Wnt signalling exhibited by *Apc*$^{min/+}$ colonoids induces a loss of tight junction proteins and increases cell motility (top panel). When coupled with an increase in extracellular matrix stiffness, Yap translocates into the nucleus activating the expression of regenerative stem cell and foetal gene markers as well as extracellular matrix remodelling proteins (middle panel). This culminates in the 2D eccentric phenotype adopted by *Apc*$^{min/+}$ colonoids in areas of increased ECM stiffness (bottom panel).

In the final chapter of this study, it was endeavoured to accurately model the subclonal dynamics and ITH present in CRC tumours. Competitive interactions between mutant and wild type clones and cooperative interactions between mutant clones have been implicated in the initiation and promotion of tumour growth[243,245,323-325]. Moreover, the considerable ITH exhibited by CRC tumours drives tumour evolution, fosters drug resistance and directly correlates with

patient prognosis[234-238]. To elucidate the complex interactions which exist between subclonal populations during the early stages of CRC tumour evolution, the behaviour and gene expression of mutant colonoids grown under co-culture conditions was analysed. Compared to standard culture conditions, each mutant genotype demonstrated an enhanced organoid forming ability, suggesting that mutant colonoids have an increased stem cell functionality when in the presence of other mutants. Findings from scRNA-seq analysis on co-cultured mutant colonoids showed that that, while most mutant genotypes showed considerable transcriptomic changes during co-culture, *Apc*$^{min/+}$ colonoids were less susceptible to modifications of their transcriptomic profile in response to the presence of other mutant genotypes. This characterisation of the behaviour of *Apc*$^{min/+}$ organoids in the presence of subclones carrying other mutations is novel, as previously *Apc*$^{min/+}$ dynamics have only been characterised in culture with wild type organoids, but the impact of organoids with single driver mutations on each other has not yet been investigated[243,244]. While further investigation is warranted, this has the potential to provide valuable insight into how mutations in driver genes influence each other and drive subclonal evolution during the early stages of CRC tumourigenesis.

Co-culture using traditional organoid culture techniques yielded important information about dynamics between mutant colonoids, but these traditional techniques are insufficient to fully recapitulate the complex ITH seen during CRC development. To this end, a novel organoid co-culture protocol which provides spatial control and patterning of mutant colonoids within the same “mixed colonoid” structure and facilitates the incorporation of cells usually present in the tumour microenvironment (TME) was developed. In this work, mixed colonoids were introduced and used as exemplars of how this protocol could be applied to generate colonoids with a variety of pre-specified mutant cell patterns. Once optimised, this highly physiologically relevant mixed colonoid model has the capacity to contribute to the understanding of direct subclonal interactions and ITH present in CRC tumours and clarify the influence that the TME has on CRC tumour evolution.

In conclusion, it has clearly been demonstrated that CRC-associated driver alterations exhibit unique spatiotemporal dynamics and gene expression profiles. It is proposed that the usual basal stem cell molecular phenotype imposed by the *Apc* mutation is superimposed by microenvironmental influences which are able to induce a phenotypic shift regardless of the mutation status. The insights gained from this study have the potential to further our understanding of the influence of *Apc* mutations in CRC tumourigenesis and progression and aid in the identification of novel biomarkers and therapeutics for CRC treatment. Additionally, it has been shown that the growth potential and molecular phenotype of single mutant colonoids are highly influenced by the presence of colonoids carrying other single driver mutations, supporting the Big Bang model and suggesting an important role for cooperative subclonal interactions during CRC development. Finally, the "mixed colonoid" model is put forward as an ideal technological innovation for the field to use to model ITH and assess other key questions about subclonal dynamics and interactions.

5. FUTURE DIRECTIONS

5.1. Investigating the Altered Stem Cell Molecular Phenotype and Morphological Change in *Apc*$^{min/+}$ Colonoids

In this study the unique spatiotemporal dynamics and gene expression profiles of colonoids harbouring CRC-associated driver mutations was determined. These findings highlighted the potential for modifications in key driver genes to alter the cellular plasticity of colonic stem cells, leading to significant morphological and transcriptional changes. Consequently, this novel discovery has emphasised the importance of thoroughly investigating the dynamic genotype-phenotype relationships present in CRC in order to further our understanding of this complex cancer type.

Of the mutant colonoids which were utilised in this study, *Apc*$^{min/+}$ colonoids were observed to adopt a distinct 2D eccentric phenotype over the course of seven days. This highly distinct phenotype even among mutant colonoids warrants further exploration to explore its causes and potential provenance for tumourigenesis. In this study, this morphological change was found to be associated with the activation of Yap signalling and the development of a regenerative stem cell (RSC) signature. This finding was further correlated with the increased expression of ECM remodelling proteins and the decreased expression of tight junction proteins. Taken together, these results suggest that *Apc*$^{min/+}$ colonoids have an increased oncogenic potential and the study of these colonoids could reveal potential targets for the treatment of advanced CRC.

5.1.1. Delineating the Role of Yap in Promoting the 2D Eccentric Phenotype and Regenerative Stem Cell Molecular Phenotype in *Apc*$^{min/+}$ Colonoids

Activation of the Yap signalling pathway has been associated with ECM remodelling and the development of a RSC signature[17,108,109,257,306]. Here it has been demonstrated that 2D eccentric *Apc*$^{min/+}$ colonoids were positive for nuclear Yap localisation, thus reflecting the activation of the Yap pathway. Despite this, it is not altogether clear whether Yap is directly responsible for the eccentric phenotype and RSC signature observed in *Apc*$^{min/+}$ colonoids, or

whether nuclear *Yap* expression is a downstream effect of a separate phenomenon which also induces eccentricity in *Apc*$^{min/+}$colonoids. Treatment with an inhibitor which prevents Yap nuclear localisation could help determine whether Yap plays a causal role in development of the unique phenotype displayed by *Apc*$^{min/+}$ colonoids. If so, this could reveal Yap as a biomarker or potential target in the treatment of advanced CRC harbouring *Apc* mutations or Wnt pathway alterations.

Interestingly, Yap undergoes increased nuclear translocation with increased 3D matrix stiffness, a characteristic associated with the regenerating epithelium[313,369,370]. Culturing the *Apc*$^{min/+}$ colonoids in Matrigel of differing stiffnesses could further contribute to our understanding of the role that Yap plays in these colonoids. According to our proposed mechanistic model, it is believed that *Apc*$^{min/+}$ colonoids grown in a stiffer matrix will exhibit increased nuclear Yap localisation and accelerated development of the observed 2D eccentric phenotype and RSC molecular phenotype.

Several groups have further shown that organoids cultured in a collagen ECM induce Yap activation and these Yap-activated organoids have been used to investigate matrix mechanotransduction and the RSC signature[108,110,371,372]. It would be interesting to determine whether culturing *Apc*$^{min/+}$ colonoids in collagen instead of Matrigel has an impact on the RSC signature observed in these colonoids. Clarifying the role of Yap in the *Apc*$^{min/+}$ RSC signature would help to understand the complex relationship between CRC-associated driver mutations, molecular stem cell phenotype and microenvironmental signalling pathways more clearly.

5.1.2. Determining the Function of Ahr in *Apc*$^{min/+}$ Colonoids

In addition to the RSC signature expressed by *Apc*$^{min/+}$ colonoids-derived cells, these cells also exhibited elevated expression of *Aryl hydrocarbon receptor* (*Ahr*, Figure 5.1). While this was not focused on in this study, the upregulation of *Ahr* still warrants further investigation, as it is known to play a role in CRC tumourigenesis and has recently been identified as a key gene inducing termination of the RSC molecular phenotype.

Aberrations in the Ahr pathway are associated with an elevated intestinal inflammatory response and predispose mice to the development of colitis[373,374]. Furthermore, Ahr has been implicated in crypt base columnar (CBC) stem cell differentiation and regulation of the Wnt pathway[375]. In a mouse model of CRC, the absence of *Ahr* was demonstrated to promote tumourigenesis through activation of the Wnt pathway causing increased proliferation and impaired differentiation in CBC stem cells.

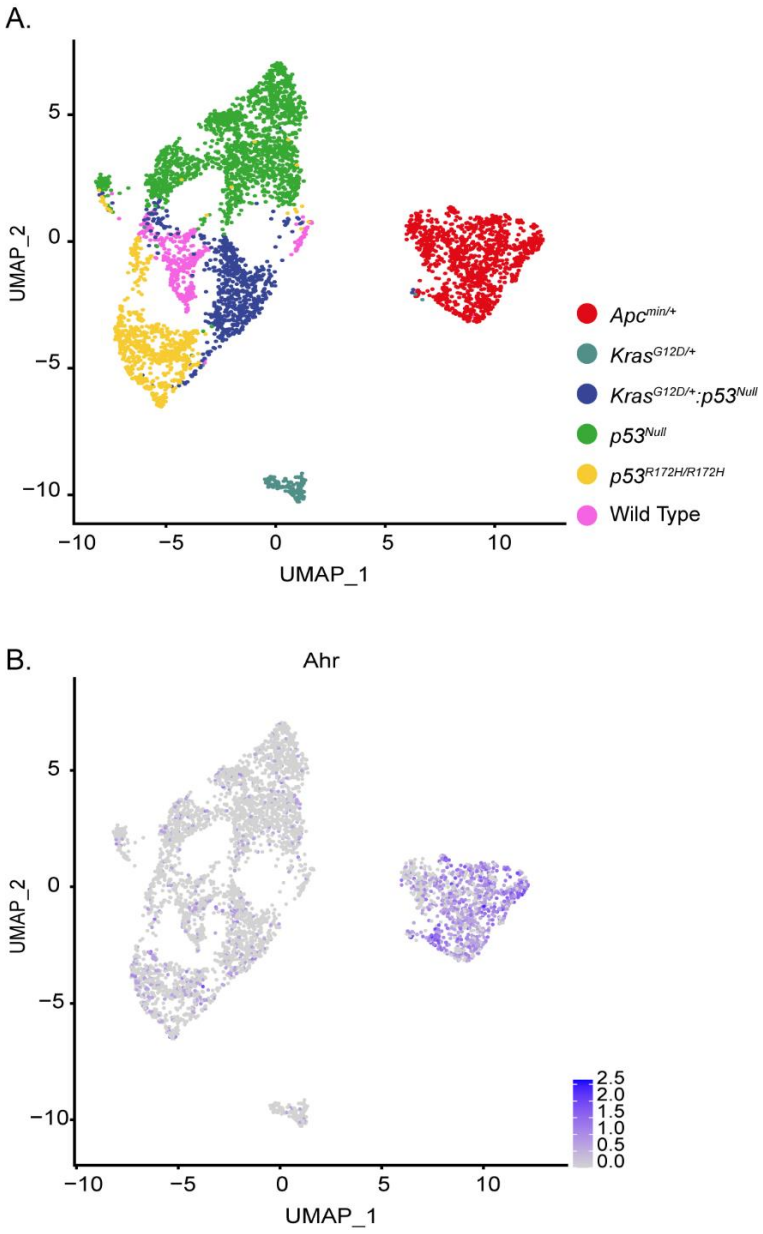


Figure 5.1. *Apc*$^{min/+}$ colonoid-derived cells have elevated expression of *Ahr*. Wild type and mutant colonoids were individually seeded in a 384-well plate and cultured for seven days before processing. scRNA-seq was conducted using a 5' scRNA-seq gene expression workflow. Sequencing of final libraries was conducted on the Illumina NextSeq 550 and data analysis was conducted using Cell Ranger and Seurat. **A.** Overall UMAP clustering of colonoid-derived cells and **B**. Visualisation of *Aryl hydrocarbon receptor* (*Ahr*) expression by FeaturePlot. Colour scale represents normalized expression values for each cell as calculated by Seurat. Analysis performed by Thomas Carroll and Brittany-Amber Jacobs.

Recently, Shah *et al.* revealed that *Ahr* knockout mouse which were exposed to a colitis-inducing agent (dextran sulphate sodium or DSS) were unable to terminate the regenerative response[376]. The colonic epithelium of DSS treated mice reverted to a foetal-like state and expressed genes associated with a RSC response (*Ly6a*) in a Yap-dependent manner. However, mice lacking *Ahr* expression had persistent *Ly6a* expression and failed to reacquire mature epithelial cell identity. Through analysis of wild type and *Ahr* knockout organoids, the mechanism behind the *in vivo* observations was revealed. It was shown that Ahr is required to restrict chromatin accessibility to regeneration-associated genes including *Yap*. Moreover, Ahr contributed to the termination of the repair process by repressing proto-oncogenes *Sox9* and *Myc* and promoting the reversion to ISC differentiation from the RSC molecular phenotype. Interestingly, the same study showed that Ahr is a transcriptional activator of *Cdx2*, thereby promoting the differentiation and specification of cells post regeneration[376]. Consequently, in the absence of *Ahr* the regenerative response is lengthened and differentiation is limited which has the potential to promote an environment conducive for CRC development. These findings could suggest that upregulation of *Ahr* in *Apc*$^{min/+}$ colonoids could serve as a negative feedback mechanism limiting the extent of RSC molecular phenotype development.

However, in contrast to the seemingly anti-tumourigenic role described above, *Ahr* has also been implicated in promoting tumourigenesis by influencing ECM remodelling processes and cell-to-cell interactions[302,377,378]. Ahr activation has been demonstrated to enhance gastric cancer migration and invasion by increasing the expression and activity of ECM MMP remodelling proteins[379]. Furthermore, Ahr has been shown to activate pathways which cause the loss of substratum adhesion and cell-to-cell contact resulting in increased cell motility and the promotion of EMT[377]. Therefore, it is not yet clear whether *Ahr* upregulation is limiting or contributing to the aberrant phenotype displayed by *Apc*$^{min/+}$ colonoids.

In the present study, it was shown that *Apc*$^{min/+}$ colonoid-derived cells have decreased expression of *Cdx2* (Figure 3.19. B). Although the precise reason for the loss of *Cdx2* expression in these colonoids is unclear, it is plausible that Ahr is unable to efficiently terminate the regenerative response due to its loss, as previous studies have shown this is a key Ahr

target gene promoting specification of cell identity[376]. Importantly, *Apc*$^{min/+}$ colonoid-derived cells were also observed to have increased expression of *Mmp7* (Figure 3.19. A) and decreased expression tight junction proteins (Figure 3.19. C and D). Accordingly, perhaps the elevated expression of *Ahr* targets these proteins and in doing so is responsible for the increased mean speed (Figure 3.8) and ECM remodelling demonstrated by these colonoids.

Here scRNA-seq was performed on *Apc*$^{min/+}$ colonoid-derived cells after one week of culture, perhaps if these colonoids were cultured over longer periods of time and sequenced again the expression of *Cdx2*, RSC markers, *Mmp7* and tight junction proteins could be reanalysed. These findings have the potential to reveal a novel role for Ahr in *APC* mutant CRC.

5.2. Examining the Unique Gene Expression Profile of *Kras*$^{G12D/+}$ Colonoids

While the primary focus of this study was the unique phenotype and RSC gene signature exhibited by *Apc*$^{min/+}$ colonoids, it is worth acknowledging the distinct clustering of *Kras*$^{G12D/+}$ colonoids, which could also represent a uniquely important subclonal phenotype conferred by this mutant within the growing tumour (Figure 5.2. A). Accordingly, the implications of the unique gene expression profile of this mutant genotype, and some of the key questions to be answered by further study will be discussed.

Preliminary analysis of the scRNA-seq data revealed that the top upregulated genes expressed by *Kras*$^{G12D/+}$ colonoid-derived cells were *Ectonucleotide pyrophosphatase/phosphodiesterase 2* (*Enpp2*, Figure 5.2. B) and *Keratin23* (*Krt23*, Figure 5.2. C). *Enpp2,* commonly referred to as Autotaxin*,* is a secreted lysophospholipase D which is responsible for the production of lysophosphatidic acid (LPA)[380]. LPA is a lipid mediator acting on G-protein-coupled receptors (GPCRs) to execute multiple functions. Dietary and endogenous lipids have been associated with the development of IBD due to their capacity to modulate inflammation[380]. Consequently, LPA, which is a naturally occurring phospholipid, has been linked to the development and promotion of several intestinal pathologies including IBD and tumour progression[380,381]. Furthermore, the secretion of Autotaxin by melanoma cells has been shown to exhibit chemorepulsive qualities by supressing tumour infiltration of cytotoxic CD8+ T cells and impairing tumour regression[382]. Although the exact role of Autotaxin in CRC

is unclear, the literature suggests that Autotaxin which was found upregulated in *Kras*$^{G12D/+}$ mutant colonoids likely plays a key role in its contribution to CRC tumour progression. Future studies should be conducted to characterise the role of this highly differentially expressed genes in *Kras* mutant colonoids, and whether it plays a central role in driving its unique molecular phenotype.

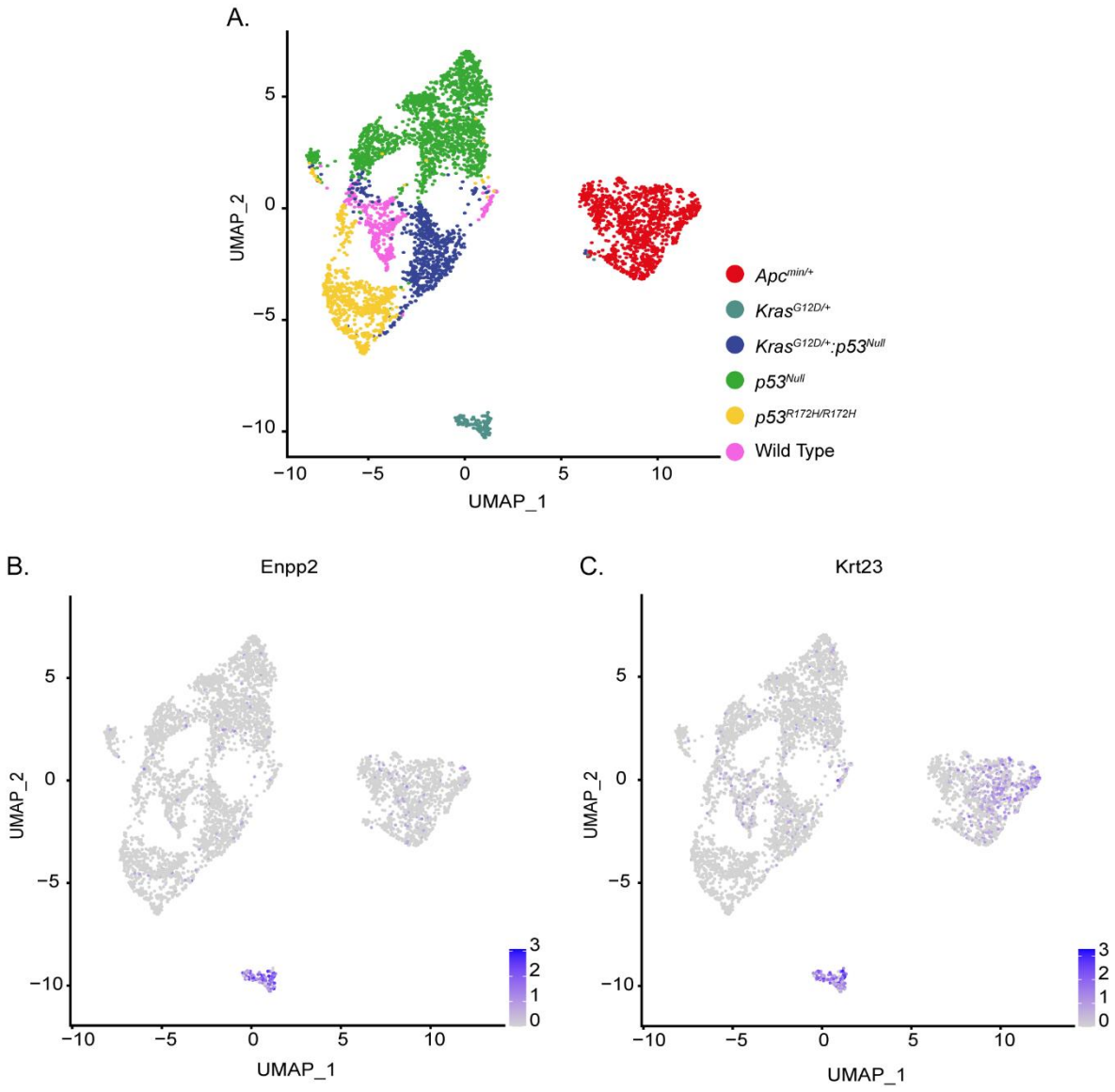


Figure 5.2. *Kras*$^{G12D/+}$ colonoids exhibit a unique gene expression profile. **A.** Overall UMAP clustering of colonoid-derived cells and visualisation of **B**. *Ectonucleotide pyrophosphatase/phosphodiesterase 2* (*Enpp2*) and **C.** *Keratin23* (*Krt23*) expression by FeaturePlot. Colour scale represents normalized expression values for each cell as calculated by Seurat.

Keratins are intermediate filament forming proteins vital to the maintenance of epithelial cell structural integrity[383]. Indeed several keratins have been associated with the development of epithelial cell cancers, including CRC[384]. Specifically, KRT23, which is usually absent in the healthy colon epithelium, has been implicated in the promotion of CRC tumour growth and migration by promoting ISC properties[385]. Unfortunately, this means that CRC patients with high *KRT23* expression have a significantly shorter overall survival time[385]. Importantly, *KRT23* knockdown in CRC cells lines renders cells more sensitive to irradiation and led to decreased proliferation, suggesting this gene could be a potential target to improve outcomes of patients with *KRAS* mutated CRC tumours[386].

A more thorough analysis into the gene expression profile of *Kras*$^{G12D/+}$ colonoids is required, however these preliminary investigations have identified highly upregulated biomarkers which warrant further exploration in the context of *KRAS* mutant CRC.

5.3. Investigating the Potential Function of Wnt Antagonists in Mutant Colonoid Co-Culture Models

As previously mentioned, CRC is characterised by significant genetic diversity, clonal expansion and clonal selection[321,322]. The Big Bang model postulates that the ITH in CRC tumours is the result of diverse subclone populations which arise early during tumour development[233]. Despite this, the exact mechanism behind which these subclones interact is still unclear. Defining this will contribute to the understanding of CRC tumour evolution and contribute to improving patient prognosis.

Several experiments exploring CRC ITH have been conducted using the mutant colonoid library developed in this study. Namely, scRNA-seq was performed on mutant colonoid-derived cells which had been co-cultured for seven days (Figure 5.3. A). Analysis revealed that the gene expression profile of *Apc*$^{min/+}$ colonoid-derived cells was less altered under co-culture conditions, while the opposite was true for the remaining mutants. However, co-cultured *Apc*$^{min/+}$ colonoids did still show highly significant changes in the expression of a few genes.

Interestingly, co-cultured *Apc*$^{min/+}$ colonoid-derived cells were observed to have elevated expression of the Wnt antagonist *Notum* (Figure 5.3. B).

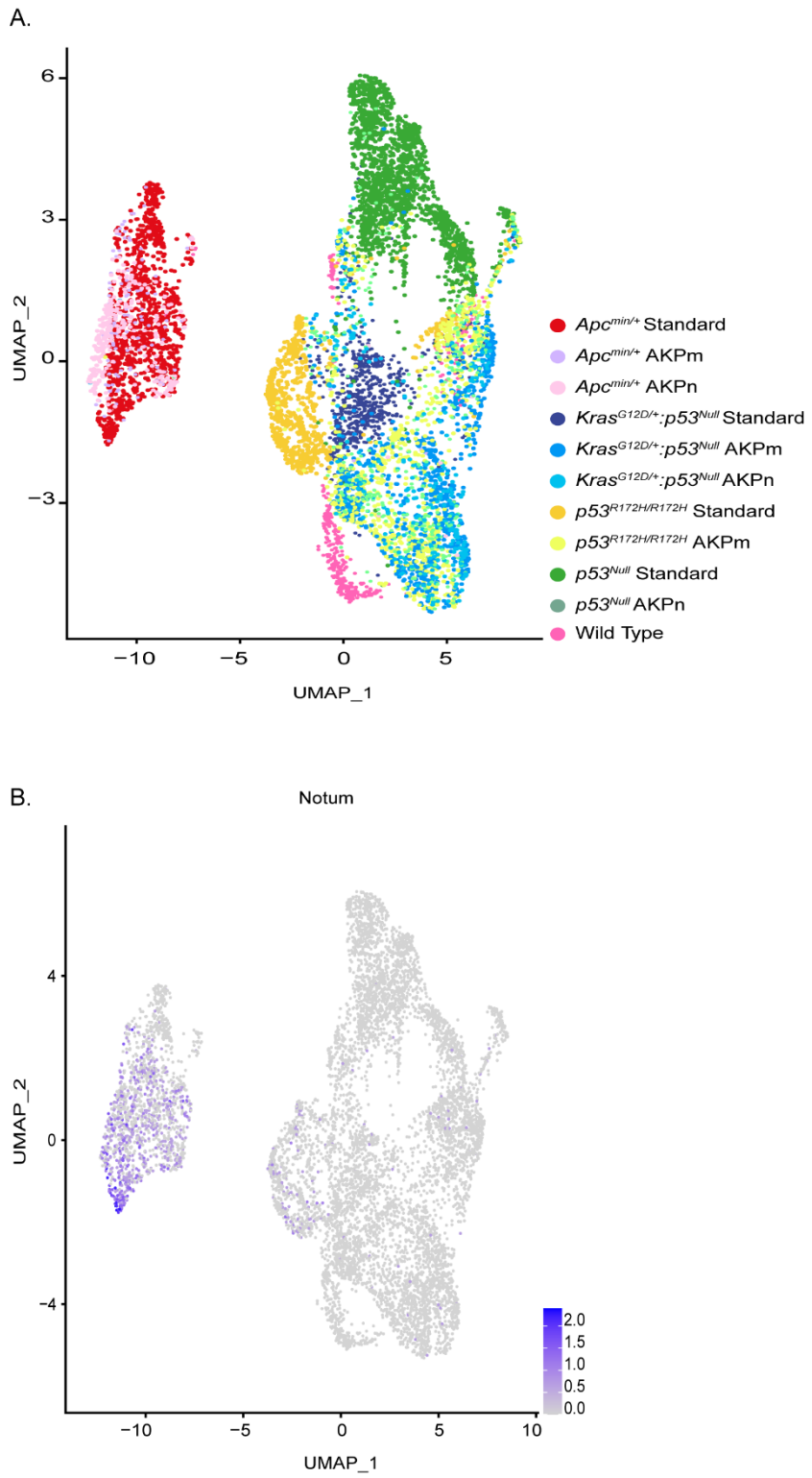


Figure 5.3. Standard and co-cultured *Apc*$^{min/+}$ colonoids exhibit increased expression of Wnt antagonist *Notum*. A. Overall UMAP clustering of colonoid-derived cells grown under standard or co-culture conditions and **B**. visualisation of *Notum* expression by FeaturePlot. Colour scale represents normalized expression values for each cell as calculated by Seurat.

Notum has previously been identified as a Wnt antagonist secreted by *Apc* mutant ISCs[244]. In this setting *APC* mutant ISCs acted as “supercompetitors” and outcompeted wild type ISCs to establish clonal fixation and initiate CRC. Accordingly, it is possible that the *Apc*$^{min/+}$ colonoids are interacting with the other mutant colonoids through the secretion of Notum. This interaction could be studied by treating the colonoid co-cultures with a Notum inhibitor and performing scRNA-seq on the colonoid-derived cells, to determine whether this supercompetition-mediator plays a key role driving the large phenotypic changes seen in other mutants during co-culture. Despite analysis of the top unregulated genes expressed by co-cultured mutant colonoids not being conclusive in whether co-culture conditions inhibited or promoted CRC tumourigenesis, it would still be insightful to determine whether Notum is able to drive the large changes in gene expression seen in colonoids harbouring different CRC-associated mutations.

The influence of Notum on non-*Apc* mutant colonoids could be further elucidated by culturing these colonoids in the conditioned medium from *Apc*$^{min/+}$ colonoids with and without Notum inhibition. If this induced Yap activation and a shift in stem cell molecular phenotype in other mutant colonoids in a Notum-dependent manner, it would reveal the role of Wnt antagonists in ECM remodelling and metastatic CRC.

5.4. Optimisation and Characterisation of Mixed Colonoids

Here a novel organoid co-culture model which facilitates spatial control and patterning of fluorescently labelled colonoids has been developed. By culturing different mutant colonoids in close proximity and in a predetermined pattern, mixed colonoids have the potential to accurately mimic subclonal interactions and ITH present in CRC. Due to the ability for the mutant colonoids to self-assemble and migrate between compartments within the mixed colonoids, it would be insightful to perform SAM analysis on the mixed colonoids and compare it to the spatiotemporal dynamics already determined under standard culture conditions. Results from the analysis would elucidate the influence that CRC-associated mutations have on one another and how it depends on their proximity and spatial architecture, thus providing further insight into the subclonal dynamics in CRC and how ITH arises.

In addition to SAM analysis, scRNA-seq should be performed on mixed colonoid-derived cells. As mentioned, scRNA-seq on mutant colonoid-derived cells grown under co-culture conditions revealed that the gene expression profile of *Apc*$^{min/+}$ colonoid-derived cells was less altered compared to standard culture conditions, while the opposite was true for the remaining mutants genotypes. scRNA-seq on mixed colonoid-derived cells could help to determine whether the proximity and arrangement of co-cultured mutant colonoids influences their gene expression. This would provide further insight into the importance of subclonal dynamics in CRC progression.

scRNA-seq would undoubtedly provide an unbiased transcriptome analysis of the mixed colonoids, however the spatial context within these samples would be lost, which is a key benefit of using the mixed colonoid model. To determine whether the gene expression of individual mutant colonoids is uniquely altered by physical contact with other mutants, spatial transcriptomics could be performed. Spatial transcriptomics is a relatively new and unbiased technology that allows for the sequencing of polyadenylated transcripts from a tissue section, which is then spatially mapped onto histological brightfield images of the tissue section[387]. This innovative sequencing technology would enable the detailed investigation into whether the pre-defined pattern of mixed colonoids influences the gene expression profile of the mutant colonoids. For example, would the transcriptome of *p53*$^{R172H/R172H}$ colonoids be altered in a similar manner if in contact with *Apc*$^{min/+}$ and *Kras*$^{G12D/+}$ colonoids (triangle pattern) compared to if in contact with *Apc*$^{min/+}$ colonoids (straight line pattern) only? If not, this would highlight the importance of paracrine signalling between mutant populations in CRC tumours over contact-mediated signalling. The resolution of spatial transcriptomics could even allow for distinguishing between local effects between mutant cells in direct contact with each other, which may only be present in border regions, and more distant effects mediated through secreted effectors. The knowledge gained through spatial transcriptomic analysis of the mixed colonoids has the potential to provide further appreciation for the complex interactions between mutant clones and how these dynamics drive tumour evolution and foster drug resistance in CRC tumours. Furthermore, by incorporating colonic fibroblasts into mixed colonoid cultures,

the impact that the TME has on the transcriptome of mutant populations can be interrogated, providing high-resolution analysis of a more physiological model of CRC tumours.

Recently, spatial transcriptomics has been performed on tissue derived from the regenerating murine colon epithelium[388]. This study was able to identify and spatially map transcriptional signatures of tissue repair processes, immune cell recruitment, pro-regenerative pathways, and tissue remodelling. Moreover, the authors performed targeted mapping of genes associated with disease outcome in human IBD patients and IBD risk variants and inferred their involvement in specific pathological processes based on their localisation in areas with distinct histological properties. This emphasises the ability of spatial transcriptomics to map clinically relevant CRC-associated genes and pathways in patient-derived tissue and assist with patient stratification for tailored therapies and predicting disease outcome.

While the preliminary optimisation experiments characterising mixed colonoids have been performed, further optimisation and characterisation are required before spatial transcriptomics analysis can be carried out, which will be the focus of further study. As an initial step towards this aim, seven-day-old mixed colonoids were embedded in optimal cutting temperature (OCT) compound, stored at -80 °C and cryosectioned at 10 µm thickness as advised by the Visium Spatial Gene Expression protocol, a commonly used protocol for spatial transcriptomics. The RNA was extracted from the individual sections and had an acceptable RNA integrity number (RIN) score of 6.4. These preliminary experiments demonstrate that mixed colonoids are robust structures which maintain RNA integrity after embedding and are easily cryosectioned thus suggesting their suitability for spatial transcriptomics.

Continuing to develop mixed colonoids for spatial transcriptomics applications has great promise to make optimal use of the spatial and molecular information provided by this unique CRC model, in order to dissect the complex ITH that is a hallmark of this disease.

6. REFERENCES

1 (NCI), N. C. I. *Small & Large Intestine*, 2022).

2 Azzouz LL, S. S. *Physiology, Large Intestine.*, 2021).

3 Hill, M. J. Intestinal flora and endogenous vitamin synthesis. *Eur J Cancer Prev* **6 Suppl 1**, S43-45, doi:10.1097/00008469-199703001-00009 (1997).

4 Turnberg, L. A. Electrolyte absorption from the colon. *Gut* **11**, 1049-1054, doi:10.1136/gut.11.12.1049 (1970).

5 Snippert, H. J. Colonic Crypts: Safe Haven from Microbial Products. *Cell* **165**, 1564-1566, doi:https://doi.org/10.1016/j.cell.2016.06.003 (2016).

6 Noah, T. K., Donahue, B. & Shroyer, N. F. Intestinal development and differentiation. *Exp Cell Res* **317**, 2702-2710, doi:10.1016/j.yexcr.2011.09.006 (2011).

7 Gayer, C. P. & Basson, M. D. The effects of mechanical forces on intestinal physiology and pathology. *Cell Signal* **21**, 1237-1244, doi:10.1016/j.cellsig.2009.02.011 (2009).

8 Leblond, C. P. & Walker, B. E. Renewal of Cell Populations. *Physiological Reviews* **36**, 255-276, doi:10.1152/physrev.1956.36.2.255 (1956).

9 Barker, N., van de Wetering, M. & Clevers, H. The intestinal stem cell. *Genes Dev* **22**, 1856-1864, doi:10.1101/gad.1674008 (2008).

10 Barker, N. *et al.* Identification of stem cells in small intestine and colon by marker gene Lgr5. *Nature* **449**, 1003-1007, doi:10.1038/nature06196 (2007).

11 Sato, T. *et al.* Single Lgr5 stem cells build crypt-villus structures in vitro without a mesenchymal niche. *Nature* **459**, 262-265, doi:10.1038/nature07935 (2009).

12 van der Flier, L. G., Haegebarth, A., Stange, D. E., van de Wetering, M. & Clevers, H. OLFM4 is a robust marker for stem cells in human intestine and marks a subset of colorectal cancer cells. *Gastroenterology* **137**, 15-17, doi:10.1053/j.gastro.2009.05.035 (2009).

13 van der Flier, L. G. *et al.* Transcription factor achaete scute-like 2 controls intestinal stem cell fate. *Cell* **136**, 903-912, doi:10.1016/j.cell.2009.01.031 (2009).

14 Lopez-Garcia, C., Klein, A. M., Simons, B. D. & Winton, D. J. Intestinal stem cell replacement follows a pattern of neutral drift. *Science* **330**, 822-825, doi:10.1126/science.1196236 (2010).

15 Snippert, H. J. *et al.* Intestinal crypt homeostasis results from neutral competition between symmetrically dividing Lgr5 stem cells. *Cell* **143**, 134-144, doi:10.1016/j.cell.2010.09.016 (2010).

16 Sei, Y., Feng, J., Chow, C. C. & Wank, S. A. Asymmetric cell division-dominant neutral drift model for normal intestinal stem cell homeostasis. *Am J Physiol Gastrointest Liver Physiol* **316**, G64-g74, doi:10.1152/ajpgi.00242.2018 (2019).

17 Ayyaz, A. *et al.* Single-cell transcriptomes of the regenerating intestine reveal a revival stem cell. *Nature* **569**, 121-125, doi:10.1038/s41586-019-1154-y (2019).

18 Gregorieff, A., Liu, Y., Inanlou, M. R., Khomchuk, Y. & Wrana, J. L. Yap-dependent reprogramming of Lgr5+ stem cells drives intestinal regeneration and cancer. *Nature* **526**, 715-718, doi:10.1038/nature15382 (2015).

19 Delacour, D., Salomon, J., Robine, S. & Louvard, D. Plasticity of the brush border — the yin and yang of intestinal homeostasis. *Nature Reviews Gastroenterology & Hepatology* **13**, 161-174, doi:10.1038/nrgastro.2016.5 (2016).

20 Slifer, Z. M. & Blikslager, A. T. The Integral Role of Tight Junction Proteins in the Repair of Injured Intestinal Epithelium. *International Journal of Molecular Sciences* **21**, 972 (2020).

21 Cobo, E. R. & Chadee, K. Antimicrobial Human β-Defensins in the Colon and Their Role in Infectious and Non-Infectious Diseases. *Pathogens* **2**, 177-192, doi:10.3390/pathogens2010177 (2013).

22 Furuta, G. T. *et al.* Hypoxia-Inducible Factor 1–Dependent Induction of Intestinal Trefoil Factor Protects Barrier Function during Hypoxia. *Journal of Experimental Medicine* **193**, 1027-1034, doi:10.1084/jem.193.9.1027 (2001).

23 Litvak, Y., Byndloss, M. X., Tsolis, R. M. & Bäumler, A. J. Dysbiotic Proteobacteria expansion: a microbial signature of epithelial dysfunction. *Current Opinion in Microbiology* **39**, 1-6, doi:https://doi.org/10.1016/j.mib.2017.07.003 (2017).
24 Smith, P. M. *et al.* The microbial metabolites, short-chain fatty acids, regulate colonic Treg cell homeostasis. *Science* **341**, 569-573, doi:10.1126/science.1241165 (2013).
25 Byndloss, M. X. *et al.* Microbiota-activated PPAR-γ signaling inhibits dysbiotic Enterobacteriaceae expansion. *Science* **357**, 570-575, doi:10.1126/science.aam9949 (2017).
26 Shin, N. R., Whon, T. W. & Bae, J. W. Proteobacteria: microbial signature of dysbiosis in gut microbiota. *Trends Biotechnol* **33**, 496-503, doi:10.1016/j.tibtech.2015.06.011 (2015).
27 Vollaard, E. J., Clasener, H. A. & Janssen, A. J. Co-trimoxazole impairs colonization resistance in healthy volunteers. *J Antimicrob Chemother* **30**, 685-691, doi:10.1093/jac/30.5.685 (1992).
28 Martinez-Medina, M. *et al.* Western diet induces dysbiosis with increased E coli in CEABAC10 mice, alters host barrier function favouring AIEC colonisation. *Gut* **63**, 116-124, doi:10.1136/gutjnl-2012-304119 (2014).
29 Carroll, I. M., Ringel-Kulka, T., Siddle, J. P. & Ringel, Y. Alterations in composition and diversity of the intestinal microbiota in patients with diarrhea-predominant irritable bowel syndrome. *Neurogastroenterol Motil* **24**, 521-530, e248, doi:10.1111/j.1365-2982.2012.01891.x (2012).
30 Morgan, X. C. *et al.* Dysfunction of the intestinal microbiome in inflammatory bowel disease and treatment. *Genome Biol* **13**, R79, doi:10.1186/gb-2012-13-9-r79 (2012).
31 Normann, E., Fahlén, A., Engstrand, L. & Lilja, H. E. Intestinal microbial profiles in extremely preterm infants with and without necrotizing enterocolitis. *Acta Paediatr* **102**, 129-136, doi:10.1111/apa.12059 (2013).
32 Arthur, J. C. *et al.* Intestinal inflammation targets cancer-inducing activity of the microbiota. *Science* **338**, 120-123, doi:10.1126/science.1224820 (2012).
33 Steinert, R. E. & Beglinger, C. Nutrient sensing in the gut: interactions between chemosensory cells, visceral afferents and the secretion of satiation peptides. *Physiology & Behavior* **105**, 62-70, doi:https://doi.org/10.1016/j.physbeh.2011.02.039 (2011).
34 Sjölund, K., Sandén, G., Håkanson, R. & Sundler, F. Endocrine cells in human intestine: an immunocytochemical study. *Gastroenterology* **85**, 1120-1130 (1983).
35 Varndell, I. M., Lloyd, R. V., Wilson, B. S. & Polak, J. M. Ultrastructural localization of chromogranin: a potential marker for the electron microscopical recognition of endocrine cell secretory granules. *Histochem J* **17**, 981-992, doi:10.1007/bf01417947 (1985).
36 Wiedenmann, B., Franke, W. W., Kuhn, C., Moll, R. & Gould, V. E. Synaptophysin: a marker protein for neuroendocrine cells and neoplasms. *Proc Natl Acad Sci U S A* **83**, 3500-3504, doi:10.1073/pnas.83.10.3500 (1986).
37 Gunawardene, A. R., Corfe, B. M. & Staton, C. A. Classification and functions of enteroendocrine cells of the lower gastrointestinal tract. *Int J Exp Pathol* **92**, 219-231, doi:10.1111/j.1365-2613.2011.00767.x (2011).
38 Modlin, I. M., Kidd, M., Pfragner, R., Eick, G. N. & Champaneria, M. C. The functional characterization of normal and neoplastic human enterochromaffin cells. *J Clin Endocrinol Metab* **91**, 2340-2348, doi:10.1210/jc.2006-0110 (2006).
39 Spiller, R. Serotonin and GI clinical disorders. *Neuropharmacology* **55**, 1072-1080, doi:10.1016/j.neuropharm.2008.07.016 (2008).
40 Gustafsson, B. I., Bakke, I., Tømmerås, K. & Waldum, H. L. A new method for visualization of gut mucosal cells, describing the enterochromaffin cell in the rat gastrointestinal tract. *Scand J Gastroenterol* **41**, 390-395, doi:10.1080/00365520500331281 (2006).
41 Lördal, M., Wallén, H., Hjemdahl, P., Beck, O. & Hellström, P. M. Concentration-dependent stimulation of intestinal phase III of migrating motor complex by circulating serotonin in humans. *Clin Sci (Lond)* **94**, 663-670, doi:10.1042/cs0940663 (1998).
42 Coleman, N. S. *et al.* Effect of a novel 5-HT3 receptor agonist MKC-733 on upper gastrointestinal motility in humans. *Aliment Pharmacol Ther* **18**, 1039-1048, doi:10.1046/j.1365-2036.2003.01797.x (2003).

43 Costedio, M. M., Hyman, N. & Mawe, G. M. Serotonin and its role in colonic function and in gastrointestinal disorders. *Dis Colon Rectum* **50**, 376-388, doi:10.1007/s10350-006-0763-3 (2007).
44 Rubin, G. *et al.* Identification and diagnosis of patients with irritable bowel syndrome in primary care: nominal group technique. *Gut* **54**, A3 (2005).
45 Garfield, A. S. & Heisler, L. K. Pharmacological targeting of the serotonergic system for the treatment of obesity. *J Physiol* **587**, 49-60, doi:10.1113/jphysiol.2008.164152 (2009).
46 Saras, J., Grönberg, M., Stridsberg, M., Oberg, K. E. & Janson, E. T. Somatostatin induces rapid contraction of neuroendocrine cells. *FEBS Lett* **581**, 1957-1962, doi:10.1016/j.febslet.2007.04.019 (2007).
47 Hope, N. *et al.* Somatostatin enhances cAMP-dependent short-circuit current in human colon via somatostatin receptor subtype-2. *Dig Dis Sci* **46**, 2499-2503, doi:10.1023/a:1012392307462 (2001).
48 Low, M. J. Clinical endocrinology and metabolism. The somatostatin neuroendocrine system: physiology and clinical relevance in gastrointestinal and pancreatic disorders. *Best Pract Res Clin Endocrinol Metab* **18**, 607-622, doi:10.1016/j.beem.2004.08.005 (2004).
49 Wren, A. M. & Bloom, S. R. Gut Hormones and Appetite Control. *Gastroenterology* **132**, 2116-2130, doi:https://doi.org/10.1053/j.gastro.2007.03.048 (2007).
50 Ballantyne, G. H. Peptide YY(1-36) and peptide YY(3-36): Part I. Distribution, release and actions. *Obes Surg* **16**, 651-658, doi:10.1381/096089206776944959 (2006).
51 Mari, A. *et al.* Meal and oral glucose tests for assessment of beta -cell function: modeling analysis in normal subjects. *Am J Physiol Endocrinol Metab* **283**, E1159-1166, doi:10.1152/ajpendo.00093.2002 (2002).
52 Drucker, D. J. Biological actions and therapeutic potential of the glucagon-like peptides. *Gastroenterology* **122**, 531-544, doi:10.1053/gast.2002.31068 (2002).
53 Dao DPD, L. P. *Histology, Goblet Cells*, 2022).
54 Birchenough, G. M. H., Johansson, M. E., Gustafsson, J. K., Bergström, J. H. & Hansson, G. C. New developments in goblet cell mucus secretion and function. *Mucosal Immunology* **8**, 712-719, doi:10.1038/mi.2015.32 (2015).
55 Antoni, L. *et al.* Human colonic mucus is a reservoir for antimicrobial peptides. *Journal of Crohn's and Colitis* **7**, e652-e664, doi:10.1016/j.crohns.2013.05.006 (2013).
56 Hase, K., Eckmann, L., Leopard, J. D., Varki, N. & Kagnoff, M. F. Cell differentiation is a key determinant of cathelicidin LL-37/human cationic antimicrobial protein 18 expression by human colon epithelium. *Infect Immun* **70**, 953-963, doi:10.1128/iai.70.2.953-963.2002 (2002).
57 Johansson, M. E. V. *et al.* The inner of the two Muc2 mucin-dependent mucus layers in colon is devoid of bacteria. *Proceedings of the National Academy of Sciences* **105**, 15064-15069, doi:doi:10.1073/pnas.0803124105 (2008).
58 Round, A. N. *et al.* Lamellar Structures of MUC2-Rich Mucin: A Potential Role in Governing the Barrier and Lubricating Functions of Intestinal Mucus. *Biomacromolecules* **13**, 3253-3261, doi:10.1021/bm301024x (2012).
59 Ambort, D. *et al.* Calcium and pH-dependent packing and release of the gel-forming MUC2 mucin. *Proceedings of the National Academy of Sciences* **109**, 5645-5650, doi:doi:10.1073/pnas.1120269109 (2012).
60 Halm, D. R. & Halm, S. T. Secretagogue response of goblet cells and columnar cells in human colonic crypts1. *American Journal of Physiology-Cell Physiology* **278**, C212-C233, doi:10.1152/ajpcell.2000.278.1.C212 (2000).
61 Knoop, K. A., McDonald, K. G., McCrate, S., McDole, J. R. & Newberry, R. D. Microbial sensing by goblet cells controls immune surveillance of luminal antigens in the colon. *Mucosal Immunology* **8**, 198-210, doi:10.1038/mi.2014.58 (2015).
62 Mach, J., Hshieh, T., Hsieh, D., Grubbs, N. & Chervonsky, A. Development of intestinal M cells. *Immunological Reviews* **206**, 177-189, doi:https://doi.org/10.1111/j.0105-2896.2005.00281.x (2005).

63 Mörbe, U. M. *et al.* Human gut-associated lymphoid tissues (GALT); diversity, structure, and function. *Mucosal Immunology* **14**, 793-802, doi:10.1038/s41385-021-00389-4 (2021).
64 Mabbott, N. A., Donaldson, D. S., Ohno, H., Williams, I. R. & Mahajan, A. Microfold (M) cells: important immunosurveillance posts in the intestinal epithelium. *Mucosal Immunol* **6**, 666-677, doi:10.1038/mi.2013.30 (2013).
65 Sansonetti, P. J. & Phalipon, A. M cells as ports of entry for enteroinvasive pathogens: mechanisms of interaction, consequences for the disease process. *Semin Immunol* **11**, 193-203, doi:10.1006/smim.1999.0175 (1999).
66 Fotopoulos, G. *et al.* Transepithelial transport of HIV-1 by M cells is receptor-mediated. *Proc Natl Acad Sci U S A* **99**, 9410-9414, doi:10.1073/pnas.142586899 (2002).
67 Heppner, F. L. *et al.* Transepithelial prion transport by M cells. *Nature Medicine* **7**, 976-977, doi:10.1038/nm0901-976 (2001).
68 Gerbe, F., Legraverend, C. & Jay, P. The intestinal epithelium tuft cells: specification and function. *Cellular and Molecular Life Sciences* **69**, 2907-2917, doi:10.1007/s00018-012-0984-7 (2012).
69 Ting, H.-A. & von Moltke, J. The Immune Function of Tuft Cells at Gut Mucosal Surfaces and Beyond. *The Journal of Immunology* **202**, 1321-1329, doi:10.4049/jimmunol.1801069 (2019).
70 Bezençon, C., le Coutre, J. & Damak, S. Taste-Signaling Proteins Are Coexpressed in Solitary Intestinal Epithelial Cells. *Chemical Senses* **32**, 41-49, doi:10.1093/chemse/bjl034 (2006).
71 Gerbe, F. & Jay, P. Intestinal tuft cells: epithelial sentinels linking luminal cues to the immune system. *Mucosal Immunology* **9**, 1353-1359, doi:10.1038/mi.2016.68 (2016).
72 Howitt, M. R. *et al.* Tuft cells, taste-chemosensory cells, orchestrate parasite type 2 immunity in the gut. *Science* **351**, 1329-1333, doi:doi:10.1126/science.aaf1648 (2016).
73 Gerbe, F. *et al.* Intestinal epithelial tuft cells initiate type 2 mucosal immunity to helminth parasites. *Nature* **529**, 226-230, doi:10.1038/nature16527 (2016).
74 von Moltke, J., Ji, M., Liang, H.-E. & Locksley, R. M. Tuft-cell-derived IL-25 regulates an intestinal ILC2–epithelial response circuit. *Nature* **529**, 221-225, doi:10.1038/nature16161 (2016).
75 McKenzie, G. J., Bancroft, A., Grencis, R. K. & McKenzie, A. N. A distinct role for interleukin-13 in Th2-cell-mediated immune responses. *Curr Biol* **8**, 339-342, doi:10.1016/s0960-9822(98)70134-4 (1998).
76 Biswas, S. *et al.* Microenvironmental control of stem cell fate in intestinal homeostasis and disease. *The Journal of Pathology* **237**, 135-145, doi:https://doi.org/10.1002/path.4563 (2015).
77 Gregorieff, A. & Clevers, H. Wnt signaling in the intestinal epithelium: from endoderm to cancer. *Genes Dev* **19**, 877-890, doi:10.1101/gad.1295405 (2005).
78 Clevers, H., Loh, K. M. & Nusse, R. An integral program for tissue renewal and regeneration: Wnt signaling and stem cell control. *Science* **346**, 1248012, doi:doi:10.1126/science.1248012 (2014).
79 Janda, C. Y., Waghray, D., Levin, A. M., Thomas, C. & Garcia, K. C. Structural basis of Wnt recognition by Frizzled. *Science* **337**, 59-64, doi:10.1126/science.1222879 (2012).
80 Kim, K. A. *et al.* R-Spondin family members regulate the Wnt pathway by a common mechanism. *Mol Biol Cell* **19**, 2588-2596, doi:10.1091/mbc.e08-02-0187 (2008).
81 de Lau, W. *et al.* Lgr5 homologues associate with Wnt receptors and mediate R-spondin signalling. *Nature* **476**, 293-297, doi:10.1038/nature10337 (2011).
82 Hao, H. X. *et al.* ZNRF3 promotes Wnt receptor turnover in an R-spondin-sensitive manner. *Nature* **485**, 195-200, doi:10.1038/nature11019 (2012).
83 Koo, B. K. *et al.* Tumour suppressor RNF43 is a stem-cell E3 ligase that induces endocytosis of Wnt receptors. *Nature* **488**, 665-669, doi:10.1038/nature11308 (2012).
84 Fevr, T., Robine, S., Louvard, D. & Huelsken, J. Wnt/β-Catenin Is Essential for Intestinal Homeostasis and Maintenance of Intestinal Stem Cells. *Molecular and Cellular Biology* **27**, 7551-7559, doi:doi:10.1128/MCB.01034-07 (2007).
85 Hata, A. & Chen, Y. G. TGF-β Signaling from Receptors to Smads. *Cold Spring Harb Perspect Biol* **8**, doi:10.1101/cshperspect.a022061 (2016).

86 Zhang, Y. E. Non-Smad pathways in TGF-β signaling. *Cell Research* **19**, 128-139, doi:10.1038/cr.2008.328 (2009).
87 Hardwick, J. C. *et al.* Bone morphogenetic protein 2 is expressed by, and acts upon, mature epithelial cells in the colon. *Gastroenterology* **126**, 111-121, doi:10.1053/j.gastro.2003.10.067 (2004).
88 Qi, Z. *et al.* BMP restricts stemness of intestinal Lgr5+ stem cells by directly suppressing their signature genes. *Nature Communications* **8**, 13824, doi:10.1038/ncomms13824 (2017).
89 Auclair, B. A., Benoit, Y. D., Rivard, N., Mishina, Y. & Perreault, N. Bone morphogenetic protein signaling is essential for terminal differentiation of the intestinal secretory cell lineage. *Gastroenterology* **133**, 887-896, doi:10.1053/j.gastro.2007.06.066 (2007).
90 Brink, G. R. v. d. Hedgehog Signaling in Development and Homeostasis of the Gastrointestinal Tract. *Physiological Reviews* **87**, 1343-1375, doi:10.1152/physrev.00054.2006 (2007).
91 Varjosalo, M. & Taipale, J. Hedgehog: functions and mechanisms. *Genes Dev* **22**, 2454-2472, doi:10.1101/gad.1693608 (2008).
92 van den Brink, G. R. *et al.* Indian Hedgehog is an antagonist of Wnt signaling in colonic epithelial cell differentiation. *Nat Genet* **36**, 277-282, doi:10.1038/ng1304 (2004).
93 Kosinski, C. *et al.* Indian hedgehog regulates intestinal stem cell fate through epithelial-mesenchymal interactions during development. *Gastroenterology* **139**, 893-903, doi:10.1053/j.gastro.2010.06.014 (2010).
94 Büller, N. V., Rosekrans, S. L., Westerlund, J. & van den Brink, G. R. Hedgehog signaling and maintenance of homeostasis in the intestinal epithelium. *Physiology (Bethesda)* **27**, 148-155, doi:10.1152/physiol.00003.2012 (2012).
95 Ramalho-Santos, M., Melton, D. A. & McMahon, A. P. Hedgehog signals regulate multiple aspects of gastrointestinal development. *Development* **127**, 2763-2772, doi:10.1242/dev.127.12.2763 (2000).
96 Artavanis-Tsakonas, S., Rand, M. D. & Lake, R. J. Notch signaling: cell fate control and signal integration in development. *Science* **284**, 770-776, doi:10.1126/science.284.5415.770 (1999).
97 Liang, S. J., Li, X. G. & Wang, X. Q. Notch Signaling in Mammalian Intestinal Stem Cells: Determining Cell Fate and Maintaining Homeostasis. *Curr Stem Cell Res Ther* **14**, 583-590, doi:10.2174/1574888x14666190429143734 (2019).
98 VanDussen, K. L. *et al.* Notch signaling modulates proliferation and differentiation of intestinal crypt base columnar stem cells. *Development* **139**, 488-497, doi:10.1242/dev.070763 (2012).
99 Fre, S. *et al.* Notch signals control the fate of immature progenitor cells in the intestine. *Nature* **435**, 964-968, doi:10.1038/nature03589 (2005).
100 Milano, J. *et al.* Modulation of Notch Processing by γ-Secretase Inhibitors Causes Intestinal Goblet Cell Metaplasia and Induction of Genes Known to Specify Gut Secretory Lineage Differentiation. *Toxicological Sciences* **82**, 341-358, doi:10.1093/toxsci/kfh254 (2004).
101 Noah, T. K. & Shroyer, N. F. Notch in the Intestine: Regulation of Homeostasis and Pathogenesis. *Annual Review of Physiology* **75**, 263-288, doi:10.1146/annurev-physiol-030212-183741 (2013).
102 Barker, N. Adult intestinal stem cells: critical drivers of epithelial homeostasis and regeneration. *Nature Reviews Molecular Cell Biology* **15**, 19-33, doi:10.1038/nrm3721 (2014).
103 Tao, S. *et al.* Wnt activity and basal niche position sensitize intestinal stem and progenitor cells to DNA damage. *The EMBO Journal* **36**, 2920-2921, doi:https://doi.org/10.15252/embj.201797813 (2017).
104 Metcalfe, C., Kljavin, Noelyn M., Ybarra, R. & de Sauvage, Frederic J. Lgr5+ Stem Cells Are Indispensable for Radiation-Induced Intestinal Regeneration. *Cell Stem Cell* **14**, 149-159, doi:https://doi.org/10.1016/j.stem.2013.11.008 (2014).
105 Li, L. & Clevers, H. Coexistence of Quiescent and Active Adult Stem Cells in Mammals. *Science* **327**, 542-545, doi:doi:10.1126/science.1180794 (2010).
106 Muñoz, J. *et al.* The Lgr5 intestinal stem cell signature: robust expression of proposed quiescent '+4' cell markers. *The EMBO Journal* **31**, 3079-3091, doi:https://doi.org/10.1038/emboj.2012.166 (2012).

107 Wang, F. *et al.* Isolation and Characterization of Intestinal Stem Cells Based on Surface Marker Combinations and Colony-Formation Assay. *Gastroenterology* **145**, 383-395.e321, doi:https://doi.org/10.1053/j.gastro.2013.04.050 (2013).
108 Yui, S. *et al.* YAP/TAZ-Dependent Reprogramming of Colonic Epithelium Links ECM Remodeling to Tissue Regeneration. *Cell Stem Cell* **22**, 35-49.e37, doi:https://doi.org/10.1016/j.stem.2017.11.001 (2018).
109 Nusse, Y. M. *et al.* Parasitic helminths induce fetal-like reversion in the intestinal stem cell niche. *Nature* **559**, 109-113, doi:10.1038/s41586-018-0257-1 (2018).
110 Vasquez, E. G. *et al.* Dynamic and adaptive cancer stem cell population admixture in colorectal neoplasia. *Cell Stem Cell* **29**, 1213-1228.e1218, doi:10.1016/j.stem.2022.07.008 (2022).
111 Patel, N. & Shackelford, K. in *StatPearls* (StatPearls Publishing Copyright 2022, StatPearls Publishing LLC., 2022).
112 Molodecky, N. A. *et al.* Increasing incidence and prevalence of the inflammatory bowel diseases with time, based on systematic review. *Gastroenterology* **142**, 46-54.e42; quiz e30, doi:10.1053/j.gastro.2011.10.001 (2012).
113 Podolsky, D. K. Inflammatory bowel disease. *N Engl J Med* **347**, 417-429, doi:10.1056/NEJMra020831 (2002).
114 Heuckeroth, R. O. Hirschsprung's disease, Down syndrome, and missing heritability: too much collagen slows migration. *J Clin Invest* **125**, 4323-4326, doi:10.1172/jci85003 (2015).
115 Lambrichts, D. P. V. *et al.* The Multidisciplinary Management of Acute Complicated Diverticulitis. *Inflamm Intest Dis* **3**, 80-90, doi:10.1159/000486677 (2018).
116 Jensen, C. & Teng, Y. Is It Time to Start Transitioning From 2D to 3D Cell Culture? *Frontiers in Molecular Biosciences* **7**, doi:10.3389/fmolb.2020.00033 (2020).
117 Kapałczyńska, M. *et al.* 2D and 3D cell cultures - a comparison of different types of cancer cell cultures. *Arch Med Sci* **14**, 910-919, doi:10.5114/aoms.2016.63743 (2018).
118 Clevers, H. Modeling Development and Disease with Organoids. *Cell* **165**, 1586-1597, doi:10.1016/j.cell.2016.05.082 (2016).
119 Dutta, D., Heo, I. & Clevers, H. Disease Modeling in Stem Cell-Derived 3D Organoid Systems. *Trends Mol Med* **23**, 393-410, doi:10.1016/j.molmed.2017.02.007 (2017).
120 Simian, M. & Bissell, M. J. Organoids: A historical perspective of thinking in three dimensions. *J Cell Biol* **216**, 31-40, doi:10.1083/jcb.201610056 (2017).
121 Kretzschmar, K. & Clevers, H. Organoids: Modeling Development and the Stem Cell Niche in a Dish. *Dev Cell* **38**, 590-600, doi:10.1016/j.devcel.2016.08.014 (2016).
122 Weiss, P. & Taylor, A. C. Reconstitution of Complete Organs from Single-Cell Suspensions of Chick Embryos in Advanced Stages of Differentiation. *Proceedings of the National Academy of Sciences* **46**, 1177-1185, doi:doi:10.1073/pnas.46.9.1177 (1960).
123 Bissell, D. M., Arenson, D. M., Maher, J. J. & Roll, F. J. Support of cultured hepatocytes by a laminin-rich gel. Evidence for a functionally significant subendothelial matrix in normal rat liver. *J Clin Invest* **79**, 801-812, doi:10.1172/jci112887 (1987).
124 Petersen, O. W., Rønnov-Jessen, L., Howlett, A. R. & Bissell, M. J. Interaction with basement membrane serves to rapidly distinguish growth and differentiation pattern of normal and malignant human breast epithelial cells. *Proc Natl Acad Sci U S A* **89**, 9064-9068, doi:10.1073/pnas.89.19.9064 (1992).
125 Barcellos-Hoff, M. H., Aggeler, J., Ram, T. G. & Bissell, M. J. Functional differentiation and alveolar morphogenesis of primary mammary cultures on reconstituted basement membrane. *Development* **105**, 223-235, doi:10.1242/dev.105.2.223 (1989).
126 Hofer, M. & Lutolf, M. P. Engineering organoids. *Nature Reviews Materials* **6**, 402-420, doi:10.1038/s41578-021-00279-y (2021).
127 Huch, M. & Koo, B. K. Modeling mouse and human development using organoid cultures. *Development* **142**, 3113-3125, doi:10.1242/dev.118570 (2015).
128 Lancaster, M. A. & Huch, M. Disease modelling in human organoids. *Dis Model Mech* **12**, doi:10.1242/dmm.039347 (2019).
129 Xu, H. *et al.* Organoid technology and applications in cancer research. *Journal of Hematology & Oncology* **11**, 116, doi:10.1186/s13045-018-0662-9 (2018).

130 Beumer, J. & Clevers, H. Cell fate specification and differentiation in the adult mammalian intestine. *Nature Reviews Molecular Cell Biology* **22**, 39-53, doi:10.1038/s41580-020-0278-0 (2021).
131 Pérez-González, C. *et al.* Mechanical compartmentalization of the intestinal organoid enables crypt folding and collective cell migration. *Nature Cell Biology* **23**, 745-757, doi:10.1038/s41556-021-00699-6 (2021).
132 Spence, J. R. *et al.* Directed differentiation of human pluripotent stem cells into intestinal tissue in vitro. *Nature* **470**, 105-109, doi:10.1038/nature09691 (2011).
133 Ootani, A. *et al.* Sustained in vitro intestinal epithelial culture within a Wnt-dependent stem cell niche. *Nature Medicine* **15**, 701-706, doi:10.1038/nm.1951 (2009).
134 Sato, T. *et al.* Long-term expansion of epithelial organoids from human colon, adenoma, adenocarcinoma, and Barrett's epithelium. *Gastroenterology* **141**, 1762-1772, doi:10.1053/j.gastro.2011.07.050 (2011).
135 Sato, T. & Clevers, H. Growing Self-Organizing Mini-Guts from a Single Intestinal Stem Cell: Mechanism and Applications. *Science* **340**, 1190-1194, doi:doi:10.1126/science.1234852 (2013).
136 Wilson, S. S. *et al.* Optimized Culture Conditions for Improved Growth and Functional Differentiation of Mouse and Human Colon Organoids. *Frontiers in Immunology* **11**, doi:10.3389/fimmu.2020.547102 (2021).
137 de Jong, P. R. *et al.* Ion channel TRPV1-dependent activation of PTP1B suppresses EGFR-associated intestinal tumorigenesis. *The Journal of Clinical Investigation* **124**, 3793-3806, doi:10.1172/JCI72340 (2014).
138 Dignass, A. U. & Sturm, A. Peptide growth factors in the intestine. *Eur J Gastroenterol Hepatol* **13**, 763-770, doi:10.1097/00042737-200107000-00002 (2001).
139 Matano, M. *et al.* Modeling colorectal cancer using CRISPR-Cas9–mediated engineering of human intestinal organoids. *Nature Medicine* **21**, 256-262, doi:10.1038/nm.3802 (2015).
140 Wong, V. W. Y. *et al.* Lrig1 controls intestinal stem-cell homeostasis by negative regulation of ErbB signalling. *Nature Cell Biology* **14**, 401-408, doi:10.1038/ncb2464 (2012).
141 Powell, A. E. *et al.* The pan-ErbB negative regulator Lrig1 is an intestinal stem cell marker that functions as a tumor suppressor. *Cell* **149**, 146-158, doi:10.1016/j.cell.2012.02.042 (2012).
142 Puschhof, J. *et al.* Intestinal organoid cocultures with microbes. *Nature Protocols* **16**, 4633-4649, doi:10.1038/s41596-021-00589-z (2021).
143 Kim, H. J., Li, H., Collins, J. J. & Ingber, D. E. Contributions of microbiome and mechanical deformation to intestinal bacterial overgrowth and inflammation in a human gut-on-a-chip. *Proceedings of the National Academy of Sciences* **113**, E7-E15, doi:doi:10.1073/pnas.1522193112 (2016).
144 Kaiko, G. E. *et al.* The Colonic Crypt Protects Stem Cells from Microbiota-Derived Metabolites. *Cell* **165**, 1708-1720, doi:10.1016/j.cell.2016.05.018 (2016).
145 Nigro, G., Rossi, R., Commere, P. H., Jay, P. & Sansonetti, P. J. The cytosolic bacterial peptidoglycan sensor Nod2 affords stem cell protection and links microbes to gut epithelial regeneration. *Cell Host Microbe* **15**, 792-798, doi:10.1016/j.chom.2014.05.003 (2014).
146 Hill, D. R. *et al.* Bacterial colonization stimulates a complex physiological response in the immature human intestinal epithelium. *Elife* **6**, doi:10.7554/eLife.29132 (2017).
147 Engevik, M. A. *et al.* Loss of NHE3 alters gut microbiota composition and influences Bacteroides thetaiotaomicron growth. *Am J Physiol Gastrointest Liver Physiol* **305**, G697-711, doi:10.1152/ajpgi.00184.2013 (2013).
148 Bar-Ephraim, Y. E., Kretzschmar, K. & Clevers, H. Organoids in immunological research. *Nature Reviews Immunology* **20**, 279-293, doi:10.1038/s41577-019-0248-y (2020).
149 Biton, M. *et al.* T Helper Cell Cytokines Modulate Intestinal Stem Cell Renewal and Differentiation. *Cell* **175**, 1307-1320.e1322, doi:10.1016/j.cell.2018.10.008 (2018).
150 Waddell, A., Vallance, J. E., Hummel, A., Alenghat, T. & Rosen, M. J. IL-33 Induces Murine Intestinal Goblet Cell Differentiation Indirectly via Innate Lymphoid Cell IL-13 Secretion. *J Immunol* **202**, 598-607, doi:10.4049/jimmunol.1800292 (2019).

151 Lindemans, C. A. *et al.* Interleukin-22 promotes intestinal-stem-cell-mediated epithelial regeneration. *Nature* **528**, 560-564, doi:10.1038/nature16460 (2015).
152 Schreurs, R. *et al.* Human Fetal TNF-α-Cytokine-Producing CD4(+) Effector Memory T Cells Promote Intestinal Development and Mediate Inflammation Early in Life. *Immunity* **50**, 462-476.e468, doi:10.1016/j.immuni.2018.12.010 (2019).
153 de Lau, W. *et al.* Peyer's patch M cells derived from Lgr5(+) stem cells require SpiB and are induced by RankL in cultured "miniguts". *Mol Cell Biol* **32**, 3639-3647, doi:10.1128/mcb.00434-12 (2012).
154 Haber, A. L. *et al.* A single-cell survey of the small intestinal epithelium. *Nature* **551**, 333-339, doi:10.1038/nature24489 (2017).
155 Porotto, M. *et al.* Authentic Modeling of Human Respiratory Virus Infection in Human Pluripotent Stem Cell-Derived Lung Organoids. *mBio* **10**, doi:10.1128/mBio.00723-19 (2019).
156 Drost, J. *et al.* Sequential cancer mutations in cultured human intestinal stem cells. *Nature* **521**, 43-47, doi:10.1038/nature14415 (2015).
157 Li, X. *et al.* Organoid cultures recapitulate esophageal adenocarcinoma heterogeneity providing a model for clonality studies and precision therapeutics. *Nature Communications* **9**, 2983, doi:10.1038/s41467-018-05190-9 (2018).
158 Yan, H. H. N. *et al.* A Comprehensive Human Gastric Cancer Organoid Biobank Captures Tumor Subtype Heterogeneity and Enables Therapeutic Screening. *Cell Stem Cell* **23**, 882-897.e811, doi:10.1016/j.stem.2018.09.016 (2018).
159 Steele, N. G. *et al.* An Organoid-Based Preclinical Model of Human Gastric Cancer. *Cell Mol Gastroenterol Hepatol* **7**, 161-184, doi:10.1016/j.jcmgh.2018.09.008 (2019).
160 Chakrabarti, J. *et al.* Mouse-Derived Gastric Organoid and Immune Cell Co-culture for the Study of the Tumor Microenvironment. *Methods Mol Biol* **1817**, 157-168, doi:10.1007/978-1-4939-8600-2_16 (2018).
161 Riordan, J. R. *et al.* Identification of the Cystic Fibrosis Gene: Cloning and Characterization of Complementary DNA. *Science* **245**, 1066-1073, doi:doi:10.1126/science.2475911 (1989).
162 Dekkers, J. F. *et al.* A functional CFTR assay using primary cystic fibrosis intestinal organoids. *Nature Medicine* **19**, 939-945, doi:10.1038/nm.3201 (2013).
163 Dekkers, J. F. *et al.* Characterizing responses to CFTR-modulating drugs using rectal organoids derived from subjects with cystic fibrosis. *Science Translational Medicine* **8**, 344ra384-344ra384, doi:doi:10.1126/scitranslmed.aad8278 (2016).
164 Organization, W. H. *Burden Of Enteric Diseases*, <https://www.who.int/teams/immunization-vaccines-and-biologicals/product-and-delivery-research/burden-of-enteric-diseases> (2022).
165 Yin, Y. *et al.* Modeling rotavirus infection and antiviral therapy using primary intestinal organoids. *Antiviral Research* **123**, 120-131, doi:https://doi.org/10.1016/j.antiviral.2015.09.010 (2015).
166 Ettayebi, K. *et al.* Replication of human noroviruses in stem cell-derived human enteroids. *Science* **353**, 1387-1393, doi:10.1126/science.aaf5211 (2016).
167 Lamers, M. M. *et al.* SARS-CoV-2 productively infects human gut enterocytes. *Science* **369**, 50-54, doi:doi:10.1126/science.abc1669 (2020).
168 Zhou, J. *et al.* Infection of bat and human intestinal organoids by SARS-CoV-2. *Nature Medicine* **26**, 1077-1083, doi:10.1038/s41591-020-0912-6 (2020).
169 Engevik, M. A. *et al.* Human Clostridium difficile infection: inhibition of NHE3 and microbiota profile. *Am J Physiol Gastrointest Liver Physiol* **308**, G497-509, doi:10.1152/ajpgi.00090.2014 (2015).
170 Mileto, S. J. *et al.* Clostridioides difficile infection damages colonic stem cells via TcdB, impairing epithelial repair and recovery from disease. *Proceedings of the National Academy of Sciences* **117**, 8064-8073, doi:doi:10.1073/pnas.1915255117 (2020).
171 Zhang, Y.-G., Wu, S., Xia, Y. & Sun, J. Salmonella-infected crypt-derived intestinal organoid culture system for host–bacterial interactions. *Physiological Reports* **2**, e12147, doi:https://doi.org/10.14814/phy2.12147 (2014).
172 Heo, I. *et al.* Modelling Cryptosporidium infection in human small intestinal and lung organoids. *Nature Microbiology* **3**, 814-823, doi:10.1038/s41564-018-0177-8 (2018).

173 Caponigro, G. & Sellers, W. R. Advances in the preclinical testing of cancer therapeutic hypotheses. *Nat Rev Drug Discov* **10**, 179-187, doi:10.1038/nrd3385 (2011).
174 Kamb, A. What's wrong with our cancer models? *Nat Rev Drug Discov* **4**, 161-165, doi:10.1038/nrd1635 (2005).
175 Drost, J. & Clevers, H. Organoids in cancer research. *Nature Reviews Cancer* **18**, 407-418, doi:10.1038/s41568-018-0007-6 (2018).
176 Noben, M. *et al.* Epithelial organoid cultures from patients with ulcerative colitis and Crohn's disease: a truly long-term model to study the molecular basis for inflammatory bowel disease? *Gut* **66**, 2193-2195, doi:10.1136/gutjnl-2016-313667 (2017).
177 Dotti, I. *et al.* Alterations in the epithelial stem cell compartment could contribute to permanent changes in the mucosa of patients with ulcerative colitis. *Gut* **66**, 2069-2079, doi:10.1136/gutjnl-2016-312609 (2017).
178 Xu, P., Becker, H., Elizalde, M., Masclee, A. & Jonkers, D. Intestinal organoid culture model is a valuable system to study epithelial barrier function in IBD. *Gut* **67**, 1905-1906, doi:10.1136/gutjnl-2017-315685 (2018).
179 d'Aldebert, E. *et al.* Characterization of Human Colon Organoids From Inflammatory Bowel Disease Patients. *Frontiers in Cell and Developmental Biology* **8**, doi:10.3389/fcell.2020.00363 (2020).
180 Sarvestani, S. K. *et al.* Induced organoids derived from patients with ulcerative colitis recapitulate colitic reactivity. *Nature Communications* **12**, 262, doi:10.1038/s41467-020-20351-5 (2021).
181 Stidham, R. W. & Higgins, P. D. R. Colorectal Cancer in Inflammatory Bowel Disease. *Clin Colon Rectal Surg* **31**, 168-178, doi:10.1055/s-0037-1602237 (2018).
182 van de Wetering, M. *et al.* Prospective derivation of a living organoid biobank of colorectal cancer patients. *Cell* **161**, 933-945, doi:10.1016/j.cell.2015.03.053 (2015).
183 Fujii, M. *et al.* A Colorectal Tumor Organoid Library Demonstrates Progressive Loss of Niche Factor Requirements during Tumorigenesis. *Cell Stem Cell* **18**, 827-838, doi:10.1016/j.stem.2016.04.003 (2016).
184 Weeber, F. *et al.* Preserved genetic diversity in organoids cultured from biopsies of human colorectal cancer metastases. *Proc Natl Acad Sci U S A* **112**, 13308-13311, doi:10.1073/pnas.1516689112 (2015).
185 Cristobal, A. *et al.* Personalized Proteome Profiles of Healthy and Tumor Human Colon Organoids Reveal Both Individual Diversity and Basic Features of Colorectal Cancer. *Cell Rep* **18**, 263-274, doi:10.1016/j.celrep.2016.12.016 (2017).
186 Fumagalli, A. *et al.* Genetic dissection of colorectal cancer progression by orthotopic transplantation of engineered cancer organoids. *Proc Natl Acad Sci U S A* **114**, E2357-e2364, doi:10.1073/pnas.1701219114 (2017).
187 Fumagalli, A. *et al.* A surgical orthotopic organoid transplantation approach in mice to visualize and study colorectal cancer progression. *Nat Protoc* **13**, 235-247, doi:10.1038/nprot.2017.137 (2018).
188 O'Rourke, K. P. *et al.* Transplantation of engineered organoids enables rapid generation of metastatic mouse models of colorectal cancer. *Nature Biotechnology* **35**, 577-582, doi:10.1038/nbt.3837 (2017).
189 Roper, J. *et al.* In vivo genome editing and organoid transplantation models of colorectal cancer and metastasis. *Nat Biotechnol* **35**, 569-576, doi:10.1038/nbt.3836 (2017).
190 de Sousa e Melo, F. *et al.* A distinct role for Lgr5+ stem cells in primary and metastatic colon cancer. *Nature* **543**, 676-680, doi:10.1038/nature21713 (2017).
191 Fumagalli, A. *et al.* Plasticity of Lgr5-Negative Cancer Cells Drives Metastasis in Colorectal Cancer. *Cell Stem Cell* **26**, 569-578.e567, doi:10.1016/j.stem.2020.02.008 (2020).
192 Junttila, M. R. & de Sauvage, F. J. Influence of tumour micro-environment heterogeneity on therapeutic response. *Nature* **501**, 346-354, doi:10.1038/nature12626 (2013).
193 Neal, J. T. *et al.* Organoid Modeling of the Tumor Immune Microenvironment. *Cell* **175**, 1972-1988.e1916, doi:10.1016/j.cell.2018.11.021 (2018).

194 Dijkstra, K. K. *et al.* Generation of Tumor-Reactive T Cells by Co-culture of Peripheral Blood Lymphocytes and Tumor Organoids. *Cell* **174**, 1586-1598.e1512, doi:10.1016/j.cell.2018.07.009 (2018).
195 Verissimo, C. S. *et al.* Targeting mutant RAS in patient-derived colorectal cancer organoids by combinatorial drug screening. *Elife* **5**, doi:10.7554/eLife.18489 (2016).
196 Vlachogiannis, G. *et al.* Patient-derived organoids model treatment response of metastatic gastrointestinal cancers. *Science* **359**, 920-926, doi:10.1126/science.aao2774 (2018).
197 Ganesh, K. *et al.* A rectal cancer organoid platform to study individual responses to chemoradiation. *Nature Medicine* **25**, 1607-1614, doi:10.1038/s41591-019-0584-2 (2019).
198 Ooft, S. N. *et al.* Patient-derived organoids can predict response to chemotherapy in metastatic colorectal cancer patients. *Science Translational Medicine* **11**, eaay2574, doi:doi:10.1126/scitranslmed.aay2574 (2019).
199 Yao, Y. *et al.* Patient-Derived Organoids Predict Chemoradiation Responses of Locally Advanced Rectal Cancer. *Cell Stem Cell* **26**, 17-26.e16, doi:10.1016/j.stem.2019.10.010 (2020).
200 Bray, F. *et al.* Global cancer statistics 2018: GLOBOCAN estimates of incidence and mortality worldwide for 36 cancers in 185 countries. *CA Cancer J Clin* **68**, 394-424, doi:10.3322/caac.21492 (2018).
201 Division of Cancer Prevention and Control, C. f. D. C. a. P. *What Are the Risk Factors for Colorectal Cancer?*, 2022).
202 Song, M., Garrett, W. S. & Chan, A. T. Nutrients, foods, and colorectal cancer prevention. *Gastroenterology* **148**, 1244-1260.e1216, doi:10.1053/j.gastro.2014.12.035 (2015).
203 Durko, L. & Malecka-Panas, E. Lifestyle Modifications and Colorectal Cancer. *Curr Colorectal Cancer Rep* **10**, 45-54, doi:10.1007/s11888-013-0203-4 (2014).
204 Bogaert, J. & Prenen, H. Molecular genetics of colorectal cancer. *Ann Gastroenterol* **27**, 9-14 (2014).
205 Conradi, L.-C. *et al.* Combined targeting of HER-2 and HER-3 represents a promising therapeutic strategy in colorectal cancer. *BMC Cancer* **19**, 880, doi:10.1186/s12885-019-6051-0 (2019).
206 Cunningham, D. *et al.* Colorectal cancer. *Lancet* **375**, 1030-1047, doi:10.1016/s0140-6736(10)60353-4 (2010).
207 Tariq, K. & Ghias, K. Colorectal cancer carcinogenesis: a review of mechanisms. *Cancer Biol Med* **13**, 120-135, doi:10.28092/j.issn.2095-3941.2015.0103 (2016).
208 Vogelstein, B. *et al.* Cancer genome landscapes. *Science* **339**, 1546-1558, doi:10.1126/science.1235122 (2013).
209 Tran, E. *et al.* Cancer immunotherapy based on mutation-specific CD4+ T cells in a patient with epithelial cancer. *Science* **344**, 641-645, doi:10.1126/science.1251102 (2014).
210 Nguyen, L. H., Goel, A. & Chung, D. C. Pathways of Colorectal Carcinogenesis. *Gastroenterology* **158**, 291-302, doi:10.1053/j.gastro.2019.08.059 (2020).
211 Bond, C. E. *et al.* Oncogenic BRAF mutation induces DNA methylation changes in a murine model for human serrated colorectal neoplasia. *Epigenetics* **13**, 40-48, doi:10.1080/15592294.2017.1411446 (2018).
212 Guinney, J. *et al.* The consensus molecular subtypes of colorectal cancer. *Nature Medicine* **21**, 1350-1356, doi:10.1038/nm.3967 (2015).
213 Miller, S. A., Ghobashi, A. H. & O'Hagan, H. M. Consensus molecular subtyping of colorectal cancers is influenced by goblet cell content. *Cancer Genetics* **254-255**, 34-39, doi:https://doi.org/10.1016/j.cancergen.2021.01.009 (2021).
214 Fodde, R., Smits, R. & Clevers, H. APC, signal transduction and genetic instability in colorectal cancer. *Nat Rev Cancer* **1**, 55-67, doi:10.1038/35094067 (2001).
215 Leoz, M. L., Carballal, S., Moreira, L., Ocaña, T. & Balaguer, F. The genetic basis of familial adenomatous polyposis and its implications for clinical practice and risk management. *Appl Clin Genet* **8**, 95-107, doi:10.2147/tacg.S51484 (2015).
216 De Filippo, C. *et al.* Mutations of the APC gene in human sporadic colorectal cancers. *Scand J Gastroenterol* **37**, 1048-1053, doi:10.1080/003655202320378248 (2002).

217 Rowan, A. J. *et al.* APC mutations in sporadic colorectal tumors: A mutational "hotspot" and interdependence of the "two hits". *Proc Natl Acad Sci U S A* **97**, 3352-3357, doi:10.1073/pnas.97.7.3352 (2000).
218 Conlin, A., Smith, G., Carey, F. A., Wolf, C. R. & Steele, R. J. The prognostic significance of K-ras, p53, and APC mutations in colorectal carcinoma. *Gut* **54**, 1283-1286, doi:10.1136/gut.2005.066514 (2005).
219 Miyaki, M. *et al.* Characteristics of somatic mutation of the adenomatous polyposis coli gene in colorectal tumors. *Cancer Res* **54**, 3011-3020 (1994).
220 Armaghany, T., Wilson, J. D., Chu, Q. & Mills, G. Genetic alterations in colorectal cancer. *Gastrointest Cancer Res* **5**, 19-27 (2012).
221 Nussinov, R., Tsai, C. J. & Jang, H. Independent and core pathways in oncogenic KRAS signaling. *Expert Rev Proteomics* **13**, 711-716, doi:10.1080/14789450.2016.1209417 (2016).
222 Downward, J. Targeting RAS signalling pathways in cancer therapy. *Nat Rev Cancer* **3**, 11-22, doi:10.1038/nrc969 (2003).
223 Dinu, D. *et al.* Prognostic significance of KRAS gene mutations in colorectal cancer--preliminary study. *J Med Life* **7**, 581-587 (2014).
224 Wrana, J. L. Signaling by the TGFβ superfamily. *Cold Spring Harb Perspect Biol* **5**, a011197, doi:10.1101/cshperspect.a011197 (2013).
225 Maitra, A., Molberg, K., Albores-Saavedra, J. & Lindberg, G. Loss of Dpc4 expression in colonic adenocarcinomas correlates with the presence of metastatic disease. *Am J Pathol* **157**, 1105-1111, doi:10.1016/s0002-9440(10)64625-1 (2000).
226 Goswami, R. S. *et al.* Hotspot mutation panel testing reveals clonal evolution in a study of 265 paired primary and metastatic tumors. *Clin Cancer Res* **21**, 2644-2651, doi:10.1158/1078-0432.Ccr-14-2391 (2015).
227 Vousden, K. H. & Lu, X. Live or let die: the cell's response to p53. *Nat Rev Cancer* **2**, 594-604, doi:10.1038/nrc864 (2002).
228 Li, X. L., Zhou, J., Chen, Z. R. & Chng, W. J. P53 mutations in colorectal cancer - molecular pathogenesis and pharmacological reactivation. *World J Gastroenterol* **21**, 84-93, doi:10.3748/wjg.v21.i1.84 (2015).
229 Committee, U. N. S. *Bowel Cancer*, <https://view-health-screening-recommendations.service.gov.uk/bowel-cancer/> (2018).
230 Vogelstein, B. *et al.* Genetic alterations during colorectal-tumor development. *N Engl J Med* **319**, 525-532, doi:10.1056/nejm198809013190901 (1988).
231 Short, S. P., Costacurta, P. W. & Williams, C. S. Using 3D Organoid Cultures to Model Intestinal Physiology and Colorectal Cancer. *Curr Colorectal Cancer Rep* **13**, 183-191, doi:10.1007/s11888-017-0363-8 (2017).
232 Smith, G. *et al.* Mutations in APC, Kirsten-ras, and p53 - alternative genetic pathways to colorectal cancer. *Proceedings of the National Academy of Sciences* **99**, 9433-9438, doi:doi:10.1073/pnas.122612899 (2002).
233 Sottoriva, A. *et al.* A Big Bang model of human colorectal tumor growth. *Nat Genet* **47**, 209-216, doi:10.1038/ng.3214 (2015).
234 Losi, L., Baisse, B., Bouzourene, H. & Benhattar, J. Evolution of intratumoral genetic heterogeneity during colorectal cancer progression. *Carcinogenesis* **26**, 916-922, doi:10.1093/carcin/bgi044 (2005).
235 Saito, T. *et al.* A temporal shift of the evolutionary principle shaping intratumor heterogeneity in colorectal cancer. *Nat Commun* **9**, 2884, doi:10.1038/s41467-018-05226-0 (2018).
236 Wood, L. D. *et al.* The genomic landscapes of human breast and colorectal cancers. *Science* **318**, 1108-1113, doi:10.1126/science.1145720 (2007).
237 Uchi, R. *et al.* Integrated Multiregional Analysis Proposing a New Model of Colorectal Cancer Evolution. *PLoS Genet* **12**, e1005778, doi:10.1371/journal.pgen.1005778 (2016).
238 Oh, B. Y. *et al.* Intratumor heterogeneity inferred from targeted deep sequencing as a prognostic indicator. *Sci Rep* **9**, 4542, doi:10.1038/s41598-019-41098-0 (2019).
239 Misale, S. *et al.* Emergence of KRAS mutations and acquired resistance to anti-EGFR therapy in colorectal cancer. *Nature* **486**, 532-536, doi:10.1038/nature11156 (2012).

240 Mamlouk, S. *et al.* Malignant transformation and genetic alterations are uncoupled in early colorectal cancer progression. *BMC Biol* **18**, 116, doi:10.1186/s12915-020-00844-x (2020).
241 Sievers, C. K. *et al.* Subclonal diversity arises early even in small colorectal tumours and contributes to differential growth fates. *Gut* **66**, 2132-2140, doi:10.1136/gutjnl-2016-312232 (2017).
242 Ling, S. *et al.* Extremely high genetic diversity in a single tumor points to prevalence of non-Darwinian cell evolution. *Proc Natl Acad Sci U S A* **112**, E6496-6505, doi:10.1073/pnas.1519556112 (2015).
243 van Neerven, S. M. *et al.* Apc-mutant cells act as supercompetitors in intestinal tumour initiation. *Nature* **594**, 436-441, doi:10.1038/s41586-021-03558-4 (2021).
244 Flanagan, D. J. *et al.* NOTUM from Apc-mutant cells biases clonal competition to initiate cancer. *Nature* **594**, 430-435, doi:10.1038/s41586-021-03525-z (2021).
245 Hobor, S. *et al.* TGFα and amphiregulin paracrine network promotes resistance to EGFR blockade in colorectal cancer cells. *Clin Cancer Res* **20**, 6429-6438, doi:10.1158/1078-0432.Ccr-14-0774 (2014).
246 Cleary, A. S., Leonard, T. L., Gestl, S. A. & Gunther, E. J. Tumour cell heterogeneity maintained by cooperating subclones in Wnt-driven mammary cancers. *Nature* **508**, 113-117, doi:10.1038/nature13187 (2014).
247 Heijmans, J. *et al.* ER Stress Causes Rapid Loss of Intestinal Epithelial Stemness through Activation of the Unfolded Protein Response. *Cell Reports* **3**, 1128-1139, doi:https://doi.org/10.1016/j.celrep.2013.02.031 (2013).
248 O'Rourke, K. P., Ackerman, S., Dow, L. E. & Lowe, S. W. Isolation, Culture, and Maintenance of Mouse Intestinal Stem Cells. *Bio Protoc* **6**, doi:10.21769/bioprotoc.1733 (2016).
249 Langlands, A. J., Carroll, T. D., Chen, Y. & Näthke, I. Chir99021 and Valproic acid reduce the proliferative advantage of Apc mutant cells. *Cell Death Dis* **9**, 255, doi:10.1038/s41419-017-0199-9 (2018).
250 Wang, N. *et al.* Adenovirus-mediated efficient gene transfer into cultured three-dimensional organoids. *PLoS One* **9**, e93608, doi:10.1371/journal.pone.0093608 (2014).
251 Fujii, M. *et al.* Human Intestinal Organoids Maintain Self-Renewal Capacity and Cellular Diversity in Niche-Inspired Culture Condition. *Cell Stem Cell* **23**, 787-793.e786, doi:10.1016/j.stem.2018.11.016 (2018).
252 Villar, G., Graham, A. D. & Bayley, H. A tissue-like printed material. *Science* **340**, 48-52, doi:10.1126/science.1229495 (2013).
253 Zhou, L. *et al.* Lipid-Bilayer-Supported 3D Printing of Human Cerebral Cortex Cells Reveals Developmental Interactions. *Advanced Materials* **32**, 2002183, doi:https://doi.org/10.1002/adma.202002183 (2020).
254 Zhou, L. *et al.* Bioengineered Gastrointestinal Tissues with Fibroblast-Induced Shapes. *Advanced Functional Materials* **31**, 2007514, doi:https://doi.org/10.1002/adfm.202007514 (2021).
255 Shen, S. & Clairambault, J. Cell plasticity in cancer cell populations. *F1000Res* **9**, doi:10.12688/f1000research.24803.1 (2020).
256 Buczacki, S. Fate plasticity in the intestine: The devil is in the detail. *World J Gastroenterol* **25**, 3116-3122, doi:10.3748/wjg.v25.i25.3116 (2019).
257 de Sousa, E. M. F. & de Sauvage, F. J. Cellular Plasticity in Intestinal Homeostasis and Disease. *Cell Stem Cell* **24**, 54-64, doi:10.1016/j.stem.2018.11.019 (2019).
258 Shimokawa, M. *et al.* Visualization and targeting of LGR5(+) human colon cancer stem cells. *Nature* **545**, 187-192, doi:10.1038/nature22081 (2017).
259 Lenos, K. J. *et al.* Stem cell functionality is microenvironmentally defined during tumour expansion and therapy response in colon cancer. *Nat Cell Biol* **20**, 1193-1202, doi:10.1038/s41556-018-0179-z (2018).
260 Lin, C. C., Liao, T. T. & Yang, M. H. Immune Adaptation of Colorectal Cancer Stem Cells and Their Interaction With the Tumor Microenvironment. *Front Oncol* **10**, 588542, doi:10.3389/fonc.2020.588542 (2020).

261 Kemper, K. *et al.* Monoclonal antibodies against Lgr5 identify human colorectal cancer stem cells. *Stem Cells* **30**, 2378-2386, doi:10.1002/stem.1233 (2012).
262 Schepers, A. G. *et al.* Lineage tracing reveals Lgr5+ stem cell activity in mouse intestinal adenomas. *Science* **337**, 730-735, doi:10.1126/science.1224676 (2012).
263 Lukonin, I., Zinner, M. & Liberali, P. Organoids in image-based phenotypic chemical screens. *Experimental & Molecular Medicine* **53**, 1495-1502, doi:10.1038/s12276-021-00641-8 (2021).
264 Lukonin, I. *et al.* Phenotypic landscape of intestinal organoid regeneration. *Nature* **586**, 275-280, doi:10.1038/s41586-020-2776-9 (2020).
265 Serra, D. *et al.* Self-organization and symmetry breaking in intestinal organoid development. *Nature* **569**, 66-72, doi:10.1038/s41586-019-1146-y (2019).
266 Hof, L. *et al.* Long-term live imaging and multiscale analysis identify heterogeneity and core principles of epithelial organoid morphogenesis. *BMC Biol* **19**, 37, doi:10.1186/s12915-021-00958-w (2021).
267 Yang, Q. *et al.* Cell fate coordinates mechano-osmotic forces in intestinal crypt formation. *Nat Cell Biol* **23**, 733-744, doi:10.1038/s41556-021-00700-2 (2021).
268 Bolhaqueiro, A. C. F. *et al.* Ongoing chromosomal instability and karyotype evolution in human colorectal cancer organoids. *Nat Genet* **51**, 824-834, doi:10.1038/s41588-019-0399-6 (2019).
269 Bollen, Y. *et al.* Reconstructing single-cell karyotype alterations in colorectal cancer identifies punctuated and gradual diversification patterns. *Nat Genet* **53**, 1187-1195, doi:10.1038/s41588-021-00891-2 (2021).
270 Albanese, A. *et al.* Multiscale 3D phenotyping of human cerebral organoids. *Sci Rep* **10**, 21487, doi:10.1038/s41598-020-78130-7 (2020).
271 Mergenthaler, P. *et al.* Rapid 3D phenotypic analysis of neurons and organoids using data-driven cell segmentation-free machine learning. *PLoS Comput Biol* **17**, e1008630, doi:10.1371/journal.pcbi.1008630 (2021).
272 Freckmann, E. C. *et al.* Traject3d allows label-free identification of distinct co-occurring phenotypes within 3D culture by live imaging. *Nature Communications* **13**, 5317, doi:10.1038/s41467-022-32958-x (2022).
273 Hashimoto, K. *et al.* Cellular context-dependent consequences of Apc mutations on gene regulation and cellular behavior. *Proceedings of the National Academy of Sciences* **114**, 758-763, doi:doi:10.1073/pnas.1614197114 (2017).
274 Dow, L. E. *et al.* Apc Restoration Promotes Cellular Differentiation and Reestablishes Crypt Homeostasis in Colorectal Cancer. *Cell* **161**, 1539-1552, doi:10.1016/j.cell.2015.05.033 (2015).
275 Zhang, T. *et al.* APC mutations in human colon lead to decreased neuroendocrine maturation of ALDH+ stem cells that alters GLP-2 and SST feedback signaling: Clue to a link between WNT and retinoic acid signalling in colon cancer development. *PLOS ONE* **15**, e0239601, doi:10.1371/journal.pone.0239601 (2020).
276 Solé, L. *et al.* p53 wild-type colorectal cancer cells that express a fetal gene signature are associated with metastasis and poor prognosis. *Nature Communications* **13**, 2866, doi:10.1038/s41467-022-30382-9 (2022).
277 Hammond, D. E. *et al.* Differential reprogramming of isogenic colorectal cancer cells by distinct activating KRAS mutations. *J Proteome Res* **14**, 1535-1546, doi:10.1021/pr501191a (2015).
278 Moser, A. R. *et al.* ApcMin: A mouse model for intestinal and mammary tumorigenesis. *European Journal of Cancer* **31**, 1061-1064, doi:https://doi.org/10.1016/0959-8049(95)00181-H (1995).
279 Moser, A. R., Pitot, H. C. & Dove, W. F. A Dominant Mutation That Predisposes to Multiple Intestinal Neoplasia in the Mouse. *Science* **247**, 322-324, doi:doi:10.1126/science.2296722 (1990).
280 Boman, B. M. & Fields, J. Z. An APC:WNT Counter-Current-Like Mechanism Regulates Cell Division Along the Human Colonic Crypt Axis: A Mechanism That Explains How APC Mutations Induce Proliferative Abnormalities That Drive Colon Cancer Development. *Front Oncol* **3**, 244, doi:10.3389/fonc.2013.00244 (2013).

281 Zhu, G., Pei, L., Xia, H., Tang, Q. & Bi, F. Role of oncogenic KRAS in the prognosis, diagnosis and treatment of colorectal cancer. *Molecular Cancer* **20**, 143, doi:10.1186/s12943-021-01441-4 (2021).
282 Olmedillas-López, S. *et al.* Detection of KRAS G12D in colorectal cancer stool by droplet digital PCR. *World J Gastroenterol* **23**, 7087-7097, doi:10.3748/wjg.v23.i39.7087 (2017).
283 Betzler, A. M. *et al.* Differential Effects of Trp53 Alterations in Murine Colorectal Cancer. *Cancers (Basel)* **13**, doi:10.3390/cancers13040808 (2021).
284 Liu, G. *et al.* High metastatic potential in mice inheriting a targeted p53 missense mutation. *Proc Natl Acad Sci U S A* **97**, 4174-4179, doi:10.1073/pnas.97.8.4174 (2000).
285 Fearon, E. R. Molecular Genetics of Colorectal Cancer. *Annual Review of Pathology: Mechanisms of Disease* **6**, 479-507, doi:10.1146/annurev-pathol-011110-130235 (2011).
286 Young, M. A. *et al.* Subtle Deregulation of the Wnt-Signaling Pathway Through Loss of Apc2 Reduces the Fitness of Intestinal Stem Cells. *Stem Cells* **36**, 114-122, doi:10.1002/stem.2712 (2018).
287 Cai, Z., Cao, Y., Luo, Y., Hu, H. & Ling, H. Signalling mechanism(s) of epithelial-mesenchymal transition and cancer stem cells in tumour therapeutic resistance. *Clin Chim Acta* **483**, 156-163, doi:10.1016/j.cca.2018.04.033 (2018).
288 Vermeulen, L. & Snippert, H. J. Stem cell dynamics in homeostasis and cancer of the intestine. *Nat Rev Cancer* **14**, 468-480, doi:10.1038/nrc3744 (2014).
289 Zhao, H. *et al.* Wnt signaling in colorectal cancer: pathogenic role and therapeutic target. *Molecular Cancer* **21**, 144, doi:10.1186/s12943-022-01616-7 (2022).
290 Kalluri, R. & Weinberg, R. A. The basics of epithelial-mesenchymal transition. *J Clin Invest* **119**, 1420-1428, doi:10.1172/jci39104 (2009).
291 Boumahdi, S. & de Sauvage, F. J. The great escape: tumour cell plasticity in resistance to targeted therapy. *Nat Rev Drug Discov* **19**, 39-56, doi:10.1038/s41573-019-0044-1 (2020).
292 Davidson, L. A. *et al.* Alteration of colonic stem cell gene signatures during the regenerative response to injury. *Biochimica et Biophysica Acta (BBA) - Molecular Basis of Disease* **1822**, 1600-1607, doi:https://doi.org/10.1016/j.bbadis.2012.06.011 (2012).
293 Gil Vasquez, E. *et al.* Molecular phenotyping of colorectal neoplasia shows dynamic and adaptive cancer stem cell population admixture. *bioRxiv*, 2022.2006.2011.495729, doi:10.1101/2022.06.11.495729 (2022).
294 Barker, N. *et al.* Crypt stem cells as the cells-of-origin of intestinal cancer. *Nature* **457**, 608-611, doi:10.1038/nature07602 (2009).
295 Schwitalla, S. *et al.* Intestinal tumorigenesis initiated by dedifferentiation and acquisition of stem-cell-like properties. *Cell* **152**, 25-38, doi:10.1016/j.cell.2012.12.012 (2013).
296 Davis, H. *et al.* Aberrant epithelial GREM1 expression initiates colonic tumorigenesis from cells outside the stem cell niche. *Nat Med* **21**, 62-70, doi:10.1038/nm.3750 (2015).
297 Bolós, V., Gasent, J. M., López-Tarruella, S. & Grande, E. The dual kinase complex FAK-Src as a promising therapeutic target in cancer. *Onco Targets Ther* **3**, 83-97, doi:10.2147/ott.s6909 (2010).
298 Azzolin, L. *et al.* Role of TAZ as mediator of Wnt signaling. *Cell* **151**, 1443-1456, doi:10.1016/j.cell.2012.11.027 (2012).
299 Azzolin, L. *et al.* YAP/TAZ incorporation in the β-catenin destruction complex orchestrates the Wnt response. *Cell* **158**, 157-170, doi:10.1016/j.cell.2014.06.013 (2014).
300 Scott, K. E., Fraley, S. I. & Rangamani, P. A spatial model of YAP/TAZ signaling reveals how stiffness, dimensionality, and shape contribute to emergent outcomes. *Proceedings of the National Academy of Sciences* **118**, e2021571118, doi:doi:10.1073/pnas.2021571118 (2021).
301 Zanconato, F., Cordenonsi, M. & Piccolo, S. YAP/TAZ at the Roots of Cancer. *Cancer Cell* **29**, 783-803, doi:10.1016/j.ccell.2016.05.005 (2016).
302 Hanahan, D. & Weinberg, R. A. Hallmarks of cancer: the next generation. *Cell* **144**, 646-674, doi:10.1016/j.cell.2011.02.013 (2011).
303 Winkler, J., Abisoye-Ogunniyan, A., Metcalf, K. J. & Werb, Z. Concepts of extracellular matrix remodelling in tumour progression and metastasis. *Nature Communications* **11**, 5120, doi:10.1038/s41467-020-18794-x (2020).

304 Della Chiara, G. *et al.* Epigenomic landscape of human colorectal cancer unveils an aberrant core of pan-cancer enhancers orchestrated by YAP/TAZ. *Nature Communications* **12**, 2340, doi:10.1038/s41467-021-22544-y (2021).
305 Jiang, L. *et al.* YAP promotes the proliferation and migration of colorectal cancer cells through the Glut3/AMPK signaling pathway. *Oncol Lett* **21**, 312, doi:10.3892/ol.2021.12573 (2021).
306 Nukuda, A. *et al.* Stiff substrates increase YAP-signaling-mediated matrix metalloproteinase-7 expression. *Oncogenesis* **4**, e165-e165, doi:10.1038/oncsis.2015.24 (2015).
307 Panarelli, N. C., Yantiss, R. K., Yeh, M. M., Liu, Y. & Chen, Y.-T. Tissue-Specific Cadherin CDH17 Is a Useful Marker of Gastrointestinal Adenocarcinomas With Higher Sensitivity Than CDX2. *American Journal of Clinical Pathology* **138**, 211-222, doi:10.1309/ajcpkshxi3xehw1j (2012).
308 Silberg, D. G., Swain, G. P., Suh, E. R. & Traber, P. G. Cdx1 and cdx2 expression during intestinal development. *Gastroenterology* **119**, 961-971, doi:10.1053/gast.2000.18142 (2000).
309 Bae, J. M., Lee, T. H., Cho, N. Y., Kim, T. Y. & Kang, G. H. Loss of CDX2 expression is associated with poor prognosis in colorectal cancer patients. *World J Gastroenterol* **21**, 1457-1467, doi:10.3748/wjg.v21.i5.1457 (2015).
310 Zhang, B. Y. *et al.* Lack of Caudal-Type Homeobox Transcription Factor 2 Expression as a Prognostic Biomarker in Metastatic Colorectal Cancer. *Clin Colorectal Cancer* **16**, 124-128, doi:10.1016/j.clcc.2016.09.003 (2017).
311 Cai, J., Maitra, A., Anders, R. A., Taketo, M. M. & Pan, D. β-Catenin destruction complex-independent regulation of Hippo-YAP signaling by APC in intestinal tumorigenesis. *Genes Dev* **29**, 1493-1506, doi:10.1101/gad.264515.115 (2015).
312 Cheung, P. *et al.* Regenerative Reprogramming of the Intestinal Stem Cell State via Hippo Signaling Suppresses Metastatic Colorectal Cancer. *Cell Stem Cell* **27**, 590-604.e599, doi:10.1016/j.stem.2020.07.003 (2020).
313 Dupont, S. *et al.* Role of YAP/TAZ in mechanotransduction. *Nature* **474**, 179-183, doi:10.1038/nature10137 (2011).
314 Kwak, J. M. *et al.* The prognostic significance of E-cadherin and liver intestine-cadherin expression in colorectal cancer. *Dis Colon Rectum* **50**, 1873-1880, doi:10.1007/s10350-007-9034-1 (2007).
315 Takamura, M. *et al.* Reduced expression of liver-intestine cadherin is associated with progression and lymph node metastasis of human colorectal carcinoma. *Cancer Lett* **212**, 253-259, doi:10.1016/j.canlet.2004.03.016 (2004).
316 Yang, L. *et al.* Evaluation of the Prognostic Relevance of Differential Claudin Gene Expression Highlights Claudin-4 as Being Suppressed by TGFβ1 Inhibitor in Colorectal Cancer. *Front Genet* **13**, 783016, doi:10.3389/fgene.2022.783016 (2022).
317 Kohn, K. W., Zeeberg, B. M., Reinhold, W. C. & Pommier, Y. Gene expression correlations in human cancer cell lines define molecular interaction networks for epithelial phenotype. *PLoS One* **9**, e99269, doi:10.1371/journal.pone.0099269 (2014).
318 Kyuno, D. *et al.* Role of tight junctions in the epithelial-to-mesenchymal transition of cancer cells. *Biochimica et Biophysica Acta (BBA) - Biomembranes* **1863**, 183503, doi:https://doi.org/10.1016/j.bbamem.2020.183503 (2021).
319 Kim, M. S. *et al.* Extracellular Matrix Biomarkers in Colorectal Cancer. *Int J Mol Sci* **22**, doi:10.3390/ijms22179185 (2021).
320 Karlsson, S. & Nyström, H. The extracellular matrix in colorectal cancer and its metastatic settling – Alterations and biological implications. *Critical Reviews in Oncology/Hematology* **175**, 103712, doi:https://doi.org/10.1016/j.critrevonc.2022.103712 (2022).
321 Greaves, M. & Maley, C. C. Clonal evolution in cancer. *Nature* **481**, 306-313, doi:10.1038/nature10762 (2012).
322 Dang, H. X. *et al.* The clonal evolution of metastatic colorectal cancer. *Science Advances* **6**, eaay9691, doi:doi:10.1126/sciadv.aay9691 (2020).
323 Krotenberg Garcia, A. *et al.* Active elimination of intestinal cells drives oncogenic growth in organoids. *Cell Rep* **36**, 109307, doi:10.1016/j.celrep.2021.109307 (2021).
324 Yum, M. K. *et al.* Tracing oncogene-driven remodelling of the intestinal stem cell niche. *Nature* **594**, 442-447, doi:10.1038/s41586-021-03605-0 (2021).

325 Bose, D. *et al.* Chemoresistant colorectal cancer cells and cancer stem cells mediate growth and survival of bystander cells. *Br J Cancer* **105**, 1759-1767, doi:10.1038/bjc.2011.449 (2011).
326 Andersen, J. *et al.* Generation of Functional Human 3D Cortico-Motor Assembloids. *Cell* **183**, 1913-1929.e1926, doi:10.1016/j.cell.2020.11.017 (2020).
327 Graham, A. D. *et al.* High-Resolution Patterned Cellular Constructs by Droplet-Based 3D Printing. *Scientific Reports* **7**, 7004, doi:10.1038/s41598-017-06358-x (2017).
328 Dunbar, K. *et al.* Aspirin Rescues Wnt-Driven Stem-like Phenotype in Human Intestinal Organoids and Increases the Wnt Antagonist Dickkopf-1. *Cellular and Molecular Gastroenterology and Hepatology* **11**, 465-489, doi:https://doi.org/10.1016/j.jcmgh.2020.09.010 (2021).
329 Knight, J. R. P. *et al.* MNK Inhibition Sensitizes KRAS-Mutant Colorectal Cancer to mTORC1 Inhibition by Reducing eIF4E Phosphorylation and c-MYC Expression. *Cancer Discov* **11**, 1228-1247, doi:10.1158/2159-8290.Cd-20-0652 (2021).
330 Reischmann, N. *et al.* BRAF(V600E) drives dedifferentiation in small intestinal and colonic organoids and cooperates with mutant p53 and Apc loss in transformation. *Oncogene* **39**, 6053-6070, doi:10.1038/s41388-020-01414-9 (2020).
331 Li, C. *et al.* GDF15 promotes EMT and metastasis in colorectal cancer. *Oncotarget* **7**, 860-872, doi:10.18632/oncotarget.6205 (2016).
332 Bueno-Fortes, S. *et al.* A Gene Signature Derived from the Loss of CDKN1A (p21) Is Associated with CMS4 Colorectal Cancer. *Cancers* **14**, 136 (2022).
333 Thompson, C. A., DeLaForest, A. & Battle, M. A. Patterning the gastrointestinal epithelium to confer regional-specific functions. *Developmental Biology* **435**, 97-108, doi:https://doi.org/10.1016/j.ydbio.2018.01.006 (2018).
334 Cui, H.-Y. *et al.* CD147 receptor is essential for TFF3-mediated signaling regulating colorectal cancer progression. *Signal Transduction and Targeted Therapy* **6**, 268, doi:10.1038/s41392-021-00677-2 (2021).
335 Park, H. S. *et al.* Deleted in malignant brain tumor 1 is a novel prognostic marker in colorectal cancer. *Oncol Rep* **39**, 2279-2287, doi:10.3892/or.2018.6287 (2018).
336 Xu, J. *et al.* LYPD8 regulates the proliferation and migration of colorectal cancer cells through inhibiting the secretion of IL-6 and TNF-α Corrigendum in /10.3892/or.2021.8004. *Oncol Rep* **41**, 2389-2395, doi:10.3892/or.2019.7034 (2019).
337 Kim, S.-A. *et al.* Amphiregulin can predict treatment resistance to palliative first-line cetuximab plus FOLFIRI chemotherapy in patients with RAS wild-type metastatic colorectal cancer. *Scientific Reports* **11**, 23803, doi:10.1038/s41598-021-03197-9 (2021).
338 Gemoll, T., Strohkamp, S., Schillo, K., Thorns, C. & Habermann, J. K. MALDI-imaging reveals thymosin beta-4 as an independent prognostic marker for colorectal cancer. *Oncotarget* **6**, 43869-43880, doi:10.18632/oncotarget.6103 (2015).
339 Tang, Q. *et al.* TM4SF1 promotes EMT and cancer stemness via the Wnt/β-catenin/SOX2 pathway in colorectal cancer. *Journal of Experimental & Clinical Cancer Research* **39**, 232, doi:10.1186/s13046-020-01690-z (2020).
340 Ji, L., Wei, Y., Jiang, T. & Wang, S. Correlation of Nrf2, NQO1, MRP1, cmyc and p53 in colorectal cancer and their relationships to clinicopathologic features and survival. *Int J Clin Exp Pathol* **7**, 1124-1131 (2014).
341 Deng, J. *et al.* CRYAB predicts clinical prognosis and is associated with immunocyte infiltration in colorectal cancer. *PeerJ* **9**, e12578, doi:10.7717/peerj.12578 (2021).
342 Wang, R. *et al.* HSPA5 repressed ferroptosis to promote colorectal cancer development by maintaining GPX4 stability. *Neoplasma*, doi:10.4149/neo_2022_220331N363 (2022).
343 Zhang, J. *et al.* p62 functions as an oncogene in colorectal cancer through inhibiting apoptosis and promoting cell proliferation by interacting with the vitamin D receptor. *Cell Proliferation* **52**, e12585, doi:https://doi.org/10.1111/cpr.12585 (2019).
344 Zong, Y. *et al.* Combination of FOXD1 and Plk2: A novel biomarker for predicting unfavourable prognosis of colorectal cancer. *Journal of Cellular and Molecular Medicine* **26**, 3471-3482, doi:https://doi.org/10.1111/jcmm.17361 (2022).

345 Yuan, H. *et al.* SHP-2 Interacts with CD81 and Regulates the Malignant Evolution of Colorectal Cancer by Inhibiting Epithelial-Mesenchymal Transition. *Cancer Manag Res* **12**, 13273-13284, doi:10.2147/cmar.S270813 (2020).
346 LI, X., MARTIN, T. A. & JIANG, W. G. COM-1/p8 Acts as a Tumour Growth Enhancer in Colorectal Cancer Cell Lines. *Anticancer Research* **32**, 1229-1237 (2012).
347 Huang, W. S. *et al.* Expression of PRDX6 Correlates with Migration and Invasiveness of Colorectal Cancer Cells. *Cellular Physiology and Biochemistry* **51**, 2616-2630, doi:10.1159/000495934 (2018).
348 Luo, Y. *et al.* Long non-coding RNA NEAT1 promotes colorectal cancer progression by competitively binding miR-34a with SIRT1 and enhancing the Wnt/β-catenin signaling pathway. *Cancer Lett* **440-441**, 11-22, doi:10.1016/j.canlet.2018.10.002 (2019).
349 Zhang, X. *et al.* Selenium binding protein 1 inhibits tumor angiogenesis in colorectal cancers by blocking the Delta-like ligand 4/Notch1 signaling pathway. *Transl Oncol* **18**, 101365, doi:10.1016/j.tranon.2022.101365 (2022).
350 He, Y., Chen, Y., Dai, X. & Huang, S. Dysregulation of Circadian Clock Genes Associated with Tumor Immunity and Prognosis in Patients with Colon Cancer. *Computational and Mathematical Methods in Medicine* **2022**, 4957996, doi:10.1155/2022/4957996 (2022).
351 Jang, B. G. *et al.* SMOC2, an intestinal stem cell marker, is an independent prognostic marker associated with better survival in colorectal cancers. *Scientific Reports* **10**, 14591, doi:10.1038/s41598-020-71643-1 (2020).
352 Li, D. *et al.* KLF4-Mediated Negative Regulation of IFITM3 Expression Plays a Critical Role in Colon Cancer Pathogenesis. *Clinical Cancer Research* **17**, 3558-3568, doi:10.1158/1078-0432.Ccr-10-2729 (2011).
353 Cho, W. C., Jang, J. E., Kim, K. H., Yoo, B. C. & Ku, J. L. SORBS1 serves a metastatic role via suppression of AHNAK in colorectal cancer cell lines. *Int J Oncol* **56**, 1140-1151, doi:10.3892/ijo.2020.5006 (2020).
354 Oltedal, S. *et al.* Expression profiling and intracellular localization studies of the novel Proline-, Histidine-, and Glycine-rich protein 1 suggest an essential role in gastro-intestinal epithelium and a potential clinical application in colorectal cancer diagnostics. *BMC Gastroenterology* **18**, 26, doi:10.1186/s12876-018-0752-8 (2018).
355 Zhao, Q. *et al.* Circulating galectin-3 promotes metastasis by modifying MUC1 localization on cancer cell surface. *Cancer Res* **69**, 6799-6806, doi:10.1158/0008-5472.Can-09-1096 (2009).
356 Tomasi, M. L. *et al.* S-adenosylmethionine and methylthioadenosine inhibit cancer metastasis by targeting microRNA 34a/b-methionine adenosyltransferase 2A/2B axis. *Oncotarget* **8**, 78851-78869, doi:10.18632/oncotarget.20234 (2017).
357 Wu, R. *et al.* The long noncoding RNA LUCAT1 promotes colorectal cancer cell proliferation by antagonizing Nucleolin to regulate MYC expression. *Cell Death & Disease* **11**, 908, doi:10.1038/s41419-020-03095-4 (2020).
358 Shao, K. *et al.* DNA hypermethylation contributes to colorectal cancer metastasis by regulating the binding of CEBPB and TFCP2 to the CPEB1 promoter. *Clinical Epigenetics* **13**, 89, doi:10.1186/s13148-021-01071-z (2021).
359 Lewis, M. A. *et al.* Increased IFRD1 Expression in Human Colon Cancers Predicts Reduced Patient Survival. *Digestive Diseases and Sciences* **62**, 3460-3467, doi:10.1007/s10620-017-4819-0 (2017).
360 Sakthianandeswaren, A. *et al.* PHLDA1 expression marks the putative epithelial stem cells and contributes to intestinal tumorigenesis. *Cancer Res* **71**, 3709-3719, doi:10.1158/0008-5472.Can-10-2342 (2011).
361 Hu, L. *et al.* Overexpression of CHKA contributes to tumor progression and metastasis and predicts poor prognosis in colorectal carcinoma. *Oncotarget* **7**, 66660-66678, doi:10.18632/oncotarget.11433 (2016).
362 He, G. *et al.* Cysteine-Rich Intestinal Protein 1 Silencing Inhibits Migration and Invasion in Human Colorectal Cancer. *Cell Physiol Biochem* **44**, 897-906, doi:10.1159/000485357 (2017).

363 Yang, Y., Huycke, M. M., Herman, T. S. & Wang, X. Glutathione S-transferase alpha 4 induction by activator protein 1 in colorectal cancer. *Oncogene* **35**, 5795-5806, doi:10.1038/onc.2016.113 (2016).
364 Polari, L. *et al.* Keratin intermediate filaments in the colon: guardians of epithelial homeostasis. *Int J Biochem Cell Biol* **129**, 105878, doi:10.1016/j.biocel.2020.105878 (2020).
365 Saha, S. K., Yin, Y., Chae, H. S. & Cho, S. G. Opposing Regulation of Cancer Properties via KRT19-Mediated Differential Modulation of Wnt/β-Catenin/Notch Signaling in Breast and Colon Cancers. *Cancers (Basel)* **11**, doi:10.3390/cancers11010099 (2019).
366 Zhang, H. *et al.* Integrated Analysis of Oncogenic Networks in Colorectal Cancer Identifies GUCA2A as a Molecular Marker. *Biochemistry Research International* **2019**, 6469420, doi:10.1155/2019/6469420 (2019).
367 Olive, K. P. *et al.* Mutant p53 Gain of Function in Two Mouse Models of Li-Fraumeni Syndrome. *Cell* **119**, 847-860, doi:https://doi.org/10.1016/j.cell.2004.11.004 (2004).
368 Hamers, P. A. H. *et al.* Informing metastatic colorectal cancer patients by quantifying multiple scenarios for survival time based on real-life data. *Int J Cancer* **148**, 296-306, doi:10.1002/ijc.33200 (2021).
369 Panciera, T., Azzolin, L., Cordenonsi, M. & Piccolo, S. Mechanobiology of YAP and TAZ in physiology and disease. *Nat Rev Mol Cell Biol* **18**, 758-770, doi:10.1038/nrm.2017.87 (2017).
370 Aragona, M. *et al.* A mechanical checkpoint controls multicellular growth through YAP/TAZ regulation by actin-processing factors. *Cell* **154**, 1047-1059, doi:10.1016/j.cell.2013.07.042 (2013).
371 Koppens, M. A. J. *et al.* Bone Morphogenetic Protein Pathway Antagonism by Grem1 Regulates Epithelial Cell Fate in Intestinal Regeneration. *Gastroenterology* **161**, 239-254.e239, doi:https://doi.org/10.1053/j.gastro.2021.03.052 (2021).
372 Ramadan, R. *et al.* The extracellular matrix controls stem cell specification and crypt morphology in the developing and adult gut. *bioRxiv*, 2021.2004.2014.439776, doi:10.1101/2021.04.14.439776 (2021).
373 Stockinger, B., Shah, K. & Wincent, E. AHR in the intestinal microenvironment: safeguarding barrier function. *Nature Reviews Gastroenterology & Hepatology* **18**, 559-570, doi:10.1038/s41575-021-00430-8 (2021).
374 Wang, Q. *et al.* Aryl hydrocarbon receptor inhibits inflammation in DSS-induced colitis via the MK2/p-MK2/TTP pathway. *Int J Mol Med* **41**, 868-876, doi:10.3892/ijmm.2017.3262 (2018).
375 Metidji, A. *et al.* The Environmental Sensor AHR Protects from Inflammatory Damage by Maintaining Intestinal Stem Cell Homeostasis and Barrier Integrity. *Immunity* **49**, 353-362.e355, doi:10.1016/j.immuni.2018.07.010 (2018).
376 Shah, K. *et al.* Cell-intrinsic Aryl Hydrocarbon Receptor signalling is required for the resolution of injury-induced colonic stem cells. *Nature Communications* **13**, 1827, doi:10.1038/s41467-022-29098-7 (2022).
377 Dietrich, C. & Kaina, B. The aryl hydrocarbon receptor (AhR) in the regulation of cell–cell contact and tumor growth. *Carcinogenesis* **31**, 1319-1328, doi:10.1093/carcin/bgq028 (2010).
378 Feng, S., Cao, Z. & Wang, X. Role of aryl hydrocarbon receptor in cancer. *Biochimica et Biophysica Acta (BBA) - Reviews on Cancer* **1836**, 197-210, doi:https://doi.org/10.1016/j.bbcan.2013.05.001 (2013).
379 Peng, T. L., Chen, J., Mao, W., Song, X. & Chen, M. H. Aryl hydrocarbon receptor pathway activation enhances gastric cancer cell invasiveness likely through a c-Jun-dependent induction of matrix metalloproteinase-9. *BMC Cell Biol* **10**, 27, doi:10.1186/1471-2121-10-27 (2009).
380 Lin, S. *et al.* Autotaxin determines colitis severity in mice and is secreted by B cells in the colon. *Faseb j* **33**, 3623-3635, doi:10.1096/fj.201801415RR (2019).
381 Lin, S. *et al.* The absence of LPA2 attenuates tumor formation in an experimental model of colitis-associated cancer. *Gastroenterology* **136**, 1711-1720, doi:10.1053/j.gastro.2009.01.002 (2009).
382 Matas-Rico, E. *et al.* Autotaxin impedes anti-tumor immunity by suppressing chemotaxis and tumor infiltration of CD8(+) T cells. *Cell Rep* **37**, 110013, doi:10.1016/j.celrep.2021.110013 (2021).

383 Moll, R., Divo, M. & Langbein, L. The human keratins: biology and pathology. *Histochem Cell Biol* **129**, 705-733, doi:10.1007/s00418-008-0435-6 (2008).
384 Karantza, V. Keratins in health and cancer: more than mere epithelial cell markers. *Oncogene* **30**, 127-138, doi:10.1038/onc.2010.456 (2011).
385 Zhang, N. *et al.* Keratin 23 promotes telomerase reverse transcriptase expression and human colorectal cancer growth. *Cell Death Dis* **8**, e2961, doi:10.1038/cddis.2017.339 (2017).
386 Birkenkamp-Demtröder, K. *et al.* Keratin23 (KRT23) knockdown decreases proliferation and affects the DNA damage response of colon cancer cells. *PLoS One* **8**, e73593, doi:10.1371/journal.pone.0073593 (2013).
387 Ståhl, P. L. *et al.* Visualization and analysis of gene expression in tissue sections by spatial transcriptomics. *Science* **353**, 78-82, doi:10.1126/science.aaf2403 (2016).
388 Parigi, S. M. *et al.* The spatial transcriptomic landscape of the healing mouse intestine following damage. *Nature Communications* **13**, 828, doi:10.1038/s41467-022-28497-0 (2022).

Generated with BioRender.com

7. APPENDIX

7.1. Cell Culture Media

- HEK293T Rspo1-Fc Cells

  Advanced DMEM/F-12 (ThermoFisher Scientific/12634010)

  5% foetal bovine serum (FBS, ThermoFisher Scientific/10082147)

  2 mM L-glutamine (ThermoFisher Scientific/25030081)

  1 M 4-(2-hydroxyethyl)-1-piperazineethanesulfonic Acid (HEPES, ThermoFisher Scientific/15630080)

  Selectable medium only: 0.3 mg/ml Zeocin (ThermoFisher Scientific/R25001)

- HEK293T Nog-Fc Cells

  Advanced DMEM/F-12

  5% FBS

  2 mM L-glutamine

  1 M HEPES

  Selectable medium only: 10 µg/ml Puromycin (ThermoFisher Scientific/A1113803)

- HEK293T Wnt3A Luciferase Reporter Cells

  DMEM

  10% FBS

  2 mM L-glutamine

  1 M HEPES

  Selectable medium only: 0.4 mg/ml G418 (Sigma-Aldrich/A1720)

- L Wnt3A Cells

  DMEM (ThermoFisher Scientific/31966021)

  5% FBS

  2mM L-glutamine

  1 M HEPES

Selectable medium only: 0.4 mg/ml G418 (Sigma-Aldrich/A1720)

- Phoenix Cells

  10% FBS

  2 mM L-glutamine

  200 units/ml penicillin/streptomycin

7.2. Conditioned Medium Activity Assay

The HEK293T Wnt3A luciferase reporter cell line (gifted by the laboratory of Professor Fiona Powrie, University of Oxford) was used to test the quality of the R-Spondin and Wnt3a conditioned medium. Cells were expanded in the relevant selectable medium (Appendix 8.1), plated at confluency in a 24-well plate (in non-selectable medium) and allowed to adhere overnight. The appropriate wells (Figure 6.1) were then transfected with 0.4 ng/ml of Renilla, using Lipofectamine2000 (ThermoFisher Scientific/11668019) and Opti-MEM (ThermoFisher Scientific/ 31985062) as the transfection reagents, and five hours later 500 µl of conditioned medium was added to each well.

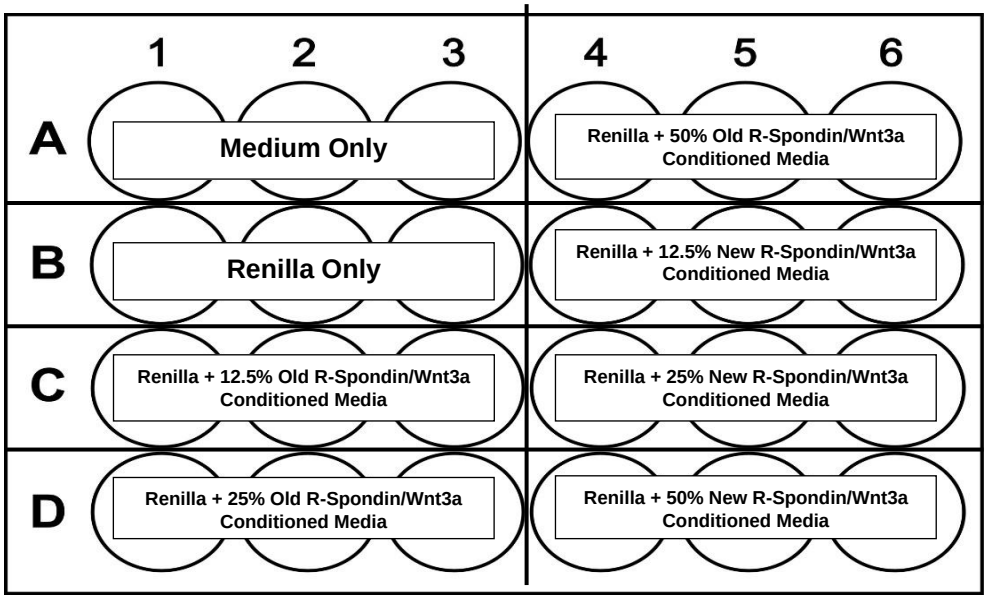


Figure 6.1. HEK293T luciferase reporter cell plate layout and medium requirements. HEK293T Wnt3A luciferase reporter cells were expanded in the relevant selectable medium and plated at confluency in triplicate in a 24-well plate (in non-selectable medium) and allowed to adhere overnight. The appropriate wells were transfected with Renilla, using Liopfectamine2000 and Opti-MEM as the transfection reagents, and five hours later conditioned medium was added to each well.

The cells were left to incubate overnight, following which the Dual-Luciferase® Reporter Assay System (Promega) and GloMax Multi Detection Plate Reader (Promega) were used to determine the luminescence of each well. Figure 6.2 illustrates an optimal luciferase assay result comparing the quality of an old and new batch of conditioned medium.

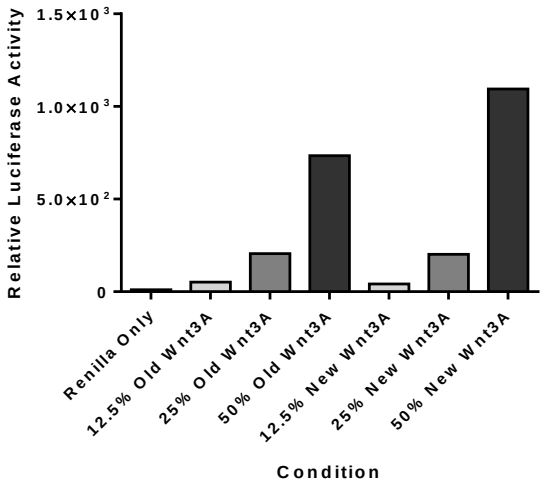


Figure 6.2. An optimal luciferase assay result comparing the quality of an old and new batch of Wnt3a conditioned medium. HEK293T Wnt3a luciferase reporter cells were expanded in the relevant selectable medium and plated at confluency in a 24-well plate (in non-selectable medium) and allowed to adhere overnight. The appropriate wells were transfected with 0.4 ng/ml of Renilla, using Liopfectamine2000 and Opti-MEM as the transfection reagents, and five hours later 500 µl of conditioned medium was added to each well. The Dual-Luciferase® Reporter Assay System (Promega) and GloMax Multi Detection Plate Reader (Promega) were used to determine the luminescence of each well.

In order to test the quality of the Noggin conditioned medium, 500 µl of organoid medium containing the newly made Noggin conditioned medium was placed on growing organoids and the growth monitored for 7-10 days. If the organoids began to die or grow at a slower rate, the batch was discarded. Once tested, all conditioned medium was aliquoted and stored at -80 °C.

7.3. Lentiviral Transduction

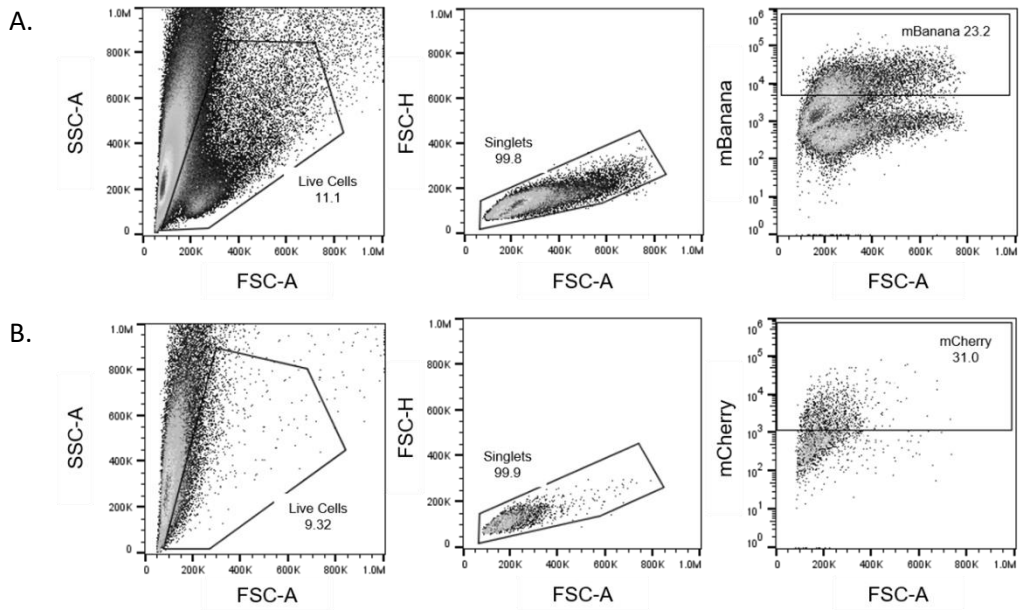


Figure 6.3. Gating strategy applied to isolate successfully transduced organoid populations. The proximal colon was removed from *p53*$^{LSL\text{-}R172H/R172H}$ (Cre untreated therefore *p53*^{Null}) and *Apc*$^{min/+}$ mice and derived into organoids. Subsequent *p53*^{Null} and *Apc*$^{min/+}$ colonoids were transduced with lentivirus expressing the fluorescent proteins mBanana and mCherry respectively. Live singlet cells were sorted using a MA900 Multi-Application Cell Sorter (Sony Biotechnology). Only those colonoids which were positive **A.** mCherry or **B.** mBanana were collected and expanded further.

7.4. Polymerase Chain Reaction

Table 6.1. Polymerase Chain Reaction primers used to confirm the colonoid genotypes. In order to confirm the genotype of wild type and mutant colonoids, the DNA was extracted from, and PCR performed on wild type, *Apc*$^{min/+}$, *Kras*$^{LSL\text{-}G12D/+\ CreERT2\text{-}EYFP}$*:p53*^{Null} (Tamoxifen treated), *Kras*$^{LSL\text{-}G12D/+\ CreERT2\text{-}EYFP}$ (Cre treated), *p53*$^{LSL\text{-}R172H/R172H}$ (Cre untreated) and *p53*$^{LSL\text{-}R172H/R172H}$ (Cre treated) colonoids using the appropriate primers stated below.

Genotype	Forward Primer	Reverse Primer
Apc Wild Type	5' GCCATCCCTTCACGTTAG 3'	5' TTCCACTTTGGCATAAGGC 3'
Apc^{min}	5' TTCTGAGAAAGACAGAAGTTA 3'	5' TTCCACTTTGGCATAAGGC 3'
Kras Wild Type	5' ATGTCTTTCCCCAGCACAGT 3'	5' TCCGAATTCAGTGACTACAGATG 3'
Kras^{G12D} Conditional Allele	5' CTAGCCACCATGGCTTGAGT 3'	5' TCCGAATTCAGTGACTACAGATG 3'
Kras^{G12D} Recombined Allele	5' ATGTCTTTCCCCAGCACAGT 3'	5' TCCGAATTCAGTGACTACAGATG 3'
p53 Wild Type	5' TTACACATCCAGCCTCTGTGG 3'	5' CTTGGAGACATAGCCACACTG 3'
p53^{R172H} Conditional Allele	5' AGCTAGCCATGGCTTGAGTAAGTCTGC 3'	5' CTTGGAGACATAGCCACACTG 3'
p53^{R172H} Recombined Allele	5' TTACACATCCAGCCTCTGTGG 3'	5' CTTGGAGACATAGCCACACTG 3'

Table 6.2. Polymerase Chain Reaction components and volumes used to confirm the colonoid genotypes.

Component	Company/Catalogue Number	20 µl Reaction
2X GoTaq® Green Master Mix	Promega/M712	10 µl
10 µM Forward Primer	See Table 8.1	1 µl
10 µM Reverse Primer	See Table 8.1	1 µl
<1000 ng DNA	-	0.5 µl
Nuclease-Free Water	Qiagen/129115	7.5 µl

Table 6.3. ProFlex PCR System conditions used to confirm the colonoid genotypes.

	Step	Temperature	Time
	Initial Denaturation	98 °C	2 minutes
35 Cycles	Denaturation	98 °C	40 seconds
	Annealing	60 °C	40 seconds
	Extension	72 °C	45 seconds
	Final Extension	72 °C	10 minutes
	Hold	4 °C	∞

7.5. Antibodies for Immunofluorescence Staining

Table 6.4. Primary and secondary antibodies used for immunofluorescent staining of colonoids.

Primary Antibody	Company/Catalogue Number
Annexin A1 (Anxa1)	Abcam/ab214486
Clusterin (Clu)	ThermoFisher Scientific/bs-1354R
Cytokeratin 14 (Krt14)	BioLegend/Poly19053
Osteopontin (Spp1)	ThermoFisher Scientific/702184
Small Proline Rich Protein 1A (Sprr1a)	ThermoFisher Scientific/PA5-110423
Yap	Cell Signaling/14074
Secondary Antibody	**Company/Catalogue Number**
Donkey Anti-Rabbit Alexa Fluor 488	ThermoFisher Scientific/A21206
Donkey Anti-Mouse Alexa Fluor 488	ThermoFisher Scientific/A21202
DAPI	Sigma Aldrich/D9542

7.6. Reagents for Mixed Colonoid Culture

- Oil

  4 mg/ml 1,2-diphytanoyl-sn-glycero-3-phosphocholine (DPhPC, Avanti/850356)

- Lipid

  1:4 (v/v) Undecane (Sigma Aldrich/W510505) and Silicone Oil AR20 (Sigma Aldrich/10836)

- Collagen Type I (Corning/354249) was diluted with co-culture medium to a final concentration of 1.6 mg/ml and neutralized to pH 7.3. The prepared collagen was kept on ice prior to use.